Papers presented to the

SEVENTEENTH SYMPOSIUM ON ANTARCTIC METEORITES

August 19–21, 1992

NATIONAL INSTITUTE OF POLAR RESEARCH, 国立極地研究所
TOKYO

Papers presented to the

SEVENTEENTH SYMPOSIUM ON ANTARCTIC METEORITES

August 19–21, 1992

NATIONAL INSTITUTE OF POLAR RESEARCH,
TOKYO

国立極地研究所

Wednesday, August 19, 1992

0830 - 1200 Registration Auditorium (6th Floor)

0925 - 0930 Opening Address **Takao Hoshiai**
Director-General
National Institute of
Polar Research

* Speaker

Chairmen: Yukio Ikeda and Kazushige Tomeoka

1 0930 - 0945 **Nishio F.*, Cho K., Seko K. and Fukuoka T.**
Role of tephra layers on satellite images in Meteorite Ice Field near Yamato Mountains, Antarctica

2 0945 - 1000 **Yanai K.* and Kojima H.**
Asuka-88 meteorites collection: Preliminary report of discoveries, initial processing and breif classification

3 1000 - 1015 **Miura Y.*, Imai M. and Kato T.**
Shock metemorphic evolution process applied by shock impact experiments

4 1015 - 1030 **Xie Xiande* and Chen Ming**
Micromineralogical studies on the severely shocked Yanzhuang H6 chondrite

5 1030 - 1045 **Akai J.***
Voids structure in some constituent minerals in Antarctic carbonaceous chondrites

6 1045 - 1100 **Scorzelli R. B.*, E.Galvao da Silva and Azevedo I. S.**
A mössbauer study of two thermal metamorphosed carbonaceous chondrites: Yamato-82162 and Yamato-86720

7 1100 - 1115 **Nakamura T.*, Tomeoka K. and Takeda H.**
Metamorphosed carbonaceous chondrites, Y-82104 and Y-82002: Mineralogy and petrology

8 1115 - 1130 **Tomeoka K.*, Nomura K. and Takeda H.**
Nepheline and albite in the Yamato-791717 CO carbonaceous chondrite: Evidence for nebular alteration

9 1130 - 1145 **Kojima T*, Tomeoka K. and Takeda H.**
Unusual clasts in the Vigarano CV3 chondrite

10 1145 - 1200 **Fudaki M* and Kitamura M.**
Cathodoluminescence study of olivines in the Allende meteorite

1200 - 1300 Lunch Time

Chairmen: **Makoto Kimura and Akira Shimoyama**

11 1300 - 1315 **Murakami T.*, Ikeda Y., Kimura M. and Noguchi T.**
Petrology and mineralogy of Yamato-86751 (CV3)

12 1315 - 1330 **Kimura M.* and Ikeda Y.**
Pre-accretionary alteration of chondrules in Allende meteorite

13 1330 - 1345 **Fujita T* and Kitamura M.**
Origin of fine fragment in matrix of chondrites

14 1345 - 1400 **Sekine T.***
Shock-induced phase transformation in nepheline

15 1400 - 1415 **Kojima H.*, and Yanai K.**
Type A CAI with core-mantle structure

16 1415 - 1430 **Nagahara H.***
Genetic relationships among Type IA and II chondrules and matrix in ordinary and carbonaceous chondrites

17 1430 - 1445 **Noguchi T.***
Reverse zoning of matrix plagioclase in CK chondrites

18 1445 - 1500 **Matsunami S.* and El Goresy A.**
Constraints to the formation of martix reduced olivine in Yamato-691 (EH3) chondrite: Implications for the evolution of EH chondrites

19 1500 - 1515 **Yamaguchi A.*, Saiki K. and Takeda H.**
Heterogeneous mixing of fall out deposits as seen in the Yamato polymict eucrites

1515 - 1530 **Tea Time**

20 1530 - 1545 **Hiroi T.*, Bell J. F., Takeda H. and Pieters C. H.**
Spectral comparison between olivine-rich asteroids and pallasites

21 1545 - 1600 **Komiya M.* and Shimoyama A.**
Examination of insoluble organic matter in some Antarctic and Murchison carbonaceous chondrites by a DTA/TG-GC/MS method

22 1600 - 1615 **Shimoyama A.* and Shigematsu R.**
Dicarboxylic acids in the Yamato 791198 and Murchison carbonaceous chondrites

23 1615 - 1630 **Murae T.***
Spectroscopic study of major organic matter in carbonaceous chondrites by microscopic FT-IR

24 1630 - 1645 **Kitajima F.* and Masuda A.**
A comparative structural study of the carbonaceous macromolecular materials in carbonaceous chondrites with several synthetic polymers

-- Special Lecture (I) --

Chairman: Akira Shimoyama

25 1645 - 1745 **Kerridge J. (Invited Speaker)**

Title: Origins of organic matter in meteorites

1745 - 2000 **Reception** **Lecture Room (2F)**

Thursday, August 20, 1992

Chairmen: Noboru Nakamura and Akira Tsuchiyama

26 0900 - 0915 **Miyamoto M.* and Takeda H.**
Thermal evolution of a primitive achondrite parent body: ^{26}Al heating.

27 0915 - 0930 **Uegomori H.*, Kurita K., Yurimoto H. and Sueno S.**
Size distribution and shape analysis of metal particles in ordinary chondrites

28 0930 - 0945 **Shimamura T.*, Honda M., Nagai H. and Yoshioka Y.**
Elemental distributions of unique iron meteorite Yamato-791694 by SIMS

29 0945 - 1000 **Inoue M.* and Nakamura N.**
REE constraints on the formation of Murchison (CM) chondrules

30 1000 - 1015 **Palme H.*, Spettel B., Wänke H. and Ikeda Y.**
The composition of chondrules in the H3-4 chondrite Y-790986

31 1015 - 1030 **Kagi H.*, Russel S. S., Pillinger C. T., Takahashi K. and Masuda A.**
Optical and isotopic properties of diamonds in ureilites

32 1030 - 1045 **Yamanaka C.*, Toyoda S. and Ikeya M.**
Possibility of classification and characteristic estimation of meteorites with ESR spectroscopy

33 1045 - 1100 **Flynn G. J.*, Sutton S. R. and Klöck W.**
Unmelted polar micrometeorites: Compositions, mineralogies, and similarities/differences with IDPs and meteorites

34 1100 - 1115 **Miono S.***
Comparison between carbonaceous chondrite and microspherule in Paleozoic-Mesozoic bedded chert

35 1115 - 1130 **Ping Kong* and Chifang Chai**
Implications of iridium distribution and some micro-spherules in Cretaceous-Tertiary boundary clays

36 1130 - 1145 **Li Chun-lai* and Ouyang Ziyuan**
Chemical Compositions of microtektites in loess

37 1145 - 1200 **Lin Wenzhu***
A evidence for the impact origin of tektites

1200 - 1300 Lunch Time

-- Special Session: Lunar Meteorites --

Chairmen: Hiroshi Takeda and Nobuo Takaoka

38 1300 - 1315 **Takeda H.*, Arai T. and Saiki K.**
Mineralogical studies of lunar meteorite Y-793169, a crystalline basalt

39 1315 - 1330 **Warren P. H.* and Kallemeyn G. W.**
Lithophile, siderophile, and volatile geochemistry (consortium investigations) of two mare-basaltic meteorites

40 1330 - 1345 **Snyder G. A. and Taylor L. A.***
The genesis and evolution of the moon's magma ocean as supported by lunar Antarctic meteorites

41 1345 - 1400 **Takahashi K.* and Masuda A.**
Geochemical and chronological studies for Asuka-881757 lunar meteorite

42 1400 - 1415 **Misawa K.*, Tatsumoto M., Dalrymple G. B. and Yanai K.**
U-Th-Pb, Sm-Nd, and Rb-Sr isotopic systematics and $^{40}Ar/^{39}Ar$ age of lunar meteorite Asuka-881757

43 1415 - 1430 **Torigoye N., Misawa K. and Tatsumoto M.***
U-Th-Pb chronology of Yamato-793169 lunar meteorite

44 1430 - 1445 **Nagao K.* and Miura Y.**
Noble gases and ^{81}Kr-terrestrial age of Asuka-31

45 1445 - 1500 **Nishiizumi K.*, Arnold J. R., Caffee M. W., Finkel R. C. and Reedy R. C.**
Cosmic ray exposure histories of lunar meteorites Asuka-881757, Yamato-793169, and Calcalong Creek

46 1500 - 1515 **Kaneoka I.* and Nagao K.**
^{40}Ar- ^{39}Ar analyses of a lunar meteorite (Y-86032) and a few LL3 and LL4 chondrites from Antarctica

1515 - 1530 Tea Time

47 1530 - 1545 **Matsubara K.*, and Matsuda J.**
Heavy noble gas constraint on the origin of tektites

48 1545 - 1600 **Matsuda J.*, Kusumi A., Yajima H., Kusaba K. and Syono Y.**
Noble gases in shock-produced diamonds: Their relationship with shock pressure and porosity

49 1600 - 1615 **Ozima M.* and Zahnle K.**
Evolution of terrestrial noble gas

50 1615 - 1630 **Takaoka N.*, Nagao K. and Miura Y.**
Noble gases in unique meteorites Yamato -74063 and -74357

-- Special Lecture (II) --

Chairman: Yukio Ikeda

51 1630 - 1730 **Wänke H.*(Invited Speaker) and Dreibus G.**

Title: On the martian volatiles as inferred from SNC-meteorites

Friday, August 21,1992

Chairmen: Jun-ichi Matsuda and Hirokazu Fujimaki

52 0900 - 0915 **Kiyota K.*, Sugiura N. and Hashizume K.**
On the carriers of anomalous nitrogen components in primitive meteorites

53 0915 - 0930 **Miura Y.* and Sugiura N.**
Nitrogen isotopic compositions in eucrites

54 0930 - 0945 **Fujimaki H.*, Aoki K., Ishikawa K., Kojima H. and Yanai K.**
Rb-Sr age of an impact event recorded in the Yamato-791088 H-chondrite

55 0945 - 1000 **Tsuchiyama A.* and Uyeda C.**
Effects of total gas pressure on Mg isotopic mass fractionation in condensation experiments of Mg-silicates

56 1000 - 1015 **Uyeda C* and Tsuchiyama A.**
Isotope line analysis on primitive meteorites using ion microprobe

57 1015 - 1030 **Koike O.*, Yurimoto H. Nagasawa H. and Sueno S.**
Ion microprobe measurements of Mg isotopes in Type-B1 CAI of Allende meteorite

58 1030 - 1045 **Clayton R. N.* and Mayeda T. K.**
Oxygen isotopic compositions of achondrites

59 1045 - 1100 **Kano N.*, Yamakoshi K. and Nogami K.**
Chemical and isotopic compositions in acid residues from various meteorites

60 1100 - 1115 **Alexander C. M. O'D., Xia Gao, Swan P. D. and Walker R. M.***
Non-chemical methods for the isolation and study of interstellar grains in primitive meteorites

61 1115 - 1130 **Amari S.*, Zinner E. and Lewis R. S.**
Isotopic compositions of corundum and hibonite grains from the Murchison meteorite

62 1130 - 1145 **Ninagawa K.*, Matoba A., Yamamoto I., Wada T., Matsunami S., Takaoka N., Sears D. W. G., Kojima H. and Yanai K.**
Proposal for measuring the TL of Japanese Antarctic meteorites

63 1145 - 1200 **Bhandari N.***
Depth profiles of cosmogenic isotopes: Implications to terrestrial ages of Antarctic meteorites

1200 - 1300 Lunch Time

Chairman: Keisuke Nagao

64 1300 - 1315 **Osadchii Eu.* and Kulikov Al.**
Concentration of electronic paramagnetic centers (EPC) in carbonaceous chondrites

65 1315 - 1330 **Pesonen L. J.*, Terho M. and Kukkonen I. T.**
Physical properties of 368 meteorites: Implications of early solar system magnetic fields

66 1330 - 1345 **Yamanaka A.*, Funaki M. and Nagai H.**
Magnetic properties of the Willard L6 chondrite and its NRM record

67 1345 - 1400 **Funaki M.***
Temperature dependent changes in magnetic coercivity in some ordinary chondrites

68 1400 - 1415 **Cresswell R. G.*, Miura Y., Beukens R. P. and Rucklidge J. C.**
Radiocarbon measurements on meteorites I: CO and CO_2 separations from temperature fractions

69 1415 - 1430 **Jakes P.* and Padevet V.**
Comets, asteroids and meteorites: Relationships witnessed by fireballs

70 1430 - 1445 **Nayak V. K.***
Shocked and unshocked basalt fragments and impactite glasses in monomict breccia from the Lonar impact crater, India

-- Special Lecture (III) --

Chairman: Noboru Nakamura

71 1445 - 1545 **Palme H.* (Invited Speaker)**

Title: Formation of Allende chondrules and matrix

-- Poster Session --

72 1230 - 1300 **Funaki M.***
Identification of the fine magnetic structures in chondrites by magnetotactic bacterial technique

Waiting List

73 **Chen Ming and Xie Xiande***
Vapour phase crystallization of Fe_3S_4 in the severely shocked Yanzhuang chondrite

74 **Miura Y., Cresswell R. G.*, Beukens R. P. and Rucklidge J.**
Radiocarbon Measurements on Meteorites II: Terrestrial ages and weathering activeities in some Antarctic chondrites.

Abstruct only

75 **Akai J. and Yagi K.**
Electron Microscopic observation of shocked minerals from Siljan crater, central Sweden and from some reference specimens

76 **Eugster O.**
Basaltic lunar meteorites Asuka-881757 and Yamato-793169: Comparison with EET87521 and Yamato 793274

77 **Hou Wei and Xie Hong-sen**
Gas-Liquid condensation evidences in meteorites and solar nebular condensation model

78 **Kimura M., Yabuki H., Ikeda Y. and EL Goresy A.**
Spinels in unquilibrated ordinary chondrites: correlation between their Al/Al+Cr ratios and petrologic types

79 **Kimura M., Lin Y-T., Ikeda Y., EL Goresy A., Yanai K. and Kojima H.**
Petrology and mineralogy of Antarctic aubrites, Y-793592 and ALH-78113, in comparison with non-Antarctic aubrites and E-chondrites

80 **Koeberl C., Kurat G. and Brandstätter F.**
Geochemical and mineralogical study of gabbroic lunar mare meteorites Asuka-881757 (Asuka-31) and Yamato-793169

Wednesday, August 19, 1992

0830-1200	*Registration, 6th Floor*
0925-0930	*Opening address, Auditorium*
0930-1645	*Symposium, Auditorium*
1645-1745	*Special Lecture (I)*

Dr. J. Kerridge (Invited Speaker)
University of California at Los Angels
U.S.A.

1745-2000 *Reception, Lecture Room, 2nd Floor*

Role of Tephra Layers on Satellite Images in Meteorite Ice Field n ear Yamato Mountains, Antarctica

Fumihiko NISHIO*1, Kohei Cho*2, Katsumoto Seko*3
and Takaaki Fukuoka*4

*1 Hokkaido University of Education,1-15-55, Shiroyama, Kushiro-Shi, Japan 085 (Fax:0154-43-0855)
*2 Remote Sensing Technology Center of Japan.
*3 Water Research Institute, Nagoya University, Japan.
*4 Gakushuin University, Tokyo, Japan.

1. Tephra layer

Dirt layers of tephra were found on the bare ice surface in the Meteorite Ice Field near the Yamato Mountains, Antarctica. The grain-size analyses of volcanic ash fragments and the geochemical composition of glass shards of the tephra indicate that the volcanic sources of the dirt layers in the Yamato Mountains region are far away and are some volcanoe in the South Sandwich Islands.

All of dirt layers was found to contain abundunt volcanic ash fragments. This fact shows that most of the dirt layers in the bare ice area are tephra layer. Tephra in glacier ice offers great potential as marker levels for stratigraphic studies and should be useful in providing isochronous planes in the ice sheet.

Englacial dirt layers outcropping on the bare ice surface can be observed easily when there is no snow deposited but may be missed when the dirt is in low concentrations. Since albedo decreases locally on the surface of a dirt layer, the ice within the dirt layer ablates faster than the surrounding ice to form narrow shallow troughs. Individual dirt layers showed great differences in length, width and their concentration of materials. Two types of layers are distinguished by the difference in colour tone. The darkest layer is very dark brown to black with a high concentration of materials. The other type of layer is characterized by low concentrations of materials. The thickness of the dirt layer varies from a few centimeters to about 15 cm, and the layers dip steeply up-glacier. The dirt layers generally have a sharp dirt/ice boundary in the bottom of the dirt layer, whereas in the upper part of the layer it is diffuse.

2. Role of tephra layers in satellite image

The satellite images of SPOT in the Yamato Meteorite Ice Field have shown more tephra layers than the dirt layers which were surveyed on the ground by eye during the traversing. Many patterns of tephra layers on the bare ice field would suggest the very complicated flow mode of ice in the vicinity of nunataks.

It is confirmed that tephras in the Antarctic ice are very fruitful tool for correlations of age of distant sites even if the absolute age of tephra is unknown. From the uranium-series age of Yamato ice contained Tephra, the age of approximately 35 x 10^3 years is obtained.

ASUKA-88 METEORITES COLLECTION; PRELIMINARY REPORT OF DISCOVERIES, INITIAL PROCESSING AND BREIF CLASSIFICATION; **Keizo Yanai** and **Hideyasu Kojima**, Department of Meteorites, National Institute of Polar Research (NIPR) 9-10, Kaga 1-chome, Itabashi-ku, Tokyo 173, Japan

Introduction

Asuka meteorites collections include Asuka-86, Asuka-87, Asuka-88 and Asuka-90 meteorites. Asuka-86 and Asuka-87 meteorites have been reported as the catalog (Yanai and Kojima, 1987) and in the last symposium of NIPR (Yanai, 1991) respectively. We report preliminary the discoveries and initial processing of Asuka-88 meteorites with their breif classification.

Search and discovery of the Asuka-88 meteorites

Asuka-88 meteorites have been found on the southern bare ice fields of the Sör Rondane Mountains by the Asuka wintering party of the 29th Japanese Antarctic Research Expedition (JARE-29, 1987-89). The party carried out the search for meteorites on the bare ice fields where located southern of **Mt. Bamse - Mt. Nils Larsen** in October 1988, and **Nansenisen** in 1988 field season (Fig.1).

Mt. Bamse - Mt. Nils Larsen area was poor for meteorite concentration. Several fragments of chondrite covered partly with fusion crust were collected in the southern bare ice of the point A118. A lot of doubtful specimens over few hundred were found in the moraine field near the A118. Those specimens are dark brown in color and deeply weathered, and collected as doubtful meteoritic specimens. Larger bare ice field located at the southern A140 to A180 was expected as high potential for meteorite concentration. But there are no meteorite and no terrestrial with some light colored dirt layers.

The "Nausenisen" (Nansen Ice field), on which more than 200 meteorites have been found by the reconnaissance search in February-March 1988, is new site of the most productive meteorite in Antarctica. The meteorite search party have been searched and investigated in detail in the period from November 1988 to January 1989. Almost 1,500 meteorites have been collected on the several bare ice areas, which included various type of irons, stony-irons, achondrites, carbonaceous meteorites and chondrites. There are some characteristic feature of meteorite occurrences in the Nausenisen. In general, relative large and mostly unweathered meteorites with complete

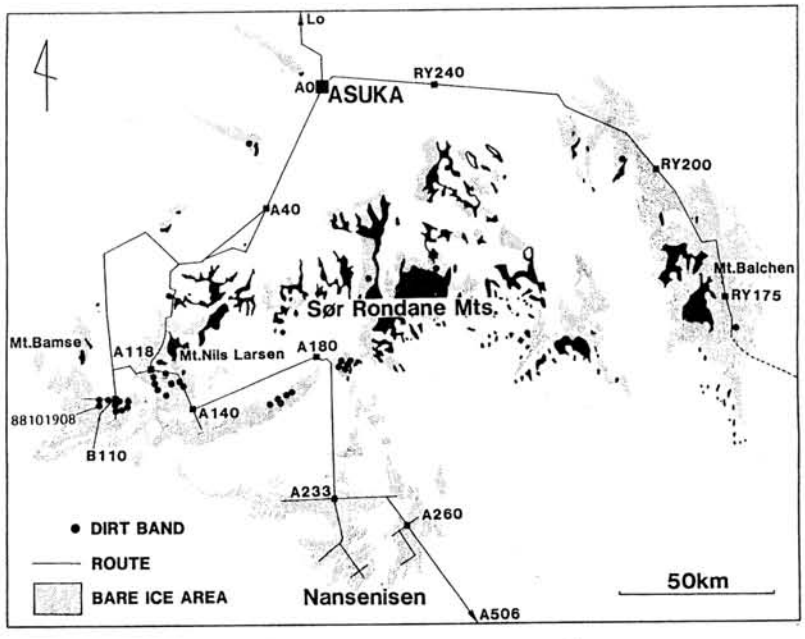

Fig.1 Field locations of the meteorite search in 1988 field season around the Sör Rondane Mountains, Queen Maud Land, East Antarctica.

fusion crust distributed in the bare ice area at an upstream where is relatively high elevation, plateau side and far from the Mountains. However at the down stream, much smaller, fragmental and more weathered meteorites were concentrated much more than those of the upstream. This features might be caused by sensitive wind effect, mechanical weathering and length of exposed period. Only four moraines with in small size are recognized on the bare ice field in the Nansenisen.

Initial processing of Asuka-88 meteorites

The Asuka-88 meteorites collection was put in a clean teflon bag and maintained together with Asuka-87 collection in frozen conditions under-20°C at the NIPR. The meteorites were returned to room temperature in a dry nitrogen-filled cabinet at the NIPR. Then each specimens were officially named Asuka-880001 to Asuka-882124 in order of discovery. All meteorites of the Asuka-88 were listed with their date of find, dimensions, weight and most brief identification and classification. Initial processing shows with other Asuka collections in Table 1. The Asuka-88 meteorites is over 2,100 specimens weighing almost 400kg including irons, stony-irons, achondrites, carbonaceous meteorites and chondrites with number of doubtful specimens. Iron contains few type briefly. Stony-Irons are tiny pallasite and relatively large mesosiderite weighing 1.1kg. Achondrites have much varieties such as lunar gabbro, Ca-pyroxene plagioclase crystalline basalt, coarse-midum-fine grained crystalline-unbrecciated eucrites and eucrite breccias, few types of diogenite, eucrite-howardites and ureilites without aubrite and martin meteorite. Carbonaceous meteorites include several types as possible C1(?), numbers of CM, CO, CV, C4 and C5(?). Chondrites have the majority in Asuka-88 collection similar to the other collections. After brief identification most of chondrites are ordinary types including lot of low petrologic types, and some of them are possibly unique types.

Asuka-31 (named officially as an Asuka-881757) lunar gabbro is one of the most unique and representative specimen of Asuka-88 collection, because Asuka-31 have been classified as the new type of the lunar rock (Yanai, 1991).

References:

Yanai, K. and Kojima, H.(1987) Photographic Catalog, NIPR Tokyo, 298p.
Yanai, K.(1991) Symposium on Anterctic Meteorites 16th, NIPR Tokyo, 1-2.
Yanai, K.(1991) Proc. Lunar Conf., 21, LPI Houston, 317-324.

Table 1 Asuka meteorites collections

Name (year)	Asuka-86 (1986/87)	Asuka-87 (1988)	Asuka-88 (1988/89)
Total	3	352	2,124
The largest(kg)	1.5(L)	46(LL)	43(H)
Irons	–	1	7
Stony-Irons	–	1	5
Achondrites	–	9	53
C. chondrites	–	2	31
Chondrites	3	326	] 2,028
Doubtful	–	13	
Total weight	2.2kg	129.0kg	394.0kg

SHOCK METAMORPHIC EVOLUTION PROCESS APPLIED BY SHOCK IMPACT EXPERIMENTS

Yasunori MIURA, MAsashi IMAI and Toshio KATO
Fuculty of Science, Yamaguchi University, Yoshida, Yamaguchi 753, Japan.

It has been considered that quartz minerals and decrease of anorthite-content can be formed by magmatic crystallization of the Earth or Earth-type planets under high temperature condition of the magma. However, if similar high-temperature can be obtained at impact processes, silica minerals and An-poor plagioclase phase will be formed even under impact condition [1,2,3,4]. The purpose of the present study is to explain the formation of silica and plagioclase phases on meteorite parent body, primordial lunar and Earth-type planetary bodies by shock metamorphism (i.e. shock metamorphic evolution).

1. Silica phases by impact experiments

The various silica minerals can be obtained in the artificial impact crater experiments of various type target rocks.

Fine-grained shocked quartz aggregates crystallized from vaporization of feldspar compositions shows are shown by the increased abundance of shocked quartz (SQ) and feldspar(F) at the "fine ejecta"; that is, SQ/F=3.0 and 5.6 in the granite and gabbroic anorthosite, respectively [3] (cf. Fig.1). This type of shock metamorphism is the largest shock wave under solid-melt-vapour reaction (cf. Table 1).

Impact effects of density change and shocked quartz formation (SQ/F) show larger in fine-grained target rock of gabbroic anorthosite than hard coarse-grained target rock of granite.

Shocked stishovite and coesite crystals could not observed in small space of laboratory experiments.

The highest density of shocked quartz crystal (SQ) in fine-grained ejecta can be obtained in quartz-rich target-rock of sandstone, which is the same implication to the Barringer impact crater with sanstone [1,3].

2. Compositional change of plagioclase by impact experiment

There are two types of shocked (diaplectic) plagioclase (cf. Table 1) [1,2,4]:

1) Chemical compositions of "large coarse-grained fragments" broken by impact processes reveal partly anomalous diaplectic feldspar grains with irregularly wavy extinction and nonstoichiometric composition. The similar anomalous composition of plagioclase can be found at wall rocks of artificial and natural impact craters. This type of diaplectic plagioclase shows small change of composition and atomic arrangement within solid-solid reaction by shock wave.

2) "Fine-grained plagioclase(-like)" composition found in ejecta of artificial impact crater experiments reveals decrease of An-content and mixture of projectile. For example, plagioclase from Kohyama gabbroic anorthosite (bytownite-labradorite) changes to albite (i.e. decrease of An_{40} mol.%). There are various mixture phases between plagioclase and projectile element (i.e. Fe). The type of diaplectic plagioclase shows intermediate degree of shock wave (i.e. reaction under melt condition).

Table 1. Various types of shock metamorphism in silica-plagioclase-projectile aggregates.

Target rock, plagioclase	Shocked materials	Reaction	Shock wave
1) **Gabbroic anorthosite**			
Labradorite-bytownite	a) Shocked quartz A.	Solid-vapour	The largest
	b) Albite	Melt	Intermediate
	Andesine+Fe	Melt	Intermediate
	c) Nonstoichiometric labradorite	Solid-solid	Smaller
2) **Granite**			
Albite (quartz)	a) Shocked quartz A.	Solid-vapour	The largest
	b) Albite+Fe	Melt	Intermediate
	Projectile mixture	Melt	Intermediate
	c) Nonstoichiometric albite	Solid-solid	Small
3) **Sandstone**			
Quartz	a) Shocked quartz A.	Solid-vapour	The largest

3. Evidence of shocked material by shock metamorphism

The shocked materials formed by larger shock metamorphism can be found in shocked quartz agrregates and projectile mixture, as follows:

1) Analytical data of SEM with EDX indicate that shocked quartz formed by the largest shock wave shows fine-grained aggregate of silica composition (about 10 μm) with large parts of amorphous state (cf. Fig.1).

2) Projectile of Fe (mainly in steel) and Cu (mainly in plastic) has been melted to produce mixtures of Cu/Fe and plagioclase, and various types of droplets and mantle-core structure (cf. Fig.2).

4. Shock metamorphic evolution of planetary materials

By using the experimental results of shock metamorphism [4], plagioclase minerals of anorthositic rock formed by magmatic ocean processes on the primordial planetary and lunar surfaces, can be changed to shocked silica minerals, An-poor plagioclase, diaplectic plagioclase (with mixture of iron elements) by impact shock effects, resulting in the formation of shocked quartz (SQ) by rapid crystallization. The SQ phases formed by impact can be changed to normal quartz (Q) by magmatic evolution process under high temperature, as shown in Table 2. The present results of shock metamorphic evolution will be applied to lunar impactand recrystallized rocks (cf. KREEPy lunar rocks with feldspar and quartz aggregates) [2,4].

Table 2. Shock metamorphic evolution on primordial and evolved surfaces of Earth-type planets and the Moon.

Feldspar (F) → (shock waves) →
- a) → (vaporization; rapid depression) → Shocked quartz (SQ)
- b) → (melt condition) → An-poor plagioclase (+Fe)*
- c) → (solid-solid reaction) → diaplectic plagioclase*

Quartz (Q) → (shock waves) → High-pressure type silica
- a) → (rapid depression) → Shocked quartz (high density)
- b) → (rapid cooling) → Cristobalite/Tridymite
- → (transformation) → Quartz (normal)

* Maskelynite (found in the meteorites).
The similar phases can be found in lunar rocks, and wall rocks of terrestrial and artificial impact craters.

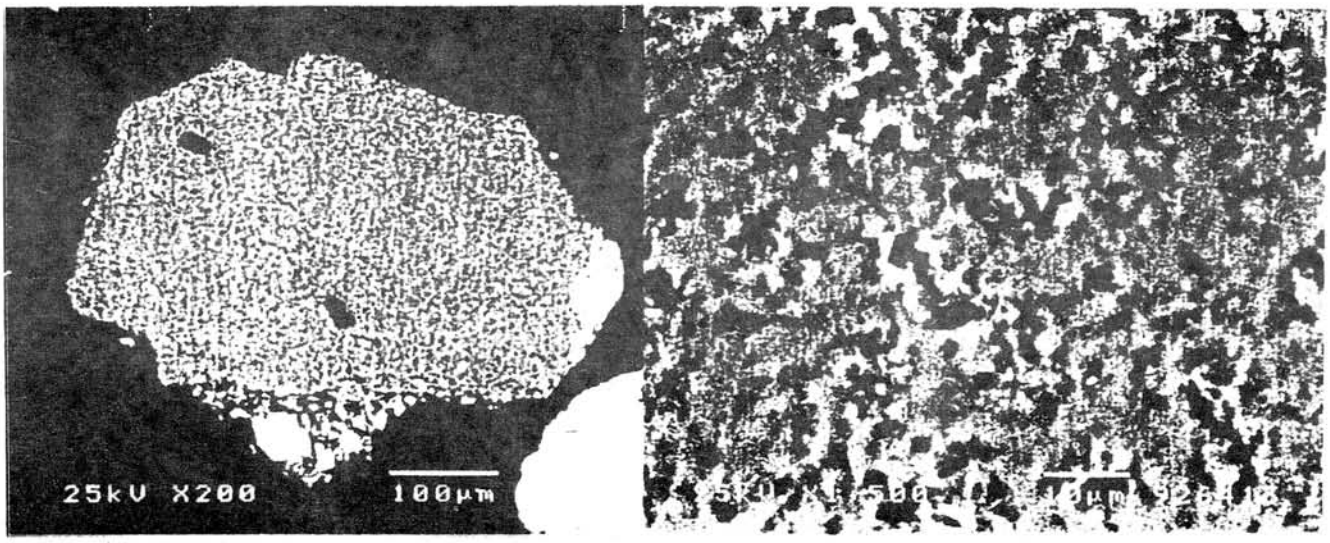

Fig.1. Fine-grained quartz silica aggregates with 10 μm in width and large parts of X-ray amorphous state found in ejecta from gabbroic anorthosite. BEI image.

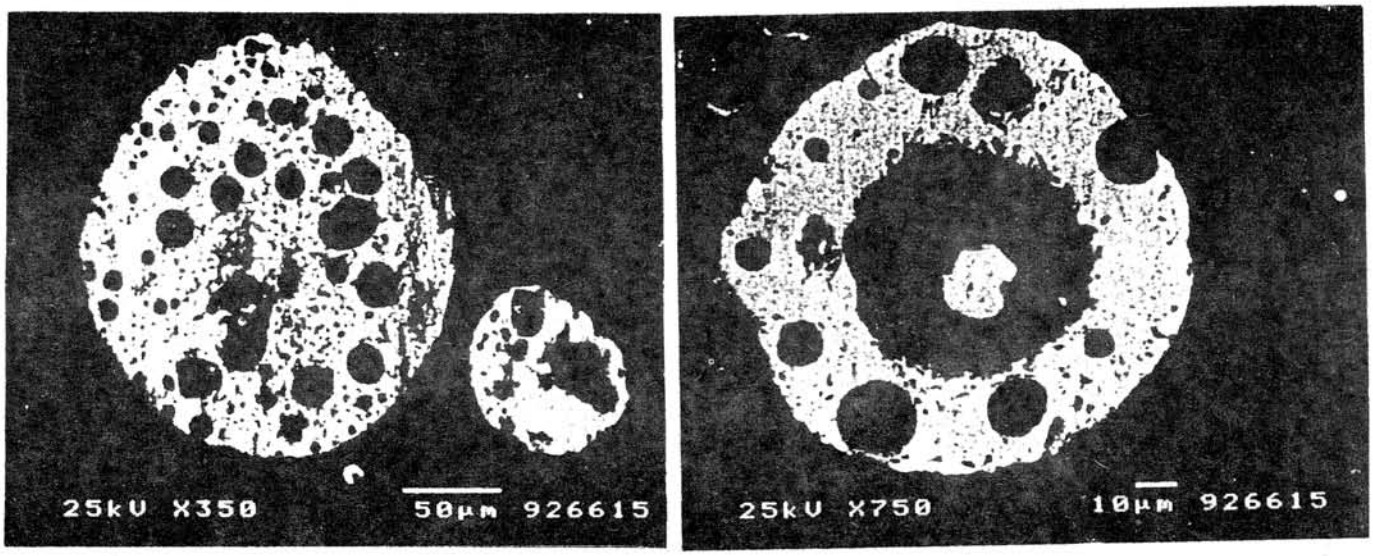

(a) (b)

Fig.2. Evidence of melt reaction of shock metamorphism. Various types of droplets (a) and mantle-core structure (b) can be observed in fine ejecta of granitic target rocks of plastic-Cu/Fe projectile.

Main references

[1] Miura Y. (1991): Shock Waves (Springer-Verlag), 1, 35-41.
[2] Miura Y., Kato T., Kawashima N., Yamori A. and Imai M. (1991): Lunar and Planet Sci. (ISAS, Tokyo), 24, 46-52.
[3] Miura Y., Takayama K. Kato T., Kawashima N. and Yamori A. (1992): Proc. 18th Intern. Sympo. Shock Wave (Springer-Verlag). 7 pp. (in press).
[4] Miura Y. and Kato T. (1992): Celestial Mechanics (July issue), 4 pp. (in press).

MICROMINERALOGICAL STUDIES ON THE SEVERELY SHOCKED YANZHUANG H6 CHONDRITE

XIE Xiande, CHEN Ming (Institute of Geochemistry, Academia Sinica, Guangzhou Branch, Guangzhou, 510640, China)

Yanzhuang (H_6) is a new meteorite fall in China (October 31, 1990)[1]. It is a partly shock-melted chondrite and consists of severely deformed chondritic mass and black veins of molten materials. The shock effects in Yanzhuang have been studied by transmission electron microscopy (TEM), energy dispersive X-ray microanalysis (EDX), Raman microprobe spectra (RMS) and X-ray diffraction analysis (XRD). Here, we report some results on micromineralogical features of silicates.

RESULTS:

(1) Pyroxene

Most of pyroxenes in chondritic mass are bronzite, in which many exsolution lamellae of Ca-rich pyroxene can be found. The shock effects of pyroxenes include:

Dislocation: Dislocations have three kinds of stretching direction -- parallel to (100) plane, parallel to (110) plane, and network dislocation.

Mosaic block: Mosaic blocks of pyroxene can easily be seen due to the result of intersection of fractures and dislocations.

Mechanical twins: The twins usually coexist with the dislocations in fixed direction.

Brreciation: Brrecia belts in pyroxenes are composed of small crystals (<0.001 -- 1 μm in size). The belts have a width of 1--5 μm and stretch in no fixed direction of crystals (Photo 1).

Amorphous mass: Parts of pyroxenes had been transformed into amorphous mass. Usually, the amorphous mass keeps pyroxene pseudomorph, and consists of some sub-round and irregular grains(0.1--0.001 μm in size) (Photo 2).

Thetomorphic and melt glasses: Thetomorphic glass is associated together with high density dislocation areas. Then, melt glass often located in the brrecia belts and amorphous areas of pyroxenes.

Recrystallization: XRD analyses show the pyroxenes in and near the black veins mostly have clino-structure. EDX analyses reveal the composition of the pyroxenes is still same to that of bronzite. TEM studies indicate the clinopyroxenes consist of high density lamellar crystals (twins). These lamellae were possibly produced from martensite transform due to the fast cooling after shock.

Photo 1 TEM images showing the brrecia belts in pyroxene, Bright Field (BF)

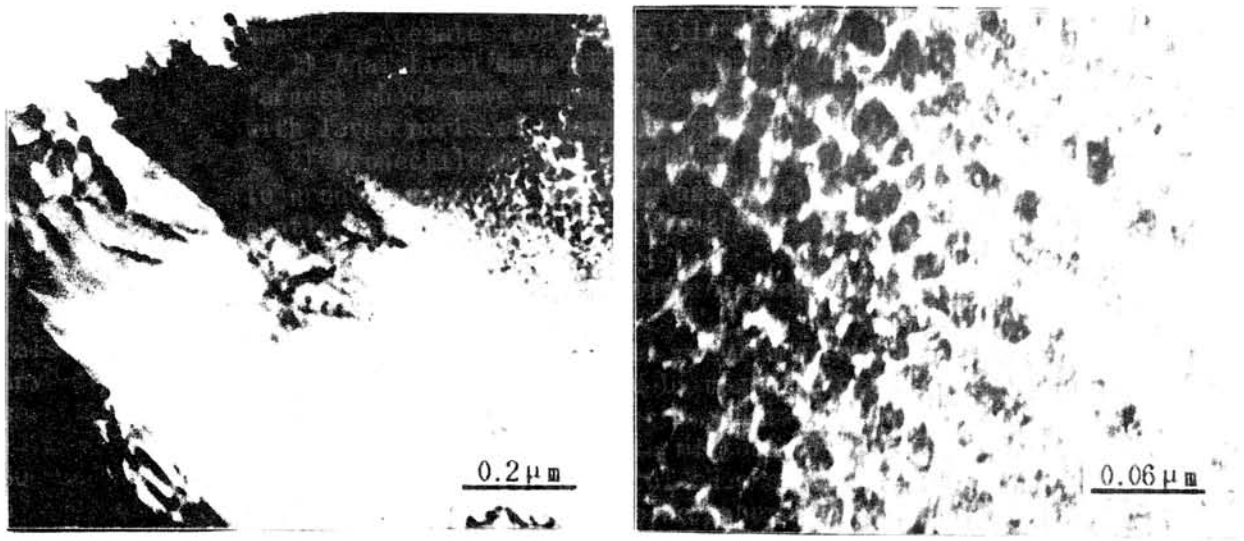

Photo 2 TEM images showing the amorphous mass in pyroxene, BF

(2) Olivine

Olivines have also undergone extensive changes in microstructure.

Dislocation: The predominant dislocation lines in olivine are along [001]. The others include ring dislocation and network dislocation, which are produced from dislocation climbing in higher temperature.

Mosaic blocks and subgrain structure: The formation of mosaic blocks and subgrain structure is due to the intersection of several sets of dislocations and fractures. Dislocation climbing had promoted their development.

Thetomorphic glass: Thetomorphic glass is found in the areas with high density dislocations. RMS analyses show that the glass is clearly identified by the intense band near 1100 cm^{-1} [2] (Fig.1).

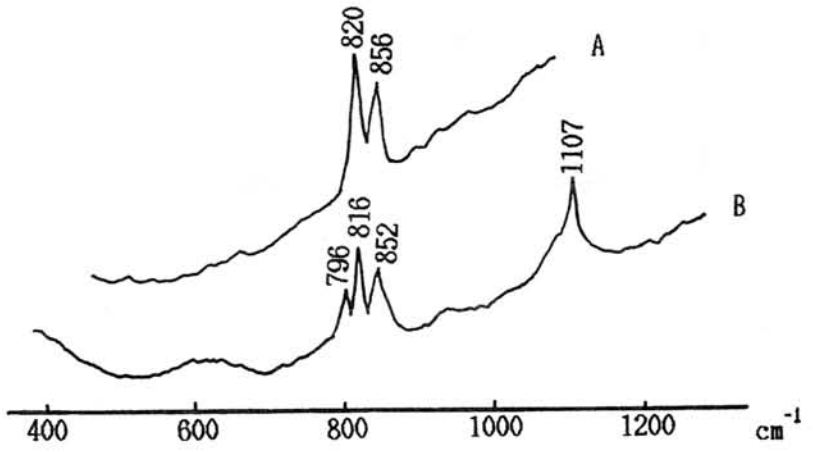

Fig.1 Raman spectra of olivine and ringwoodite
A. Olivine B. Ringwoodite + Olivine

High-pressure phase: RMS analyses for the "olivine" with isotrope or low birefringence reveal the existence of ringwoodite. In Raman spectra, ringwoodite is identified by the intense band at 796 cm^{-1} [3]. Fig.1 shows the coexisting of olivine and ringwoodite in a crystal. The revealed antiphase and twin boundaries in crystal are due to the inversion of γ-spinel to β modified spinel[4] (Photo 3).

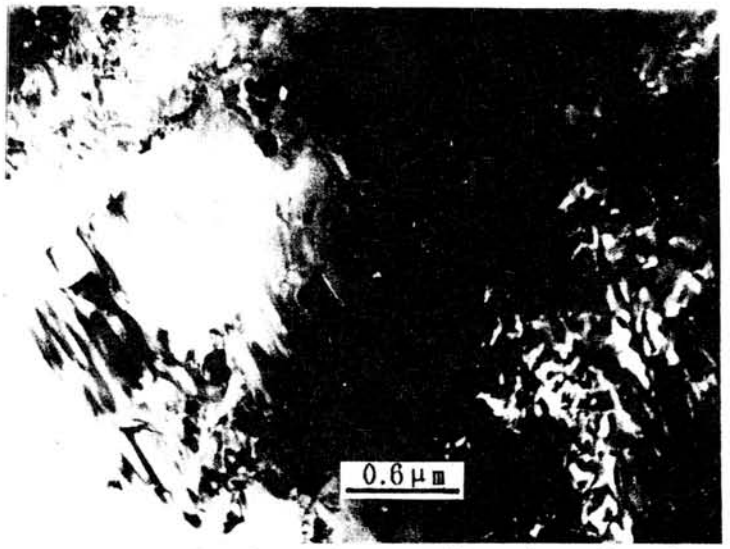

Photo 3 TEM image showing ringwoodite microstructure, BF

Melt glass: The melt glass mainly locate in some edges of olivine. The occurrence of the melt glass reflect the critical environment -- shock induced high temperature and fast cooling.

Recrystallization: Recrystallization of olivine is very wide-spread in Yanzhuang. Three cases are observed: one is the recovery from shock-metamorphised crystal by healing of dislocations and fractures, back transformation of high pressure phase; second is crystallization from thetomorphic and melt glass; third is crystallization from silicate melt (molten chondritic mass), in which some dendritic and euhedral crystals have formed (Photo 4).

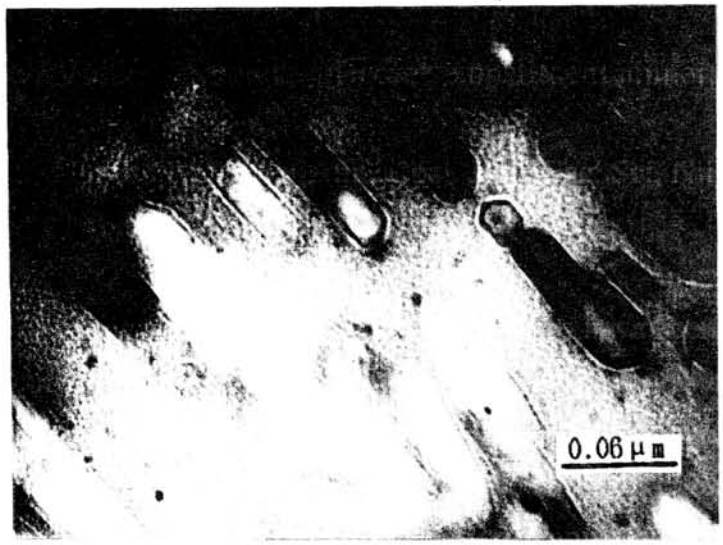

Photo 4 TEM image showing dendritic and euhedral crystals of olivine, BF

(3) Plagioclase

Most of plagioclases in chondritic mass have been transformed into maskelynite.

CONCLUSIONS:

(1) The disequilibrium shock effect effects of minerals in Yanzhuang can be summarized as follows:

Pyroxene: Dislocations -- Mosaic blocks -- Mechanical twins -- Brrecciation -- Amorphous mass -- Thetomorphic glass -- Melt glass -- Recrystallization -- martensite transformation

Olivine: Linear, ring and network dislocations -- Mosaic blocks and subgrain structures -- Thetomorphic glass -- High pressure phase (ringwoodite) -- Melt glass -- Recrystallization

Plagioclase: Maskelynite

(2) The shock effects of minerals reflect two important physico-chemical conditions of Yanzhuang after the impact -- high temperature and fast cooling. This made some shock-induced microstructures either to be dimmed, or remained, and even intensified.

(3) Since the strongly shocked H chondrites are rare, Yanzhuang, the most heavily shocked H chondrite ever found, is a good sample for study. The shock peak pressure acted on Yanzhuang is estimated as >100 GPa and the residual peak temperature >2000^{0}C.

REFERENCES: [1] XIE Xiande et al. (1991) Abstract 54th. Annual Meeting Meteorite Soc. p254; [2] Heymann D. et al. (1988) Meteoritics 23 353--357; [3] McMillan P. et al. (1987) Am. Mineral. 72 261--364; [4] Putnis A. et al. (1979) Nature 280 217--218

Voids structure in some constituent minerals in Antarctic carbonaceous chondrites

Junji Akai : Departm. Geol. Min. Fac. Sci. Niigata Univ. Ikarashi 2-nocho, Niigata 950-21

Many unique carbonaceous chondrites have been found from Antactica : some have unique petrographic features(Tomeoka et al. 1989a,b; Zolensky at al.,1989; Ikeda,1991) or some have experienced thermal metamorphism (Akai,1984, 1988) which have not been found from non-Antarctic carbonaceous chondrites. Evidences for thermal metamorphism have been found in Yamato (Y)-793321, Y-86720, Y- 82162 and Belgica (B)-7904. Their heating degrees were also estimated using T-T-T diagrams experimentally obtained (Akai,1992).

Examining these specimens by High Resolution Transmission Electron Microscopy (HRTEM) and Analytical Electron Microscopy (AEM), some characteristic textures were found in the constituent minerals of some of these specimens; Voids structures were found and are described here.

Spercimens and Experimental : Antarctic carbonaceous chondrites, B-7904, Y-86720, Y-82162 and Y-793321 were used. Ion-thinned specimens previously prepared were again examined by HRTEM and AEM . Experimental procedures are the same as those in Akai (1990 ,1992).

Results and Discussions : Examining the Antarctic carbonaecous chondrites voids structures were sometimes found . Abundant voids structures were characteristic in constituent minerals in B-7904. However, the voids structures are not found in all the constituent minerals but in some restricted mineral species. The constituent minerals with voids structures were usually olivine grains. Fig. 1 shows some characteristic voids structures in olivine found.

Fig. 1a,b shows EM images of olivine in B-7904 matrix. Frequent and characteristic voids structures are found in the figure. their shapes are crystallographically controled. Fig.1c shows another voids structure in B-7904, which indicates a little irregular type of voids structures. Fig.2 is an EM image of constituent minerals in Y-86720. In Y-82162 ,the voids are not always clear (Fig.3).

Voids structures are widely found in these three Antarctic carbonaceous chondrites. However the origin of these voids cannot yet be definitely determined but the following possibilities , in general, can be suggested:

1) fine textures related to acceptor & donor region structure in thermal metamorphism
2) structures produced by irradiation
3) structure formed by shock effects
4) artifacts in specimen preparation
5) reaction texture in alteration process which might have occurred in the earlier stage

Possibility 4 can be denied because only some characteristic specimen has this typical texture although the same preparation method of ion-eching is used for every specimen. Possibility 3 of textures by shock effect can be considered to be small because textural characteristic is a little different form those by shock effects and no other shock evidence is found. Possibility 5 may also be very small because textural features are different and no alteration products are present in adjascent position of the mineral .

The most probable cause of this texture may be related to heating events because these meteorites suffered thermal metamorphism of some degree. The voids structures are not found in all the mineral grains but often in olivine grains,and this fact is consistent with the supposed thermal metamorphic origin.

However, the textural characteristic is also very similar to the fine textures found in metal specimens irradiated by high energy particles (eg. Ohnuki et al.,1986 ; Kodama et al.,1988). The other small possibility of the texture is 2 (by some irradiation damage or some similar origin) . It cannot be denied completely.

The possibility of heating origin has already been discussed (Akai, 1992) and some of the voids structures found may be explained by this origin . In this case, such voids structures may correspond to some spcific degree of thermal metamorphism. This may be typically the degree of metamorphism in B-7904 , which has the strongest degree of metamorphism among the four carbonaceous chondrites. Specimen with the second strongest degree of heating is Y-86720. The degrees well correspond to the character of the voids structures. Trsansformation process was also discussed using schematic figures (Akai, 1992) ,and it is estimated that donor and acceptor region structure model may be related to this voids structures. Many of the voids structures origin may be related to this process.

However, the strong similarity of the textures between these voids structures and voids produced by irradiations (eg. Kodama et al.,1988) forces the possibility of irradiation origin not to be denied completely. Natural irradiation damage by high energy particles may not be ignored in the early solar system or pre solar nubula stages. This process may

also be related to the cause of heating. In this case, the formation process of this voids structure might have occurred separately i.e. in isolated place ; not in parent body, because only restricted minerals have the voids structures.

Similar textures have not been found in artificially heated spcimens of serpentine or saponite hitherto; but experimental heating duration is very short and this may be different from natural process .

To ascertain these problems , more detailed examinations are necessay.

References

Akai,J.(1984) Paper to 9th Symp.Ant.Meteo.Natl.Inst.Polar Res.,59 ;
----- (1988) GCA,52,1593. ; ---- (1990) Proc.NIPR Symp.Ant.Meteo.,3,55.;
----- (1992) ibid (in print) ; Ikeda,Y. (1991) Proc.NIPR Ant.Meteo.,4,461.;
Tomeoka,K. et al.(1989a) Proc.NIPR Symp.Ant.Meteo.,2,36.; ----- (1989b) ibid 2,55.; Zolensky,M.E. et al.(1989) Pap.to 14th Symp.Ant.Meteo.,Natl.Inst.Polar Res.,24.

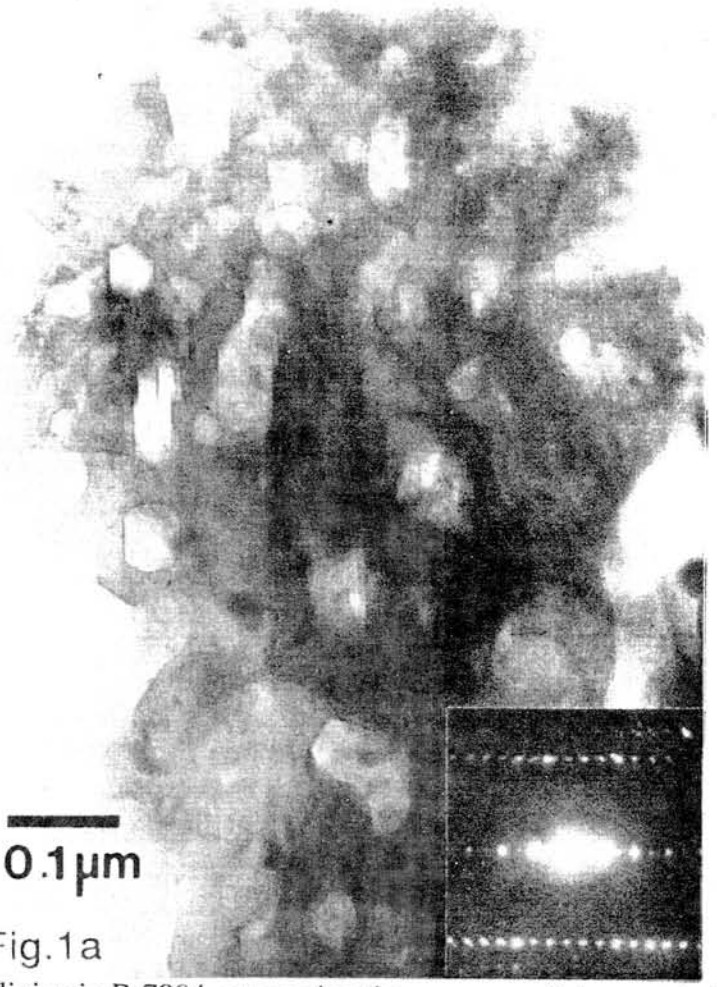

Fig.1a

Fig.1a EM image of olivine in B-7904, suggesting the presence of characteristic voids structures.

Fig.1b Lattice image of the olivine of Fig.1a. The shape is crystallographically controled and characteristic lattice defects are found.

Fig.1c EM image of another olivine grain in B-7904. Voids are irregularly contained.

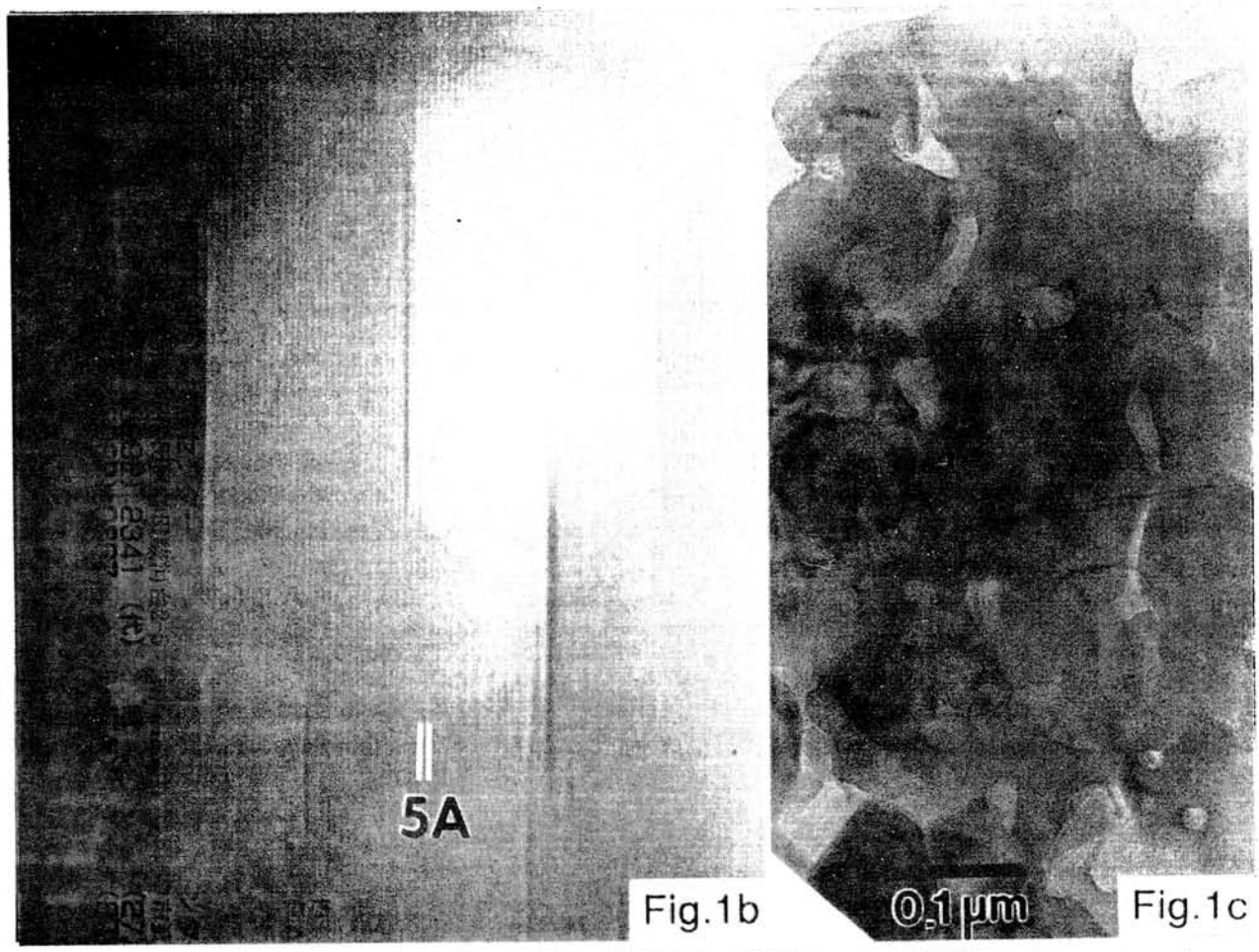

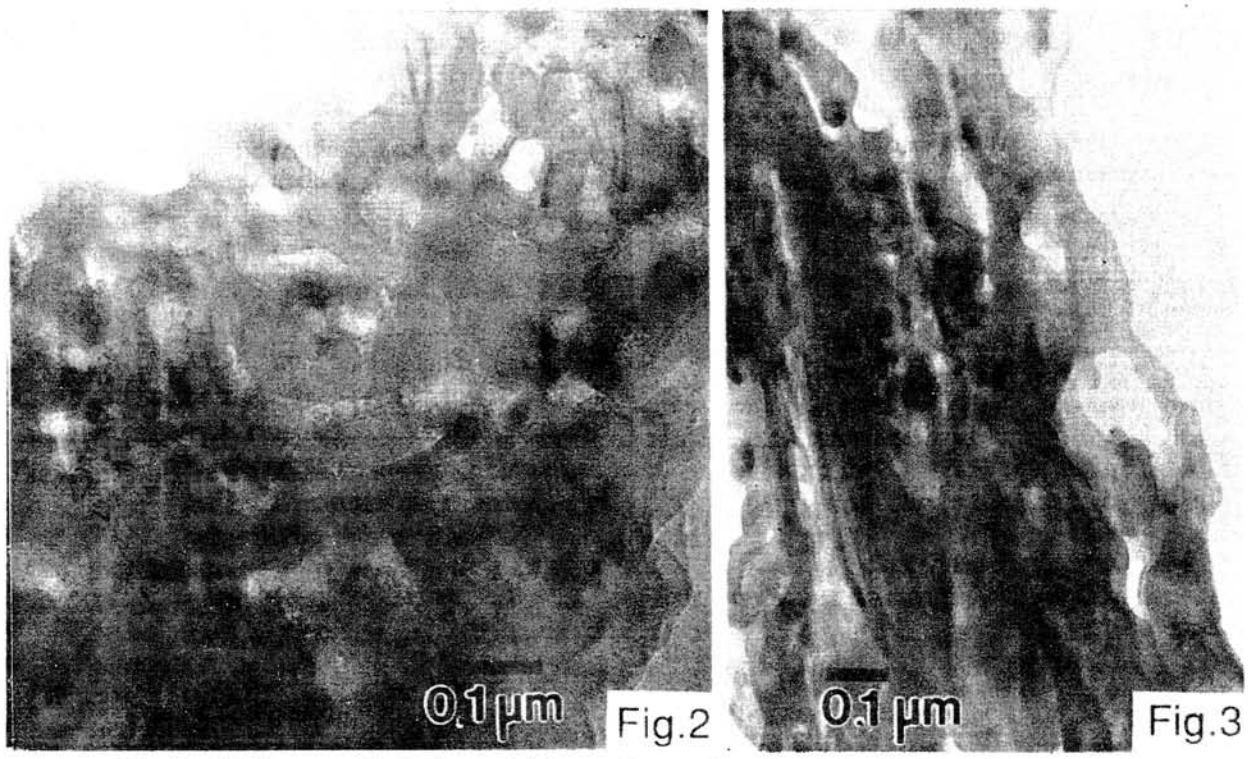

Fig.2 EM image of olivine with irregular voids structures in Y-86720.

Fig.3 EM image of Y-82162 matrix. Small voids are rarely found.

A MÖSSBAUER STUDY OF TWO THERMAL METAMORPHOSED CARBONACEOUS CHONDRITES: YAMATO-82162 AND YAMATO-86720

R. B. Scorzelli, E. Galvao da Silva* and I. Souza Azevedo. Centro Brasileiro de Pesquisas Fisicas - R. Xavier Sigaud, 150 -22290 Rio de Janeiro, Brazil * Departamento de Fisica - Universidade Federal de Minas Gerais - 31270 Belo Horizonte - Brazil

INTRODUCTION The oxygen isotopic characteristics of the Antarctic carbonaceous chondrites Yamato-82162 (Y-82162) and Yamato-86720 (Y-86720) are CI-like [1] but their details of mineralogy and chemistry are different from those of non-Antarctic CI or CM chondrites.TEM and SEM studies [2] showed that the phylosilicate matrix in both chondrites is probably serpentine and saponite. They exibit evidences that these phylosilicates were thermally metamorphosed before their entry to the Earth. Serpentine was almost entirely transformed in olivine or in an intermediate phase during transformation from serpentine to olivine.

The Y-82162 chondrite seems to represent an unique pre-metamorphic material different from Y-86720, exhibiting many mineralogical features suggesting that it has an unique formation history compared to other CI chondrites [3]. In particular, it seems to have largely escaped the late aqueous alteration stage that affected other chondrites.

The results of petrographic, SEM and TEM studies [3] of Y-86720 indicate that it is petrographically closer to CM than to CI chondrites. However it shows many mineralogical and chemical features distinct from the known CM chondrites. The mineralogy and textures suggest that this meteorite probably has experienced more extensive aqueous alteration than any other CM chondrite, and also considerable thermal metamorphism after the aqueous alteration.The mineralogical comparison shows that the degree of thermal metamorphism is higher in Y-86720 than in Y-82162.

In this paper we present the results of ^{57}Fe Mössbauer spectroscopy studies. This is a very useful technique for the identification of the Fe compounds, their magnetic state, ionicity of the iron atom, and relative amount of each phase in meteorites. It can also be used for the study of the local environment around the iron atom, which can be correlated with the thermal and metamorphic history of the meteorites.

EXPERIMENTAL The samples of the meteorites were ground into a powder and Mössbauer absorbers were prepared in a plexi-glass sample holder. Transmission Mössbauer spectra were taken using a ^{57}Co/Rh source through the temperature range 4.2K<T<300K.

RESULTS AND DISCUSSION A) Figure 1 shows the Mössbauer spectra (MS) of Y-82162 at room temperature (RT) and 4.2 K. The spectrum at RT indicates mainly the presence of a magnetically splitted component, due to iron in sulphides and two quadrupole doublets attributed to paramagnetic Fe^{2+} and Fe^{3+} compounds. In addition to that, a second magnetic sextet can be observed in very low proportion (5%). By lowering the temperature, a drastic transition is observed at 4.2 K. The best fitting was obtained

considering, in addition to the phases previously identified, a large contribution due to several paramagnetic modified phases which can only be resolved at 4.2 K. The Mössbauer parameters at RT and 4.2 K can be seen in Table I.

B) The results obtained for Y-86720 can also be seen in Figure 1 and Table I. The fitting of the spectra from RT up to 25 K is similar to that of Y-82162. In contrast to the narrow linewidth found for the Y-82162 RT spectrum, that of Y-86720 shows very broad lines for the paramagnetic as well as for the magnetic phases. At 4.2 K a second magnetic phase in small proportion (8%) appears with an internal magnetic field of 250 kOe.

From the relative spectral areas (see Table I) we can see that this phase results from the contribution of an Fe^{2+} compound which could not be yet identified. We have to emphasize the behaviour of the linewidth of the magnetic component with temperature. The lines are very broadened up to 7 K, becoming very sharp at 4.2 K (Γ = 0.42 mm/s). In addition, a large broadening of the Fe^{2+} paramagnetic compounds is observed which is similar to that of Y-82162.

The Mössbauer results indicate in both meteorites the presence of a very well resolved magnetic phase due to iron in troilite. Its relative proportion remains almost constant with temperature and the apparent increase of the outer lines of the spectra (Fig. 1) only reflects the increase of the linewidth of the paramagnetic contribution.

As can be seen in Table I the Mössbauer parameters at RT for the Fe^{2+} component are in accordance with Fe^{2+} in olivines [5]. However in the case of Y-86720, even at RT, we observed a much broad line that indicates the presence of other compounds besides olivine.

The Fe^{3+} doublet in Y-86720 can be attributed to ferryhidrite [2] while in Y-82162 can be due to an overlap of different compounds as Fe and Mg carbonates and Fe-poor magnetite [4].

The magnetic component with an hyperfine field of 250 kOe at RT in Y-82162 seems to be the same as that observed at 4.2 K (which originated from the Fe^{2+} paramagnetic compounds) for the Y-86720 chondrite. If that is the case, the later should be present at temperatures higher than 4.2 K in a superparamagnetic state. The differences observed in the other Mössbauer parameters are due to difficulties in the fitting because of the small contribution from that phase to the spectrum.

The results obtained by Mössbauer spectroscopy and other techniques indicate that the abundance of troilite in these Antarctic CC is unusual as compared with the non-Antarctic ones. From the Mössbauer results we can observe that the linewidths of the magnetic and paramagnetic Fe components are less broadened for Y-82162 than for Y-86720 (see Table I). This may reflect a more homogeneous Fe environment for the phases present in Y-82162, what is compatible with a less metamorphosed material. The relative area of olivine is almost the half in this chondrite as compared with Y-86720 in good agreement with the mineralogical and chemical features above described. The fact that ferryhidrite was not detected in our spectra for Y-82162 can be explained by the lack of the late aqueous alteration in this meteorite. In the case of Y-86720 in which the mineralogy and textures suggest that

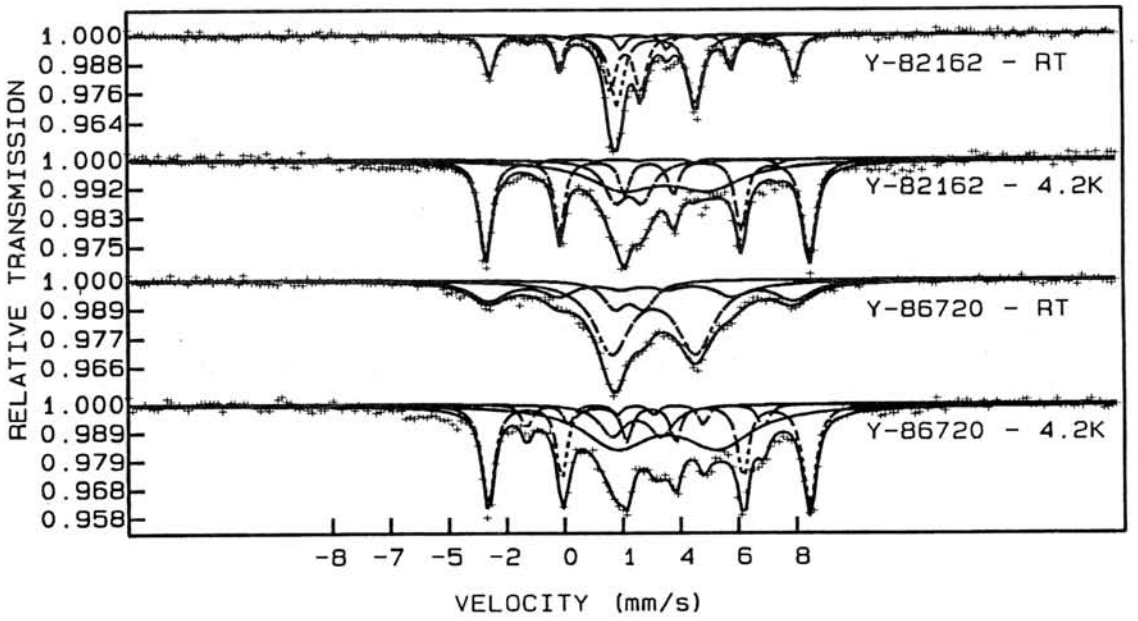

Figure 1 - Mössbauer spectra for the Yamato Y-82162 and Y-86720 meteorites at room temperature and 4.2K.

Temp.(K)		Γ(mm/s) (±0.02)	IS(mm/s) (±0.02)	Δ(mm/s) (±0.02)	HF(kOe) (±3.0)	Area(%)
Sample Y-82162						
RT	Fe^{3+}	0.50	0.17	1.07		26.1
	Fe^{2+}	0.57	1.21	2.68		38.1
	Troilite	0.35	0.73	-0.17	313.1	30.8
		0.35	0.59	0.55	249.7	5.0
4.2K	Fe^{3+}	0.54	0.18	1.06		27.7
	Fe^{2+}	0.23	1.35	2.81		4.5
	Fe^{2+}	1.45	1.81	2.23		31.5
	Troilite	0.25	0.88	-0.17	329.2	31.8
		0.30	0.97	0.59	265.4	4.5
Sample Y-86720						
RT	Fe^{3+}	0.93	0.29	1.01		13.2
	Fe^{2+}	1.45	1.12	2.86		57.2
	Troilite	1.25	0.71	-0.18	315.3	29.6
4.2K	Fe^{3+}	1.02	0.46	1.70		12.2
	Fe^{2+}	2.76	1.49	3.49		43.2
	Troilite	0.42	0.86	-0.18	331.3	36.4
		0.35	0.56	0.28	248.7	8.2

Table I - Mössbauer parameters for the Yamato Y-82162 and Y-86720 meteorites at room temperature and 4.2K. Γ is the linewidth at half height, IS is the isomer shift relative to α-Fe, Δ is the quadrupole splitting, HF is the internal hyperfine magnetic field, and Area is the relative spectral area. The line intensity ratios I_2/I_1 and I_3/I_1 were fixed during the fitting to 0.66 and 0.33, respectively.

this meteorite has experienced more extensive aqueous alteration and considerable thermal metamorphism, the Mössbauer parameters suggest the presence of an Fe^{3+} doublet that can be attributed to ferryhidrite.
In conclusion, we can say that the present Mössbauer results show clearly the iron compounds present in both chondrites and these results are in accordance with the mineralogy, chemical composition and thermal history obtained by other techniques. In special, they agree with the results obtained by TEM and SEM, which show that these CC exhibit mineralogical evidences of thermal metamorphism, that is unknown for non-Antarctic carbonaceous chondrites. Also the degree of thermal metamorphism is higher in Y-86720 than in Y-82162.

ACKNOWLEDGMENTS We thank the National Institute of Polar Research (NIPR) for providing the meteorite samples.

REFERENCES 1 - T.K.Mayeda, R.N.Clayton and K.Yanai, Mem. Natl. Inst. Polar Res. Spec. Issue, 46, 144-150 (1987). 2 - Junji Akai, Proc. NIPR Symp. Antarct. Meteorites 3, 55-68 (1990). 3 - K. Tomeoka, H.Kojima and K.Yanai, Natl. Inst. Polar Research, 130-131 (1988) and Proc. Symp. Antarct. Meteorites 2, 55-74 (1989). 4 - K.Tomeoka, H.Kojima and K. Yanai, Proc. NIPR Symp. Antarct. Meteorites 2, 36-54 (1989). 5 - G.M.Bancroft, A. G. Maddock and R.G.Burns, Geochim. Cosmochim. Acta 31, 2219 (1967).

Metamorphosed carbonaceous chondrites, Y-82104 and Y-82002: Mineralogy and petrology

Tomoki Nakamura, Kazushige Tomeoka* and Hiroshi Takeda

Mineralogical Institute, Faculty of Science, University of Tokyo, Hongo, Tokyo 113 .

* Department of Earth Sciences, Faculty of Science, Kobe University, Nada, Kobe 657.

Introduction

Carbonaceous chondrites are believed to be the most pristine materials and have not been affected by significant metamorphism. However, in the process of parent body evolution, they are expected to have experienced increasing degrees of thermal metamorphism. We here present the results of our petrographic and scanning electron microscope studies of two metamorphosed carbonaceous chondrites from Antarctica, Yamato-82002 and Yamato-82104, which are classified as C5 [1]. Details of mineralogy and petrology of Antarctic metamorphosed carbonaceous chondrites are poorly known except for Yamato-693 [2].

Results

Y-82104 and Y-82002 have similar overall textures; both contain chondrules and mineral fragments of various sizes embedded in recrystallized matrix. Some chondrules are difficult to define, because they are fragmented and grade into matrix. Recognizable chondrules have diameters of typically 0.3~0.8 mm in Y-82104 and 0.2~0.5 mm in Y-82002; but in each chondrite specimen, we found one exceptionally large chondrule, ~ 2 mm in Y-82104 and ~ 3 mm in Y-82002. The matrix of Y-82104 has higher proportions of opaque phases than that of Y-82002. In both meteorites, olivines in matrix commonly exhibit strong wavy extinction, whereas those in chondrules show none or weak wavy extinction.

Y-82104: Most chondrules are porphyritic olivine type and commonly contain aggregates of magnetite, pentlandite and pyrrhotite. Matrix consists of relatively coarsely recrystallized olivine (typically >50 μm in diameter), magnetite, pentlandite, pyrrhotite, and an Al,Si,Ca-rich phase. The Al,Si,Ca-rich phase may be an alteration product formed by terrestrial weathering of plagioclase and mesostasis glass; low analytical totals of the Al,Si,Ca-rich phase (40 ~ 60 wt%) suggest that it is hydrated. Olivine and the Al,Si,Ca-rich phase are commonly intermixed with magnetite. Most magnetites contain minor amounts of Cr (< 4 wt% Cr_2O_3). Large magnetite grains commonly contain ilmenite exsolution lamellae which are 3 ~ 5 μm wide and 10 ~ 100 μm long. Apatite and chlorapatite (5 ~ 30 μm in diameter) also occur in minor amounts. Olivines in chondrules and matrix have very similar, homogeneous compositions; mean value is Fa 29.5 with 1δ value of Fa 0.53 for chondrules and Fa 29.1 with 1δ value of Fa 0.41 for matrix. Low-Ca pyroxene occurs in lesser amounts: it is also compositionally very homogenized; mean value is Fs 25.2 with 1δ value of Fs 1.86.

Y-82002: Chondrules are also mostly porphyritic olivine type; barred olivine

chondrules occur but are rare. Constituents of matrix are similar to those in Y-82104, but olivine grains are smaller (10 ~ 50 μm in diameter). Marked differences are seen in opaque mineralogy. Magnetite is absent in Y-82002, and the most abundant opaque phase is troilite. A minor amount of pentlandite also occurs. An Fe-rich phase, presumably Fe hydroxide, forms network-like veins within the sulfides; they appear to have formed by terrestrial weathering. In some places of the matrix, subhedral to euhedral chromite grains occur. Olivines in both chondrules and matrix have much higher Fe concentrations and less homogenized compositions than those in Y-82104, and unlike Y-82104, Fe concentrations differ considerably between olivines in chondrules and those in matrix; mean value is Fa 35.1 with 1δ value of Fa 5.11 for chondrules, and Fa 37.3 with 1δ value of Fa 2.39 for matrix. Low-Ca pyroxenes show a much broader range of compositions(Fs 10.5 ~ 29.7) than those in Y-82104.

Conclusions

(1) Olivines and low-Ca pyroxenes in Y-82104 are compositionally more homogenized than those in any other metamorphosed carbonaceous chondrites; thus this meteorite is probably one of the most highly metamorphosed and equilibrated carbonaceous chondrites known. (2) In contrast, olivines and low-Ca pyroxenes in Y-82002 have broader ranges of compositions, comparable to the Carlisle Lakes C4 chondrite [3]. In Y-82002, olivines in matrix show a smaller standard deviation than olivines in chondrules, suggesting that the matrix became equilibrated faster than chondrules; the same tendency is reported from other metamorphosed carbonaceous chondrites [3]. (3) The ilmenite lamellae within magnetite grains in Y-82104 are common in CK chondrites [4], suggesting that Y-82104 may be similar to the CK chondrites. High abundance of Cr-bearing magnetite and lack of Fe-Ni metal in Y-82104 support this view [5]. (4) Y-82002 contains no magnetite but abundant sulfides (troilite and pentlandite), which differ from Y-82104 and other metamorphosed carbonaceous chondrites. This suggests that Y-82002 has been metamorphosed in a more reduced condition than other metamorphosed carbonaceous chondrites.

References

[1] Yanai K and Kojima H. (1987) Photo. Catalog of the Antarctic Meteorites, 298p.

[2] Scott R. D. and Tailor G. J. (1985) Petrology of types 4-6 carbonaceous chondrites. Jour. Geophys. Res. 90, 699-799.

[3] Okada A., (1975) Petrological studies of the Yamato meteorites, part 1. Mineralog of the Yamato meteorites, Mem. Natl. Inst. Polar Res., Spec. Issue No.5, edited by T. Nagata, 67-82.

[4] Geiger T. and Bischoff A. (1990) Exsolution of spinels and ilmenite in magnetites from types 4-5 carbonaceous chondrites-Indications for metamorphic processes. Lunar Planet. Sci. 21, 409-410.

[5] Geiger T. and Bischoff A. (1990) The metamorphosed carbonaceous chondrites A new meteorite group? Abstr. 15th Symp. of Antarctic Meteorites, 78-80.

NEPHELINE AND ALBITE IN THE YAMATO-791717 CO CARBONACEOUS CHONDRITE: EVIDENCE FOR NEBULAR ALTERATION

Kazushige Tomeoka[1], **Koji Nomura**[2] and **Hiroshi Takeda**[2]

1 Department of Earth Sciences, Faculty of Science, Kobe University, Nada, Kobe 657; 2 Mineralogical Institute, Faculty of Science, University of Tokyo, Hongo, Tokyo 113

INTRODUCTION

Nepheline occurs in Ca-Al-rich inclusions (CAIs) in some CV [1-3] and CO [4,5] chondrites. Most previous workers suggested that the nepheline is a secondary alteration product formed by reaction of primary phases such as melilite, anorthite and spinel with the solar nebular gas, and their formation temperatures are significantly lower than those of most other secondary phases, probably less than 1000 K [e.g., 6-8]. We found that CAIs in the Yamato-7191717 CO chondrite contain 5 to 80 volume % of nepheline and that some chondrules contain major amounts of albite. Such a large amount of albite has not been previously reported from chondrules and CAIs in carbonaceous chondrites. Our study provides evidence that nepheline and albite were formed by reaction of primary phases with the solar nebula at relatively low temperatures.

RESULTS

Ca-Al-rich inclusions

We observed 54 inclusions within two thin sections; they range in diameter from 30 to 500 μm, but most (>80 % of the inclusions) are <150 μm in diameter. Most inclusions are single concentric objects or aggregates of concentric objects. Nepheline commonly shows irregular contacts with primary phases such as spinel, fassaite, and melilite, suggesting that the nepheline was formed by replacing these phases. For purposes of discussion, we divided these inclusions into three types based on the amounts of nepheline, i.e., lightly altered, moderately altered, and heavily altered types. Lightly altered inclusions are those containing less than ~ 25 vol% nepheline, and heavily altered inclusions are those containing more than ~ 50% nepheline. Out of 54 inclusions, 19 are lightly altered, 16 moderately altered, and 17 heavily altered; the other two inclusions show textures and mineralogy different from other inclusions and thus are not classified into the above types.

Lightly altered inclusions have cores of spinel surrounded by bands of nepheline (replacing fassaite), fassaite, and diopside. In moderately altered inclusions, spinel cores are replaced by nepheline, and fassaite is absent. In heavily altered inclusions, the major part of internal areas (50 to 80 % in volume) are replaced by nepheline. In some moderately and heavily altered inclusions, only diopside rims remain unaltered.

Spinel shows a wide range of Fe/(Mg+Fe) ratios (0.00 to 0.57 in atomic ratio). In lightly altered inclusions, spinel tends to be poorer in Fe than that in moderately and heavily altered inclusions, and commonly exhibits Fe-Mg zoning. In contrast to many CO chondrites, melilite is rare. Only inclusion Y17-21, which is described in the following section, contains abundant melilite in

its core region. Nepheline is commonly fine-grained and intermixed with tiny grains (<2 in diameter) of sodalite, Ca-rich clinopyroxene, and troilite.

A unique, melilite-rich and Fe-free-spinel-rich inclusion

Inclusion Y17-21, which is classified as lightly-altered, is by far the largest (540 x 300 μ m) of all the inclusions studied and shows unique mineralogy and texture. Approximately 40% of the core area is comprised of interlocking melilite and Fe-free spinel, and the outer area consists mostly of porous nepheline, Fe-rich spinel (<42 mol% $FeAl_2O_4$), and perovskite. Along the boundary zone between the core and the outer areas, spinels show Fe-Mg zoning (from 0 to 40 mol% $FeAl_2O_4$). Fe-free spinel and such a large amount of melilite are found only in this inclusion.

The melilite-rich and Fe-free-spinel-rich core area appears to represent some of the primary (unaltered) mineralogy and texture of the inclusions in Y791717. The texture suggests that the whole internal area of Y17-21 was previously composed of melilite and Fe-free spinel, and alteration medium, probably the nebular gas, was introduced from the surroundings and altered melilite and spinel in the outer area into nepheline.

Albite-bearing chondrules

We observed six albite-bearing chondrules; all belong to the porphyritic olivine-rich type. Olivine grains are distinctly Fe rich (Fo_{80}-Fo_{45}) compared to those in other chondrules that contain no albite, and relatively large olivine grains tend to show Fe-Mg zoning. The chondrules commonly contain relatively large grains of Ca-rich clinopyroxene (salite) and Fe-Cr-Al spinel. Albite occurs in mesostasis of the chondrules as relatively large ($\sim$ 20 μ m in diameter), homogeneous grains but commonly forms dendritic intergrowths with Ca-rich clinopyroxene. Albite appears to have formed by replacing mesostasis glass.

CONCLUSIONS

Ca-Al-rich inclusions (CAIs) in the Yamato-791717 CO chondrite contain major but variable amounts of nepheline, along with minor amounts of sodalite, Ca-rich clinopyroxene, and troilite, and thus are among the most nepheline-rich CAIs known. Our observations provide evidence that nepheline formed primarily by alteration of melilite, spinel, and fassaite. The resistance of primary phases increases in the order melilite, fassaite, spinel, diopside. Melilite was probably another major primary phase, but most of it was preferentially consumed to form nepheline; thus, it is rare in this meteorite. Our results support the view that the alteration occurred by reaction with a nebular gas rich in Na, Fe, and Cl at relatively low temperatures (<1000 K) prior to incorporation of the CAIs into the meteorite. The CAIs in Y791717 probably have experienced a much higher degree of low-temperature alteration than those in other reported meteorites. We believe that albite in the chondrules was also formed by reaction with the solar nebula gas in the same environment as for the CAIs. The precursor of albite was a residual glass in the mesostasis, and the silica-rich glass probably favored the formation of albite rather than nepheline.

REFERENCES

[1] Wark, D.A. and Lovering, J.F. (1977) Proc. Lunar Sci. Conf. 8th, 95-112.
[2] MacPherson, G.J. and Grossman, L. (1984) Geochim. Cosmochim. Acta 48, 29-46.
[3] Wark, D.A. (1986) Earth Planet. Sci. Lett. 77, 129-148.
[4] Kurat, G. (1975) Tschermaks Min. Petr. Mitt. 22, 38-78.
[5] Davis, A.M. (1985) Lunar Planet. Sci. XVI, 165-166 (abstract).
[6] MacPherson, G.J., Grossman, L., Allen, J.M. and Beckett, J.R. (1981) Proc. Lunar Planet. Sci. Conf. 12B, 1079-1091.
[7] Wark, D.A. (1981) Lunar Planet. Sci. XII, 1145-1147 (abstract).
[8] Hashimoto, A. and Grossman, L. (1987) Geochim. Cosmochim. Acta 51, 1685-1704.

UNUSUAL CLASTS IN THE VIGARANO CV3 CHONDRITE

Tomoko Kojima[1], Kazushige Tomeoka[2] and Hiroshi Takeda[1]

1) Mineralogical Institute, Faculty of Science, University of Tokyo, Hongo, Tokyo 113

2) Department of Earth Sciences, Faculty of Science, Kobe University, Nada, Kobe 657

INTRODUCTION

Dark lithic clasts are known to occur in CV3 chondrites and are generally called "dark inclusions" [e.g.1-3]. These clasts are of great interest, because they potentially provide information about processes which operated at, or prior to, the time of accretion to the meteorite parent bodies.

During our scanning electron microscope (SEM) observations of the Vigarano CV3 chondrite, we found two unusual clasts that are apparently different from the dark clasts or inclusions previously reported. Their mineralogical and textural features suggest that they may have experienced thermal metamorphism after extensive aqueous alteration.

TEXTURE AND MINERALOGY

The two unusual clasts, CL1 (1.2x1.0mm) and CL2 (0.8x0.6mm), are included in a larger clast (Fig.1). They have essentially identical mineralogy and texture, and CL1 itself is composed of several clasts suggesting that they were derived from the same accretionary rock. Both CL1 and CL2 consist mostly of fine-grained olivine (<1 μm in diameter). Tiny Fe-Ni metal grains (<1 μm in diameter) are dispersed throughout the clasts. No distinct chondrules, CAIs, and mineral fragments are contained. Defocused-electron beam analyses show that they are homogeneous in composition, and that their FeO contents (32-37 wt.%) are apparently lower than that of the host matrix (35-48 wt.%).

CL1 and CL2 are not mere aggregates of uniform fine-grained olivine but show various textures indicative of their previous history as described in the following: 1) Both CL1 and CL2 contain inclusions ranging in diameter from 100 to 300μm that are free of metal grains. In transmitted light, these inclusions exhibit distinctive outlines and have a brownish translucent appearance, resembling aqueously altered chondrules or their fragments. Narrow veins extend from these inclusions to the surrounding matrix. These textures suggest that CL1 and CL2 have been involved in aqueous alteration, although there is little compositional difference between the inclusions and the surrounding matrix, and no typical products of aqueous alteration such as phyllosilicates are present in the clasts. 2) CL1 contains a relatively large aggregate of Fe-Ni metal grains (100x30 μm), and its surrounding portions are distinctly enriched in Fe, Ni, and S, suggesting that this aggregate was originally a mixture of Fe-Ni metal and sulfide and was later affected by alteration.

DISCUSSION

The mineralogy and texture of CL1 and CL2 are clearly distinct from the host Vigarano chondrite and any previously reported dark inclusions. However, they are reminiscent of the anomalous CM chondrites found in Antarctica, Yamato-86720 and Belgica-7904. These meteorites are unusual in that they are petrologically and chemically CM like but are oxygen-isotopically CI like [4-8]. Matrices of Y-86720 and Belgica-7904 consist largely of fine grains of Mg-Fe olivine and Si-Mg-Fe-rich glass which were probably produced by thermal transformation of phyllosilicates [4,5,9,10]. Tomeoka *et al.* [4] and Tomeoka [5] showed that Fe-Ni metal particles are widespread in the matrices of both anomalous Antarctic CM chondrites. These mineralogical and textural similarities suggest that CL1 and CL2 were originally CM like but were affected by intense thermal metamorphism. In order to verify the effects of thermal metamorphism of phyllosilicates, a transmission electron microscope study is now in progress.

ACKNOWLEDGMENT

We thank Dr. G.J. MacPherson, U.S. National Museum, for providing the Vigarano sample.

REFERENCES

[1] Fruland R.M., King E.A. and McKay D.S. (1978) Proc. Lunar Planet. Sci. Conf. 9th, 1305-1329.

[2] Kracher A., Keil K., Kallemeyn G.W., Wasson J.T., Clayton R.N. and Huss G.I. (1985) Proc. Lunar Planet. Sci. Conf. 16th, D123-D135.

[3] Johnson C.A.,Prinz M.,Weisberg M.K., Clayton R.N. and Mayeda T.K. (1989) Geochim. Cosmochim. Acta 54, 819-830.

[4] Tomeoka K., Kojima H. and Yanai K. (1989b) Proc. NIPR Symp. Antarct. Meteorites, 2, 55-74.

[5] Tomeoka K. (1990) Proc. NIPR Symp. Antarct. Meteorites, 3, 40-54.

[6] Kallemeyn G.W. (1988) 13th Symp. Antarct. Meteorites (Abstr.), 132-134.

[7] Clayton R.N. and Mayeda T.K. (1989) Lunar Planet. Sci. XX (Abstr.), 169-170.

[8] Paul R.L. and Lipschutz M.E. (1989) Z. Naturf. A44, 979-987.

[9] Akai J. (1988) Geochim. Cosmochim. Acta 52, 1593-1599.

[10] Akai J. (1990a) Proc. NIPR Symp. Antarct. Meteorites, 3, 55-68.

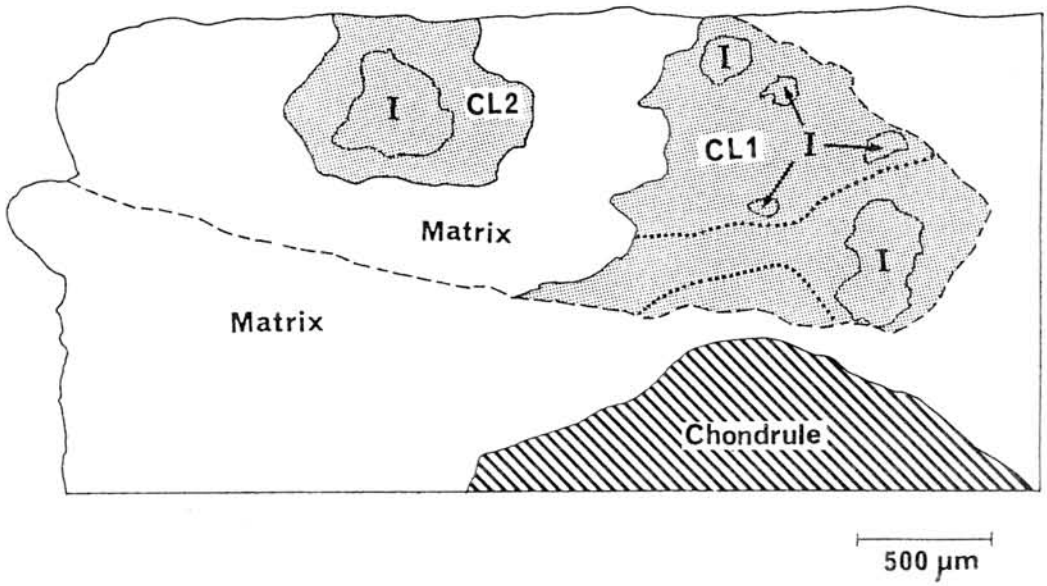

(Fig.1) Illustration of the portion containing CL1 and CL2. These clasts are included in a clast whose boundary is shown by a broken line. Both CL1 and CL2 contain inclusions indicated by (I). CL1 itself consists of several clasts whose boundaries are shown by dotted lines.

CATHODOLUMINESCENCE STUDY OF OLIVINES IN THE ALLENDE METEORITE

Mitsuru FUDAKI and Masao KITAMURA
Department of Geology and Mineralogy, Kyoto University,
Sakyo Kyoto 606, Japan

Relict olivine grains in chondrules, first described by Nagahara [1] and Rambaldi [2], appear as dusty and Fe-rich cores and have been observed in porphyritic chondrules of unequilibrated ordinary chondrites (UOC's) and less commonly in carbonaceous chondrites. Steele [3,4] documented another type of relict crystals of olivine (forsterite with less than 1.0 wt% of FeO), which emit blue cathodoluminescence (CL). This type of the relict grains have been observed commonly in UOC's and carbonaceous chondrites. In the present study, the relict crystals of olivine in chondrules of the Allende meteorite (CV3) were studied by using a newly designed CL microscope with high sensivity and a back-scattered electron imaging (BEI) technique of a scanning electron microscope.

In the Allende meteorite, it was confirmed that there were two types of relict olivines; a dusty and Fe-rich olivine grain in a porphyritic olivine chondrule [5] and Fe-poor olivines which emit blue CL. In the present study, the coexistence of the Fe-rich and Fe-poor relict olivines in a single chondrule was observed (Fig. 1).

A new type of the relict olivine grain which emit CL was also found in a large porphyritic olivine chondrule (Figs. 2 and 3 a & b). As seen in the CL image (Fig. 3b), a part with high CL intensity, brighter in contrast, surrounds a core with low CL intensity, dark in contrast. The core shows a reverse zoning from 2.2 wt% of FeO in its center to 0.6 wt% in its outer part. The brighter part shows a normal zoning from 0.4 wt% of FeO to 2.0 wt%. These zonings indicate that the core is relict. The banding in the CL contrast is clearly observed in the core (Fig. 3c), and considered to be growth zoning because the banding can be expressed by (010), (021) and (001) faces. The faint banding in the CL contrast is also observed in the brighter part, which may also be growth zoning. The growth zoning in the core suggests that the precursor olivine must have crystallized in a euhedral shape and not experienced a long annealing stage which could erase the growth zoning. However, it is not clear whether the crystal have grown from vapor or melt.

As a conclusion, there are three kinds of olivines as precursor of chondrules in the Allende meteorite.

1. FeO-rich (about 20 wt% of FeO) and dusty olivine.
2. FeO-poor (less than 1.0 wt% of FeO) olivine with high CL (blue) intensity.
3. FeO-poor (about 2.0 wt% of FeO) olivine with low CL intensity and the growth zoning.

References:

[1] Nagahara, H. (1981) Nature **292**, 135-136.
[2] Rambaldi, E.R. (1981) Nature **293**, 558-561.
[3] Steele, I.M. (1986a) Amer. Mineral. **71**, 966-970.
[4] Steele, I.M. (1986b) Geochim. Cosmochim. Acta **50**, 1379-1395.
[5] Isobe, H. (1986) Master's thesis of Kyoto Univ.

Fig. 1. BEI of a porphyritic olivine chondrule which includes two types of the relict olivines. Most of large olivine grain show dusty texture and a Fe-poor grain (dark in contrast) in the upper side of the figure emits blue CL.

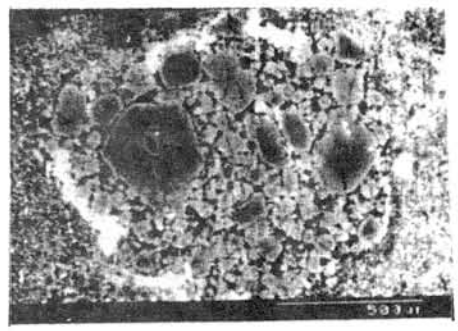

Fig. 2. BEI of a porphyritic olivine chondrule which includes new type of relict olivine crystals.

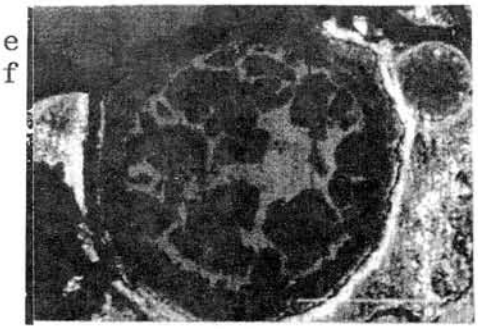

Fig. 3. A new type of relict olivine grain in the chondrule of figure 2. (a) BEI. (b) CL image (emission less than 700 nm was cut by a sharp cut filter). Brighter part surrounds a darker core part. (c) CL image of enlarged core part (emission less than 700 nm was cut by the filter). Growth banding is observed in the core.

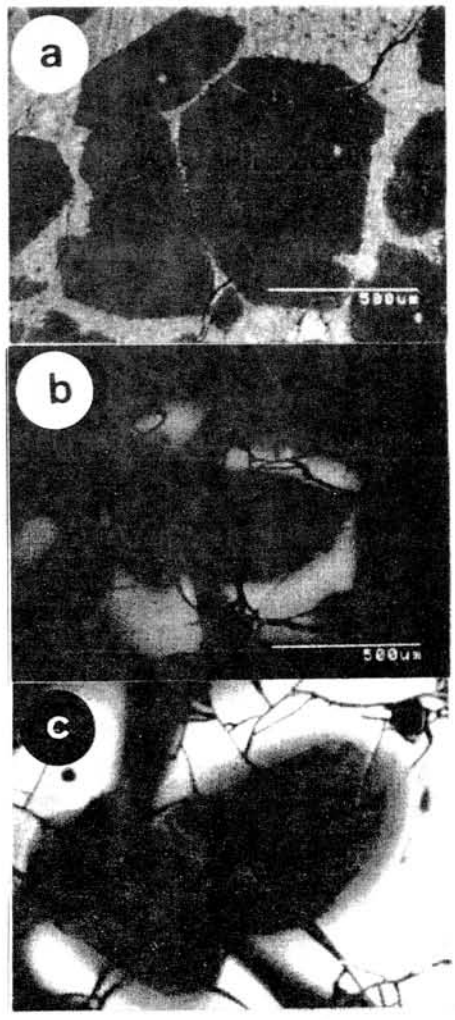

Petrology and Mineralogy of Yamato-86751 (CV3)

T. Murakami[1], Y. Ikeda[2], M. Kimura[2], and T. Noguchi[2]
1)Dept. Geology, Tokyo University, Tokyo 113, and 2)Dept. Earth Sciences, Ibaraki University, Mito 310

The Yamato 86751 chondrite (CV3) consists of chondrules, opaque mineral clasts, mineral fragments, and matrix with a minor amount of fine-grained CAI's. The major element chemical compositions of chondrules and matrix were obtained using broad beam technique of an electron-probe microanalyser. The compositions of Y-86751 chondrules differ from those of Allende chondrules; the former are poorer in Al_2O_3 and Na_2O and somewhat in CaO than the latter. Instead, the Y-86751 matrix is more enriched in Al_2O_3 and Na_2O than the Allende matrix. These suggest that the precursors of Y-86751 chondrules were depleted in an albite component probably by fractional condensation of Al_2O_3 from a solar gas or by equilibrium condensation from an Al_2O_3-depleted gas, and the Al_2O_3, in turn, was enriched as a nepheline component in the Y-86751 matrix by some process.

Y-86751 chondrules have a molar MgO/(MgO+FeO) range from 0.9-0.6, which is lower than Allende chondrules. Most of olivine in Y-86751 chondrules show a remarkable zonation from magnesian core to ferroan rim, and this zoning seems to have been produced from magnesian olivine by introduction of FeO from outside of chondrules. This is supported by an observation that all rims of enstatite in Y-86751 chondrules are replaced by ferroan olivine, which was first found in Allende chondrules by Housley and Cirline (1983).

A small amount of metals occurs in chondrules, metal-sulfide clasts, and matrix. They are mainly taenite with 1.5-2.0 wt% Co, and Co-rich metals with 22-29 wt% Co occur in metal-sulfide clasts, suggesting that they were extremely oxidized to have lost metallic Fe from the clasts, although a trace amount of kamacite still occurs in such clasts. Partition of Co between coexisting taenite and kamacite (Affiatarab and Wasson, 1980) gives a temperature range from 610-790K for metal-sulfide assemblages in clasts and chondrules. On the other hand, magnetite coexists with taenite in Y-86751 chondrules, and thermodynamic calculation for a reaction, 3Fe in taenite + $2O_2 = Fe_3O_4$, gives the oxygen fugacity of 10^{-38} bars at 630K and 10^{-33} bars at 700K, which are by 3-4 orders higher than those of the canonical solar gas with a total gas pressure of 10^{-4} bars.

Ref: Affiatarab and Wasson (1980): Geochim. Cosmochim. Acta, 44, 431-446. Housley and Cirlin (1983): Chondrules and their Origin, ed. by E.A.King, 145-161.

PRE-ACCRETIONARY ALTERATION OF CHONDRULES IN ALLENDE METEORITE.
KIMURA M. and IKEDA Y. Department of Earth Sciences, Ibaraki University, Mito 310.

Groundmasses of four chondrules in Allende (CV3) and ALH-77003 (CO3) meteorites show a chemical zonation; CaO-rich glass in the center and Na_2O-rich devitrified margin [1]. Such a zoning formed by introduction of Na_2O from the solar nebular gas and loss of CaO from chondrules. They were called zoned chondrules [1, 2]. This work follows the previous works to clarify the alteration reaction in chondrules in Allende meteorite. Four known zoned chondrules (2 from Allende and 2 from ALH-77003) were examined in detail. 47 chondrules in Allende were newly analyzed, and a new zoned chondrule was found. These chondrules cover various types of chondrule texture (porphyritic, barred and multiple), size (0.4-2.2mm in diameter), shape (spherical to fragmental) and chemistry (magnesian to ferroan chondrules).

Groundmass (zone 1) in the center of the zoned chondrules consists of clean to weakly devitrified glass, suggesting that it represents a primordial groundmass. It is usually homogeneous in composition, and is poor in FeO, Na_2O and K_2O, and rich in CaO (Table 1). On the other hand, devitrified marginal groundmass suffered alteration, and is divided into inner (zone 3) and outer (zone 4) portions. Zone 3 is richer in FeO, Na_2O and K_2O, and poorer in CaO than zone 1. Zone 4 is characterized by the highest contents of FeO, Na_2O and K_2O, and the lowest CaO content among zones. A zoned chondrule has glassy zone 2 between zone 1 and 3, in which Na_2O continuously increase forward the rim with decreasing CaO.

Each zone is characterized by the following normative mineral assemblages; zone 1 and 2 by plagioclase and diopside with minor nepheline, zone 3 by nepheline and diopside with minor plagioclase, and zone 4 by sodalite and olivine with variable contents of nepheline and plagioclase (Table 1). Molar ratios of plagioclase, nepheline and sodalite define each zone in the zoned chondrules as shown in Fig. 1. In the plot, zones 1 and 2 are defined to contain plagioclase > 50%, zone 3 nepheline >50% and zone 4 sodalite >10%.

Groundmasses of non-zoned 46 chondrules in Allende were almost altered. They have abundant nepheline and sodalite, instead of plagioclase, similar to zone 3 and 4 of the zoned chondrules (Fig. 2). Nepheline occurs in the central parts of these chondrules, and sodalite typically occurs in the marginal parts. In several chondrules, however, sodalite is encountered in the central parts. A few chondrules include relics of primordial glassy groundmass enriched in anorthite component similar to zone 1. Nepheline occurs around such a glassy groundmass, and sodalite occurs around nepheline-bearing groundmass.

Chemical similarity suggests that groundmasses of non-zoned chondrules experienced the same secondary alteration reaction to form zones 3 and 4 as the zoned chondrules. A possible predominant reaction to form devitrified groundmass of zone 3 from primordial glass of zone 1 is;

$$CaAl_2Si_2O_8 \text{ (anorthite)} + Na_2O \rightarrow 2NaAlSiO_4 \text{ (nepheline)} + CaO,$$

and a possible predominant reaction to form zone 4 from zone 3 is;

$$3NaAlSiO_4 \text{ (nepheline)} + NaCl \rightarrow Na_4Al_3Si_3O_{12}Cl \text{ (sodalite)}$$

The degree of reactions is various in Allende chondrules; the zoned chondrules suffered the alteration only in the marginal parts, but the other chondrules did extensively. The original groundmasses of wholly-altered chondrules were replaced by nepheline and sodalite even in the central parts. At any rate, all Allende chondrules have changed their primordial chemistry since they consolidated.

Low-Ca pyroxene within unaltered groundmass does not show any reaction texture, whereas that in zones 3 and 4 usually shows a replacement texture; the reaction is shown by $MgSiO_3 + Fe + 1/2O_2 \rightarrow (Mg,Fe)_2SiO_4$ [3]. Thus, the oxidation reaction to form ferroan olivine may have occurred simultaneously with the alteration reaction to form zoned chondrules in Allende.

The degree of alteration is various among Allende chondrules and seems not to be correlated with size of chondrules. Clean glass in a broken chondrule directly contacts with the Allende matrix. Therefore, the alteration may have occurred in the pre-accretionary stage of chondrules into the final parent body. It is well known that CAI's suffered a similar alteration to form secondary minerals such as nepheline, sodalite and others [e.g., 4], although reaction products in chondrule are not the same as those in CAI's, reflecting the difference in the original constituent materials between them.

References: [1] Ikeda Y. and Kimura M. (1985) Meteoritics, 20, 670. [2] Ikeda Y. (1982) Mem. Natl. Inst. Polar Res., 25, 34. [3] Housley R.M. and Cirlin E.H. (1983) in Chondrules and their origin. Lunar Planet. Inst., Houston, 145. [4] Hashimoto A. and Grossman L. (1987) GCA, 51, 1685

Table 1. Average chemical and normative compositions of groundmass in zoned chondrule.

Sample	ALH-77003						Allende							
Chondrule	1			29			I1-4				I1-8		N2-23	
Zone	1	3	4	1	3	4	1	2	3	4	1	3	1	3
SiO2	53.08	48.51	43.05	58.93	46.54	34.87	48.36	49.97	45.53	41.52	48.61	44.89	47.61	43.91
TiO2	0.61	0.50	0.56	0.28	0.20	0.16	1.17	0.97	0.84	0.36	0.65	0.34	1.12	0.83
Al2O3	20.02	19.71	20.30	17.43	16.47	19.26	24.66	23.32	20.55	23.41	22.63	24.35	24.61	23.34
Cr2O3	0.15	0.14	0.12	0.13	0.15	0.44	0.45	0.45	0.45	0.27	0.29	0.23	0.46	0.31
FeO	4.46	5.48	5.32	3.21	9.60	13.28	0.43	0.71	3.21	6.19	1.25	3.97	0.94	4.63
MnO	0.63	0.87	0.91	0.07	0.14	0.14	0.03	0.05	0.15	0.11	0.08	0.07	0.06	0.06
MgO	4.49	5.94	5.29	3.34	6.65	6.00	5.82	5.22	9.91	9.00	6.27	5.76	7.38	9.15
CaO	12.93	10.93	7.65	10.69	11.63	4.09	15.98	15.28	9.80	5.11	15.49	8.38	17.08	6.39
Na2O	4.08	8.45	11.31	6.55	7.05	13.33	1.94	2.85	8.89	11.50	3.23	10.57	1.18	10.73
K2O	0.11	1.00	0.26	0.03	0.86	0.27	0.00	0.00	0.88	0.69	0.23	0.98	0.02	1.13
Cl	0.00	0.09	2.86	0.00	0.00	3.26	0.00	0.00	0.00	1.50	0.00	0.13	0.00	0.00
Olivine	5.24	6.09	9.87	0.00	10.65	28.42	3.22	2.80	10.42	20.94	3.31	7.76	4.64	15.01
Hypersthene	0.00	0.00	0.00	0.00	0.00	0.00	2.43	0.00	0.00	0.00	0.00	0.00	3.49	0.00
Diopside	22.97	33.46	18.73	27.33	38.76	1.03	16.11	19.43	27.61	7.46	23.57	20.12	17.86	15.54
Anorthite	35.99	13.25	15.08	18.07	10.91	4.71	58.58	50.84	13.57	16.11	46.57	16.61	61.80	12.19
Albite	33.58	11.95	12.32	51.47	7.10	0.00	16.42	22.92	3.51	4.41	16.32	5.42	10.11	2.50
Nepheline	0.87	32.94	0.00	2.24	30.10	1.25	0.00	0.65	42.07	10.46	6.70	45.10	0.00	52.47
Sodalite	0.00	2.33	39.90	0.00	0.00	54.15	0.00	0.00	0.00	38.87	0.00	3.37	0.00	0.00

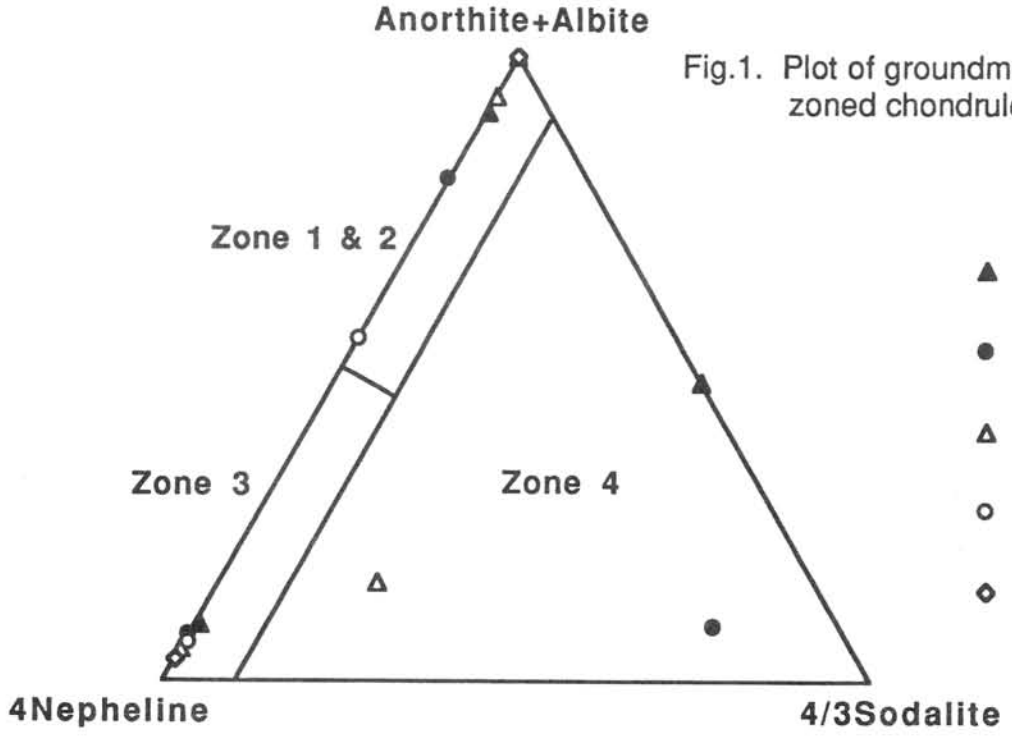

Fig.1. Plot of groundmasses in zoned chondrules.

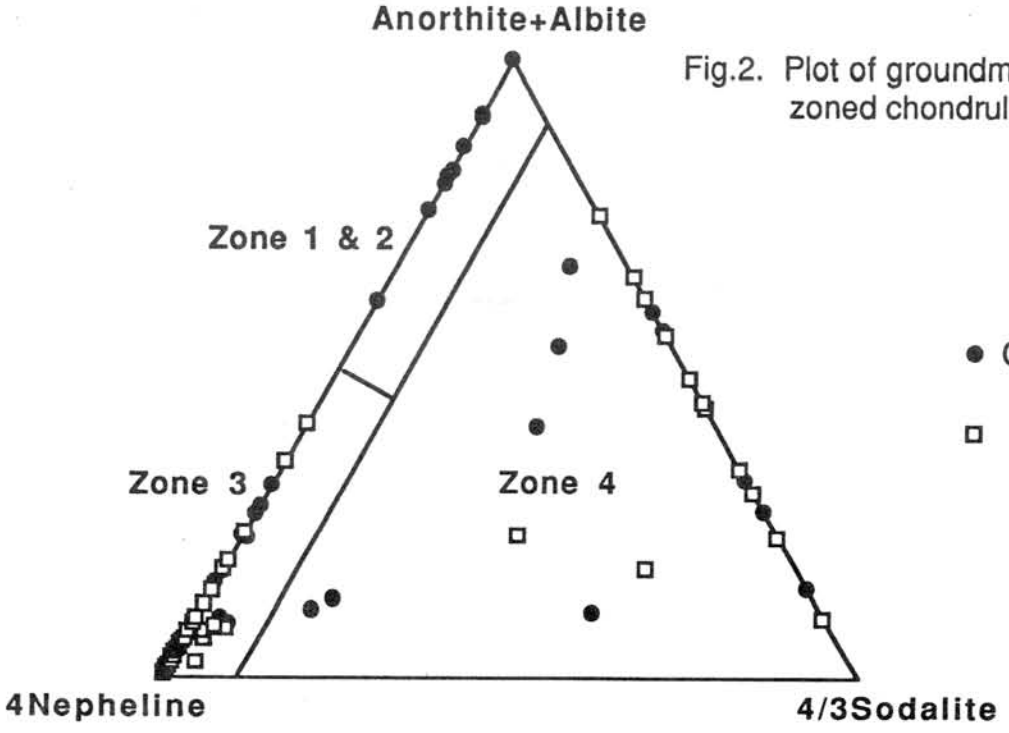

Fig.2. Plot of groundmasses in non-zoned chondrules.

ORIGIN OF FINE FRAGMENT IN MATRIX OF CHONDRITES

Takashi Fujita and Masao Kitamura

Department of Geology and Mineralogy, Kyoto University, Kyoto Sakyo 606, Japan.

Matrix of unequilibrated ordinary chondrites (UOCs) includes fine mineral fragments a few to 10 μm in size. Alexander et al. (1989) compared the compositions of the fragments with those of chondrules and concluded that matrix were the fragmented chondrules. On the other hand, relict minerals have been found as precursors of chondrules (Nagahara, 1981; Rambaldi,1981). To elucidate the origin of fine fragments critically, the relations among the fragments, relicts, and the chondrule minerals crystallized during the chondrule formation should be studied.

Olivines and pyroxenes occur as fine fragments, relict precursors and chondrule minerals. Previous studies of fine materials in matrix mainly discussed the origin of olivines for their greater amount in matrix. However, to discuss the original relation of the three materials from their compositions, it should be better to compare the compositions of pyroxenes in which diffusion rate is much slower, then the effect of secondary metamorphism are lower than those of olivines.

In this study, fine pyroxene fragments (5-20 μm in size) in the matrix materials of three UOCs, ALH-764 (LL3), Y-790448 (LL3), ALH-77015 (L3) were studied. The compositions of fine fragments were compared with the chondrule pyroxenes and relict pyroxenes in the same chondrites.

Pyroxene fragments

Pyroxene fragments in the three chondrites show the polyhedral or rounded shapes, suggesting that they are the fragments of large materials. Fig.1 shows a back scattered electron image of pyroxene fragments in ALH-77015 for example. Compositions of fine fragments are compared with those of chondrule pyroxenes, and relict pyroxenes in ALH-77015 in the quadrilateral (Fig.2).

The pyroxene fragments comprise compositional trends whose compositions range from Mg-rich enstatite to Ca-Fe-rich pyroxene (pigeonite to augite or diopside). Composition of the relict pyroxene overlaps the low-Ca pyroxene compositions of the fragments. Enstatite components of the chondrule pyroxene are similar to those of fragments, but the Ca-rich rim of the chondrule pyroxene are poorer in Fe than the fragments.

If Fe-Mg exchange in the Fe-poor Ca-rich pyroxene of fragmented chondrules formed the Ca-Fe-rich pyroxene fragments, the Ca-poor pyroxene of the same chondrules would be given Fe-rich compositions in the same process. On the contrary, the Ca-poor pyroxene fragments remains Fe-poor composition. Therefore, it is difficult to explain the origin of Ca-rich fragments by the fragmentation of the chondrule pyroxene. Furthermore, some Ca-rich pyroxene fragments are grater in size than the Ca-rich rim of chondrule pyroxenes. Those fragments cannot be formed from the fragmented chondrules. Accordingly, the fragmentation of chondrules cannot explain the origin of the fine fragments in matrix completely.

On the other hand, compositions of the relict pyroxene grains overlapping on the low-Ca compositions of the compositional trends of the pyroxene fragments suggest the existence of precursor common to the fragments and relicts. It is possible that fine fragments include the fragmented precursor common to the precursor of chondrules, although some enstatite fragments may came from the fragmented chondrules.

Implication to precursor material

Origin of the precursor material of fine fragments and chondrules can be estimated from the pyroxene composition. Under the condensation temperature of the enstatite and diopside, the coexisting pigeonite cannot be stable. Therefore, it is more possible that the precursor materials were crystallized from liquids. The observed trends resembles the compositional trends of pyroxenes in chondrules of the equilibrated chondrites (Watanabe et al. 1985), suggesting the possibility that the precursor were the rocks formed under an analogous condition of chondrules of equilibrated chondrites.

Reference

1) Alexander,C.M.O., Hutchison,R. and Barber,D.J. (1989): Earth Planet. Sci. Lett., 95,187-207.
2) Nagahara,H. (1981): Nature,292,135-136.
3) Rambaldi, E.R. (1981): Nature,293,558-561.
4) Watanabe,S. Kitamura,M. and Morimoto,N. (1985): Earth Planet. Sci.Lett.,72, 87-98

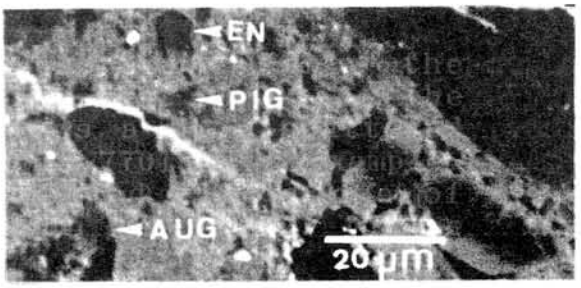

Fig.1 Back scattered electron image of matrix in ALH-77015 (L3). Fine fragments of pigeonite, augite, and enstatite are observed in the same region. PIG: pigeonite, AUG: augite, EN:enstatite

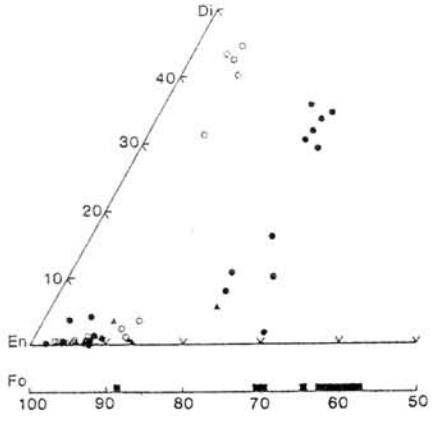

Fig.2 Compositions of pyroxenes in ALH-77015. White circles, solid circles, and solid triangles indicates the compositions of chondrule pyroxene, fine fragments and relict pyroxene respectively. Solid squares represent the forsterite contents of fine olivine in the matrix.

SHOCK-INDUCED PHASE TRANSFORMATION IN NEPHELINE

Toshimori Sekine. National Institute for Research in Inorganic Materials, 1-1 Namiki, Tsukuba 305, Japan

Introduction In our recent analyses of the shock wave data in the system $NaAlSiO_4$-SiO_2, it has been indicated that the shock-induced high-pressure candidates for nepheline and albite are of $CaFe_2O_4$ and hollandite structures, respectively[1]. The shock metamorphism of alkaline and plagioclase feldspars has been investigated in detail, based on the experimentally-shocked samples and the natural samples subjected to shock[e.g. 2]. Some high-pressure crystalline phases[3, 4] and the amorphous phases[2] have been identified in the shocked feldspars. Since there are no data available for shock-recovered nepheline, we need to know the shock effects on nepheline although nepheline is not so popular as feldspars. The purpose of the present study is to compare the structual changes in the shock-recovered nepheline with the Hugoniot data[5] to understand the shock effects on nepheline.

Experimental The nepheline employed in the present study is a Geological Survey of Japan Museum collection(GSJM 18090) from Shinjouzan, which has been described by Miyashiro and Miyashiro(1955)[6]. Our electron probe analyses and X-ray diffraction investigations revealed the presence of sodalite inclusion and a trace amount of nepheline hydrates I and II[7].

Powdered nepheline specimen was pressed into a steel container(SUS 304) and closed by two screws. The maximum sample space is about 12mm in diameter and 5mm thick. In order to get the high initial shock pressures, 90wt% copper powders with a higher shock impedance were mixed with the nepheline powders(10wt%). Figure 1 depicts the Hugoniots of nepheline(Ne), mixture of Ne and Cu, pressed copper powder with a density of 7.6 g/cm^3 as a reference, and container material(SUS 304). The shock pressure is calculated by the impedance match method using the measured impact velocity of the steel flyer plate(SUS 304). The actual peak pressure is dependent on the thicknesses of sample and flyer plate.

Recovered samples were investigated by powder X-ray diffraction technique, electron microscopy observations and Raman spectroscopy.

Results Experimental conditions are listed in Table 1. The X-ray diffractometer patterns are illustrated in Fig. 2. For the shocked nepheline powders the transition between crystalline and X-ray amorphous states occurs over a pressure interval of 30 to 35 GPa. From the electron microscope observations of shocked samples, it was found that they contains amorphous grains, detected by electron diffraction. The amorphous grains were devided into two types;one is homogeneous glass in samples #240, 272 and 248 and the other indicates many vesiculars of which diameters range between 20 and 400 nm. The latter was not found

in sample #240 and the number and average size of vesiculars increase more greatly with increasing the shock pressure. There was observed no part of amorphous phase indicating flow structures. It appears that the threshold shock pressures to produce the homogeneous glass phase and the vesiculated glass are about 20-25 GPa and 30 GPa, respectively, although there are only three data.

From the experiments of mixtures of Ne and Cu, it was found that the shocked nepheline contains albite crystals at shock pressures below 20 GPa. Since it was needed to immerse in an HNO_3 to dissolve the copper after subjected to shock, remaining crystalline nepheline was gelled. At the same time it was comfirmed that the treatment of unshocked nepheline by HNO_3 solution does not provide any albite and that albite is stable in the solution. Therefore the formation of albite must be the effect of shock.

Discussion The present shock-recovery experiments on powdered nepheline indicate that the amorphization begins in the pressure of 20-25 GPa. The Hugoniot temperature calculation of nepheline using the shock wave data[5] suggests that it is below the melting curve although the melting curve is not known precisely at high pressures. Since we employed the shock-reflection method to increase pressure, the temperatures are considered to be lower relative to that attained by a single shock. The amorphization occurs through a sold-state transition. The transition pressure is close to the threshold pressure seen on the Hugoniot curve(pressure-density plot). It is not clear, however, that the amorphous phase was formed during shock compression or in the process of presure release. The formation of diapilitic glass as shocked products of crystalline quartz and feldspars is well known[2] and also recent static high-pressure works have observed the pressure-induced amorphization of minerals such as anorthite, fayalite, quartz and others[8].

The origin of vesiculated glass is different from that of the homogeneous glass phase, because the amount of vesiculated glass increase more with increasing shock pressure. Porous samples like powdered nepheline accompany local temperature rises which are high enough to produce melting. We did not find the $CaFe_2O_4$-type high-pressure phase which was suggested based upon the analyses of the Hugoniot data[1].

References 1.Sekine T. and Ahrens T.J.(1992) Phys Chem Mineral 18, 359-364. 2.Stoffler D. et al.(1988) in Meteorites and the Early Solar System(J.K. Kerridge and M.S. Matthews, eds.) 165-202, Univ Arizona Press. 3.James O.B.(1969) Science 165, 1005-1008. 4.Mori H.(1990) Abst in 31st High Press Conf Jap 134-135. 5.Simakov G.V. and Trunin R.F.(1980) Izv Earth Phys 16, 134-137. 6.Miyashiro A. and Miyashiro T.(1955) J Fac Sci Univ Tokyo 10, 1. 7.Saha P.(1961) Am Mineral 46, 859-884. 8.Hemley R.J. et al.(1988) Nature 334, 52-54. Williams Q. and Jeanloz R.(1989) Nature 338, 413-415. Williams et al.(1990) JGR 95, 21549-21564.

Table 1. Experimental conditions of shocked nepheline

Run #	sample	thickness (mm)	impact velocity(km/s)	Pi(GPa)	Pe(GPa)
240	Ne powder	2.0	1.33	12	29
272	Ne powder	1.0	1.45	13	32
248	Ne powder	1.0	1.85	16	37
243	Ne + Cu	4.0	0.95	13	20
239	Ne + Cu	4.5	1.09	16	22
235	Ne + Cu	4.5	1.4	22	30
236	Ne + Cu	4.5	1.89	32	43

Pi = shock pressure attained by the first shock within sample.
Pe = shock pressure equilibrated with the pressure within sample container.

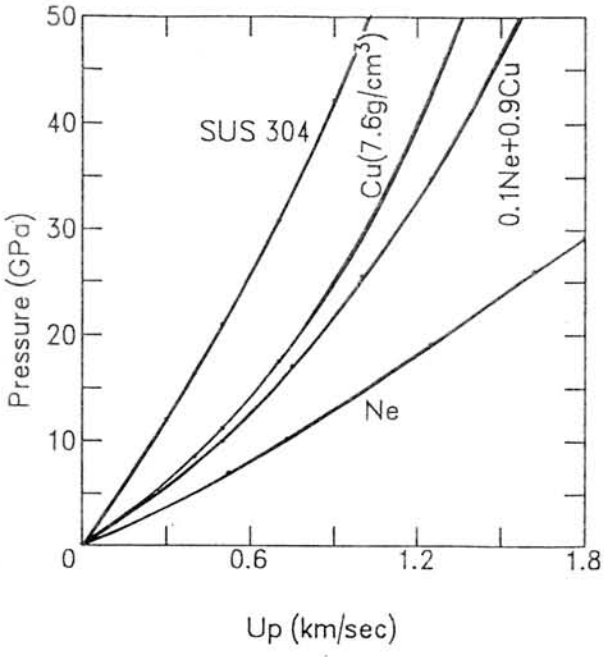

Fig. 1 Hugoniots used in the present study.

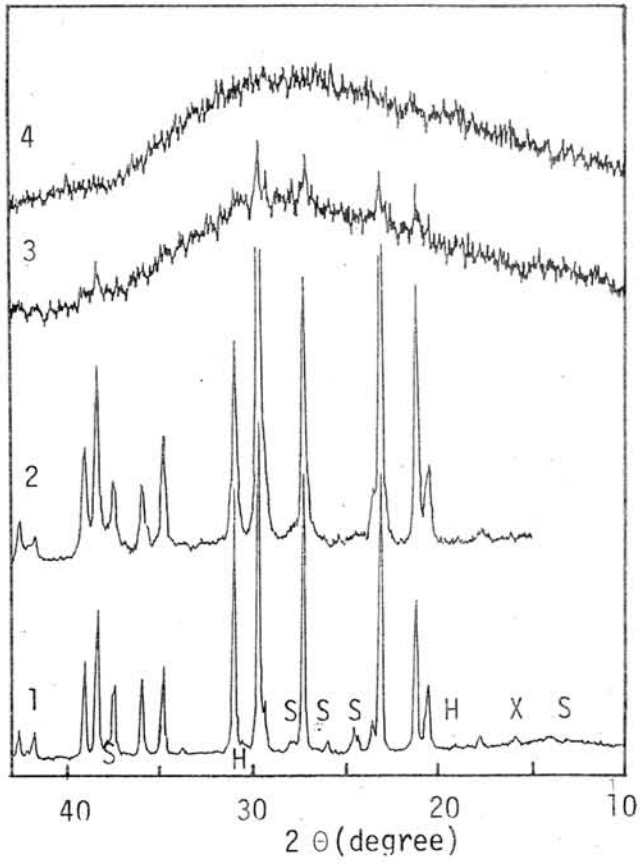

Fig. 2 X-ray diffraction patterns of unshoched(1), #240(2), #272(3), and #248 (4). S=sodalite, H=nepheline hydrates and X=unknown.

Type A CAI with core-mantle structure

Hideyasu Kojima and Keizo Yanai
Department of Antarctic Meteorites, National Institute of Polar Research, 9-10, Kaga 1-chome, Itabashi-ku, Tokyo 173, Japan

Type A calcium-aluminium inclusion(CAI) showing core-mantle structure was found from Yamato-791601 CV3 chondrite. CAI has been classified into three types; type A, B and C(Grossman, 1975 and Wark, 1987). Zoned structure was only reported in B1 CAI. So it is first report of occurence of type A CAI that has core-mantle structure.

Y-791601 is a small fragment(2.06g) of CV3 chondrite, and is mainly composed of large CAI. The long dimension of it is about 2cm. The CAI consists of 60 per cent spinel, 27 per cent melilite and 1 per cent perovskite with 13 per cent secondary phase. The mineral assemblage indicates that the CAI is classified intotype A except of the abundance of spinel and melilite. The CAI shows core-mantle structure. Core consists of mainly spinel. Mantle consists mainly of melilite with minor spinel, perovskite and hibonite.

Three types of spinel are recognized in the mode of occurence. (1) Euhedral spinel packed loosely, making a core. (2)Euhedral spinel that included in mantled melilites. (3)layered spinel making a inner most rim on the mantled melilites.

Melilite crystals are up to 1 mm in longest dimension. Many of them show signs of alteration in varying degree and are replaced by fine-grained anorthite, grossular and wollastonite. Melilite ranges in composition from Ak0.6 to Ak14.3, with a mean of Ak9. This is at the low Ak site of the lange encounted in Type A inclusions.

A narrow rims are developed as successive layers on the outside of spinel layer. From inside to outside, they consist of anorthite + grossular + andradite, Ti-Al-pyroxene + diopside and andradite + hedenbergite + anorthite + diopside. This rim sequence is similar to that of Wark and Lovering(1977).

Two rims are recognized on spinel grains of core. Inner rim consists of anorthite + grossular. Outer rim consists of Ti-Al-pyroxene + diopside. The rims are identical with inner two rims that are developed on the melilite mantle.

Petrographic study reveals the order of formation of 1601CAI as follows.

1. a core consisting of spinel
2. a mantle consisting of melilite
3. a layer of spinel
4. alteration of melilite forming fine-grained material consisting mainly of anorthite with minor grossular
5. a discontineous layer consisting of anorthite + grossular + andradite
6. a contineous layer consisting of Ti-Al-pyroxene + diopside
7. a layer consisting of andradite + hedenbergite + anorthite + diopside

References

Grossman L. (1975) Geochim. Cosmochim. Acta 39, 433-454. Wark D.A. and Lovering J.F. (1977) Proc. Lunar Sci. Conf. 8th, 95-112. Wark D.A. (1987) Geochim. Cosmochim. Acta 51, 221-242.

GENETIC RELATIONSHIPS AMONG TYPE IA AND II CHONDRULES AND MATRIX IN ORDINARY AND CARBONACEOUS CHONDRITES

Hiroko Nagahara, Geological Institute, University of Tokyo, Hongo, Tokyo 113, Japan.

Nagahara et al. [1] studied phase relation of the olivine system at low pressures on the basis of vapor pressure measurements for forsterite and fayalite. The diagram well explains the origin of Type IA and Type II chondrules and matrices in chondrites. Since chondrules are formed from pre-existing solids through incipient melting, evaporation behavior of chondrule-forming minerals, particularly olivine is important. Dynamic crystallization experiments to reproduce various chondrule textures assume that bulk composition does not change during heating, but heating at low pressures should have changed composition of the systems. Evaporation of alkalis (especially Na_2O) from chondrule liquid has been studied [2,3], but evaporation of other elements including major SiO_2, MgO, and FeO has not been studied.

Si, Mg and Fe oxides occupy about 90% of chondrites, and therefore it may be appropriate to assume chondrites roughly to be of the MgO-FeO-SiO_2 system and to apply the experimental results for the olivine system to understanding of origin of chondritic components except for highly reduced enstatite chondrites where almost all iron is metallic and the system is essentially MgO-SiO_2. The effect of SiO_2 should be taken into consideration; SiO_2, however, does not largely affect the relationship. The Mg/Fe distribution between coexisting olivine and pyroxene is nearly 1, and therefore the ratio (Mg+Fe)/Si among the phases including liquid does not change largely from that between olivine and liquid. Presence of other components (mostly CaO, Al_2O_3, and Na_2O) does not affect the Mg/Fe relationships because those elements are contained only in Ca-pyroxene, plagioclase and liquid. The amount of Ca-pyroxene is, if present, small in chondrites, and can be neglected. Plagioclase does not crystallize in most chondrules or is very small if any, thus can be also neglected. Those elements raise the vaporous and lower the liquidus and solidus, and the temperature interval for melting should becomes larger. X_{Mg} of chondrules in ordinary chondrites ranges from 0.7 to 0.95 and that in carbonaceous chondrites from 0.5 to 1.0, and mostly between 0.8 and 0.9 for both O and C chondrites. Evaporation behavior of precursor material with X_{Mg}=0.8-0.9 will be considered below.

If X_{Mg}=0.8 to 0.9 chondrules are heated at high temperatures or low pressures, they evaporate incongruently to magnesian residue and iron-rich gas. Type IA chondrules, which are characterized by (1) magnesian bulk compositions, (2) weakly zoned forsteritic olivine phenocrysts, (3) trace abundance of FeO in groundmass liquid, (4) refractory (Ca, Al, Ti-rich) groundmass, and (5) presence of Fe-Ni metal [4], are considered to be formed in the conditions where liquid is not stable and olivine evaporates incongruently to magnesian solid and iron-rich gas. FeO, Na_2O, MnO, and other volatiles should have been lost during heating and/or crystallization. The compositional zoning in olivine is hardly formed because FeO is almost lost. Groundmass of Type IA chondrules are not of SiO_2-MgO-FeO system, but is essentially of SiO_2-Al_2O_3-CaO system. This model does not require reduction during heating as has been proposed by [4,5]: absence of FeO is due to gas-solid fractionation.

At pressures 10^{-4}-10^{-5} bar, olivine (X_{Mg}<0.9) melts to become magnesian olivine and iron-rich liquid when heated, and X_{Mg} of olivine and liquid are not so largely different as is the case for the system without vapor. Type II chondrules, which are characterized by (1) having considerable amount of FeO, (2) olivine phenocrysts strongly zoned from magnesian core to iron-rich rim, (3) presence of FeO in groundmass of which composition is often disequilibrium with phenocrysts because of undercooling, (4) fairly volatile (Na_2O and FeO)-rich composition of groundmass liquid, and (5) small abundance of metallic Fe-Ni and presence of troilite [6], should have been formed in such a condition. All the characteristics suggest that melting and crystallization took place in closed systems, which are well explained by heating below the gas-solid field. Vaporization does hardly take place below the solidus of the vapor-solid loop. Therefore, the bulk composition of the system does not change during heating and subsequent cooling.

Average X_{Mg} values of olivine (0.84) and groundmass (0.79) [4] in the phase diagram shows that olivine and liquid in Type II chondrules crystallized at about 1600°C and 10^{-4} bar. If we take the same temperature for the maximum temperature for Type IA chondrules, the pressure should have been 10^{-5} to 10^{-6} bar where olivine evaporates incongruently to magnesian solid and iron-rich gas. At lower pressures, olivine evaporates totally. Difference in (olivine) pressure is due to the degree of enrichment of the dust component relative to hydrogen gas. Alternative possibility is the same pressure but different temperature; when (olivine) pressure is the same, Type IA chondrules should have been formed at higher temperature than Type II chondrules.

Although matrices of chondrites consist of several phases and their origin is in debate [7-9], matrices and chondrules are thought to be genetically related [5,10,11]. They are richer in Fe than chondrules in CV, CO, and ordinary chondrites, and the major mineral of matrices in non-altered chondrites is Fe-rich olivine, especially Fo_{50} [7,9,10]. Those olivines are fine-grained, euhedral and have similar size suggestive of condensation from gas. Although condensation of iron-rich olivine from the solar nebular gas has been discussed [13], condensed olivine from the solar nebular gas should have zoned from forsteritic olivine to iron-rich rim. However, olivine in matrices is not zoned, and is suggestive of direct condensation of Fo_{50} olivine. Therefore, the gas should not be the solar nebular gas. Condensation of iron-rich olivine from gas of iron-rich olivine composition formed by partial evaporation of magnesian olivine has been experimentally shown [14]. The Fo_{50} olivine is thus thought to have condensed from partial evaporation of the olivine component at high temperatures responsible for formation of Type I chondrules. This model is consistent with the fact that matrix is abundant in carbonaceous chondrites which have much more Type IA chondrules; whereas, matrix is less in ordinary chondrites which have much less Type IAs. Chondrules and matrix materials in the same chondrites should have originated in a dust-enriched batch in the solar nebula, which located separately from other batches.

References: [1] Nagahara, H. *et al.* (1992) *LPSC* **XXIII**, 959-960, [2] Tsuchiyama, A. et al. *GCA* **45**, 1357-1367, [3] Matsuda, H. *et al.* (1990) *Meteoritics* **25**, 137-143, [4] Jones, R. H. and Scoot, E. R. D. (1989) *Proc. LPSC* **19**, 523-536, [5] Grossman, J. N. (1991) *Meteoritics.* **26**, 340-341, [6] Jones, R. H. (1990) *GCA* **54**, 1785-1802, [7] Nagahara, H. (1984) *GCA* **48**, 2581-2595, [8] Rubin, A. and Wasson, J. T. (1987) *GCA* **51**, 1923-1937, [9] Alexander, C. M. O. (1989) *EPSL* **95**, 187-207, [10] Anders, E. (1987) *Phil. Trans. R. Soc. Lond.* A**323**, 287-304, [11] Nagahara, H. (1990) *Meteoritics*, **25**, 389-390, [12] Palme, H. and Fegley, B. (1991) *EPSL* **101**, 180-195, [13] Peck, J. A. (1983) *Metoeritics* **18**, 373-374,.[14] Nagahara, H. *et al.* (1991) *Nature* **331**, 516-518.

Reverse zoning of matrix plagioclase in CK chondrites.

Takaaki NOGUCHI
Department of Earth Sciences, Ibaraki University, Bunkyo 2-1-1, Mito 310.

Introduction: Kallemeyn et al. (1991) proposed a new chemical group of carbonaceous chondrites named CK group. Geiger and Bischoff (1991) pointed out some unique properties shown in CK chondrites. (1) Most abundant opaque mineral is magnetite, which includes ilmenite and spinel exsolution lamellae. (2) Chemical composition of plagioclase is quite heterogeneous, ~An20 to ~An75. (3) NiO content in olivine is high, 0.33-0.72 wt %. (4) Platinum-group-minerals exist in opaque mineral aggregates or grains which are composed of magnetite, pentlandite, and pyrite. (1) and (3), and perhaps (4), are related to the oxidized conditions which the CK chondrites experienced. But (2) is more problematic. I performed scanning electron microscopic observations and electron microprobe analyses of three CK chondrites: Karoonda, Maralinga, and Y-693. Here, I report on the reverse zoning of matrix plagioclase which is commonly observed in these CK chondrites.

Results: *SEM observation of plagioclase.* Matrices of Karoonda, Maralinga, and Y-693 are composed of olivine, plagioclase, opaque minerals (mainly magnetite), and pyroxenes. The abundance of pyroxenes in Maralinga is very low. Grain sizes of plagioclase in matrices are variable among these chondrites. The range of grain size of matrix plagioclase is from 10 to more than 100μm across in Karoonda and some grains exceed 100 μm across. In this meteorite, matrix minerals are fragmental. In Maralinga, most of matrix plagioclases are 20 to 50 μm across. Compared with them, while Y-693 is much more recrystallized than Karoonda and Maralinga. Therefore, matrix minerals are coarser than those in the two chondrites, and boundaries between chondrules and matrix are poorly defined. Most of matrix plagioclase exceed 100 μm across.

The cores of matrix plagioclase contain more inclusions than the rims of matrix plagioclase. In Karoonda, matrix plagioclases which are larger than several tens μm across have calcic rims of about 10 μm thick with sharp boundaries. Most of smaller plagioclase grains do not show remarkable compositional zoning, and both calcic and sodic plagioclases are observed. Matrix plagioclases in Maralinga have calcic rims of 5 to 10 μm with sharp boundaries as well as those in Karoonda. The acicular pyroxenes, both low-Ca pyroxene and augite, exist closely related to matrix plagioclase in Y-693, and there are few pyroxenes within chondrules. Matrix plagioclases in this meteorite also show reverse zoning. However, the zoning is relatively gradual and does not show sharp change of composition. Other equilibrated carbonaceous chondrites, ALH-85002, EET-87507, and EET-90007 which are recrystallized well, also have similar characteristics to those observed in Y-693.

Plagioclases in chondrules are observed as small laths or anhedral interstitial grains in mesostases, or sometimes as phenocrysts. Plagioclases are also observed in CAIs. Plagioclases in chondrules and CAIs rarely contain inclusions of magnetite, olivine and pyroxene.

Composition of plagioclase. Fig. 1 shows that plagioclase compositions are heterogeneous in these three meteorites: Karoonda: An17.9-100; Maralinga: An24.9-100; Y-693: An18.16-88.46.

This result is consistent with previous works (e. g. Scott and Taylor, 1985; Geiger and Bischoff, 1991). However, as described above, there are textural differences among plagioclases in matrices, chondrules and CAIs, and plagioclases in different occurrences have different compositions.

Fig. 2 shows the histograms of An mol% of plagioclases in matrices. It is clear that many matrix plagioclases show reverse zoning. In Maralinga, there is almost no overlap between core and rim composition of plagioclase. This result is consistent with that of Kellar et al. (1992) that there are two distinct compositional groups one of ~An_{20} and an ~An_{80} group. But Fig. 2b shows that two modes of plagioclase composition are about An_{40} (cores) and about An_{80} (rims), respectively. It is not clear whether this difference reflects heterogeneity of core composition of plagioclase or not.

Plagioclases in chondrules have as wide range of An mol% as those in matrices. But the proportion of plagioclase with >An_{80} to whole plagioclases is higher than that in matrices. In Maralinga, there are two modes in the histogram of An mol%. In the histogram, An mol% of a mode corresponds to a mode in the histogram of matrix plagioclases. CAIs are rare in CK chondrites except for Maralinga. In Karoonda, An mol% of plagioclases in CAIs is higher than 80. On the contrary, plagioclases in CAIs in Maralinga have similar range of An mol% to those in chondrules. Rims of plagioclases with ~An_{100} and plagioclases on the rims of CAIs, contain fairly amounts of Ab component, and some of them include up to Ab_{40}.

Discussion: It is a problem how these compositionally variable plagioclases were formed. Rubin (1992) stated that these plagioclases had been formed by shock metamorphism. However, compositions, grain sizes, and occurrences are different between plagioclases in CKs and feldspars in ordinary chondrite (OC) breccias. Most of feldspars in OC breccias have compositional trends from oligoclase to orthoclase (Bischoff et al., 1983), and no feldspar grain on such compositional trends was observed in this study (Fig. 1). Chemical compositions of plagioclases in OC breccias are different among veins and melt pockets. However, as described above, textures and chemical compositions of plagioclases in CKs are different among matrices, chondrules, and CAIs. These textural and compositional differences suggest that plagioclases in each occurrence are different in origin. Moreover, most of the matrix plagioclases show reverse zoning and separation between core and rim compositions are relatively well (Fig. 2). Compositionally various feldspars in OC breccias resulted from crystallization of them in veins and melt pockets with various compositions. In the veins and melt pockets, as crystallization proceeds, feldspars become more sodic and at the last stages of crystallization, potassic feldspars crystallize. Apparently, it is difficult to make reverse zoning of matrix plagioclase by this process. Therefore, it is unlikely that matrix plagioclases were formed by shock metamorphism. Although these three CK chondrites are classified as CK4, integration of chondrules with matrix, compositional variations of ferromagnesian minerals, and grain sizes of matrix minerals are various among these chondrites. However, these properties do not correlate to separation and homogeneity of core and rim compositions of matrix plagioclase. But sharpness of boundaries between cores and rims of matrix plagioclase seems to be related with grain sizes of matrix

minerals. Both original difference of chemical composition and later modification of them by thermal metamorphism seem to have been reflected to the compositions of plagioclases in CK chondrites.

References: Bischoff, Rubin, Keil, and Stöffler (1983): Earth Planet. Sci. Lett., **66**, 1-10; Geiger and Bischoff (1991): Meteoritics, **26**, 337; Kallemeyn, Rubin, and Wasson (1991): Geochim. Cosmochim. Acta, **55**, 881-892; Kellar, Clark, Lewis, and Moore (1992): Meteoritics, **27**, 87-91; Scott and Taylor (1985): J. Geophys. Res., **90**, C699-709; Rubin (1992): Geochim. Cosmochim. Acta, **56**, 1705-1714.

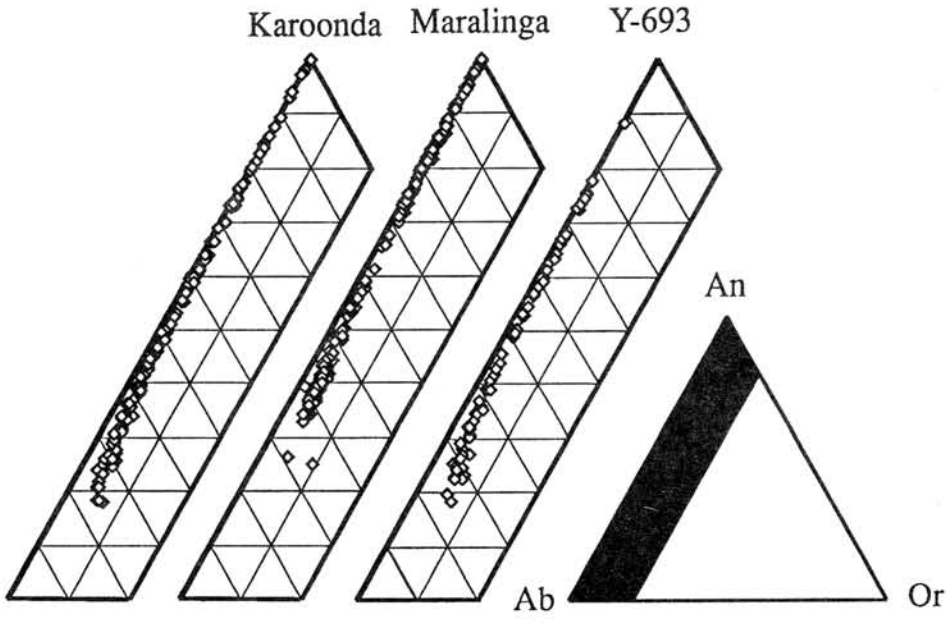

Fig. 1 Plagioclase compositions (in mol%) of Karoonda, Maralinga, and Y-693.

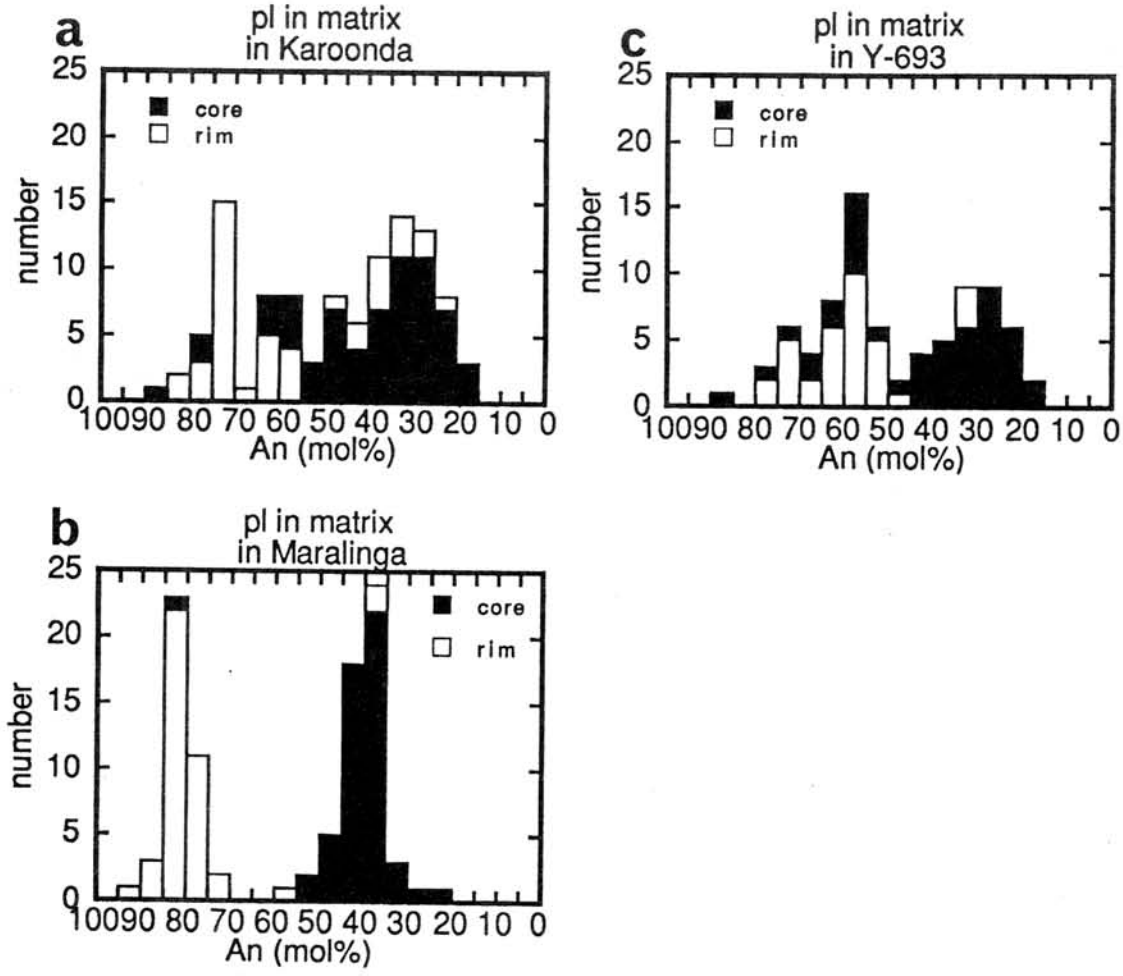

Fig. 2 Histograms of An mol% of matrix plagioclases in Karoonda, Maralinga, and Y-693.

Constraints to the Formation of Martix Reduced Olivine in Yamato-691 (EH3) Chondrite: Implications for the Evolution of EH Chondrites

S. Matsunami, Naruto University of Education, Naruto 772, Japan
A. El Goresy, Max-Planck-Institut für Kernphysik, P.O.Box 103980, D-6900 Heidelberg, F.R.Germany

In order to understand the origin of oxidized components in enstatite chondrites, matrix reduced olivine (RO) (< ~60 μm in diameter) in Yamato-691 (EH3) chondrite has been examined in detail using EPMA. It commonly shows a lamellar structure, composed of alternation (with the spacing of about 1 μm) of 'reduced olivine', which is a mixture of forsterite, metallic Fe and unreacted olivine (relict), and sub-grainboundaries (SB) partly filled with decomposition products due to reduction (Fig. 1A). The observed characteristics are (1) presence of micron-size Fe metal and troilite along SB and sub-micronsize ones in 'reduced olivine'; (2) presence of enstatite ($En_{85.9\text{-}90.2}Fs_{5.3\text{-}12.2}Wo_{1.9\text{-}4.5}$) and silicious melt ($SiO_2$=71.3-74.4wt%; MgO=10.0-20.7wt%; FeO=3.8-5.7wt%) (Fig. 2); (3) relict of initial olivine ($Fa_{6.5}$, $Fa_{13.1}$); (4) heterogeneous enrichment of CaO in 'reduced olivine' upto 2.86 wt% CaO; and (5) presence of RO with bended SB (Fig. 1A), suggesting plastic deformation of the olivine before reduction. These observations strongly suggest that the reduction of high-FeO olivine took place along SB. This is in accord with the experimental results of Boland and Duba (1986).

To constrain Temperature-Time conditions during the reduction process, we modelled theoretically the reduction kinetics of (Mg,Fe)-olivine. Fig. 3 is a schematic diagram showing diffusional and interface reaction processes during reduction of (Mg,Fe)-olivine through a cation-anion-vacancy transport mechanism. The rate-determining process is oxygen diffusion in the RO zone at high temperatures (Boland and Duba, 1986). Rate constant (RC) of reduction of (Mg,Fe)-olivine is expressed as a function of temperature, composition of olivine (X_{Fe}) and PO_2 of reducing gas (Schmalzried, 1984). Assuming that PO_2 of the reducing gas was buffered by Si-bearing Fe-Ni metal + quartz assemblage, PO_2 of the reducing gas can be easily estimated from the thermodynamic data and mixing properties of Fe-Ni-Si metal. A mean Si- and Ni-contents of kamacite in Y-691 (Si=2.09wt%; Ni=2.90wt%) was adopted from El Goresy et al. (1988) as representative ones of the metal. Oxygen diffusion data for San Carlos olivine (Gerard and Jaoul, 1989) were also used in the calculations. The effect of fast diffusion paths (grainboundaries and dislocations) to oxygen diffusivity in a RO zone is also evaluated from experimental results (Nagahara, 1986). They indicate that oxygen diffusivity in RO zone is enhanced by a factor of $\sim 10^{4.5}$ relative to lattice diffusion at high temperatures. At low temperatures the rate of reduction (progress of reaction front) is controlled by the Fe/Mg interdiffusion process in the olivine crystal. Calculated results of parabolic RC k are shown in Fig. 4, where k [cm^2/s] is defined by a parabolic rate law: $X^2=2kt$ (X[cm]: the position of reduction front from the initial surface of olivine; t[s]: reaction time). Using the obtained RC, we can estimate the time-scale for reduction of olivine with SB. To form RO with the SB spacing of 1μm within $10^{6\text{-}7}$ yr, which is a typical time-scale of thermal metamorphism at shallow parts of meteorite parent bodies (Wood, 1979), it is necessary that the temperature during reduction exceeded 700K (Fig. 5).

From these results, the formational history of matrix RO and other coexisting phases in Y-691 could be summarized as follows (Fig. 6): (1) High-FeO chondrule olivines crystallized in chondrule melts enriched in oxidized components (Stage 1). (2a) A severe impact process deformed

them plastically and generated numerous dislocations ($>10^9/cm^2$) in them (Stage 2a). (2b) Post-shock high-T (> ~1100K) annealing process formed SB in them due to dislocation climb (Stage 2b). (3) The olivine grains were then mixed with E-chondritic materials containing at least both Si-bearing Fe-Ni metals and silica (Stage 3). (4) During metamorphism and/or impact heating process (T > ~700K), reduction of the olivine proceeded along SB to precipitate reduction products (Stage 4). (5) After reduction, the ROs were comminuted to grain sizes less than ~60μm (Stage 5). (6) Finally, the fine-grained ROs were assembled with other E-chondritic components (e.g., sulfides) to form Y-691 chondrite at temperatures lower than ~500°C (Nagel, 1991) (Stage 6).

Boland J.N. and Duba A.G. (1986) *Jour. Geophys. Res.* **91**, 4711-4722.
El Goresy A. et al. (1988) *Proc. NIPR Symp. Antarct. Meteorites* **13th**, 65-101.
Gerard O. and Jaoul O. (1989) *Jour. Geophys. Res.* **94**, 4119-4128.
Nagahara H. (1986) *Lunar Planet. Sci.* (abstract) **17**, 595-596.
Nagel H.-J. (1991) *Ph.D. Thesis*, Univ. of Heidelberg, 117pp.
Schmalzried H. (1984) *Ber. Bunsenges. Phys. Chem.* **88**, 1186-1191.
Wood J.A. (1979) In *Asteroids* (ed. T. Gehrels), pp.849-891. Univ. Arizona Press, Tucson, Arizona.

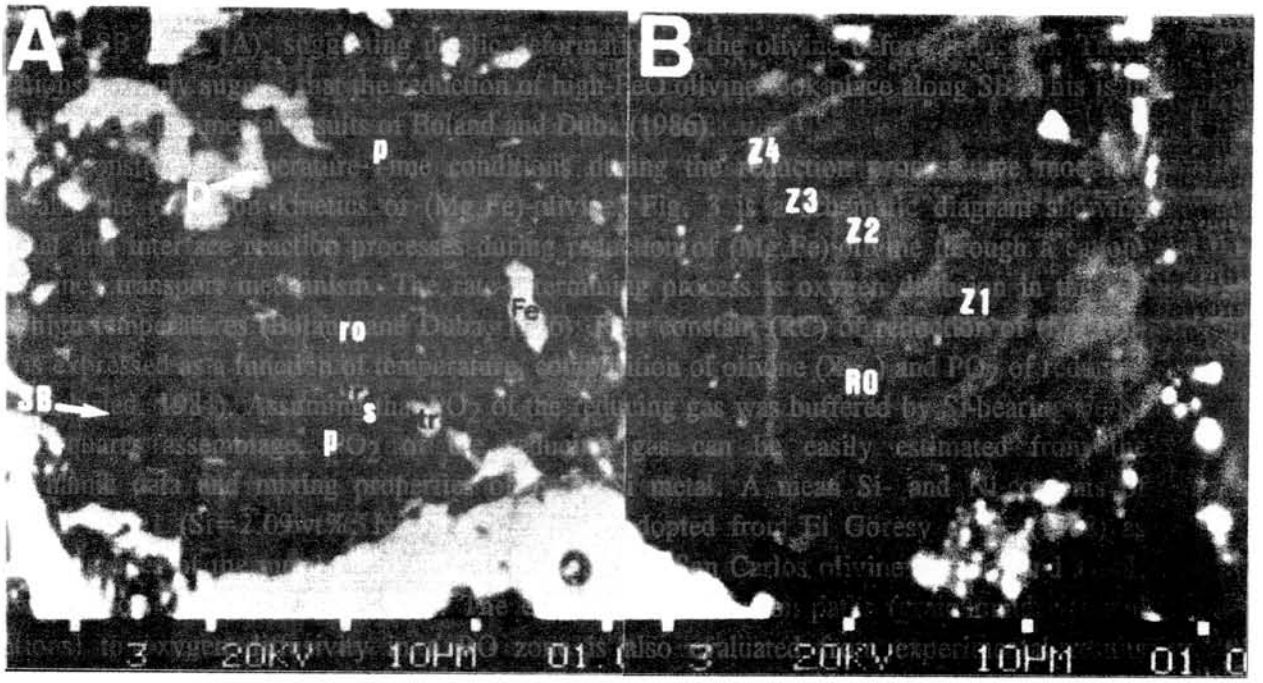

Fig. 1A. BSE image of matrix reduced olivine from Y-691. It shows a lamellar structure, composed of alternation (with the spacing of about 1μm) of reduced olivine (ro), and sub-grainboundaries (SB) partly filled with pyroxene (p), silicious melt (s), metallic Fe (Fe) and troilite (tr). The presence of bended SB (D in this figure) is suggestive of plastic deformation of the olivine before reduction.

Fig. 1B. BSE image of a reduced olivine with oscillatory zoning in matrix of Y-691. It consists of dark zones (Z1 and Z3) with magnesian composition (FeO^*=6.0-10.6wt%) and bright zones (Z2 and Z4) with ferrous composition (FeO^*=17.1-20.7wt%) and is completely converted to mixtures of forsterite and metallic Fe due to reduction, suggesting that reduction of the zoned olivine took place without homogenization through Fe/Mg interdiffusion. A tentative estimate of the reduction temperature is about 1700K. *: total Fe as FeO.

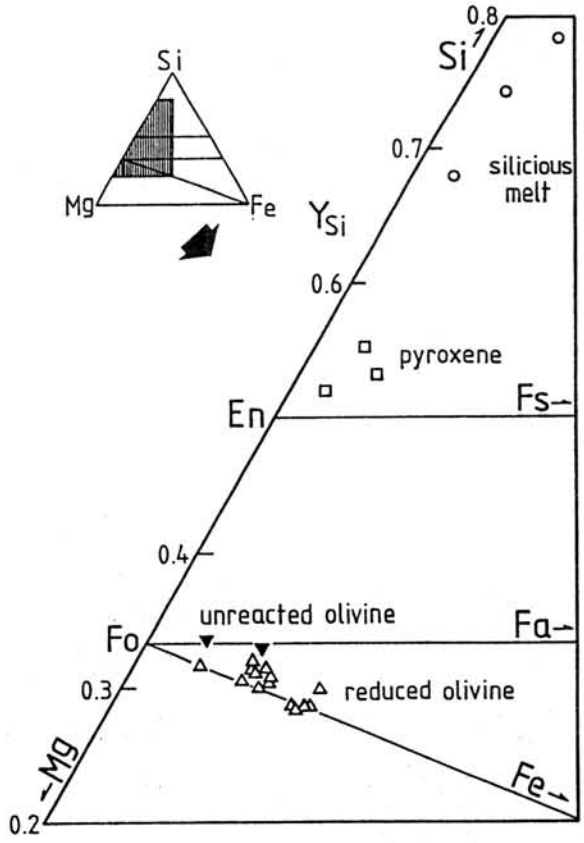

Fig. 2. Composition of decomposition products (reduced olivine, pyroxene, silicious melt, and unreacted olivine) due to reduction in matrix reduced olivines of Y-691, plotted in the Si-Mg-Fe diagram. Seven mean compositions of reduced olivine are plotted on the Fo-Fe tie-line. Pyroxene compositions are plotted slightly above the En-Fs tie-line, suggesting the formation of pyroxenes through reaction between forsterite and silicious melt.

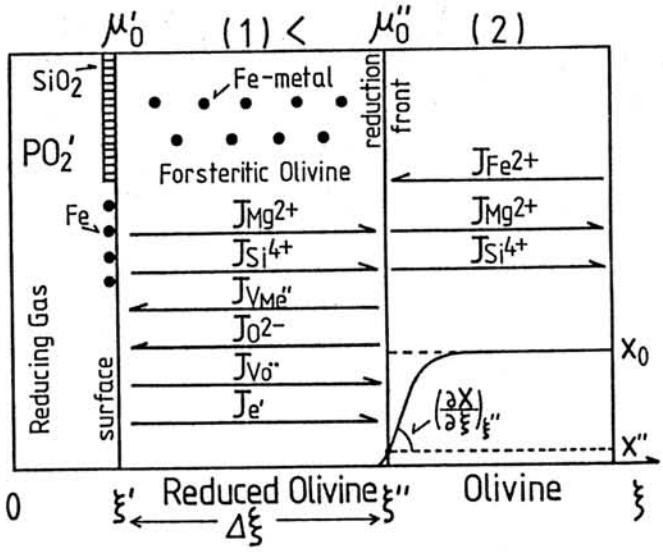

x: mole fraction of Fa component in olivine $[(Mg_{1-x},Fe_x)_2SiO_4]$.

Fig. 3. A schematic diagram showing reaction mechanism for reduction of (Mg,Fe)-olivine through a cation-anion-vacancy transport mechanism. Along the concentration gradient of Fe in olivine zone (2), Fe^{2+} ions diffuse into the reduction front to form metallic Fe, V_{Me}'' (vacancy of octahedral sites of olivine), and oxygen anion (O^{2-}) [$FeO + 2e' \rightarrow Fe + V_{Me}'' + O_O^x$]. V_{Me}'' and O^{2-} flow from the reduction front to the surface along oxygen potential gradient ($\mu_O' < \mu_O''$). At the surface, V_{Me}'' reacts with Mg_2SiO_4 component to form SiO_2, Mg^{2+} ion, O_2 and electron [$Mg_2SiO_4 + 2V_{Me}'' \rightarrow 2Mg_{Me}^x + O_2(g) + SiO_2 + 4e'$]. Along the gradient, Mg^{2+} and Si^{4+} ions also flow in the reduced olivine zone (1) from the surface into the olivine zone (2).

Fig. 4.

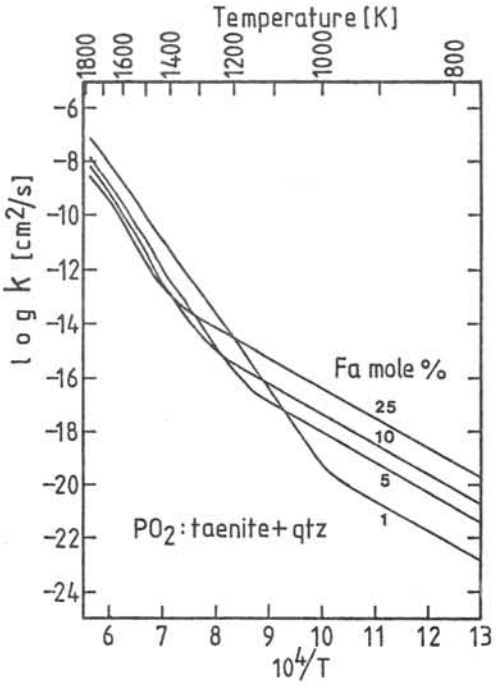

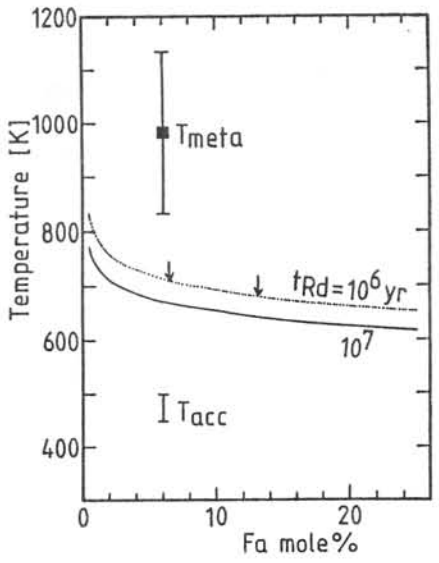

Fig. 5.

Fig. 4. Logarithm of the calculated parabolic rate constant k for reduction of olivine (Fa=25, 10, 5, 1) as a function of reciprocal temperature. At high temperatures the rate-determining process of reduction is oxygen diffusion in the reduced olivine zone (1). At low temperatures, however, it is Fe/Mg interdiffusion process in the olivine zone (2).

Fig. 5. Temperature conditions where reduction of olivine with the SB spacing of 1 μm completes for time-scale of reduction (t_{Rd})=$10^{6\text{-}7}$ yr. To form reduced olivines with initial compositions of $Fa_{6.5}$ and $Fa_{13.1}$ (small arrows), it is necessary that the reduction temperature exceeded about 700K. Metamorphism and/or impact heating may form reduced olivine.

Formational History of Matrix Reduced Olivine and other Coexisting Phases in Yamato-691

Fig. 6.

Stage I: Initial Crystallization of High-FeO Olivines in Chondrule Melts Enriched in Oxidized Components

↓

Stage IIa: Plastic Deformation of the Olivines (due to Shock) [Generation of Numerous Dislocations]

↓

Stage IIb: (Post-shock) High-Temperature Annealing [Formation of Sub-grainboundaries]

↓

Stage III: Mixing with E-chondritic Materials Containing at least both Si-bearing Fe-Ni Metals and Silica

↓

Stage IV: Reduction of the Olivines along Sub-grainboundaries to Precipitate Reduction Products during Metamorphism or Impact Heating Process [Formation of Reduced Olivine with Different Degrees of Reduction]

↓

Stage V: Comminution of the Reduced Olivines to Grain Sizes less than ~60μm

↓

Stage VI: Final Assembly of the fine-grained Reduced Olivines with other E-chondritic Components (e.g., Sulfides) to Form Y-691 Chondrite at Temperatures lower than about 500°C

Stage IIa': Fragmentation

↓

Stage IIb': Weak or No Annealing

HETEROGENEOUS MIXING OF FALL OUT DEPOSITS AS SEEN IN THE YAMATO POLYMICT EUCRITES. Akira Yamaguchi, Kazuto Saiki, and Hiroshi Takeda. Mineralogical Inst., Faculty of Science, Univ. of Tokyo, Hongo, Tokyo 113, Japan.

Introduction The polymict eucrites have been interpreted to be lithified ejecta deposits from craters produced by impact of various-sized meteorites and hence various depths of excavation of the crust on the HED (Howardites-Eucrites-Diogenites) parent body [1]. Many polymict eucrites recovered from Antarctica have been classified into several suites [2]. In order to obtain better understanding of a more comprehensive view of the Antarctic polymict eucrites and the impact and subsequent thermal histories on the HED-parent body, we have compared Yamato (Y) -793547,51-1, Y-793548,51-1 and 51-2, and Y-793570,52-2 (Y-79 eucrites) to Y-74159-type polymict eucrites. These samples have similar common components, and have high possibility of belonging to the same suite. The results may yield information about mixing of fall out deposits produced by the impact event of a surface region of the HED-parent body.

Results We have investigated a polished thin section (PTS) of Y-793547,51-1 by optical microscope, scanning electron microscope (SEM) equipped with energy dispersive spectrometer (EDS), X-ray chemical map analysis, and electron probe microanalyzer (EPMA). In addition to the samples of previous study [3], we have compared it with the Y-79 polymict eucrites (Y-793548, and Y-793570), and the Y-74159-type polymict eucrites (Y-74450, Y-75011) mineralogically and petrographically.

The PTS of Y-793547 shows textures of a typical fragmental breccia composed of lithic clasts, mineral fragments of pyroxene and plagioclase, and comminuted fine-grained matrix. Most of the lithic clasts are composed of unequilibrated mafic clasts which have variolitic to subophitic textures. The lithic clasts of Y-793547 are similar to those of the Y-793548 and Y-74159-type. Some lithic clasts have fayalite-veinlet within the zoned pyroxene crystals. Most mineral fragments are unequilibrated types. The matrix consists of comminuted fragments of eucritic materials and is not recrystallized. Chemical compositions of pyroxenes in the PTS are plotted in the pyroxene quadrilateral (Fig. 1a). There are higher proportion of exsolved pyroxenes (less than 0.1 mm) of the possible Juvinas-type [2] in a part of the matrix. There is a large grain (0.9x0.4 mm in size) of inverted pigeonite with blebby augites similar to that in Binda.

Mineralogy of Y-793548 and Y-793570 have been described previously in detail [3]. The Y-793548 and Y-793570 are breccias mostly composed of rapidly cooled materials such as chemically unequilibrated pyroxenes. Y-793548 is unequilibrated monomict breccia containing a few fragments of ordinary eucrites. The Y-793548 contains a few small exsolved pyroxene type less than 40μm in the matrix, and does not contain deeper materials. Chemical compositions of pyroxenes of Y-74450 (Y-74159-type) are shown in the pyroxene quadrilateral (Fig. 1b).

Discussion In this study of Y-793547, we found the same characteristics within Y-793547 as those of Y-74159-type and Y-793548/70. The variolitic clasts in Y-793547 are comparable with those of Y-793548. The matrix rich in zoned pyroxenes is comparable to the matrix of Y-793570 and Y-793548. All the unequilibrated mafic clasts in the Y-79 eucrites which include Pasamonte-type or a pyroxene (type-1, [4]) of pristine basaltic clast in Y-75011 are comparable to Y-74159-type polymict eucrites. Differences among these samples are presence of the Binda-type pyroxenes and high abundances of exsolved pyroxene fragments in Y-793547 and the Y-74159-type.

The presence of minor components such as the Binda or Moore County-type pyroxenes often makes classification difficult. Y-74450 was once described as similar to Pasamonte on the

basis of one clast sample available for the classification [5]. Furthermore, in the PTS of Y-793547, it was found heterogeneous distribution of exsolved pyroxene fragments. In the Y-74159-type polymict eucrites, there may be mixing of monomict breccia portions in polymict breccia portions which may be attributed to mixing heterogeneity within ejecta deposits. Mineralogical study of Y-793547 and Y-793548 [2] demonstrates that there may be local heterogeneity within the Y-74159-type suites. Y-793547 represents intermediate portions between the Y-74159-type and Y-793548.

In our previous study [3], we concluded that Y-793548 and Y-793547 do not belong to the Y-74159-type because of these specialities that these specimens are unequilibrated monomict eucrites similar to Pasamonte. Miura et al. [6] reported terrestrial ages of some eucrites, and classified Y-793547 into Yamato-I suite (Y-74159-type). In this study of Y-793547, we found the same characteristics within Y-793547 as those of Y-74159-type and Y-793548/70. There are two possibilities to consider the specialities of Y-793548 and Y-793570. (1) Y-793548 and Y-793570 belong to the single suite. (2) These meteorites have been composed of unequilibrated mafic-clast-rich portions in an original meteoroid of the Y-74159-polymict eucrite. According to the terrestrial ages determined by Miura et al. [6], the sampling location in Antarctica [7], and the present observation of Y-793547, we conclude that the specialities of Y-793548 and Y-793570 can be attributed to mixing heterogeneity of fall out deposits on the parent body.

Theoretically, any eucritic breccia represents a portion of the continuum from unequilibrated monomict eucrite such as Pasamonte to typical clastic matrix polymict eucrite depending on the degree of mixing of different lithologies on the surface of the HED-parent body. Therefore, it is natural to consider that the proportions of components differ gradually. While the components of the Y-74159-type polymict eucrites are limited in members, mixing ratio of each component in the this type polymict eucrites are variable. Thus, complete mixing of the components is difficult to achieve on the parent body. We conclude that the mixing of fall out deposit produced by impact cratering event is not always homogeneous in centimeters scale as observed in the Y-74159-type polymict eucrites.

We thank National Institute of Polar Research for the meteorites specimen and T. Ishii, E. Yoshida, and O. Tachikawa for their help in microanalysis.

References 1. Takeda, H. (1979) Icarus, 40, 445-470. 2. Delaney, J. S., Prinz, M., and Takeda, H. (1984) Proc. Lunar Planet. Sci. Conf. 15th, in J. Geophys. Res.,89, suppl., C251-C288. 3. Yamaguchi, A. and Takeda, H. (1992) Proc. NIPR Symp. Antarct. Meteorites. 5, 1992, p.242-257. 4. Takeda, H. and Graham, A. L. (1992) Meteoritics 26, 129-134. 5. Takeda, H., Miyamoto, M., Duke, M. B., and Ishii, T. (1978) Proc. Lunar Planet. Sci. Conf., 9th, 1157-1171. 6. Miura, Y., Nagao, K., and Fujitani, T. (1991) 16th Symp. Antarctic Meteorites., 129-130. 7. Yanai, K. and Kojima, H. (1987) Photographic Catalog of the Antarctic Meteorites NIPR, Tokyo, Natl. Inst. Polar Res., 298 p.

Fig. 1. Pyroxene quadrilaterals of Y-793547,51-1 and Y-74450. The tie lines with triangles connect exsolved pairs. The lines with filled circles indicate traverses from core to rim of the zoned pyroxenes.

(a) Y-793547,51-1

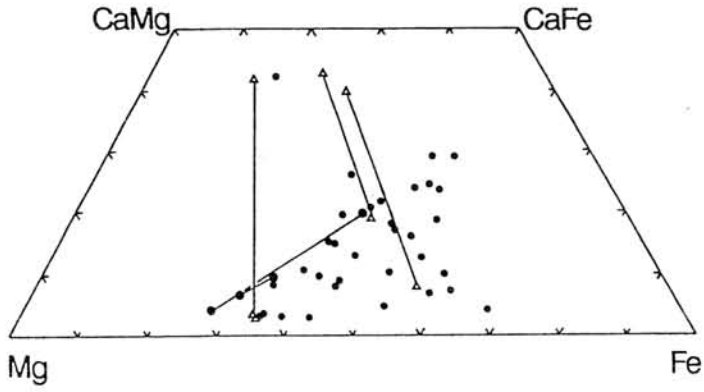

(b) Y-74450

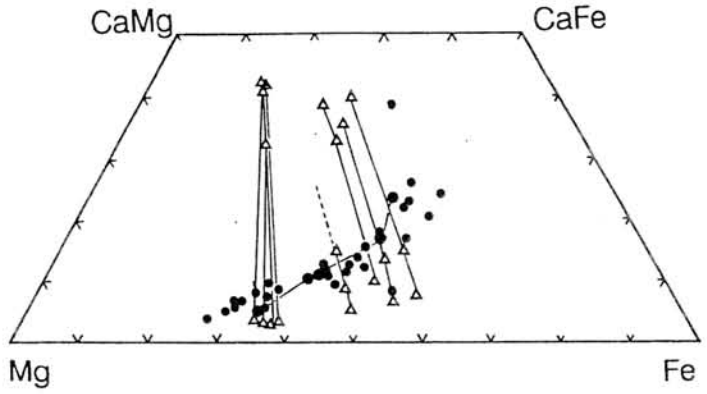

SPECTRAL COMPARISON BETWEEN OLIVINE-RICH ASTEROIDS AND PALLASITES.
Takahiro Hiroi[1], Jeffery F. Bell[2], Hiroshi Takeda[3], and Carle M. Pieters[4]. [1]SN3, NASA/JSC, Houston, TX 77058, U.S.A. [2]Planetary Geosciences, SOEST, Univ. of Hawaii, 2525 Correa Rd., Honolulu, HI 96822, U.S.A. [3]Mineralogical Institute, Univ. of Tokyo, Hongo, Tokyo 113, Japan. [4]Dept. of Geological Sciences, Brown Univ., Providence, RI 02912, U.S.A.

The similarity of reflectance spectra between olivine-rich asteroids and pallasites is one of the clearest understandings about the relationship between asteroids and meteorites together with the one between Vesta-like asteroids and HED achondrites. Two asteroids (246 Asporina and 289 Nenetta) in the main belt were the first ones that were found to be olivine-rich by high resolution near-infrared reflectance spectra, and their similarity to Chassigny and Brachina were pointed out [1]. Their similarity to pallasites was also shown by simulating the pallasite assemblage with some combinations of metallic iron and powder olivine [2]. Olivine-rich asteroids were later found also in Earth-crossing orbits [3], which increased our expectation to find their counterparts among our meteorite collections. Recent 52-color near-infrared measurements [4] found three more olivine-rich asteroids (113 Amalthea, 354 Eleonora, and 446 Aeternitas) in the main belt. In this study we have newly measured reflectance spectra of two pallasites (Y-8451 and Imilac) and compared them with those of four olivine-rich asteroids in the main belt.

Pallasites contain large amount of metallic iron, whose reflectance spectrum largely depends on the surface condition and viewing geometry not only on its chemical composition (Fe/Ni ratio). We polished one side of Imilac chip with sand paper No. 60 to roughen the surface and obtain diffuse reflection of light. The other side was a cut surface somewhat rusted. A metallic-iron portion and two olivine grains on the former rough side, and two olivine grains on the latter smooth side, were chosen for reflectance spectra measurements at the diffuse geometry (30° incidence and 0° emergence). Y-8451,20 chip was cut by National Institute of Polar Research, and three different portions of it were measured at the diffuse geometry and one portion at the specular geometry (15° incidence and -15° emergence). Those measured reflectance spectra are shown in Fig. 1.

Four olivine-rich asteroids 113 Amalthea, 354 Eleonora, 246 Asporina, and 446 Aeternitas [1, 4, 5] were chosen for linear spectral fittings with those 9 spectra of two pallasites as the end members. The method is the same with our previous work [6] that assumes the asteroidal surfaces are some kind of regional mixtures of meteorites. The results are shown in Fig. 2 and listed in Table 1. While 113 Amalthea is well-fit with mainly Y-8451 spectra, the others are not well-fit in terms of absorption band shapes and positions. The optimized albedo of Amalthea is also similar to the IRAS albedo [7]. This result suggests that Amalthea can be similar to Y-8451.

The other three asteroids are not so well-fit with two pallasites in this study. One of the spectral differences between those asteroids and pallasites, is the absorption band depth. In order to produce their reddened profiles, much metallic irons must be mixed, which decreases the absorption band depth. As the result, more iron-rich olivines should exist on the surfaces of those asteroids. Another difference is that those asteroids have linear steep slopes in visible range (0.3-0.7μm), which is difficult to produce by any combination of metallic irons and olivines.

There is much possibility that the assumption of regional mixing of metallic iron and olivine grains is not valid for those asteroids. Lunar soils show highly reddened spectral profiles without any metallic-iron domains, which is not well-understood so far [8]. Some kind of regolith formation process by heavy impact craterings may change chemical properties of mineral grains on the asteroidal surfaces as happened on the moon.

Because Y-8451 is spectroscopically very similar to 113 Amalthea, it will be meaningful to describe some mineralogical characteristics of Y-8451. Y-8451,61-1 polished thin section we examined, is composed of interconnected rounded crystals of olivine filled with thick bands of metals. The grain boundaries between olivine and metal and between olivine grains in a few cases are filled with thin films of Ni-containing iron hydroxides, and a few boundaries are intruded by thi tongue of metals. Olivine crystals have numerous fractures and are fragmented

into small pieces at some olivine-olivine boundaries, and a few metal-olivine boundaries show slight dislocations, which indicates shock deformations. The crystal sizes of olivine are 3mm or less in diameters, which are smaller than those of common pallasites such as Imilac.

At one corner of an olivine crystal facing to metal, one subrounded orthopyroxene ($Ca_{2.1}$ $Mg_{88.9}$ $Fe_{9.0}$) crystal is present. In another olivine, two joined elongated petal-shaped low-Ca pyroxenes ($Ca_{0.6}$ $Mg_{90.7}$ $Fe_{8.7}$) are present. The composition is uniform within the grains and distinctly lower in Ca than the orthopyroxene. The compositional relation indicates that these low-Ca pyroxenes may be inverted protoenstatites (orthopyroxenes). This is the second example of the coexisting proto-orthopyroxene in meteorites. By applying temperature-composition (Fe/Fe+Mg ratio) diagram for Steinbach [9], one can obtain 1135°C as their formation temperature. The presence of protoenstatite suggests that the pressure was not as high as that of a large planetary interior (diameter of Amalthea is about 48km [7]).

The chemical compositions of olivines in Y-8451 (Fa_{10-11}) are more Mg-rich than common pallasites (*e.g.* Imilac $Fa_{12.5}$ [10]). The modal abundances of minerals are: olivine 63%, metal-sulfide 30%, orthopyroxene 3%, protopyroxene 0.1%, and oxide vein 4% in volume. The small sizes and Mg-rich compositions of olivine crystals in Y-8451 imply its affinity to primitive achondrites [11]. Further determination of the oxygen isotopes is required to be sure of its classification as a pallasite. A primitive achondrite Y-791058 contains much amount of metallic iron (80 vol%) with silicate inclusions rich in plagioclase, which is the similar domain structure to pallasites.

Although meteorites are the primary candidates for asteroidal surface materials, they may have experienced some terrestrial weathering that affected their reflectance spectra significantly. Therefore, the more analytical studies should be done to obtain better information about asteroidal surface mineral assemblages by using laboratory reflectance spectra of weathering-free minerals.

Table 1. The results of spectral fits of olivine-rich asteroids with two pallasites.

	Modal abundances (area %)			Albedo %		Relative
	Y-8451 specular	Y-8451 diffuse 1	Imilac olivine 2	Optimized	IRAS*	error %
113 Amalthea	2.9	76.4	20.6	21.0	27	5.8
354 Eleonora	8.0	47.1	45.0	31.8	19	8.8
246 Asporina	15.7		84.3	45.3	13	12.5
446 Aeternitas	8.7		91.3	29.3	35	15.8

* Tedesco (1989).

ACKNOWLEDGMENT: We thank Dr. K. Yanai and National Institute of Polar Research for Y-8451 chip. Reflectance spectra of all the meteorites were measured at RELAB in Brown University, U.S.A. We thank S. F. Pratt for those measurements. RELAB is a multiuser facility supported by NASA under NAGW-748. The electron probe microanalyses were performed at Ocean Research Institute of University of Tokyo. This work was done while one of the authors (T. Hiroi) held a National Research Council-NASA/JSC Research Associateship.

REFERENCES: [1] Cruikshank D.P. and Hartmann W.K. (1984) *Science* 223, 281-283. [2] Bell J.F., Gaffey M.J., and Hawke B.R. (1984) *Bull. Am. Astron. Soc.* 16, 708-709. [3] Cruikshank D.P., Hartmann W.K., Tholen D., and Bell J.F. (1985) *Lunar and Planetary Science* XVI, 160. [4] Bell J.F., Owensby P.D., Hawke B.R., and Gaffey M.J. (1988) *Lunar and Planetary Science* XIX, 57-58. [5] Chapman C.R. and Gaffey M.J. (1979) In *Asteroids* pp. 1064-1089. [6] Hiroi T., Bell J.F., Takeda H., and Pieters C.M. (1992) *Lunar and Planetary Science* XXIII, 543-544. [7] Tedesco E.F. (1989) In *Asteroids II*, pp. 1090-1138. [8] Pieters C.M., Fischer E.M., Msustard J.F., Pratt S.F., and Basu A. (1992) *Lunar and Planetary Science* XXIII, 1071-1072. [9] Reid A.M., Williams R.J., and Takeda H. (1974) *Earth Planet. Sci. Lett.* 22, 67-74. [10] Buseck P.R. (1977) *Geochim. Cosmochim. Acta* 41, 711-740. [11] Hiroi T. and Takeda H. (1991) *Proc. NIPR Symp. Antarct. Meteorites* 4, 163-177.

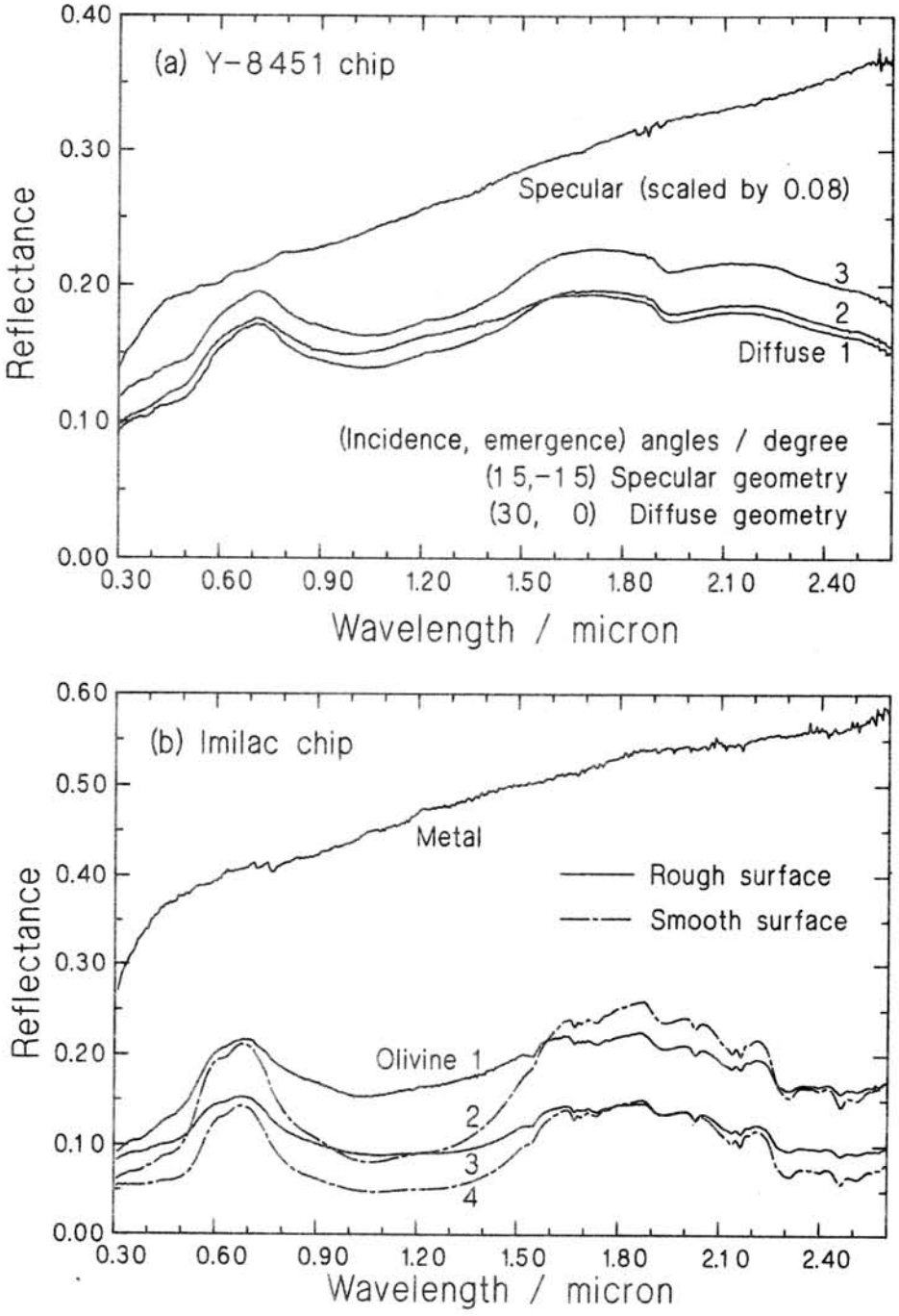

Fig. 1. Reflectance spectra of two pallasite chips. (a) Y-8451 chip with cut surfaces. Three points were measured at the diffuse geometry, and one point at the specular geometry. Actual reflectance of the specular-geometry measurement is 100/8 times higher than is shown. (b) Imilac chip with two different sides. Two olivine grains were measured on the cut surface (smooth) and are shown with broken lines. Metallic iron and two olivine grains were measured on the other side (rough) polished with sand paper No. 60 and are shown with solid lines. They were all measured at the diffuse geometry.

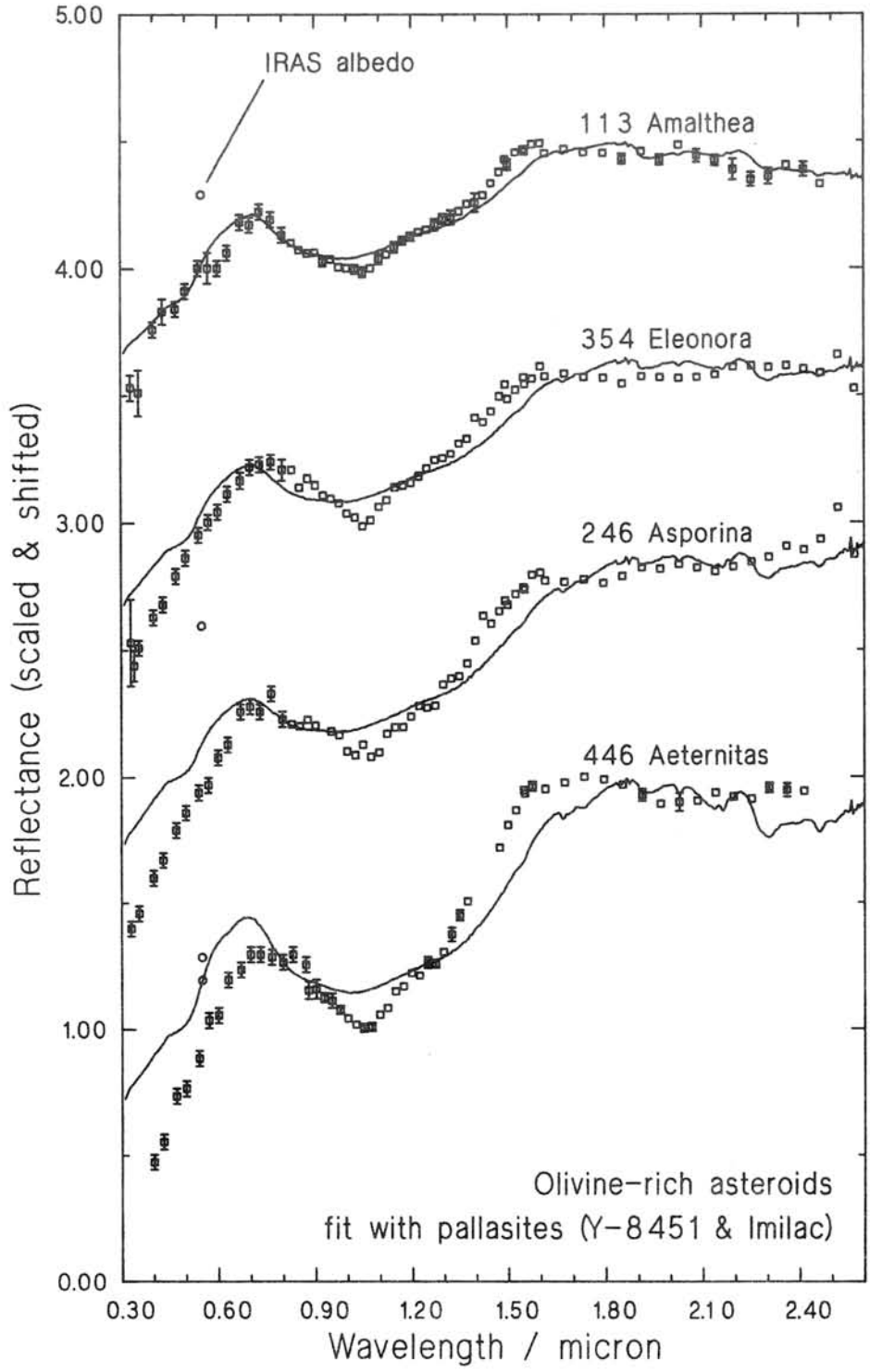

Fig. 2. Linear spectral fits of four olivine-rich asteroids [1, 4, 5] with pallasites Y-8451 and Imilac. All the reflectance spectra are scaled to 100% at 0.55μm and shifted by reflectance 100% from one another. IRAS albedos [7] are plotted with open circles at 0.55μm.

EXAMINATION OF INSOLUBLE ORGANIC MATTER IN SOME ANTARCTIC AND MURCHISON CARBONACEOUS CHONDRITES BY A DTA/TG-GC/MS METHOD

Komiya M. and Shimoyama A.
Department of Chemistry, University of Tsukuba, Tsukuba 305

We have examined organic compounds in some Antarctic carbonaceous chondrites by a DTA/TG-GC/MS (differential thermal analysis / thermogravimetry - gas chromatography / mass spectrometry) method using powdered chondrite samples[1]. Organic compounds in carbonaceous chondrites are mostly present as insoluble macromolecular organic matter. Therefore, we isolated insoluble organic matter in those Antarctic carbonaceous chondrites and examined by the method[2]. In the present study, we examined the insoluble organic matter isolated from the Murchison carbonaceous chondrite by the method and compare the results with those of Antarctic samples.

An interior piece of the Murchison chondrite was powdered and treated with HF/HCl to demineralize and concentrate the insoluble organic matter. Then it was washed with carbon disulfide, methanol, successively to remove inorganic sulfur compounds. The sample was placed in the thermal analyzer (DTA/TG instrument) and heated under helium atmosphere from room temperature to 800°C at the rate of 10°C/min. The released compounds were directly introduced into a mass spectrometer (direct-MS method) and their intensities were continuously observed along the heating temperature.

The results of the heating experiment are shown in Fig.1. In the heating, hydrocarbon generally appear at 300-400°C, and disappear at 600°C with maximum at 400-500°C. Larger molecular hydrocarbons were detected over relatively high temperature range compared with smaller ones. For example, appearance of pyrene was started at 450°C and ended at 700°C with maximum at 480-490°C. These results are basically similar to those of previous results of insoluble organic matter from Yamato-74662 and Yamato-791198, both Antarctic CM2 chondrites[2] and suggest that the constituents of insoluble organic matter of Murchison is similar to those of two Antarctic carbonaceous chondrites.

As shown in Table 1, the total weight loss from room temperature to 800°C of the Murchison sample was 32.3% and the value is close to those of Yamato-791198 and Yamato-74662 sample. The results of elemental analysis of the Murchison sample before and after the heating are also shown in Table 1 with those of Antarctic carbonaceous chondrite samples. The H/C molar ratio of Murchison before the heating is 0.70, close to the value of Yamato-74662 and Yamato-791198.

For the identification of compounds released from the insoluble organic matter of Murchison, we used a trap-GC/MS method and the results are also discussed.

We thank Dr. E. Olsen (Field Museum of Natural History, Chicago) for kindly providng a stone sample of the Murchison chondrite.

REFERENCES:
1]Shimoyama A., Komiya M. and Harada K.(1991), *Proc. NIPR Symp. Antarct. Meteor.*,**4**, 247-260, [2]Komiya M., Shimoyama A. and Harada K.(1991), *Abstr. 16th Symp. Antarct. Meteor.*, pp.45-47.

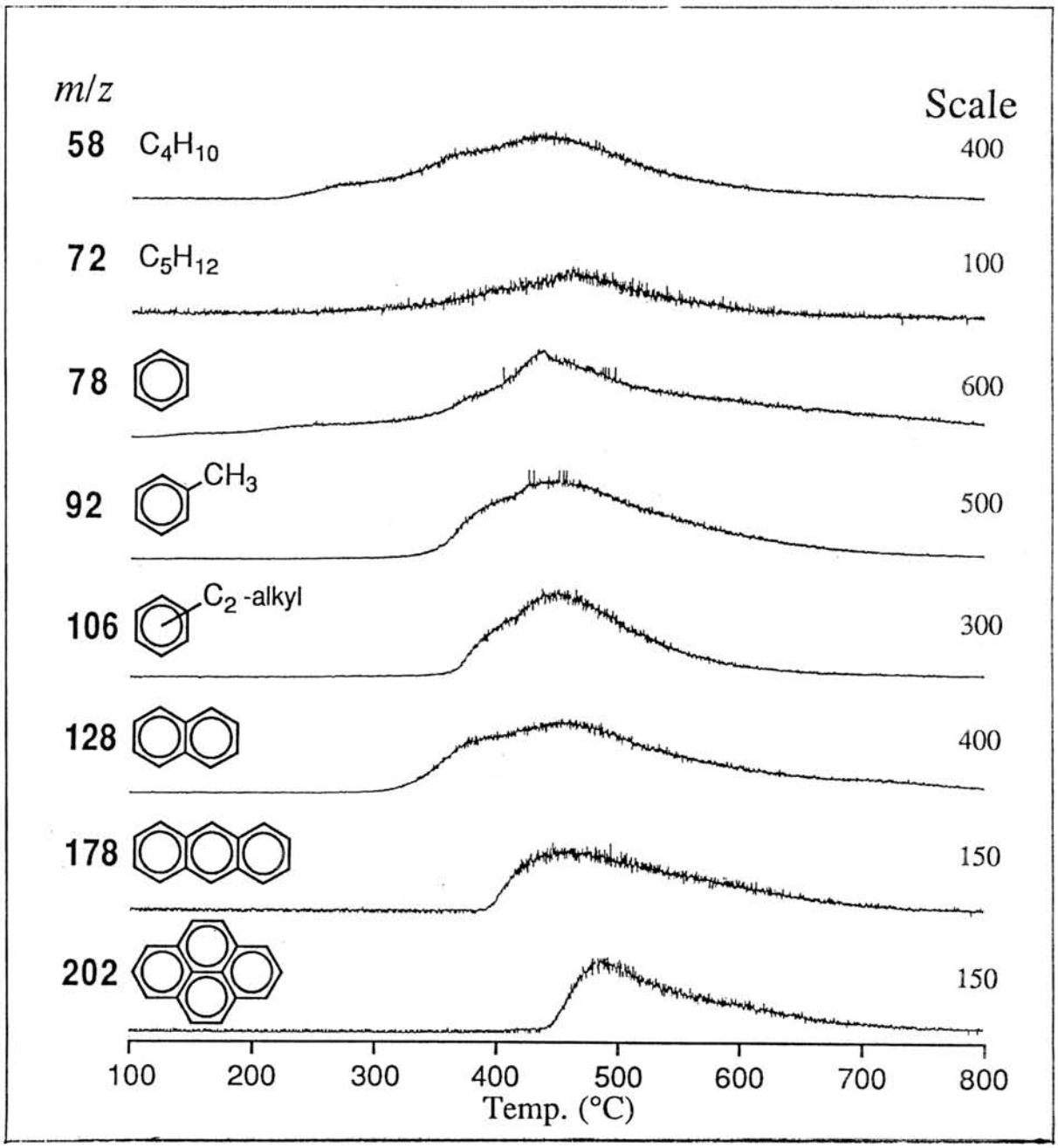

Fig. 1. Intensities of ions for compounds along the heating temperature from the insoluble organic matter isolated from Murchison by the treatment with HF/HCl.

Table 1 Elemental compositions of the insoluble organic matter isolated from carbonaceous chondrites by the treatment with HF/HCl for the heating experiment to 800°C

Chondrite	Sample wt. used(mg)	reduced(%) (r)		Contents(%) before (b)	after (a)	remained a/b(100-r)	H/C(molar ratio) before	after
Murchion	4.2	32.3	C	56.9	72.8	86.6	0.70	0.26
			H	3.3	1.6	32.8		
			N	2.6	2.3	59.9		
Y-74662	2.9	25.0	C	57.2	68.9	90.3	0.57	0.13
			H	2.7	0.75	20.8		
			N	2.7	2.3	64.0		
Y-791198	3.7	29.9	C	57.6	72.6	88.4	0.67	0.17
			H	3.2	1.0	22.6		
			N	2.5	2.2	61.6		
Y-793321	4.8	21.1	C	64.2	75.9	93.3	0.36	0.13
			H	1.9	0.80	33.6		
			N	2.9	2.9	78.4		
B-7904	4.6	16.7	C	64.3	70.5	91.3	0.15	0.10
			H	0.79	0.60	63.3		
			N	2.2	2.2	83.3		
Y-86720	4.9	12.4	C	67.3	75.5	98.3	0.11	0.05
			H	0.64	0.33	45.1		
			N	1.3	1.4	95.2		

DICARBOXYLIC ACIDS IN THE YAMATO-791198 AND MURCHISON CARBONACEOUS CHONDRITES

Shimoyama, A. and Shigematsu R.

Department of Chemistry, University of Tsukuba, Tsukuba 305

Carbonaceous chondrites contain various kinds of abiotic organic compounds. The presence of dicarboxylic acids in the Murchison chondrite has been reported by Lawless et al. (1974) and Peltzer et al.(1984). We analyzed these organic compounds in Yamato-791198 (CM2) and Murchison (CM2) and obtained useful information to report.

Powdered samples of Yamato-791198 (80 mg) and Murchison (500 mg) were extracted with water by sonication. The extracted solution of Murchison was divided into three aliquots. The Yamato-791198 extract and an aliquot of the Murchison extract were treated with 15% BF_3/methanol to make dimethyl esters of dicarboxylic acids. Another aliquot of the Murchison extract was treated with (S)-2-BuOH/2M HCl to obtain the optically active dibutyl esters of the acids. Gas chromatographic and mass spectrometric (GC-MS) analyses were performed for identification and quantification of the compounds. Elemental analyses show the Yamato-791198 powdered sample contains 2.3% carbon and 0.13% nitrogen, and the Murchison sample 2.0% carbon and 0.16% nitrogen.

A total of 27 dicarboxylic acids is identified and their concentrations are estimated(Table 1). These acids are in the C_2 (oxalic acid) to C_9 (azelaic acid) range and include eight saturated straight-chains, four unsaturated straight-chains, thirteen saturated branched-chains, one unsaturated branched-chain, and one aromatic structure.

All structural isomers of the saturated chain molecules with four, five, and six C atoms are found except some malonic acid derivatives. Six of the possible 20 isomers are found with the seven C atom molecules. As to the unsaturated molecules, the two C_4 acids (fumaric and maleic) and the three C_5 acids (mesaconic, citraconic, and itaconic) are found.

Figure 1 shows mass fragmentograms of the optical isomers as (S)-2-dibutyl esters from the Murchison sample. The S/R ratios are found to be nearly one with methylsuccinic, ethylsuccinic, 2-methylglutaric, and 2-ethylglutaric acids.

The presence of these various kinds of structures and isomers indicates abiotic origin (therefore, indigenous to the chondrites) of the dicarboxylic acids.

Oxalic acid (the smallest in size) is the most abundant of the acids in both Yamato-791198 and Murchison. The plots of log concentration vs C number of the acids give approximately straight line in the range of C_2 to C_7 straight-chain molecules (except malonic acid at C_3) as seen in Fig. 2.

The straight-line relation indicates that Yamato-791198 has not lost the dicarboxylic acids by wash with Antarctic water and likely indicates that the acids in the two chondrites are primary products in such reactions as electric discharge in the early solar nebula or ion-molecule reactions in presolar environments. Thermal reactions such as Fischer Tropsch type in the early solar nebula or thermal syntheses on the parent body may not be adequate to explain the straight-line relations. The depletion in concentration of malonic acid is probably due to its thermally very unstable property, and therefore, it still remains to be answered how pristine these acids are, if they are primary.

Similar types of the straight-line relations have been shown with monocarboxylic acids in Murchison (Yuen et al., 1984) and Aska-14 (Naraoka et al., 1991). Further detail examinations of mono- and di-carboxylic acids in carbonaceous chondrites provides more useful information on their origin and transformation during aqueous and thermal alteration of the chondrites.

We thank Dr. E. Olsen (Field Museum of Natural History, Chicago) for kindly providing a stone sample of the Murchison chondrite.

References

Lawless, J.G., Zeitmann, B., Pereira, W.E., Summons, R.E., and Duffild, A.M.(974): Nature, 251, 40.
Naraoka, H., Shimoyama, A., and Harada, K.(1991): Abst. 16th Symp. Antarct. Meteorites, 146.
Peltzer, E.T., Bada, J.L. Schesinger, G., and Miller, S.L.(1984): Adv. Space Res., 4, 69.
Yuen, G.U., Blair, N., Marais, D., and Chang, S.(1984): Nature, 307, 252.

Table 1. Concentrations of dicarboxylic acids in the water extracts of the Yamato-791198 and Murchison chondrites (nmol/g)

Compound	Yamato-791198	Murchison
Oxalic acid	1900	2100
Methylmalonic acid	3.7	9.2
Malonic acid	20	96
Ethylmalonic acid	2.3	2.3
2,2-Dimethylsuccinic acid	1.4	8.8
Fumaric acid	< 1.5	< 8.1
(meso)-2,3-Dimethylsuccinic acid	0.39	1.8
Methylsuccinic acid	16	48
(DL)-2,3-Dimethylsuccinic acid	1.0	5.9
Succinic acid	21	97
Mesaconic acid	< 0.5	< 1.9
(meso)-2,4-Dimethylglutaric acid	n.d.	n.d.
Ethylsuccinic acid	3.8	14
Maleic acid	0.3	1.0
Itaconic acid	< 0.1	< 0.4
2-Methylglutaric acid	3.1	15
3-Methylglutaric acid	1.2	4.7
Citraconic acid	3.7	19
Glutaric acid	6.8	24
Ethylglutaric acid	n.d.	2.9
2-Methyladipic acid	0.7	1.6
Adipic acid	2.3	5.8
3-Methyladipic acid	0.9	1.9
Pimeric acid	0.5	2.0
Suberic acid	0.3	1.7
Azelaic acid	0.3	3.2
Phthalic acid	3.2	3.2

n.d. : not determined

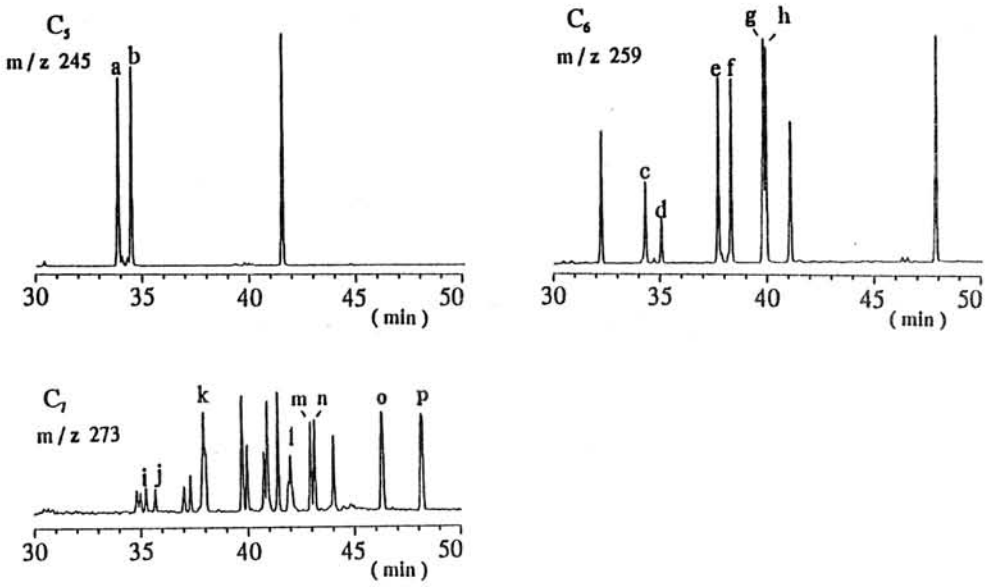

Fig. 1 Mass fragmentograms of dicarboxylic acid (S)-2-dibutyl esters from the water extract of the Murchison chondrite. Peak No., a. (S)-methylsuccinic acid, b. (R)-methylsuccinic acid, c and d. (DL and meso)-2,3-dimethylsuccinic acid, e. (S)-ethylsuccinic acid, f. (R)-ethylsuccinic acid, g. (S)-2-methylglutaric acid, h. (R)-2-methylglutaric acid, i and j. (DL)-2,4-dimethylglutaric acid, k. (meso)-2,4-dimethylglutaric acid, l. (DL)-2,3-dimethylglutaric acid, m. (S)-2-ethylglutaric acid, n. (R)-2-ethylglutaric acid, o. (RS)-2-methyladipic acid, p. (RS)-3-methyladipic acid.

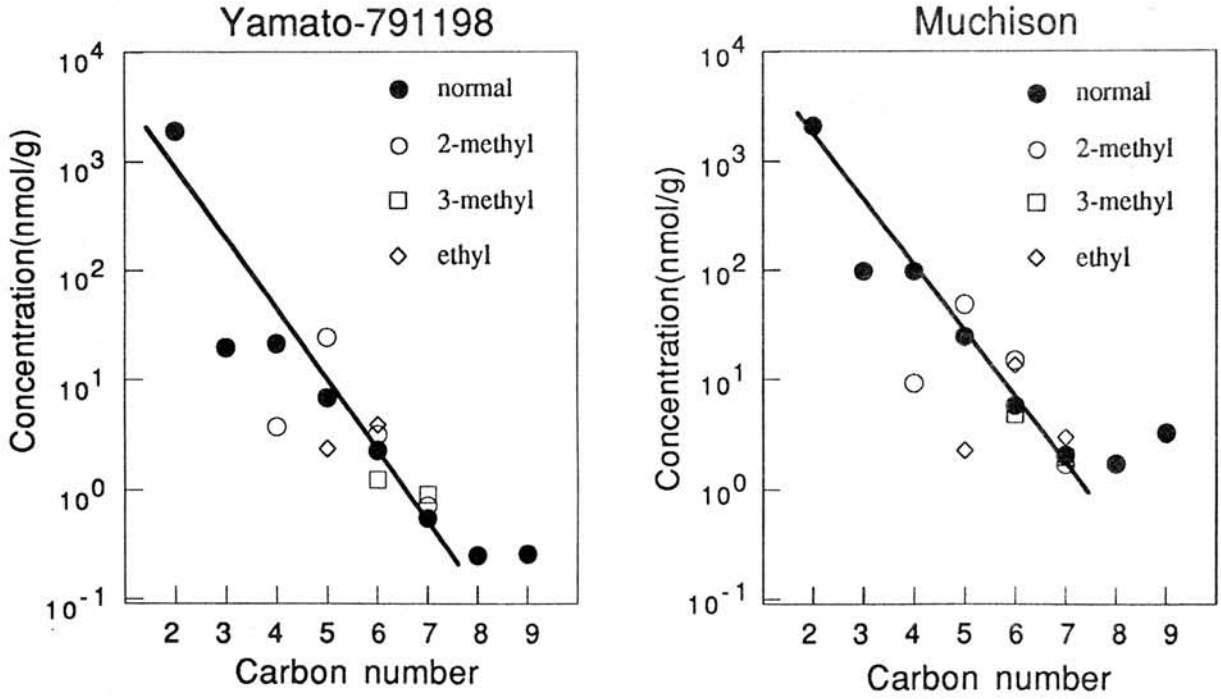

Fig. 2 Concentrations of dicarboxylic acids against carbon number in the Yamato-791198 and Murchison carbonaceous chondrites.

SPECTROSCOPIC STUDY OF MAJOR ORGANIC MATTER IN CARBONACEOUS CHONDRITES BY MICROSCOPIC FT-IR.

Tatsushi Murae.
Department of Earthand Planetary Sciences, Faculty of Science, Kyushu University, Hakozaki, Fukuoka, 812 Japan.

Introduction The major organic matter in carbonaceous chondrites is not extractable in any solvent. This insoluble material may account for from about 70 percent to essentially all of the meteoritic carbon [1,2]. A model of general structure for the solvent-unextractable organic matter has been proposed by the author and co-workers based on the data obtained by various analytical methods [3]. Partial alterations of the structure of the organic matter in carbonaceous chondrites probably reflect secondary thermal metamorphism of the meteorites [4].

Experimental methods Powdered samples of meteorites and residues obtained by partial mineral dissolution with acid treatments of the meteorites were used for the determination of the IR spectra. The samples of carbonaceous chondrites and the acid-resistant residues from the meteorites are black powder. Although IR spectra afford valuable informations on the structure of organic matters, it was difficult to observe IR spectra from black fine powdered samples. Diffuse reflection method could overcome the difficulty, but the spectral intensity was weak and enrichment of carbonaceous matter was necessary to obtain meaningful spectra [3]. We succeeded to measure IR spectra of powdered black samples containing organic matter with low concentration using recently developed microscopic FT-IR technics. The powdered samples were buried on the surface of aluminum foils with mechanical press. The buried samples gave absorption spectra on operations of the microscopic IR instrument under reflection mode. Samples less than 1 mg afforded spectra with enough intensity.

Results and discussion Table 1 lists IR data for the samples from carbonaceous chondrites and the data determined by the same methods for coronene and anthracene. Although some differences are observed in details in the spectra for the samples from meteorites, whole features of these spectra resemble each other. The spectra for meteorite samples area not so complex as those for coronene and anthracene, but most of the characteristic absorption bands for aromatic compounds were observed. This fact indicates that the major organic component in the chondrites is aromatic compound having some structural heterogeneity. In the spectra from some meteorite samples, the absorption bands assignable to C-H bonds disappeared to indicate the presence of large condensed aromatic rings. Rather simple feature of absorption bands assignable to C=C bonds also indicates the presence of large aromatic networks. Differences were observed in the spectra of the samples before and after acid treatments. It is not clear whether the difference is due to the change of aggregation form of the organic matter or due to structural changes of them.

References 1. Hayes J.M.(1967) GCA **31**, 1395-1440. 2. Han J., Simoneit B.R., Burlingame A.C. and Calvin M. (1969) Nature **222**, 364-365. 3. Murae T., Masuda A. and Takahashi T. (1990) Proc. NIPR Symp. Antarct. Meteorites **3**, 211-219. 4. Murae T., Kitajima F. and Masuda A. (1991) Proc. NIPR Symp. Antarct. Meteorites **4**, 384-389.

Table 1. IR spectral data (expressed in CM^{-1}) for the samples from carbonaceous chondrites and for coronene (1) and anthracene (2).

1[a]	2[b]	Allende[c]	Allende[d]	Murchison[d]	Y-74662[f]	Y-74662[g]	ALH-77307[d]	ALH-77307[f]	Y-791198[e]	Y-791717[f]	Y-791717[g]
3049	3050	3054									
3019	3022				3011			3011	3000		
2923	2988		2968	2972		2968	2956			2963	
2850		2825		2802	2822			2778	2754		2744
2613		2809		2731							
2568		2550									
2432	2411		2489	2448	2455	2469	2467	2467	2456	2485	2478
2290	2275	2290									
2121			2137	2153	2160	2133	2144	2155	2158	2179	2156
	2084	2070									
	1946		1940			1933					
1861	1859		1880	1883	1861	1880	1883	1894	1883	1867	1872
	1808	1820									
1616	1621	1605	1608	1604	1610	1610	1613	1594	1603	1612	1620
						1623					
1349					1349		1350				
1313	1317		1305	1322					1322	1317	1322
	1272			1272				1283			1272
	1240	1222	1231			1228				1232	
1184	1167		1183	1179			1178	1202	1189	1183	1201
1135	1147				1150	1148					
		1068	1074	1059	1039	1078	1039	1061	1050	1076	1056
	979	979					978				
958	957		956		949						
	931									928	
	906			910			917	906			917
	888		877						894		
854	859					852					
845										837	
770		779	773					772			
	753			758	763	745					
	737						739		739		744
						678	670	711		674	

a)Other remarkable absorptions for 1: 2368, 2360, 2350, 1907, 1892, 1779, 1714, 1693, 1651, 1574, 1552, 1529, 1499, 1414, 1126, 812 cm^{-1}. b)Other remarkable absorptions for 2: 2359, 2350, 2342, 2328, 2314, 1928, 1784, 1724, 1694, 1574, 1558, 1534, 1505, 1449, 1398, 1126, 998 cm^{-1}. c)Low density organic matter obtained on acid treatments. d)No acid treatments, e)No acid treatments, focused on a black part using an aperture f)Treated with HCl-HF. g)Residues obtained

A comparative structural study of the carbonaceous macromolecular materials in carbonaceous chondrites with several synthetic polymers.

Fumio Kitajima and Akimasa Masuda.
Department of Chemistry, Faculty of Science, The University of Tokyo, Hongo, Bunkyo-ku, Tokyo 113.

Carbonaceous chondrites belong to a group of primitive meteorites and one of those characteristics is relatively high carbon contents. Certain fractions of the carbon exhibit enrichments in ^{12}C, ^{13}C or D, and are considered as the host phases for isotopically anomalous noble gases such as Xe-HL, Ne-E. The isotopic heterogeneity indicates the various origins of the carbonaceous materials in the chondrites. The carbonaceous materials consist of extractable low-molecular organic compounds such as amino acids, insoluble organic macromolecular materials, carbonates, graphites, diamonds, silicon carbides, etc. Polyoxymethylene, which is suggested to exist in the core of Comet Halley, and/or Buckminsterfullerenes are/is also expected to exist in carbonaceous chondrites, however, the existence of them has not yet been confirmed. The major component of the carbon in carbonaceous chondrites is insoluble macromolecular materials. The fine-structure of those materials is considered to reflect the formation histories of them. Although the materials are considered to contain large networks of polyaromatic compounds, the fine-structure has not yet been clarified well because of the difficulty of chemical separation and the lack of satisfactory method of characterization of such insoluble macromolecular matter in a solid state.

In this investigation, we have examined the structures of carbonaceous materials in carbonaceous chondrites with pyrolysis GC-MS technique. Because the insoluble macromolecular materials have various "structural units" instead of "monomer", we compared the pyrolysis products obtained from the meteorites with those from several synthetic polymers to estimate "the partial structures" which can give such pyrolysis products as obtained from the meteorites.

Figure 1 shows the pyrograms (the gas chromatograms of the pyrolysis products) of the Murchison (CM2), Boriskino (CM2) and the Allende (CV3) carbonaceous chondrites, at 740°C (without HCl-HF treatment). The principal pyrolysis products are aromatic hydrocarbons (such as naphthalene, biphenyl, benzaldehyde), heterocyclic aromatic hydrocarbons (such as benzothiophene, dibenzofuran), normal- or branched- alkanes and alkenes ($C_{13} \sim C_{20}$). For the CM2 chondrites, the pyrograms are more similar each other than for C3 chondrites or ureilites. The pyrolysis products are considered to be derived from edge

defects of the carbonaceous macromolecular materials because complete graphite does not yield any pyrolysis products except low-molecular compounds such as CO_2 under the pyrolysis condition. Moreover, the carbonaceous materials have few chemical bonds which cleave at 386°C, because the meteorites scarcely gave any pyrolysis products at the pyrolysis temperature.

For the synthetic mechanism of the aromatic hydrocarbons (excluding heterocyclic compounds) during the pyrolysis reaction, at least two mechanisms exist. 1) The cleavage of C-C bonds which link the aromatic rings. 2) The aromatization of poly-ene generated in the course of pyrolysis reaction. For the alkanes and alkenes, the random cleavage of methylene C-C bonds is a candidate. Figure 2 shows the pyrograms of the synthetic polymers. Polyvinylchloride yielded the aromatic hydrocarbons similar to those from the meteorites as pyrolysis products at 740 and 500°C, and a few products at 386°C. The O-containing polymers, polyvinylalcohol and polyvinylacetate, gave benzaldehyde besides the aromatic compounds similar to those from polyvinylchloride. However, O-containing heterocyclic compounds such as benzofuran were not observed. Polyethylene gave n-alkanes, 1-alkenes and α,ω-alkenes as the pyrolysis products. Polypropylene gave various branched-alkanes and alkenes. These facts suggest that the reactions described above can proceed under the condition of pyrolysis concerned. A fraction of the benzaldehyde obtained from the meteorites can be derived from O-containing substituent groups such as -OH group combined to methylene bonds. However, heterocyclic compounds such as benzofuran are considered to be derived from other O-containing partial structures of the macromolecular materials. The materials also have branched C-C bonds as partial structure, however, parts of them consist of the normal C-C bonds at least C_{20} long.

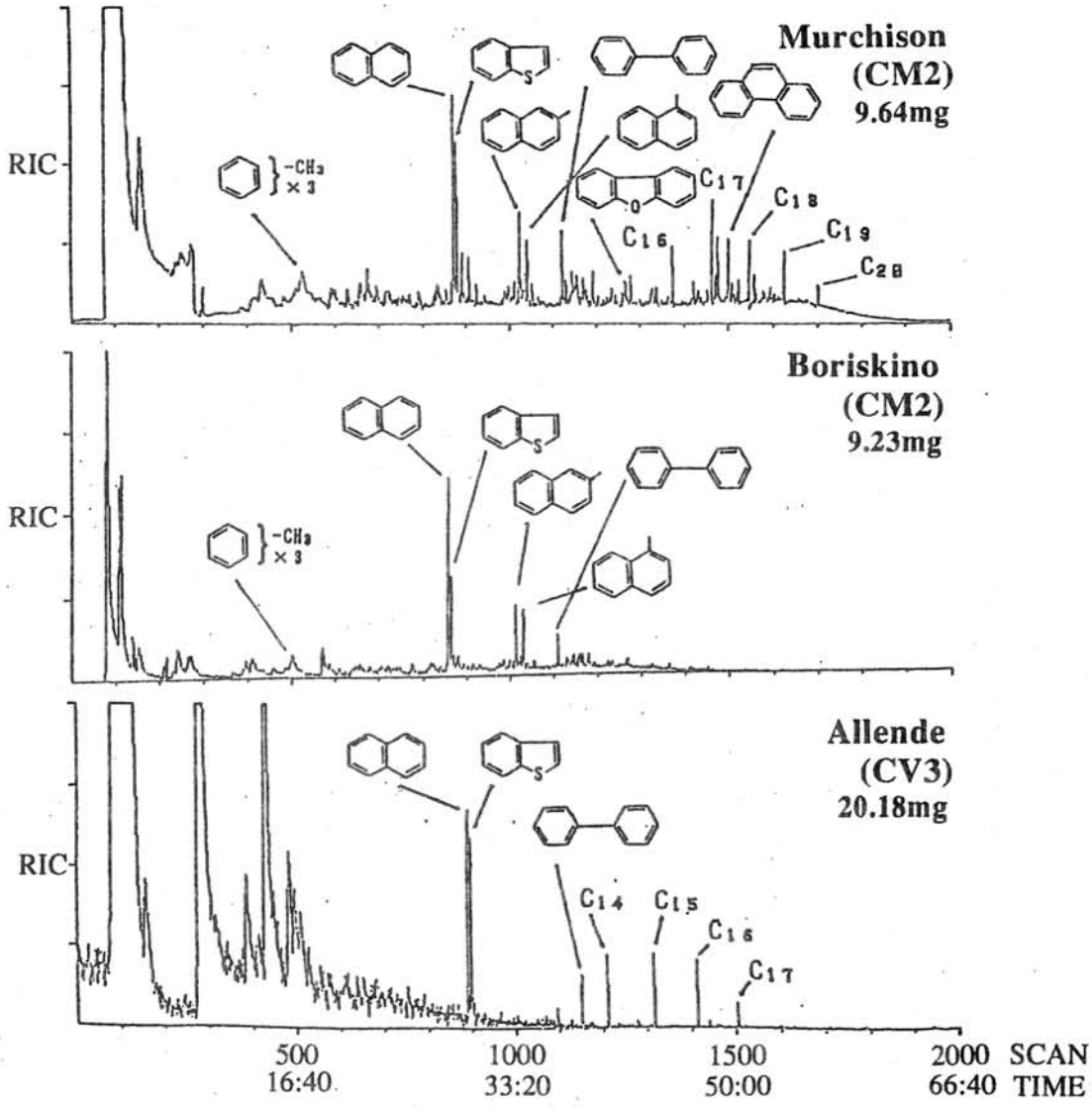

Figure 1. Pyrograms of the carbonaceous chondrites.
Column : OV-1 50m 0.25mm i.d.
Temperature : 4°C/min from 60 to 260°C
after 16 min at 60°C
Pyrolysis condition : 740°C for 3s

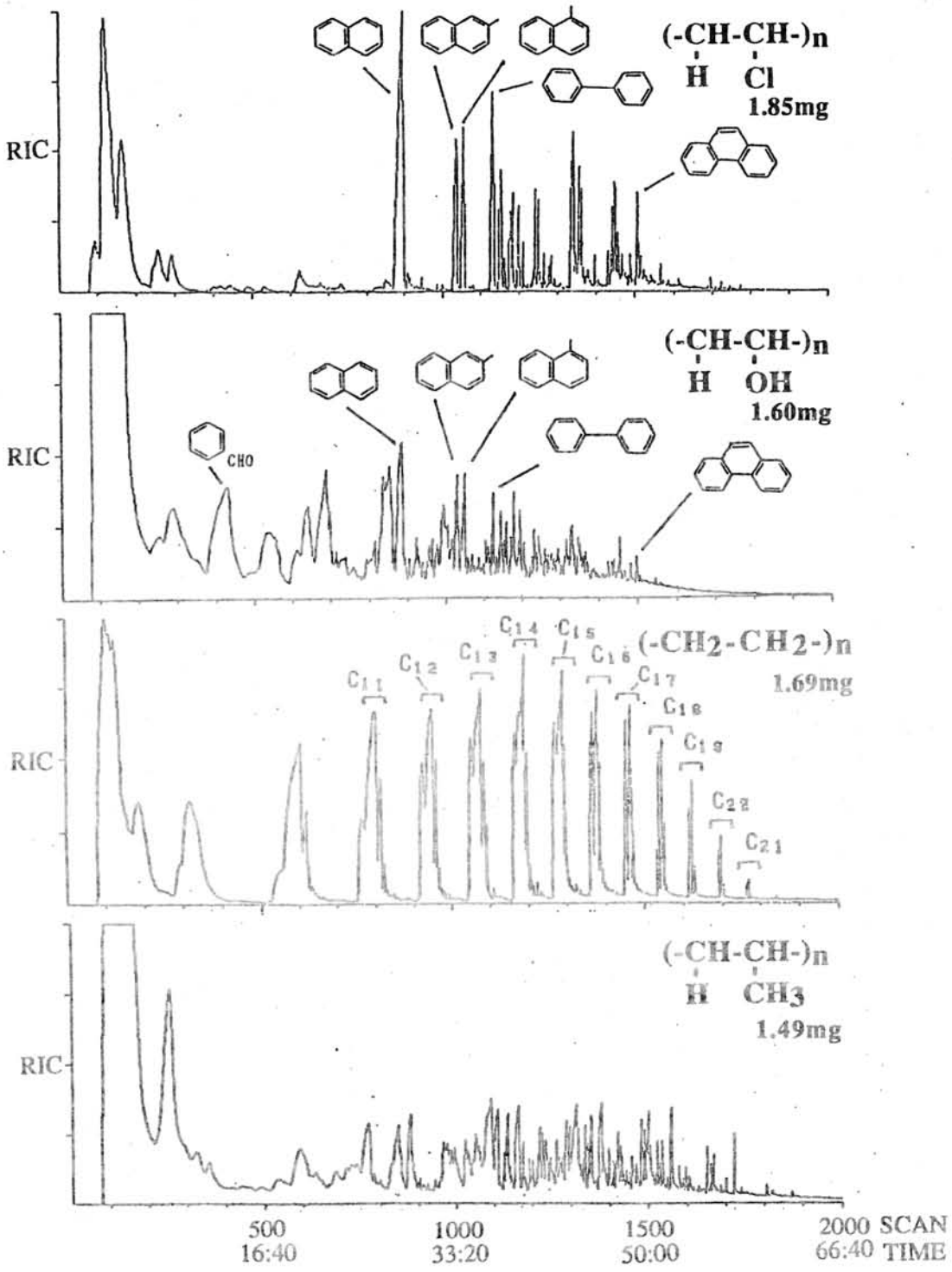

Figure 2. Pyrograms of the synthetic polymers.
Column : OV-1 50m 0.25mm i.d.
Temperature : 4°C/min from 60 to 260°C
after 16 min at 60°C
Pyrolysis condition : 740°C for 3s

Special Lecture (I)

Dr. J.F. Kerridge

ORIGINS OF ORGANIC MATTER IN METEORITES

John F.Kerridge

Institute of Geophysics, UCLA, Los Angeles, California, USA

Over 400 individual organic compounds have been identified in carbonaceous meteorites, and more undoubtedly exist below current detection limits. The observed molecular species account for 10 to 20% of the organic C in a typical carbonaceous meteorite, the balance consisting of a poorly characterised macromolecular complex resembling terrestrial kerogen. Much of the interest in meteoritic organic molecules stems from the likelihood that similar, or even identical, compounds were involved in the chemical evolution that led to the origin of life in the solar system. For that reason, much attention has been paid to understanding the mechanism(s) responsible for production of the organic matter in meteorites, even though they exhibit no evidence of biological activity.

Table 1 lists a dozen mechanisms that could plausibly have been implicated in organic synthesis in the early solar system, or before. (Note that carbonaceous meteorites are very old, having been assembled no more than a few Myr after formation of the earliest solids in the solar system [1].) Despite this plethora

Table 1. Possible sources and processes responsible for production of meteoritic organic matter.

Ion-molecule reactions in interstellar clouds
Radiation chemistry in interstellar grain mantles
Condensation in stellar outflows
Equilibrium reactions in the solar nebula
Surface catalysis (Fischer-Tropsch) in the nebula
Kinetically controlled reactions in the nebula
Radiation chemistry (Miller-Urey) in the nebula
Photochemistry in nebula surface regions
Liquid-phase reactions on parent asteroid
Surface catalysis (Fischer-Tropsch) on asteroid
Radiation chemistry (Miller-Urey) in asteroid atmosphere
Thermal reprocessing during metamorphism

of candidate mechanisms, debate has traditionally focussed on just two possible syntheses: catalysed hydrogenation of CO (Fischer-Tropsch mechanism) and chemical reactions induced by electric discharge (Miller-Urey mechanism). Recently, however, most workers have concluded that more than one mechanism was probably involved [e.g.,2,3,4]. One reason for this conclusion is the paucity of clear signatures in the meteoritic record for individual processes. Diagnostically significant patterns may be found in the meteorite data but in most cases these have not been traced to specific processes. Table 2 lists some of what now appear to be the key diagnostic indicators in meteoritic organic

matter, and in what follows we discuss these as potential constraints on mechanisms of organic synthesis in the early solar system, or before.

Table 2. Some observations of meteoritic organic matter that represent potential diagnostic indicators of sources and/or processes responsible for organic synthesis.

Structural diversity
Prevalence of branched over straight chains
Amino/hydroxy acid proportions
Deuterium enrichment of organic matter
C,H isotopic distribution within kerogen-like material
C isotope distribution in homologous series

Structural diversity

Most classes of organic compound in an uncontaminated meteorite exhibit complete structural diversity, i.e., all stable isomers are present, for virtually all species above the detection limit. This includes the higher aliphatic hydrocarbons [5] that were previously thought to show only limited structural diversity [6]. Purines and pyrimidines appear to exhibit limited structural diversity, though contamination may be a problem in those analyses [2]. The significance of structural diversity is that it is difficult to reconcile with any kind of structurally selective synthesis, such as grain-mediated catalysis, e.g., Fischer-Tropsch.

Prevalence of branched over straight-chain species

The significance of this observation, valid for all known species except the hydroxy acids [2] and possibly monocarboxylic acids [7], is similar to that of the previous one: Synthesis in most cases apparently involved random addition of C atoms, so that there was no selection for straight-chain species, as might be expected in certain catalysed reactions, such as Fischer-Tropsch [3,6].

Amino/hydroxy acid proportions

Peltzer *et al.* [8] showed that for three out of four pairs of structurally similar amino and hydroxy acids in Murchison, the proportions of the amino to the hydroxy acid were consistent with synthesis by means of the Strecker cyanohydrin reaction in an aqueous medium characterised by a unique ammonium ion concentration. The aqueous environment is consistent with the petrology of Murchison, and other carbonaceous meteorites [e.g.,9]. The reagents needed for the Strecker synthesis, aldehydes, HCN and ammonia, are all known interstellar molecules [10] whereas production in the solar nebula is contraindicated [11]. These lines of evidence lead to a scenario in which amino, and probably other

organic acids, were synthesised by equilibrium chemical reactions in liquid water in the surface regions of an asteroid, using interstellar molecules as feedstock [12].

Deuterium enrichment of organic matter

The D enrichments of all meteoritic organic species analysed to date, e.g.,amino acids [13], are so great that no known solar-system process is capable of generating them [14]. Consequently, the D enrichments are generally attributed to incorporation of molecules enriched in D by ion-molecule reactions in interstellar clouds prior to solar-system formation [e.g.,15]. What remains unknown is the molecular form in which the D-enriched hydrogen entered the primitive solar system, though there are good reasons for believing that those interstellar molecules included aliphatic hydrocarbons and aldehydes/ketones [12]. Survival of such species poses strong constraints on the thermal history of the early solar system.

C,H isotopic distribution within kerogen-like material

The insoluble kerogen-like fraction is isotopically inhomogeneous with both C and H exhibiting marked isotopic variations between the different molecular moieties analysed so far [16]. These variations rule out production of the kerogen-like material by gas-phase reactions in the solar nebula, as proposed by Morgan et al. [17]. Gas-phase production of just the aromatic moieties [17] would require substantial local D enrichment of the nebular H_2 gas, which is unlikely but cannot be ruled out. The isotopic distribution in the kerogen-like material suggests production by degradation (possibly thermal or radiation-induced) of a melange of molecular species with a variety of origins. The high proportion of unalkylated to alkylated PAHs in meteorites indicates a high formation temperature, in the range 400 to 800°C [4], consistent with production in stellar outflows [18].

C isotope distribution in homologous series

Yuen et al. [19] showed that the homologous series of both the light alkanes and the monocarboxylic acids exhibited similar systematic decreases of $^{13}C/^{12}C$ with increasing C number, at least up to C_5. The carboxylic-acid pattern is probably carried by the aliphatic C, with the carboxyl C maintaining approximately the isotopic composition of CO_2 in the meteorite. Yuen et al. argued that the C isotopic pattern was inconsistent with production of the light alkanes by "cracking" of higher hydrocarbons but pointed instead towards build-up of the homologous series by progressive addition of C atoms. The data also suggested a close relationship between the light alkanes and the aliphatic precursors to the carboxylic acids [19], a connection which might well be extended to include the amino acids as well [11,20].

Summary

The foregoing considerations strongly suggest production of meteoritic organic matter by a variety of mechanisms in a variety of environments. There is good evidence that those environments included dense molecular clouds and the surface regions of asteroid-sized objects. On the other hand, there is presently no compelling evidence for organic synthesis in the solar nebula, though this possibility certainly cannot be ruled out. Nonetheless, conditions in the solar nebula apparently permitted survival of interstellar methane and other light alkanes (as well as a variety of less volatile species), possibly trapped in icy grain mantles [e.g.,21].

References 1.Macdougall J.D.,Lugmair G.W. and Kerridge J.F.(1984) Nature 307,249. 2.Cronin J.R.,Pizzarello S. and Cruickshank D.P. (1988) In Meteorites and the Early Solar System (J.F.Kerridge and M.S.Matthews,eds.),819. 3.Anders E. (1991) Space Sci.Rev. 56,157. 4. Wing M.R. and Bada J.L. (1992) Origins of Life, in press. 5. Cronin J.R. and Pizzarello S. (1990) GCA 54,2859. 6. Hayatsu R. and Anders E. (1981) Topics Curr.Chem. 99,1. 7. Shimoyama A., Naraoka H.,Komiya M. and Harada K. (1989) Geochem.J. 23,181. 8. Peltzer E.T.,Bada J.L.,Schlesinger G. and Miller S.L. (1984) Adv. Space Res. 4,69. 9.Kerridge J.F. and Bunch T.E. (1979) In Asteroids (T.Gehrels, ed.),745. 10.Irvine W.M. and Knacke R.F.(1989) In Origin and Evolution of Planetary and Satellite Atmospheres (S.K.Atreya, J.B. Pollack and M.S.Matthews,eds.),3. 11. Fegley B. and Prinn R. (1989) In Formation and Evolution of Planetary Systems (H.A. Weaver and L.Danly,eds.),171. 12. Kerridge J.F. (1991) Origins of Life 21,19. 13. Epstein S.,Krishnamurthy R.V.,Cronin J.R. and Pizzarello S. (1987) Nature 326,477. 14. Geiss J. and Reeves H. (1981) Astron.Astrophys. 93,189. 15. Kerridge J.F. (1983) EPSL 64, 186. 16. Kerridge J.F., Chang S. and Shipp R. (1987) GCA 51, 2527. 17. Morgan W.A.,Feigelson E.D.,Wang H. and Frenklach M. (1991) Science 252,109. 18.Allamandola L.J.,Sandford S.A. and Wopenka B. (1987) Science 237,56. 19. Yuen G., Blair N., DesMarais D.J. and Chang S. (1984) Nature 307,252. 20. Shimoyama A.,Naraoka H.,Yamamoto H. and Harada K. (1986) Chem.Lett. 1986, 1561. 21. Greenberg J.M. (1982) In Comets (L.L. Wilkening,ed.), 131.

Thursday, August 20, 1992

0900-1630 *Symposium, Auditorium*

1300-1515 *Special Session; Lunar Meteorites*

1630-1730 *Special Lecture (II)*

Prof. H. Wänke (Invited Speaker)
Max-Planck-Institut für Chemie
Mainz, F.R. Germany

THERMAL EVOLUTION OF A PRIMITIVE ACHONDRITE PARENT BODY: ^{26}Al HEATING.

Miyamoto, M.[1] and Takeda, H.[2]

[1]Department of Pure and Applied Sciences, University of Tokyo, Komaba, Tokyo 153
[2]Mineralogical Institute, Faculty of Science, University of Tokyo, Hongo, Tokyo 113, Japan.

Introduction Primitive achondrite is one group of unique meteorites and is the group name suggested for all of the ungrouped chondritic meteorites and clasts that have mineralogy and bulk chemistry similar to chondrites and have achondritic texture [e.g., 1]. Acapulcoites (lodranites), brachina, forsterite chondrites, silicate inclusions in IAB and IIICD irons, and winonaites are included in this group [e.g., 2]. Studies of this group may give information on the early evolution of planetary bodies by comparison with those of other achondrites (e.g., ureilites or HED achondrites)[3] and ordinary chondrites. Hiroi and Takeda [4] related them to S-type asteroids. McCoy et al. [5] concluded that acapulcoites are samples of a parent body different from those of the ordinary chondrites, and discussed their origin.

Miyamoto et al. [6] have performed a model calculation of the ordinary chondrite parent body internally heated by the decay of ^{26}Al by using best available constraints and proposed that the ^{26}Al/^{27}Al ratio at the time when the parent body was formed was 5×10^{-6}. Since the planetesimal-scale collision model [3,4] will be applied easily to producing primitive achondrites with an additional heat source, we performed a computer simulation of their thermal history with ^{26}Al heat source.

Method A spherical body of radius R with the radiation boundary condition is heated by the decay energy of uniformly distributed ^{26}Al. The method and parameters used are similar to those of an internally heated model for the ordinary chondrite parent body proposed by Miyamoto et al. [6]. The radius of the parent body is assumed to be 100 km. Ambient temperature (T_0) is assumed to be 200 K. The ^{26}Al/^{27}Al ratio of 5×10^{-6} previously proposed for the ordinary chondrite parent body is used.

The bulk Al content of the parent body is assumed to be the average value of acapulcoites, Acapulco, Allan Hills (ALH-)77081, and Yamato (Y-)74063 (Al_2O_3= 2.31 wt%).

Results and discussion Maximum attainable temperature is about 1000 °C in the region deeper than 30 km (Fig. 1). Because melting of Fe,Ni-FeS begins at 988 °C (T_1, Fig. 1) and silicate melting at the enstatite-albite-quartz peritectic at 1062 °C (T_2, Fig. 1)[e.g., 5], maximum attainable temperature obtained by our internal heating model seems to be consistent with the previous studies of primitive achondrites [e.g., 5,7]. Because McCoy et al. [5] suggested that the heat source for producing Fe,Ni-FeS melt veins was indigenous rather than generated by impact, as indicated by the lack of shock features of acapulcoites, internal heating by the decay of ^{26}Al is a plausible heat source for the acapulcoite parent body. However, any shock texture will be annealed when the temperature reached to a point where partial melting takes place. It should be noted that maximum attainable temperature of about 1000 °C is obtained by assuming the ^{26}Al/^{27}Al of 5×10^{-6} which is the same value as that proposed for the ordinary chondrite parent body.

Another important factor to determine maximum attainable temperature is the bulk Al content of the parent body. Nagahara and Ozawa [7] suggested that Y-791493, Acapulco, ALH-77081, and Lodran originated from the same precursor in the same parent body and that the degree of melt extraction for Y-791493 was higher than that in Acapulco and ALH-77081, which were similar. The bulk Al_2O_3 contents of Y-791493 (0.93 wt%)[7] and Lodran (0.44 wt%)[8] is significantly lower than those of Acapulco (2.25 wt%)[9], ALH-77081(2.27 wt%)[7], and Y-74063(2.42 wt%)[10]. This difference may be related to the degree of partial melt and melt extraction. Therefore, Acapulco, ALH-77081, and Y-74063 seems to have the bulk Al content closer to source materials of the parent body than Y-791493 and Lodran. Because Acapulco-type meteorites tend to be enriched in plagioclase, the bulk Al content of the parent body we assumed could be higher than real source material.

Fig. 2 shows the cooling rates at temperatures of 900 and 500 ^{o}C as a function of the depth obtained by our model calculations. The cooling rates reported for primitive achondrites extend for the wide range from 10 ^{o}C/Myr to 1000 ^{o}C/Myr [e.g., 7-9, 11]. They are dependent on the method and temperature range. The cooling rates obtained by our model calculations seem to be slow, although they are within the range of the cooling rates reported. Detailed studies to obtain coolig rates of primitive achondrites are required.

Fig. 3 shows maximum attainable temperature at the center of an internally heated body having a radius of more than 50 km as a function of both the $^{26}Al/^{27}Al$ ratio (at the time when the parent body was formed) and bulk Al content. Maximum attainable temperature at the center of the body having a radius more than 50 km is not dependent on the radius of the body. H chondrite-like physical properties (thermal diffusivity, thermal conductivity, and density) are assumed. For the bulk Al contents of some meteorites shown by arrows in Fig. 2, the $^{26}Al/^{27}Al$ ratio of the order of 10^{-6} gives reasonable results for the thermal evolution of the meteorite parent bodies [12,13]. If the $^{26}Al/^{27}Al$ ratio is less than 10^{-6}, the decay energy of ^{26}Al can be neglected for the thermal metamorphism of small parent bodies, and external heat sources such as impact will be required. Although the ^{26}Mg excess related to ^{26}Al is detected in some meteorites [e.g., 14, 15], the importance of ^{26}Al as a heat source remains a major and unsolved issue.

We thank Drs. T. Fukuoka and M. Kimura for discussion.

References

[1] Yanai K., Kojima H., Prinz M., Nehru C. E., Weisberg M. K. and Delaney J. S. (1984) 9th Symp. Antarct. Meteorites, 24-28.
[2] Kimura M., Tsuchiyama A., Fukuoka T. and Iimura Y. (1992) Proc. NIPR Symp. on Antarct. Meteorites 5, 165-190.
[3] Takeda H. (1989) Earth Planet. Sci. Lett. 93, 181-194.
[4] Hiroi T. and Takeda H. (1991) Proc. NIPR Symp. Antarct. Meteorites 4, 163-177.
[5] McCoy T. J., Keil K., Mayeda T. K. and Clayton R. N. (1992) Lunar Planet. Sci. XXIII, 871-872.
[6] Miyamoto M., Fujii N and Takeda H. (1981) Proc. Lunar Planet. Sci. 12B, 1145-1152.
[7] Nagahara H. and Ozawa K. (1986) Mem. Natl. Inst. Polar Res., Spec. Issue 41, 181-205.

[8] Bild R. W. and Wasson J. T. (1976) Miner. Mag. 40, 721-735.
[9] Palme H., Schultz L., Spettel B., Weber H. W and Wanke H. (1981) Geochim. Cosmochim. Acta 45, 727-752.
[10] Fukuoka T. and Kimura M. (1990) 15th Symp. Antarct. Meteorites, 99-100.
[11] Prinz M., Klimentidis R., Harlow G. E. and Hewins R. H. (1978) Lunar Planet. Sci. IX, 919-921.
[12] Grimm R. E. and McSween H. Y. (1989) Icarus 82, 244-280.
[13] Miyamoto M. (1991) Proc. 24th ISAS Lunar Planet. Symp., 248-254.
[14] Lee T., Papanastassiou D. A. and Wasserburg G. J. (1976) Geophys. Res. Lett. 3, 41-44.
[15] Hutcheon I. D. and Hutchison R. (1989) Nature 337, 238-241.

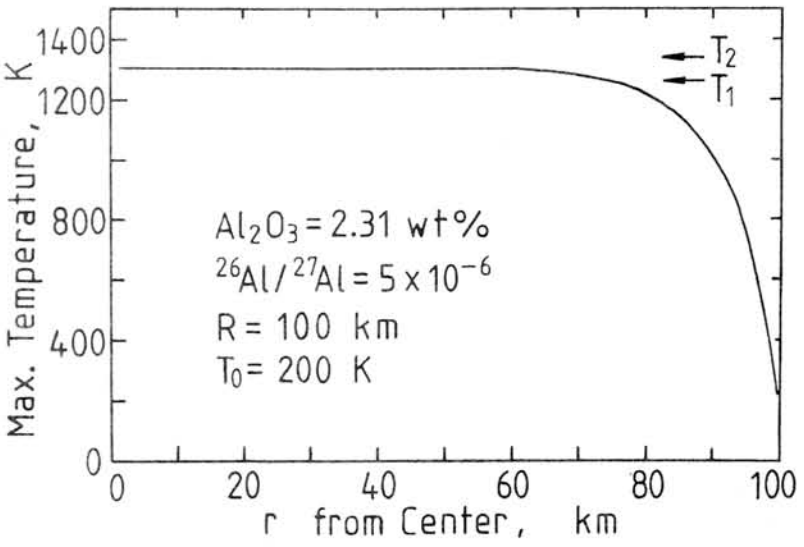

Fig. 1. The profile of maximum temperature as a function of depth for an internally heated body having a 100 km radius.

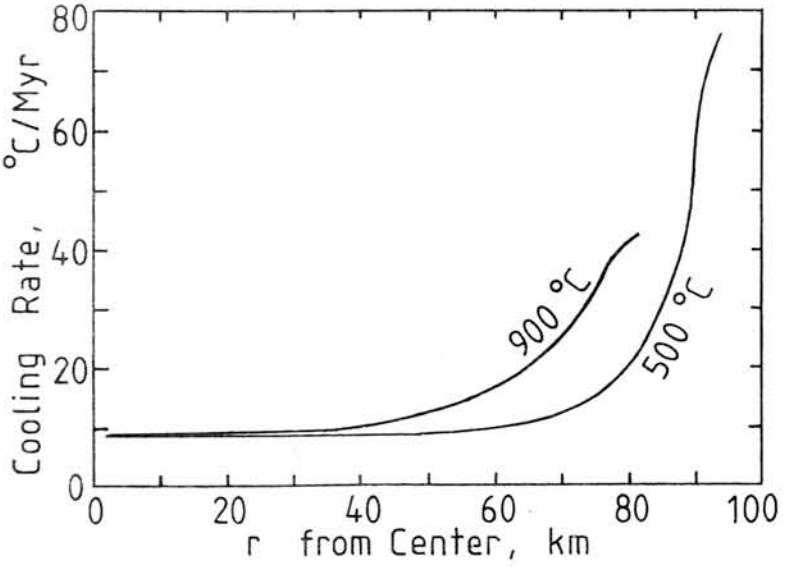

Fig. 2. Cooling rate (°C/Myr) vs. depth (km) at temperatures 900 and 500 °C.

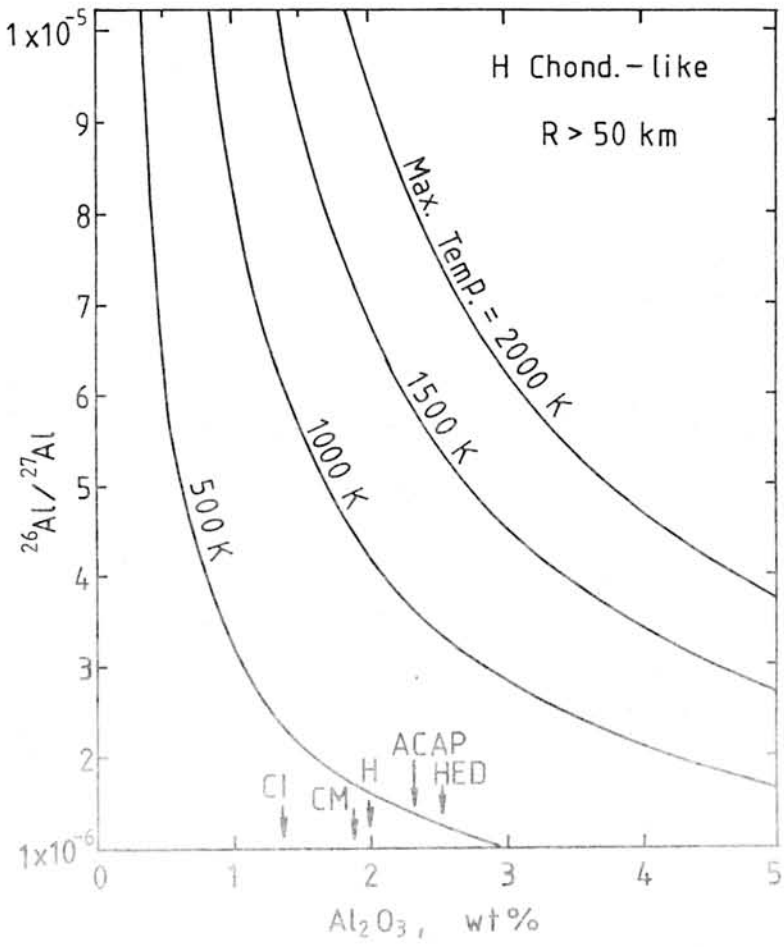

Fig. 3. Maximum attainable temperature at the center of a body having a radius more than 50 km internally heated by the decay of ^{26}Al as a function of the bulk Al content and $^{26}Al/^{27}Al$ ratio. H chondrite-like physical properties. Arrows show the bulk Al contents of meteorites. ACAP: Acapulcoite.

SIZE DISTRIBUTION AND SHAPE ANALYSIS OF METAL PARTICLES IN ORDINARY CHONDRITES

Hiroaki Uegomori, Kei Kurita, Hisayosi Yurimoto and Shigeho Sueno. Institute of Geoscience, University of Tsukuba, Tsukuba, Ibaraki, 305 Japan.

Introduction

In ordinary chondrite, metal particles mainly consisted of kamacite and taenite are dispersed. The metal particles retain the information about chondrite formation processes as well as metamorphic process in the parent body. Cooling rates of the parent body have been estimated by the compositional analysis of metal particle, and the results are compared with the conventional "onion shell" metamorphism model[1]. Shape of metal particle is sensitive to the degree of metamorphism in the chondrite parent body, whereas the size distribution carry the information about both accretion process and metamorphic process of the parent body. Fujii *et al.*[2] discussed the correlation between shape and metamorphic degree. The shape become circular with higher metamorphic stage.

In this study, we discuss the size distribution, shapes and chemical composition (Ni and Co proportion) of metal particles in three different petrologic type chondrites : Silverton (H4), Nuevo Mercurio (H5) and Big Rock Donga (H6).

Experimental

Polished surface of the meteorites were prepared for the size and shape analysis. The size distribution and the shape of metal particles were examined on the basis of back scattered electron images. Area and perimeter of the particles were measured, and $(\text{area})^{1/2}$ and $\text{perimeter}/(\text{area})^{1/2}$ were used as parameters indicative of the size and shape, respectively. Ni and Co compositions were analyzed by electron probe.

Results

Smaller particles have more circular shape than larger ones, and particles in Big Rock Donga have more circular shape than that in Silverton, which suggests higher degree of metamorphism transforms the boundary between metal particles and silicate to the round shaped. In Silverton, particles smaller than 20 μm are subject to the metamorphism and in Big Rock Donga those smaller than 100 μm are subject.

The size distribution of metal particle in Silverton follows power low type distribution, whereas Big Rock Donga has different type of distribution (Fig. 1). From the shape analysis, smaller particles are severely influenced by the metamorphism, only larger particles can carry information about the accretion process.

Ni contents of metal varies from 4 to ~50 wt%, and Ni and Co shows inverse correlation. Comparisons by size and petrologic type show no marked differences(Fig. 2).

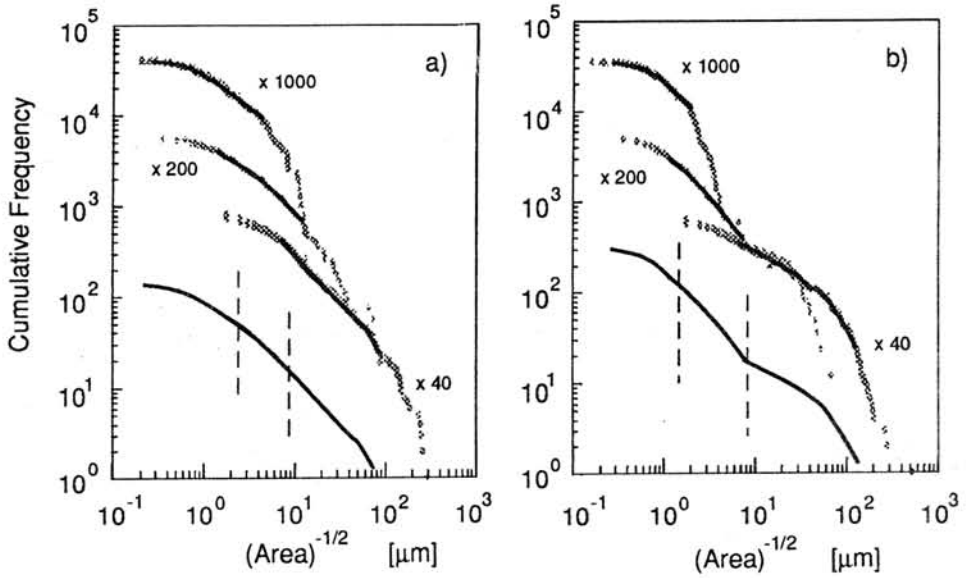

Fig.1 Size distribution of metal particles

a) Silverton (H4) b) Big Rock Donga (H6)

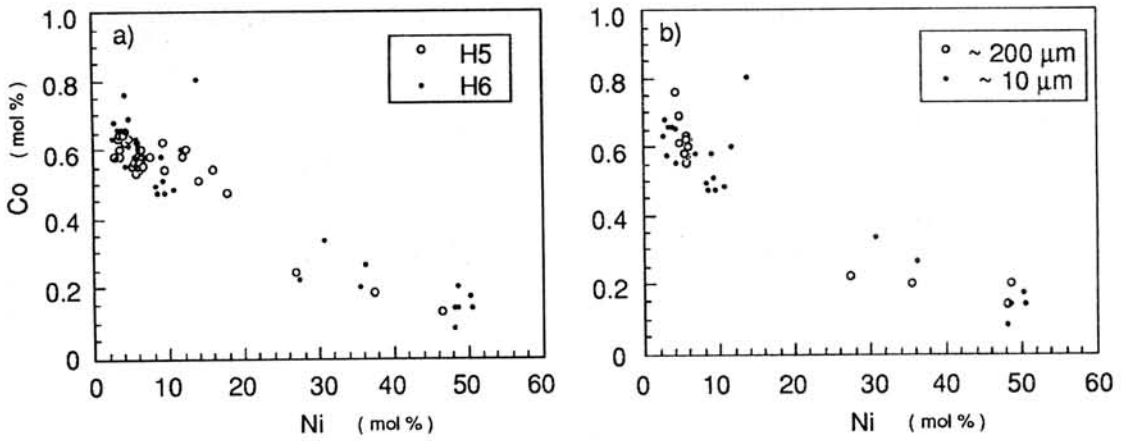

Fig.2 Co vs. Ni diagram of metal particles

a) Nuevo Meracurio(H5), Wellman(H5) and BigRock Donga(H6)

b) Compositional difference between large(~200μm) and small(~10μm) metal particles in Big Rock Donga (H6)

Reference
1. Scott, E. R. D., and R. S. Rajan (1981) GCA45, 53-67. 2. Fujii, N., Miyamoto, M., Kobayashi, Y. and Ito, K. (1982) Mem. Natl. Inst. Polar Res., Spec. Issue 25, 319-330.

ELEMENTAL DISTRIBUTIONS OF UNIQUE IRON METEORITE YAMATO791694 BY SIMS

Tadashi Shimamura, Masatake Honda*, Hisao Nagai* and Yoshiaki Yoshioka**
School of Hygienic Sciences, Kitasato University, 1-15-1 Kitasato Sagamihara Kanagawa 228, *Department of Chemistry, College of Humanities and Sciences, Nihon University, Sakurajosui 3, Setagayaku, Tokyo 156, **Matsushita Technoresearch Inc., 3-15 Yagumo-nakamachi Moriguchi, Osaka 570 ,JAPAN

Introduction Iron meteorite Yamato791694 is unique because its high concentration of Ni(35%), Cu(0.22%), In(0.12ppm), Sn(90ppm), Sb(2.4ppm), Pb (0.86ppm) and Bi(0.28ppm)[1]. The concentrations of these elements are almost the highest end among those of all known iron meteorites. Concentrations of Ni, Ge, Ga, Sb, Cu, In, Zn and Pd are similar to those of San Cristobal and Santa Catharina but S content is very much different [2][3]. Shimamura et al. [1] measured the isotopic composition of Pb using glow discharge mass spectrometer and found that the composition was very close to primordial. They pointed out that because S concentration is rather low (1.3ppm) Pb may reside in metal phase rather than troilite. Though this meteorite does not have any obvious feature or inclusions it is important to know whether element distributions are homogeneous or not. We report here the results of the distribution of eleven elements using SIMS.

Experimental The instrument used here was Cameca 4F magmetic sector type SIMS. Running conditions are listed in Table-1. To obtain sensitivity rather than spacial resolution we used RAE (Resistive Anode Encoder) mode. The isotopes used for the imaging are listed in Table-2.

Results Selected images of the results are presented in Fig.-1

Fe, Co, Ni, Cu, Ga Distributions of the major and the minor components of the meteorite were generally homogeneous and no structure larger than 5 μm was observed.

P As shown in Fig-1 P distribution was spotty with the size of 10～15 μm. There is a possiblity of interference from $^{62}Ni^{++}$. But judging from the image of Ni which has no structure, we believe P image is real. Perhaps those grains are small crystals of schreibersite.

Cr, Zn Local distributions were also observed but location of enriched area was not coincident with P.

Rh, Pd As shown in Fig-1 distributions of Rh and Pd were coincident with P, however there were possibility of spectral interferences from $^{56}Fe^{31}P^{16}O^{+}$ on $^{103}Rh^{+}$ and $^{58}Ni^{31}P^{16}O^{+}$ on $^{105}Pd^{+}$. It is difficult to eliminate those interferences without loss of sensitivity. Further investigations are necessary.

Pb No feature was observed on Pb distribution, however during course of analysis we observed sevier spectral interferences on all of the Pb isotopes perhaps caused by cluster ions like $^{56}Fe^{60}Ni_2{}^{16}O_2{}^{+}$ etc. It is also difficult to avoid such spectral interferences. Thus it is still possible that Pb has micro features.

Summary Fe, Co, Ni, Cu and Ga distributions are basically homogeneous within the spacial resolution of the instrument. Local enrichment of P was observed with a size of ～10μm. Cr and Zn also have local enrichment but no correlation was observed among Cr, Zn and P. Rh, Pd and Pb have possible spectral interferences. Further investigations are needed.

References [1] Shimamura T., Takahashi T., Honda M. and Nagai H., (1991) 16th symposium on antarctic meteorites 73-76 [2] Smales A.A., Mapper D., and Fouche K.F., (1967) G.C.A. 31 673-720 [3] Wasson J.T. (1967) G.C.A. 31 161-180

Table-1

primary ion	O_2^+
secondary ion	positive
primary ion energy(keV)	8.0
primary ion current(nA)	80, 1000
rastered area(μmxμm)	250x250
analysis area(μmϕ)	150
mass resolution	250-300

Table-2

element	P	Cr	Fe	Co	Ni	Cu	Zn	Ga	Rh	Pd	Pb
isotope	31	52	57	59	62	63	66	69	103	105	208
integration time(sec)	200	60	30	30	30	60	60	60	60	60	60

Fig-1

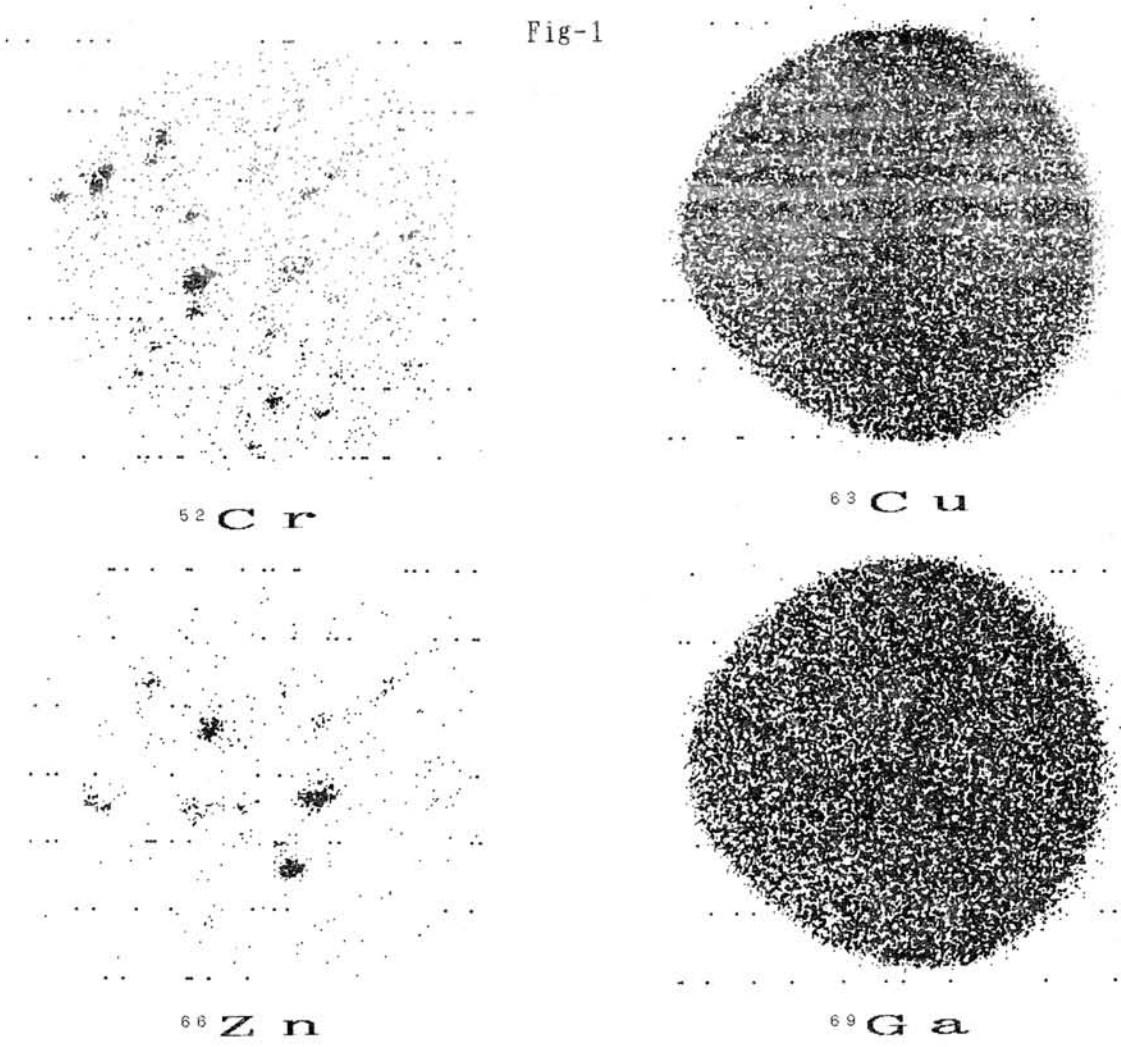

Fig-1(cont.)

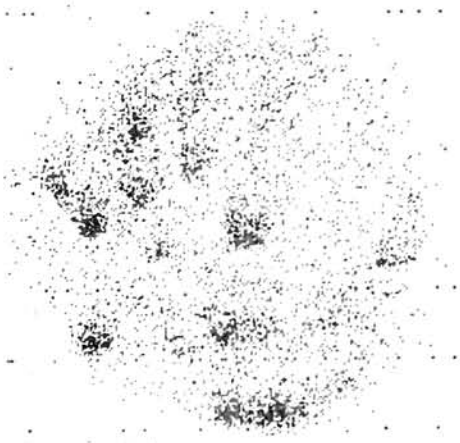

^{31}P

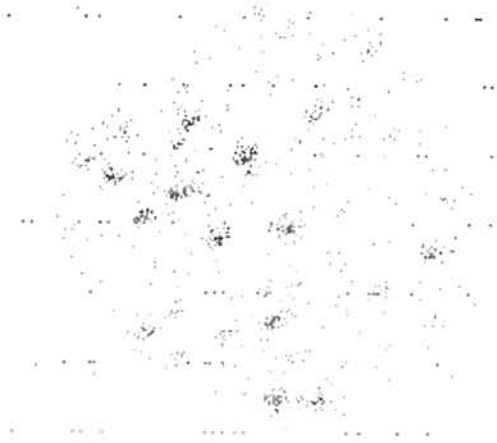

^{103}Rh

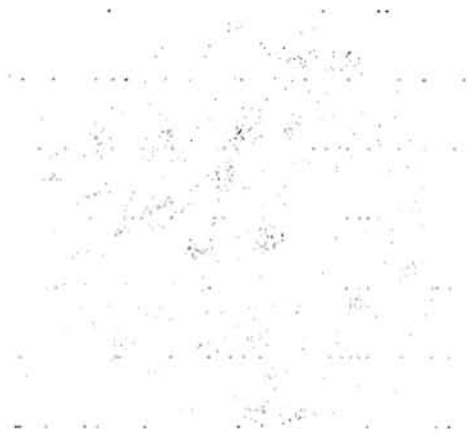

^{105}Pd

^{208}Pb

REE constraints on the formation of Murchison(CM) chondrules

Mutsuo Inoue[1] and Noboru Nakamura[1),2)]

[1)]Department of Science of Material Differentiation, Graduate School of Science and Technology, Kobe University.
[2)]Department of Earth Science, Faculty of Science, Kobe University, Nada, Kobe, Japan.

Introduction

The formation processes of chondrules of primitive chondrites are considered by the two models : nebula model (melting of dust balls) and planetary model (melting of planetesimal). Recently, the nebula model became more popular (1). The detailed isotope dilution analysis demonstrated that REE patterns of CV, CO chondrules reflect the volatilities of the elements, which is consistent with the nebula model (2,3). Because of analytical difficulty, almost no REE data of CM chondrules were reported until recent. We initiated analysis of REE of the Murchison (CM) chondrules to examine how their REE patterns look like and what the mechanism of their formations were. Our preliminary results for 7 chondrules were presented at the 16th NIPR Symposium (4). Here we report analytical results of REE for additional 6 chondrules together with the results of SEM-EDS analysis, and discuss the formation of the CM chondrules.

Petrography and compositions

Most chondrules except for MC-9 and MC-16 show porphyritic texture composed of olivine (Fa=0.3-5.0) and pyroxene (Fs=0.7-2.6) phenocrysts and mesostasis. MC-9 and MC-16 show granular olivine (Fa=38.5)(5) and radial pyroxene (Fs=4.4) textures, respectively. The results of SEM-EDS analysis suggest that the total of oxide contents in mesostasis are variable and significantly lower (100-70%) than 100%. This may be due to hydrous minerals in mesostasis. The major element contents are generally related to the total. Typically, the SiO_2 and FeO contents have positive and negative correlations with the totals, respectively (see Fig.1). It is considered that this was resulted from aqueous alteration.

REE patterns

As shown in Fig. 2, the following features are recognized for REE patterns of Murchison chondrules.

1. 10 among 13 chondrules indicate smoothly fractionated (mostly light REE depleted) REE patterns with no irregularities of Ce and Yb and of light/heavy REE.
2. They indicate large negative Eu anomalies associated with Sr depletion.

3. Only two chondrules MC-3 and MC-6 show irregularities of light/heavy REE and Yb, respectively. They also indicate the light REE depletion.
4. Abundances of alkalis (K,Rb) are lower relative to those of REE.

Aqueous alteration and REE patterns

Since the bulk chondrite has been subjected to aqueous alteration, it is necessary to see how such an alteration affects REE compositions. In this study, we employ the water contents of chondrule-mesostasis as a rough mesure of the alteration degree of each chondrule (Table.1). The water contents are estimated by subtracting the total weights of metal oxides from 100% (see table.1). It is pointed out that no correlation exists between these alteration degrees and REE patterns at all ; the least altered chondrules (MC-5 and MC-9) show surprisingly highly fractionated patterns as the others do, and on the other hand, even a severely altered chondrule (MC-1) indicat no paticular fractionation. Therefore, the REE abundances are considered not to have been influenced significantly by the hydrous alteration which established mesostasis petrography but to have preserved the memories of pre-alteration events. But the low abundances of alkalis (Fig.2-a,b) are probably due to leaching during this alteration process (5).

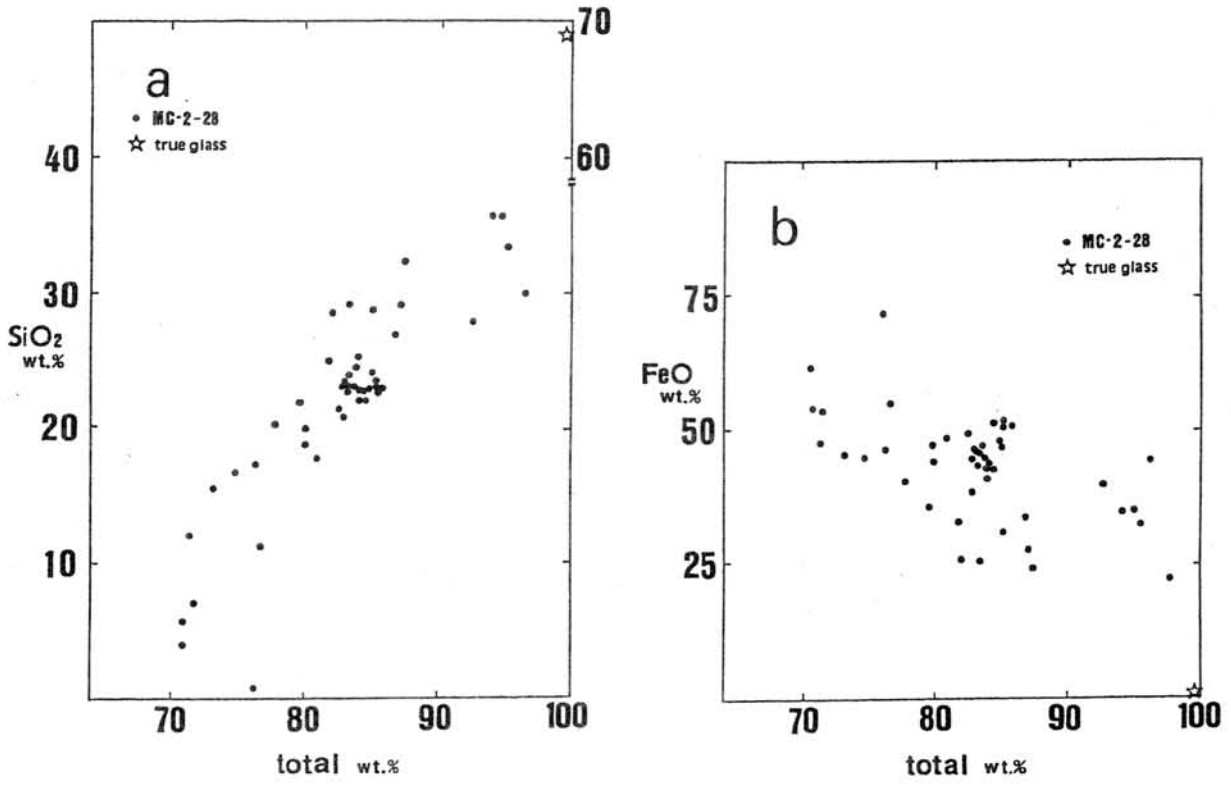

Fig.1
The correlations of SiO_2(a) and FeO(b) with total contents of oxides in the mesostasis of Murchison porphyritic chondrules.

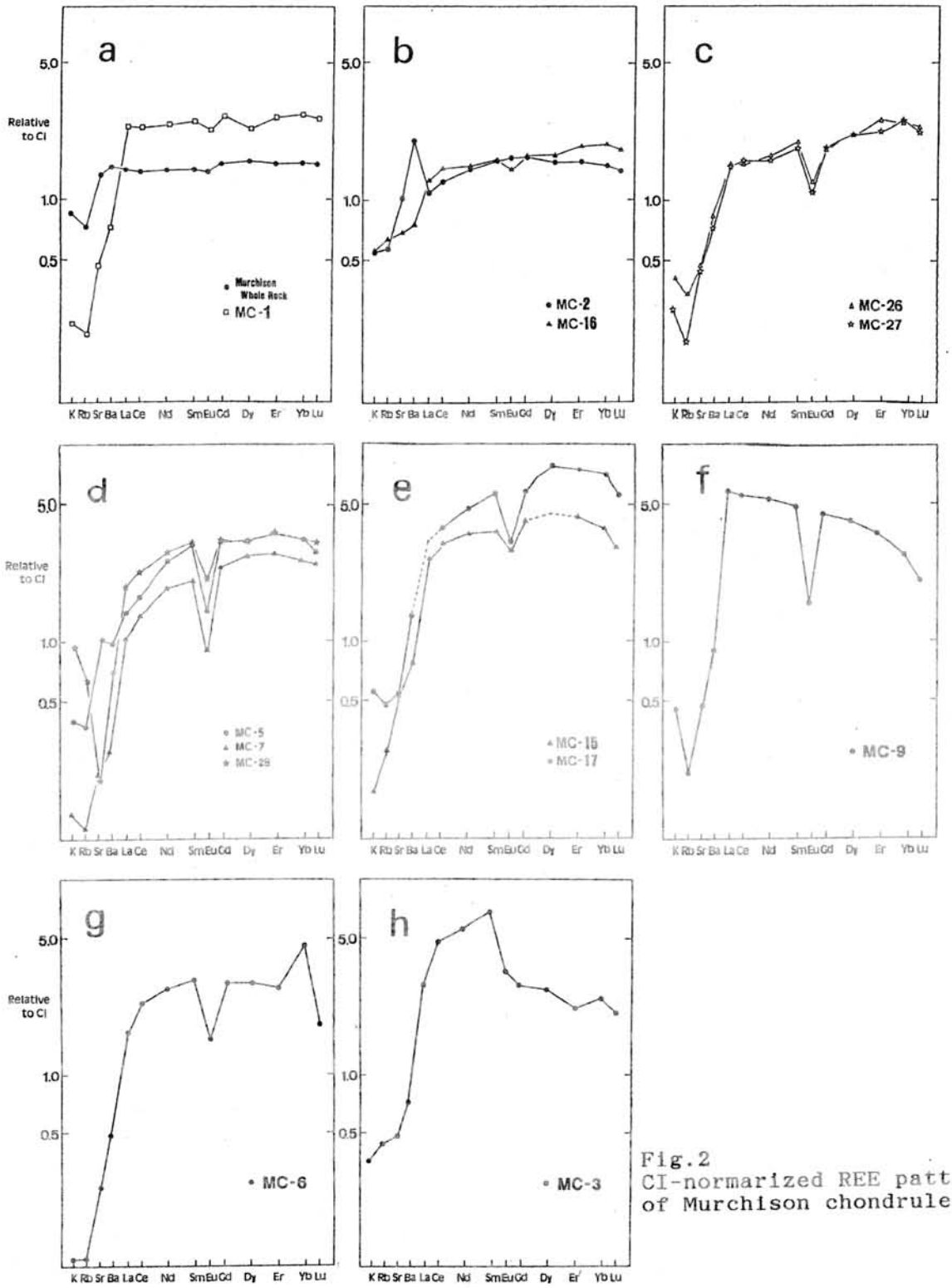

Fig.2
CI-normarized REE patterns of Murchison chondrules.

Table.1 Indexes of aqueous alteration in Murchison chondrules.

	MC-1	MC-2	MC-3	MC-5	MC-6	MC-7
Total of oxides(wt.%)	71.3	83.9	80.4	97.8	85.1	82.8
Index Alteration	3 severe	2 moderate	2 moderate	0 least	2 moderate	2 moderate

MC-9	MC-15	MC-16	MC-17	MC-26	MC-27	MC-28
	74.4	80.0	83.4	83.9	94.7	76.8
0 least	3 severe	3 severe	2 moderate	2 moderate	1 slightly	3 severe

Possible implications of the fractionated REE

Irregularities of light/heavy REE and of Ce, Eu and Yb as observed in Allende(CV) and Felix(CO) chondrules indicate that the precursors of chondrules formed by condensation/vaporization processes in the early solar nebula (2,3). On the other hand, many Murchison chondrules indicate a light REE depleted (or enriched), smooth REE fractionation which is similar to those of lunar basalts. Except for a few cases (6), meteoritic chondrules rarely have such a geochemical signature of REE. Therefore, the fractionated REE of Murchison chondrules may not be reconciled with vapor fractionation but with the solid/liquid process. If this is the case, it is considered that Murchison chondrule precursors were formed by the partial-melting of dust aggregates and separation of melts in the nebula or by an igneous activity on a grand-parent body and that later Murchison chondrules were formed from such materials and chondrules have exposed to aqueous alteration in the meteorite parent body or in the nebula. Two chondrules (MC-3, MC-6) show the REE features indicative of both vapor process and the solid/liquid fractionation and may be the key to make clear the formation model of the chondrules.

Reference

(1) Glossman L.(1988) In"Meteorites and the early solar system" (ed Kerridge J.F. and Matthews M.S.), p680-696.
(2) Misawa K. and Nakamura N.(1988a) Geochim.Cosmochim.Acta 52, 1699-1710.
(3) Misawa K. and Nakamura N.(1988b) Nature 334, 47-50.
(4) Inoue M. and Nakamura N.(1991) Papers presented to the 16th Symposium on Antarctic meteorites, 68-69.
(5) Nakamura N. and Inoue M.(1991) Meteoritics 26, 376-377.
(6) Bischoff B., Palme H. and Spettel B.(1989) Earth Planet.Sci. Lett. 52, 170-180.

THE COMPOSITION OF CHONDRULES IN THE H3-4 CHONDRITE Y-790986

H. Palme[1], B. Spettel[1], H. Wänke[1] and Y. Ikeda[2]. [1]Max-Planck-Institut für Chemie, 6500 Mainz, Germany; [2]Ibaraki University Mito 310 , Japan.

According to the olivine and pyroxene compositions (Fo_{78-83}, En_{80-89}) Y-790986 is classified as an H-chondrite. Its PMD (percent mean deviation) of olivine of 7.8 suggests a petrologic type 3.9. The rock appears very rich in chondrules with minor amounts of inclusions, mineral fragments and matrix. Most of the chondrules are porphyritic; radial-px and barred-ol chondrules are comparatively rare [1].

We have analysed 17 chondrules (in some cases chondrule fragments) by instrumental neutron activation analysis. Results are given in Table 1. Major element analyses are in progress. Petrography will be done subsequently.

Chondrules or chondrule fragments range in weight from 1.22 mg to 6.13 mg. The average chondrule composition of Y-790986 is similar to the "grand mean" for Dhajala chondrules reported by Gooding [2]. A comparison is also made with the H-chondrite bulk composition (Table 1). Chondrules are higher in refractories (e.g., Ca, Sc) and lower in Fe, Ni and associated elements than the inferred bulk (average H-chondrite). The moderately volatile elements Mn, Na and Zn are, on the average, even higher in the chondrules than in the average H-chondrite, suggesting that loss of volatiles during chondrule formation is insignificant

Nickel and Au are well correlated in Y-790986 chondrules (Fig. 1) reflecting incorporation by metal. The correlation also excludes volatility related losses of Au, as Ni is much less volatile. Heating experiments on Allende have shown that loss of volatiles during heating is strongly oxygen fugacity dependent [4]. At high fO_2 and 1050° C Au and As were found to be rapidly lost from Allende and Murchison wheras under the same conditions Zn, Na and K are almost quantitatively retained. At low fO_2 and 1050°C losses of Zn and the alkali elements occurred while Au and As were not affected. Thus the Ni-Au correlation and the high concentrations of Na, K and Zn rule out any significant loss of volatile elements at high and at low oxygen fugacities. In addition, the Mn/Na ratio in chondrules is on the average the same as the bulk H-chondrite ratio which is close to the CI-ratio. However, Mn loss was, in contrast to Na, never observed under the conditions of the experiments by Wulf and Palme [4].

The abundances of Ga in Y-790986 chondrules are rather constant and not correlated with Ni or metal, respectively, as shown in Fig. 1. Apparently, Ga was not associated with metal in the chondrule precursor material. Unequilibrated ordinary chondrites have, in general, the major fraction of Ga in silicate [5]. During thermal metamorphism Ga partitions into metal. The well equilibrated Acapulco meteorite, for example, has a Ga metal/silicate concentration ratio of about 10 [6]. During chondrule melting Ga will partition into chondrule metal. The constant Ga-contents, therefore, exclude the loss of a major fraction of a metal.

A unique characteristic of the present chondrule population are the high Zn contents. Despite comparatively high uncertainties in the analytical determination of Zn, the average Zn contents of the chondrules and most of the individual chondrule concentrations are above the H-chondrite average. A higher than average bulk Zn abundance for Y-790986 is inferred.

One chondrule (number 3) has essentially the bulk H-chondrite composition as may be seen from Table 1 and Fig. 1.

Fig. 1

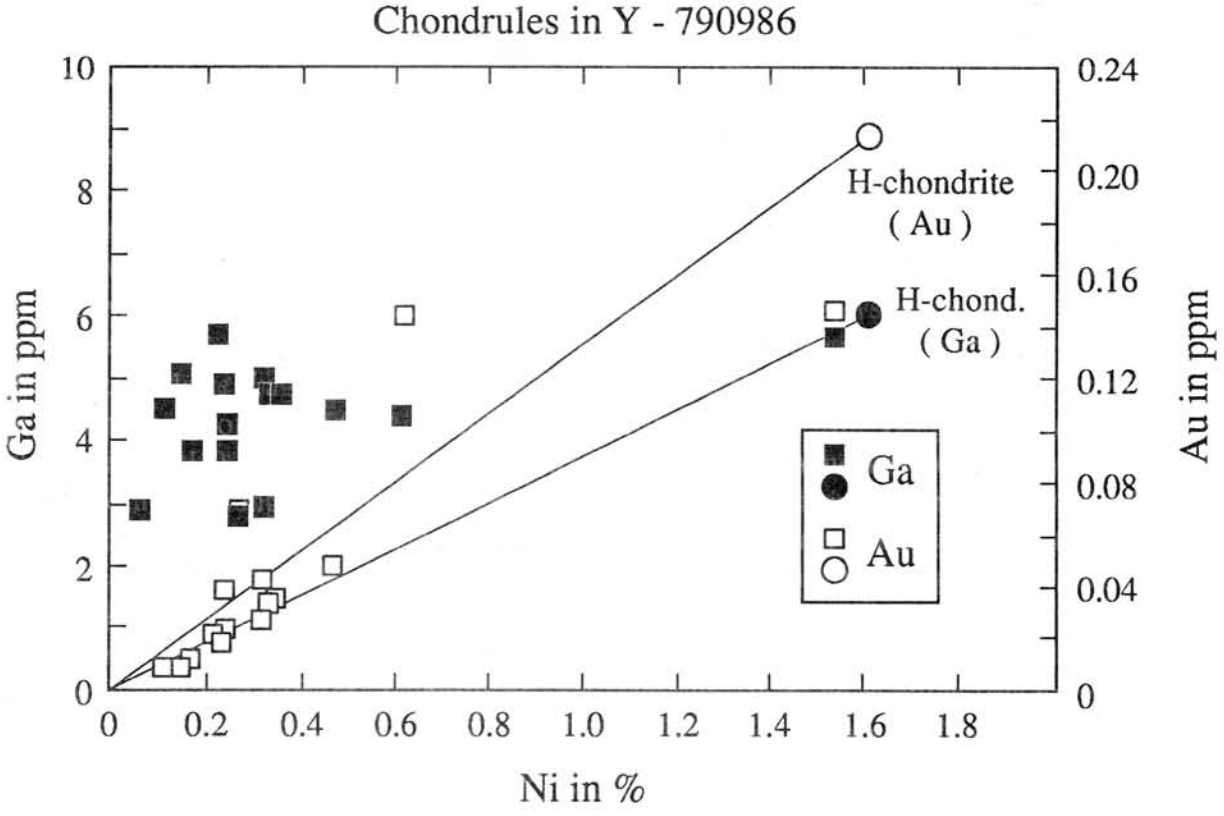

Four chondrules have a positive Eu-anomaly, nine a negative and four chondrules have a flat REE-pattern. There is a tendency for chondrules of more equilibrated chondrites to develop Eu -anomalies, while chondrules of more primitive types of chondritic meteorites show little or no Eu-anomaly (e. g. [7]). Therefore, the large fraction of chondrules with Eu-anomalies is somewhat surprising.

In summary, chondrules from Y-790986 are compositionally similar to chondrules from other H-chondrites, except for a pronounced enhancment of Zn in most chondrules. Significant losses of volatiles during chondrule formation can be excluded. Metal abundances are low but variable with one chondrule approaching the bulk H-chondrite composition. Rather constant Ga-abundances indicate that the major host phase for Ga in chondrule precursors were silicates while the Ga-host phase in chondrules should be metal. The constant Ga thus limits the amount of metal lost during chondrule formation.

Lit.: [1] Ikeda, Y. (1983) Proc. 8th Symp. Anarct. Meteor., 122-145. [2] Gooding, J. L. (1983) in: Chondrules and their origins, A. King, ed.; Lunar and Planetary Institute, Houston, pp. 61-87. [3] Wasson, J.T. and Kallemeyn, (1988) G.W. Phil. Trans. R. Soc. Lond. A 325, 535-544. [4] Wulf, A.V. and Palme, H. (1991) LPSC XXII, 1527-1528. [5] Rambaldi, R.R. and Cendales, M. (1979) Earth Planet. Sci. Lett. 44, 397-408.[6] Palme, H. et al. (1981) Geochim. Cosmochim. Acta 45, 727-752. [7] Bischoff A. et al. (1989) Earth Planet. Sci. Lett. 93, 170-180.

Table 1: Chondrules in Y-790986

nr	1	2	3	4	5	6	7	8	9	10	11	12
mg	3.19	3.92	4.53	2.74	6.13	2.90	2.73	2.62	1.61	1.94	2.06	2.36
Ca %	2.3	2	1	1.3	1.4	1.2	1.42	1.4	2.6	1.3	2.2	1.1
Fe	12.96	9.72	22.7	14.15	7.72	11.9	11.7	10.2	12.31	12.47	12.85	13.64
Na ppm	9350	10120	5090	8710	8420	6780	8050	3310	10600	8350	10710	6760
K	1680	1190	660	1430	1390	835	1370	480	1430	1890	1630	770
Sc	9.31	11.3	8.53	9.54	8.91	7.14	9.22	9.93	13.8	9.66	11.7	8.89
Cr	3890	4440	4615	4140	3950	3720	4170	4350	3160	3840	4550	4080
Mn	3980	3250	2340	3356	3070	3440	3225	2890	2890	3180	3140	2714
Co	83.3	46.4	584	60.6	57.2	106	33.7	59.0	192	41.5	81.3	155
Ni	2450	1120	15370	1740	2220	3490	1490	2730	2450	2400	2380	6190
Zn	57	43	80	84	50	50	73	46	97	76	62	100
Ga	4.22	4.50	5.69	3.80	5.69	4.70	5.05	2.81	3.80	4.84	4.90	4.39
As	<0.25		1.64	<0.2			<0.25	0.31	<0.3			0.77
Se	3.9	<6	11.7	5.4	<2	<4.5	<3	<5	<5	<15	<5	<6
Br	<0.4	0.5	0.6	<0.4	<0.2	<0.6	<0.3	<0.3	<0.3	<0.4	<0.4	<0.5
La	0.34	0.47	0.37	0.31	0.34	0.31	0.33	0.43	0.41	0.40	0.39	0.35
Sm	0.214	0.287	0.235	0.22	0.218	0.194	0.212	0.240	0.245	0.24	0.273	0.22
Eu	0.026	0.11	0.098	0.039	0.047	0.039	0.039	0.120	0.082	0.037	0.065	0.096
Yb	0.25	0.27	0.26	0.22	0.25	0.24	0.23	0.24	0.26	0.3	0.3	0.24
Lu	0.048	0.052	0.040	0.047	0.037	0.041	0.060	0.040	<0.05	0.039	0.049	<0.09
Ir	0.043	0.080	0.54	0.024	0.033	0.12	0.035	0.18	0.080	<0.015	0.05	0.33
Au	0.023	0.0082	0.146	0.012	0.021	0.035	0.0089	0.0687	0.038	0.038	0.018	0.144

nr	13	15	16	17	18	av.	Dhajala	H-chond.	av./H-chond.	s.d.
mg	2.00	1.22	1.75	1.92	2.46	(a)	(b)	(c)	(d)	(e)
Ca %	1.4	2.4	1.2	2.1	1.8	1.65	1.29	1.25	1.32	25
Fe	12.05	9.01	12.9	11.7	12.97	12.41	12.5	27.5	0.45	4
Na ppm	5670	7260	8630	6940	9235	7881	8087	6400	1.23	3
K	260	739	635	970	1510	1110		780	1.42	8
Sc	10.9	12.2	9.05	8.35	9.56	9.88	8.51	7.90	1.25	3
Cr	5075	3740	3760	2890	3550	3995	3930	3660	1.09	3
Mn	3340	2890	2990	3380	3030	3124	3108	2320	1.35	3
Co	64.9	33.4	188	219	148	127	101	810	0.16	3
Ni	3220	600	3370	4750	3220	3482	2030	16000	0.22	5
Zn	80	75	81	53	66	69	40	47	1.47	20
Ga	2.90	2.87	4.73	4.48	5.00	4.37		6.0	0.73	20
As	0.29		0.50	0.38	0.27			2.05	0.00	20
Se	<4	<3	<3	<3				7.7	0.00	20
Br	<0.3	<0.3	<0.3	<0.3	<0.3			0.5	0.00	25
La	0.35	0.35	0.34	0.25	0.36	0.36	0.39	0.295	1.22	15
Sm	0.220	0.201	0.213	0.175	0.215	0.22	0.26	0.185	1.22	5
Eu	0.14	0.071	0.11	0.039	0.063	0.072	0.076	0.073	0.98	20
Yb	0.24	0.22	0.26	0.16	0.25	0.25	0.27	0.205	1.20	20
Lu	0.039	0.049	0.061	<0.04	0.050	0.047	0.042	0.031	1.50	25
Ir	0.021	0.025	0.12	0.13	0.20	0.12	0.096	0.76	0.16	15
Au	0.0261	<0.005	0.0328	0.047	0.042	0.044	0.028	0.215	0.21	15

All analyses by INAA;(a)-average 18 chondrules; (b) Average Dhajala Chondrules [2]
(c) average H-chondrite [3]; (d) average Y 790986 chondrules/average H-chondrites;
(e) s.d.-representative standard deviation in %.

Optical and Isotopic Properties of Diamonds in Ureilites

H. Kagi[1], S. S. Russell[2], C. T. Pillinger[2], K. Takahashi[3] and A. Masuda[4],
1.Inst. of Materials Science, Univ. of Tsukuba, Ibaraki 305, Japan. 2.Planetary Sciences Unit, Open Univ., Milton Keynes, MK7 6AA, UK. 3.RIKEN, Wako, Saitama 351-01, Japan. 4.Univ. of Electro-Communications, Chofu, Tokyo 182, Japan.

Introduction

Raman spectra of micro-diamonds in ureilites reveal some unusual profiles, whose vibrational energy is significantly lower than that of the ordinary diamonds (Fig. 1; Kagi et al.,1990a). In our previous study, the observed energy shift of about 10 cm^{-1} was open to three possibilities; the presence of lonsdaleite (hexagonal polymorphism of diamond), the extraordinarily concentrated ^{13}C and remained structural strain derived from the shock events. Taking into acount the luminescence (Kagi et al., 1990b), the third possibility can be excluded. The estimated ^{13}C enrichment corresponding to the shift of 10 cm^{-1} is about 0.1 in the ratio of ^{13}C / ^{12}C. In this study, we investigated the isotope composition of carbon for the diamond contained in the antarctic ureilite Y-791538 and the most suitable interpretation was explored.

Experimental

A powdered sample of Y-791538 was decomposed with HF and HCl at room temperature, and Raman spectra were observed using a micro-Raman spectrometer. The number of the energy-shifted diamond grains was comparable to that of the ordinary diamond grains. If the energy shift is attributed to the ^{13}C enrichment, then the obtained carbon isotope ratio should be distinct from that of solar abundance.

Before making measurements of carbon isotopes, the acid residue of Y-791538 consisting of graphite and diamond was treated with $H_2Cr_2O_7$ and $HClO_4$ to ensure that all the graphite was reduced, as this would interfere with the diamond measurement.

Results and Discussion

The obtained results are shown in Fig. 2. The mean $\delta^{13}C$ was -5.0‰ with a peak value at -3.6‰. This is similar to values measured by Grady *et al.* (1985) for a suite of ureilites and means the anomalous Raman spectra we recorded are not due to an enrichment in ^{13}C but to hexagonal diamond. No well-defined Raman spectra have been reported for hexagonal diamond (lonsdaleite), because obtained hexagonal diamonds by various methods have a small crystallite size and give only faint signals. Thus the energy-shifted Raman spectrum we recorded can be acknowledged as the standard spectrum of hexagonal diamond.

In the case of hexagonal diamond, carbon atoms are configured in *eclipse* form while the configuration of cubic diamond (ordinary diamond) is *staggered*. Interatomic repulsion between *eclipsed* carbon atoms should be larger than that of *staggered* carbon atoms, therefore the interatomic distance of the hexagonal diamond is expected to be expanded, which result in the

diffraction, and it was proved that the observed lattice volume was slightly larger than an ideal value for the hexagonal diamond (Utsumi and Yagi, 1991), which is consistent with our speculation. This study would be a unique case that meteoritical information contributes to molecular mechanics and materials sciences.

References

Grady, M.M., Wright, I.P., Swart, P.K. and Pillinger, C.T. (1985): Geochim. Cosmochim. Acta., **49**, 903-916.

Kagi, H., Takahashi, K. and Masuda, A. (1990a): Proc. Japan Acad., **66**, Ser. B, 101-104.

Kagi, H., Takahashi, K. and Masuda, A. (1990b): Naturwissenschaften, **77**, 531-532.

Utsumi, W. and Yagi, T. (1991): Proc. Japan Acad., **67**, Ser. B, 159-164.

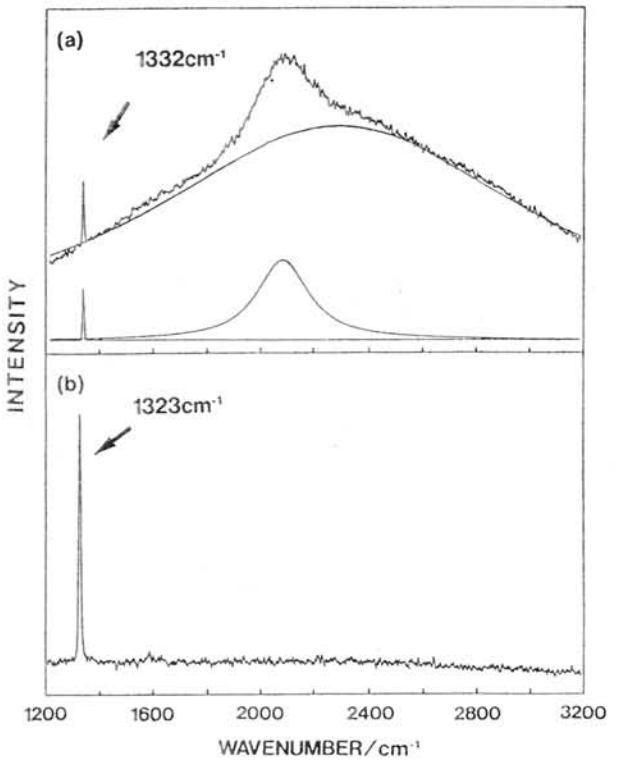

Fig. 1. (a) Laser induced spectrum of micro-diamond in Yamato-791538, which consists of sharp Raman band at 1332 cm^{-1} and broad photo-luminescence band. The smooth curves are deconvoluted components of the spectrum. (b) Strange Raman spectrum of micro-diamond. Peak position is about 1323 cm^{-1} and lower than that of ordinary diamonds in wavenumber.

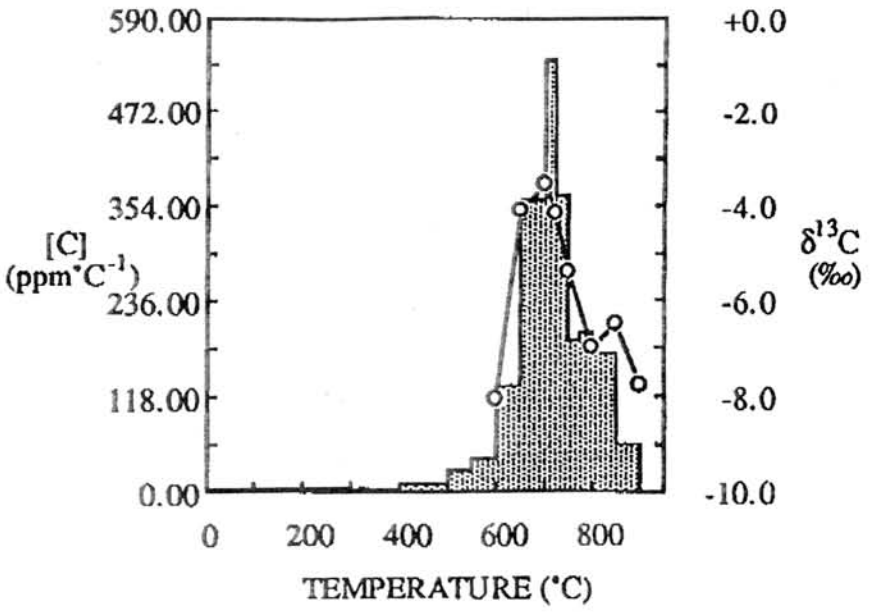

Fig. 2. Release profile of the carbon in Y-791538

POSSIBILITY OF CLASSIFICATION AND CHARACTERISTIC ESTIMATION OF METEORITES WITH ESR SPECTROSCOPY

Chihiro Yamanaka, Shin Toyoda and Motoji Ikeya
Department of Earth and Space Science, Osaka University, Toyonaka, Osaka 560 Japan

Introduction

Classification of stony meteorites is a complicated work including identification of minerals and estimation of metamorphic level and oxidization degree. Thermoluminescence (TL) is an effective method to distinguish the petrographic type in chondrites [1]. In this method, difference of TL sensitivity for radiation damage in each sample is used.

ESR (Electron Spin Resonance) technique is also effective for detection of radiation damage in minerals, however, reports are few for meteorite samples. This reason is iron components in meteorites have been considered disturbance of ESR measurements. Exceptionally, Ostertag performed ESR measurement to Fe^{3+} in shocked olivine[2].
In this paper, we consider the possibility of meteorite classification using ESR signals of Fe^{3+} ion. We also found an ESR signal considered due to the radiation damage in ALH765 sample.

Results and discussion

Figure shows the ESR spectra of meteorites. Clearly, difference in spectra is seen between chondrites and Ca-rich achondrites. ESR signals due to Fe^{3+} (g=9, g=4.3 and g=2) reflect the coordination of Fe ion. The ESR signal seen at g=2.001 in ALH765 did not increase for γ-ray irradiation up to 540 kR and saturated by microwave power of 1 mW. These tendencies are similar to those of E' center (unpaired electron trapped in the oxygen vacancy) in quartz, therefore we estimate this signal is due to the E' like radiation damage in silicate. Additionally, another ESR signal of an electron center at g=1.939 was observed in the CAI of the Allende meteorite. Details are investigating.

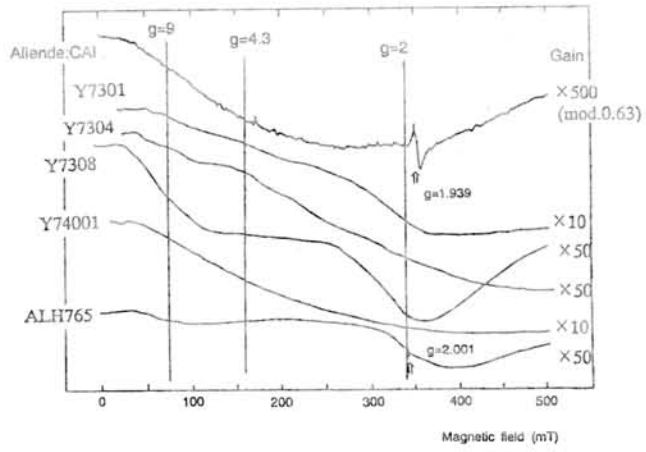

Sample (100mg)		
Yamato 7301.90	H5-6	chondrite
Yamato 7304.96	L6	chondrite
Yamato 7308.106	howardite	Ca-rich achondrite
Yamato 74001.90	H5	chondrite
ALH 765.89	eucrite	Ca-rich achondrite

measured at X band 1-2mW
modulation 100kHz 0.1mT

Figure: ESR spectra of meteorites.

References

1) Sears D.W.G. (1988) Nucl. Tracks Radiat. Meas.,14, 5-17.
2) Ostertag R., Amthauer G., Rager H. and McSween. H.Y., Jr. (1984) Earth Planet. Sci. Lett.,67, 162-166.

UNMELTED POLAR MICROMETEORITES: COMPOSITIONS, MINERALOGIES, AND SIMILARITIES/DIFFERENCES WITH IDPs AND METEORITES.

G. J. Flynn[1], S. R. Sutton[2], and W. Klöck[3].

1) Dept. of Physics, SUNY-Plattsburgh, Plattsburgh, NY 12901
2) Dept. of the Geophysical Sciences, The Univ. of Chicago, Chicago IL 60637
3) Institut für Planetologie, Westfälische Wilhelms-Universität, Münster

Micrometeorites up to several hundred microns in diameter have been recovered from polar ices in Greenland (Maurette et al., 1987), Antarctica (Maurette et al., 1991), and northern Canada (Cresswell and Herd, 1992). Although smaller micrometeorites, up to ~60 μm in diameter, are recovered from the stratosphere of the Earth by NASA sampling aircraft, micrometeorites >100 μm in size settle so rapidly that their concentration in the stratosphere is too low to allow efficient aircraft collection. Particles >60 μm in diameter are important to the understanding of the meteoritic flux at the Earth because the accreted meteoritic mass peaks sharply in the size range from 60 to 1200 μm (see Figure 1), with 80% of the continuous meteoritic mass accretion occurring in the mass range from 10^{-7} to 10^{-3} grams (Hughes, 1978). Thus particles in the 60 to 1200 μm size range, unsampled by either the stratospheric collections or the recovered meteorites but abundant in the polar collections, constitute the large majority of the meteoritic mass accreted on a continuous, planet-wide basis by the Earth.

Maurette et al. (1991) report the major element compositions and mineralogies of 51 irregular shaped micrometeorites from the Antarctic ices are similar to both the fine-grained matrix of primitive carbonaceous chondrite meteorites and to the 5 to 60 μm interplanetary dust particles (IDPs) collected from the Earth's stratosphere, but that they are not identical to either type of material. They suggest that the large micrometeorites (50 μm to 1 mm) recovered from the polar ices may be a new population of solar system material, distinct from both the smaller stratospheric IDPs and the larger (>1 cm) meteorites. If so, then the bulk of the meteoritic material accreted by the Earth may be compositionally and mineralogically distinct from the well characterized meteorites and IDPs.

The abundances of volatile trace elements have previously proven useful in establishing genetic links among or distinguishing between the types of meteorites, and in identifying the IDPs recovered from the Earth's stratosphere as compositionally distinct from the chondritic meteorites (Flynn and Sutton, 1991; 1992b). To examine the similarities and differences between the polar micrometeorites and both the IDPs and the chondritic meteorites, sixteen irregularly shaped polar micrometeorites were analyzed for trace element contents. Because of their irregular shapes these particles are not believed to have melted on atmospheric entry, and may thus better preserve the record of their pre-atmospheric chemical compositions and mineralogies than do the melted, spherical micrometeorites also recovered from the polar ices. The sixteen micrometeorites, four recovered from the Greenland ice and twelve recovered from the Antarctic ice, range from 50 to 150 μm in diameter.

Chemical Composition

Minor and trace element contents were measured in each particle by Synchrotron X-Ray Fluorescence (SXRF), which has high sensitivity for elements from Fe to Br (Sutton and Flynn, 1988). The Greenland micrometeorites were analyzed in epoxy mounts following polishing for mineralogical analyses. The twelve Antarctic micrometeorites were analyzed as whole particles prior to mounting and polishing. Because of the low SXRF sensitivity for Si, we report Fe normalized element abundances. Table 1 gives each abundance ratioed to the CI meteorite abundance for that element. Br contents of the Greenland particles are uncertain because they were analyzed in a Br bearing epoxy.

One Antarctic micrometeorite, B1 #7, broke into two fragments prior to SXRF analysis, and each fragment was analyzed separately. All element abundances are in good agreement between the two fragments (see Table 1), suggesting chemical homogenity. The abundances of Fe, Ni, Zn, and Pb in Greenland particle #16 were mapped by stepping the 8 μm x-ray beam across the sample in 5 μm steps in a 2-dimensional grid pattern. The Ni/Fe, Zn/Fe, and Pb/Fe ratios were relatively constant, indicating chemical homogenity. However, the particles are generally distinct from each other in chemical composition, with each trace element showing more than an order-of-magnitude

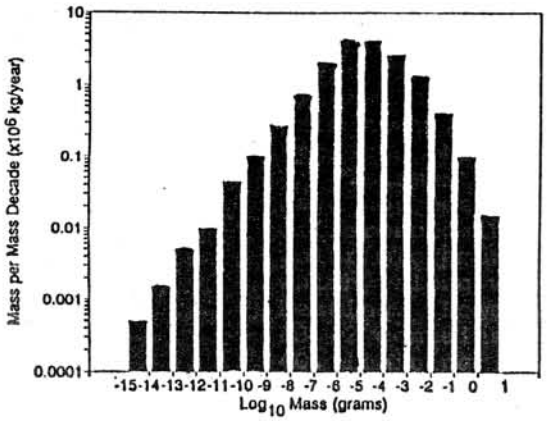

Figure 1: Mass-frequency distribution of dust entering the Earth's atmosphere (from Hughes, 1978) showing the peak between 10^{-7} and 10^{-3} grams (~60 to 1200 μm in diameter).

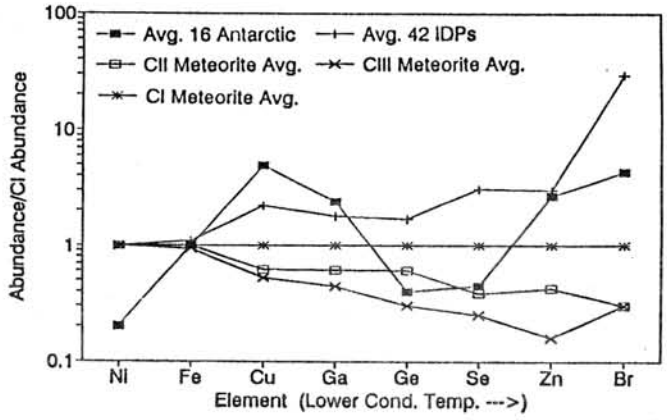

Figure 2: Average CI normalized trace element abundances in 16 polar micrometeorites, 42 IDPs from the stratosphere (data from Flynn and Sutton, 1992b), and CI, CII, and CIII carbonaceous chondrite meteorites.

variation among the set of particles. This is consistent with the wide range of major element (Fe/Si, Mg/Si, Al/Si, and Ca/Si) concentrations reported by Maurette et al. (1991) for similar Antarctic particles.

The average composition of the 16 polar micrometeorites is plotted in Figure 2 and compared with the average composition of 42 stratospheric IDPs and the CI, CII and CIII carbonaceous chondrite meteorites. The polar micrometeorites are enriched above the CI meteorite concentrations in the volatiles Cu, Zn, Ga, Br and Pb. The enrichments (except Pb) are comparable to the enrichments measured in the 5 to 35 μm diameter chondritic IDPs collected from the stratosphere (Flynn and Sutton, 1992b). However the polar micrometeorites are depleted relative to the CI composition in Ge and Se, both of which are enriched relative to CI in the IDPs (Flynn and Sutton, 1992). The Ge and Se contents of the polar micrometeorites compare with those in CII and CIII meteorites. The polar micrometeorites are also depleted in Ni, which is present at approximately CI concentration in the IDPs, CII and CII meteorites. There is no obvious correlation of element enrichment or depletion in the polar micrometeorites with nebula condensation temperature, suggesting the measured abundance pattern is not a nebula condensation effect.

Although the sample set is small, the Greenland micrometeorites have lower concentrations of Cu, Zn, and Ga than the Antarctic micrometeorites. This may indicate a time variation in the composition of the micrometeorite flux, as previously suggested for melted spherules by Taylor and Brownlee (1991).

Only one of the particles, #20 from Greenland, shows a substantial depletion in Zn, an effect previously linked to significant atmospheric entry heating (Flynn et al. 1992; Thomas et al., 1992) for the stratospheric IDPs. This suggests the abundances we measured for the other volatile elements have not been altered significantly by atmospheric entry heating since order-of-magnitude Zn depletions are observed in the stratospheric particles before any of the other volatile elements we measure by SXRF show significant deviations from CI abundances (Flynn and Sutton, 1992a).

Mineralogy

Eleven of these polar micrometeorites have been studied by Analytical Transmission Electron Microscopy. The mineralogical results are reported in Table 1. One important question is the survival of layer-lattice silicates during atmospheric entry. None of these particles contained recognizable hydrated phases, such as the serpentines and smectites which occur frequently in IDPs. Some particles, however, are so fine grained (grains <<20 nm) that specific mineralogical identifications were not possible, so we cannot exclude the possibility that fine grained particles or fine grained areas in some particles might be relics of thermally altered hydrated phases.

Mineral assemblages in the slightly coarser grained particles (grains 30 to 200 nm) consist of euhedral crystals of high-Ca and low-Ca pyroxenes, olivines, chromites, spinels, magnetites, and glass. Two olivine populations have been identified so far in these particles: low-Fe olivines (Fa 7 to 25), which usually occur as small crystals (<100 nm) embedded in glass, and high-Fe olivines with Fe/Mg ratios from Fa 30 to 60. Mineral grains in Greenland particles #20 and #22 are approximately 100 nm and consist of olivines, pyroxenes, chromites, and magnetites embedded in glass.

The polar micrometeorites studied are texturally unlike the primitive anhydrous IDPs but show some similarities to heated IDPs with respect to their grain sizes, porosity, mineral assemblages and olivine compositions. The mineral assemblages of the polar micrometeorites are different from the primitive (CI and CM) carbonaceous chondrite matrices which consist mainly of hydrated phases such as smectite, serpentine, and tochilinite.

Thermal alteration of hydrated phases during atmospheric entry heating have not been well studied, and these alterations might explain the observed differences in mineral assemblages between hydrated meteorite matrices and polar micrometeorites. Many of the polar micrometeorites contain magnetite which, along with some of the olivine, may have been formed during entry heating. However some particles contain unequilibrated olivines. For example B3 #2 contains 1 to 2 μm olivines which range in composition from Fa 8 to Fa 40, limiting its peak temperature to about 1000° C. B1 #4 contains enstatite, high-Ca pyroxene, pyroxene high in Fe (Fs 20) and olivines from Fa 14 to 55 in contact with each other. Other particles contain silica rich glasses, which might indicate they were partially molten. The irregularly shaped polar micrometeorites appear to sample a wide range of entry temperatures.

Sources

The peak temperature reached on atmospheric entry increases with particle size, density, and entry velocity. Computer simulations show interplanetary dust particles >75 μm in diameter survive atmospheric entry without melting only for entry velocities near earth escape velocity, the lower limit of the entry velocity distribution. This suggests main-belt asteroidal parent bodies for the unmelted polar micrometeorites (Flynn, 1990b; Love and Brownlee, 1991; Flynn 1992). However, because these particles sample only the lowest portion of the velocity distribution, they represent a highly-biased sample of the total interplanetary dust population in this size range (Flynn, 1990a).

Alterations

Maurette et al. (1987) estimate that the Greenland micrometeorites fell within the past 3,000 years. The particles may be altered by interactions with the polar ice/water during their long residence times or by the process of extraction from the ice. The high Pb content of the Greenland and Antarctic micrometeorites is distinct from both the stratospheric IDPs and the chondritic meteorites. This led us to suggest that a significant fraction of the Pb may be contamination from the ice/water (Flynn et al., 1991). However,

Table 1: CI NORMALIZED CHEMICAL CONTENTS AND MINERALOGIES OF POLAR MICROMETEORITES

Particle	Fe*	Ni	Cu	Zn	Ga	Ge	Se	Br	Pb	Minerals#	Fa Olivine	Bulk FeO
Greenland												
#16	1	0.13	2.4	0.72	1.6	0.15	nd@	1200$	696	fg	----	17.0
#20	1	<0.005	0.11	0.07	<0.2	<0.04	nd@	643$	27	P,O,G	14-22	8.7
#21	1	0.08	1.1	0.54	0.4	0.351	nd@	2420$	247	fg, M	-----	7.5
#22	1	0.2	1.4	0.41	2.7	0.29	nd@	681$	847	P,O,G,C,M	12-30	15.3
Antarctic (B154 Sample)												
B1 #2	1	0.19	6.2	9.4	9.6	1.4	0.95	7.4	53	not analyzed		
B1 #4	1	0.02	4.8	4.9	7.0	0.08	0.08	5.1	65	O,P,M,S	14-55	34.6
B1 #5	1	0.41	1.3	2.6	0.61	0.62	0.47	2.5	37	O,P,G,C,M,S	30-50	27.3
B1 #7 Lg&	1	0.26	4.0	1.9	0.86	0.11	0.18	0.57	60	O,P,M,G,S	44-50	35.4
B1 #7 Sm&	1	0.28	3.0	1.3	1.0	0.05	0.15	0.94	58	not analyzed		
B1 #8	1	0.12	2.1	1.2	0.43	0.1	<0.08	0.61	41	O,P,M,G	30-68	35.1
B1 #17	1	0.20	4.9	6.4	9.1	0.54	0.67	10.8	323	O,M,S	40-50	27.5
B1 #19	1	0.61	2.3	2.7	0.26	0.31	0.54	6.5	35	Enstatite,Metal	----	10.5
B1 #20	1	0.04	1.5	2.5	1.4	0.93	0.34	3.8	40	fg	-----	33.3
B1 #22	1	0.42	2.5	1.8	0.16	0.12	1.2	3.8	19	O,P,G	36-55+	24.5
B3 #1	1	0.12	38	6.1	3.6	1.4	0.32	15	228	O,M,C	55-67	19.0
B3 #2	1	0.07	5.5	3.1	2.0	0.08	0.42	7.4	210	O	8-56***	42.2
B3 #3	1	0.33	2.1	0.85	0.54	0.22	0.49	8.5	10.6	not analyzed		
Average	1	0.2	4.9	2.7	2.4	0.4	0.45	4.3**	176			

* All chemical data are normalized to Fe = 1xCI.
\# Identified by Analytical Transmission Electron Microscopy: O=olivine, P=pyroxene, C= chromite, M=magnetite, S=spinel, G=glass, fg=fine grained (<<20nm) mineralogy not determined.
@ nd = not detected.
$ Br contents of Greenland micrometeorites include a contribution from the epoxy.
& B1 #7 broke into 2 fragments, denoted Lg and Sm, which were analyzed by SXRF separately.
\+ Large olivine grains were Fa 36-55, smaller olivine grains in glass were Fa 7-11.
** Average excludes Br in Greenland particles because of possible epoxy contribution.
*** Large grains Fa 8 to 40, small grains Fa 21-56.

when we mapped the Pb distribution in Greenland micrometeorite #16 we found a relatively uniform Pb/Fe ratio at the 5 μm scale across a section of the ~60 μm particle, with no evidence for Pb concentrations near the particle surface. If the Pb is contamination it appears to be relatively uniformly distributed throughout the micrometeorite. Experiments are presently in progress to quantify the contamination by examining the depth profile of Pb in outer surfaces of Antarctic meteorites.

The cause of the large Ni depletion measured in almost all polar micrometeorites (avg. Ni/Fe = 0.2xCI for this set of particles) also remains unexplained. Stratospheric particles, even those with low Zn abundances suggestive of significant heating on atmospheric entry, have Ni abundances consistent with the CI concentration (Flynn and Sutton, 1992a). Thus Ni loss during atmospheric entry seems an unlikely explanation. The Ni content may reflect the pre-atmospheric composition. Presper and Palme (1991) suggest spherical micrometeorites with low Ni/Ir ratios are chondrules, which have low Ni content, which remelted on atmospheric entry. Alternatively, Ni-bearing sulfides may be lost during their residence in the polar ices.

Conclusions

The average composition of the polar micrometeorites is enriched above CI meteorite concentrations for the volatiles Cu, Zn, Ga, and Br by amounts comparable to the enrichments measured in the 5 to 30 μm chondritic IDPs collected from the Earth's stratosphere. However the polar micrometeorites are depleted relative to CI in Ge and Se, both of which are enriched relative to CI in the IDPs, and depleted in Ni, which is present at approximately the CI concentration in the IDPs. In accord with earlier major element measurements by Maurette et al. (1991) we find similarities in the trace element contents between the polar micrometeorites and both the IDPs and the carbonaceous chondrite meteorites, but the polar micrometeorites are not identical in composition to either type of material.

Because aqueous alterations giving rise to both the addition and the removal of various elements (particularly Pb and Ni) from the polar micrometeorites are possible, convincing identification of the polar micrometeorites as a new and distinct type of solar system material may have to wait until the recovery of large micrometeorites either from the stratosphere or in space (eg. by the proposed Cosmic Dust Collection Facility on the Space Station). However, the present chemical data are consistent with the large micrometeorites being a new type of solar system material.

These polar micrometeorites also appear to be more compact (ie. higher density) than the anhydrous, porous IDPs which constitute about 45% of the smaller (5 to 30 μm) chondritic particles collected from the Earth's stratosphere (Schramm et al., 1989). This could indicate the volatile-rich, porous IDPs have higher geocentric velocities than the more compact particles, resulting in the larger porous IDPs melting or vaporizing on atmospheric entry. Alternatively, larger porous IDPs may fragment into smaller particles by the dynamic pressure experienced on atmospheric entry, or they may be more easily broken down during residence in or collection from the polar ices.

Thermal alteration effects, resulting from atmospheric entry heating, have not been well-studied. Laboratory simulations of these effects are required to determine if the polar micrometeorites might be alteration products from IDP or chondritic meteorite starting material.

The range of compositions and mineralogies of irregularly shaped polar micrometeorites indicates the main-belt asteroids contribute a diverse variety of particles to the interplanetary dust cloud.

ACKNOWLEDGEMENTS: We thank M. Maurette for providing the polar micrometeorites used in this study. This work was supported by NASA Grants NAG-9-459 (G.J.F.) and NAG-9-109 (S.R.S.).

REFERENCES

Cresswell R.G. and R.K. Herd (1992) Meteoritics, 27, 81-85.
Flynn G.J. (1990a) Proc. 20th Lunar Planet. Sci. Conf., 363-371.
Flynn G.J. (1990b) Meteoritics, 25, 365.
Flynn G.J. (1992) "Atmospheric Entry Survival of Large Micrometeorites: Implications for Their Sources and for the Cometary Contribution to the Zodiacal Cloud," Asteroids, Comets, Meteors 1991 (in press).
Flynn G.J. and S.R. Sutton (1991) Meteoritics, 26, 334.
Flynn G.J. and S.R. Sutton (1992a) Proc. Lunar Planet. Sci. Conf., Vol. 22, 171-184.
Flynn G.J. and S.R. Sutton (1992b) "Trace Elements in Chondritic Cosmic Dust" (abstract) Meteoritics in press.
Flynn G.J., S.R. Sutton and W. Klock (1991) Meteoritics, 26, 334-335.
Flynn G.J. et al. (1992) Lunar Planet. Sci. XXIII, 375-376.
Hughes D.M. (1978) in Cosmic Dust (ed. J.A.M. McDonnell), Wiley, New York, 123-185.
Love S.G. and D.E. Brownlee (1991) Icarus, 89, 26-43.
Maurette M. et al. (1987) Nature, 328, 699-702.
Maurette M. et al. (1991) Nature, 351, 44-47.
Presper T. and H. Palme (1991) Meteoritics, 26, 386.
Schramm L.S, D.E. Brownlee and M.M. Wheelock (1989) Meteoritics, 24, 99-112.
Sutton S.R. and G.J. Flynn (1988) Proc. Lunar Planet. Sci. Conf. 18th, 607-614.
Taylor S. and D.E. Brownlee (1991) Meteoritics, 26, 203-211.
Thomas K.L. et al. (1992) Lunar Planet. Sci. XXIII, 1427-1428.

Comparison between carbonaceous chondrite and microspherule in Paleozoic-Mesozoic bedded chert

Shigeyoshi Miono

Osaka City University, Sumiyoshi-ku, Sugimoto,Osaka,Japan.

〈Abstract〉

In our previous study[1] we had given PIXE analysis results of magnetic spherules collected from Paleozoic-Mesozoic bedded chert in southwest Japan. On the basis of these results, I have suggested that the Solar System encountered interstellar molecular cloud in the past. Furthermore data have been obtained as to the comparison between carbonaceous chondrite and magnetic spherule. Also internal texture of magnetic spherules were observed which is shown in Fig.1. The former suggestion that the ancient cosmic dust originated in interstellar medium similar to a carbonaceous chondrite was still confirmed. In 1978 at this symposium, Prof.N.Onuma of Tsukuba University suggested that the chondrite is rather interstellar in origin than interplanetary estimated by oxygen isotope analysis data. Recently Prof. E. Anders *et al.* have presented evidence from the insolble residues of meteorite for interstellar origin.[2] This admits of no doubt now, also it should be better to take into consideration that interstellar dust grains can penetrate the Solar System directly even after its formation.

References.

1)S.Miono *et al.* Proceedings of the NIPR Sympo. No4, 436-441.1991

2)E.Anders *et al.* Nature Vol. 326, 160-162, 1987

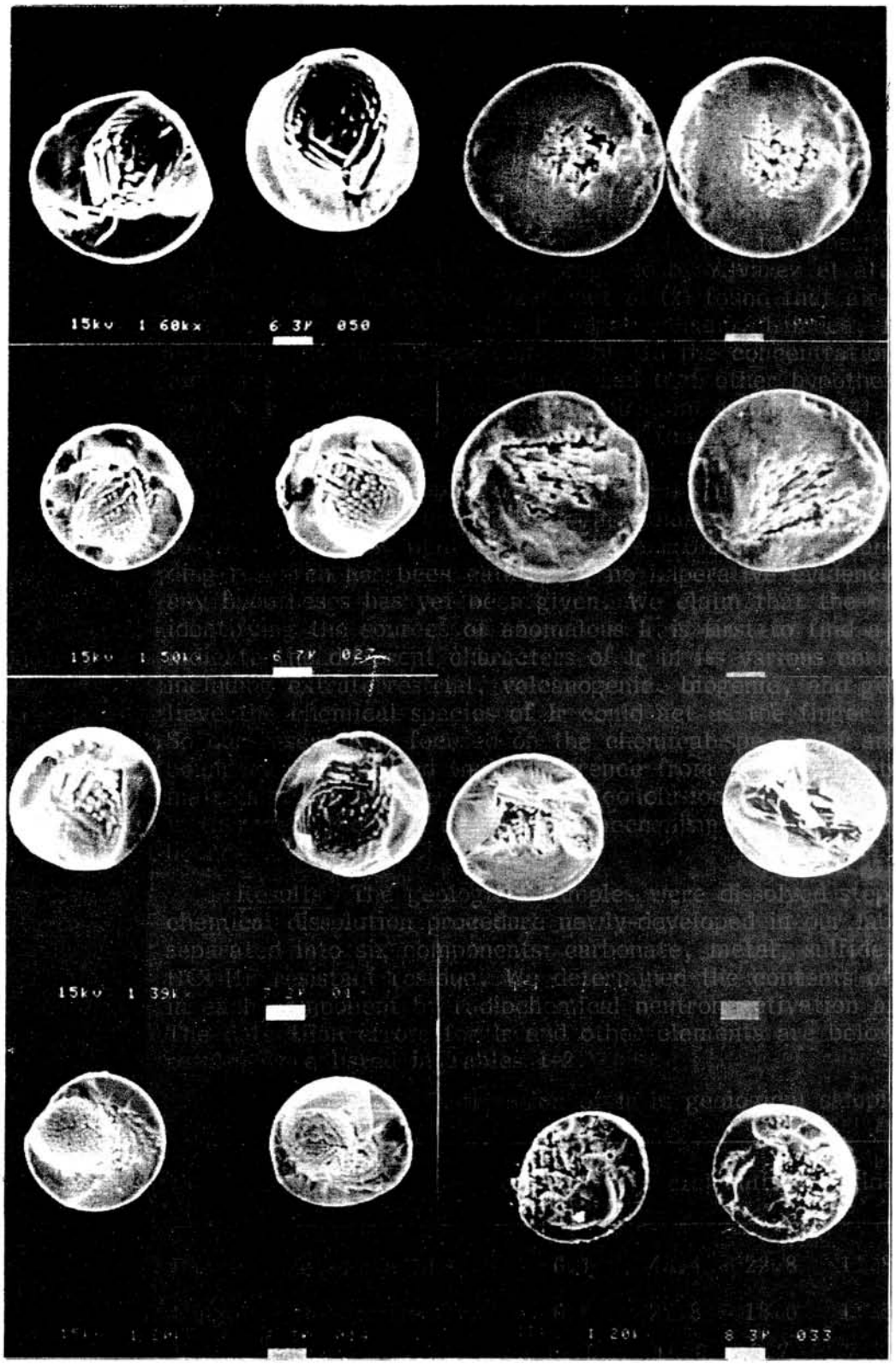

Fig.1 Internal texture of microspherules by scanning electron micrograph. Most of the spherules are hollow, it seems likely that CO_2 gas or vaporizing water were escaped.

Implications of iridium distribution and some micro-spherules in Cretaceous-Tertiary boundary clays

Ping Kong and Chifang Chai

Institute of High Energy Physics, Academia Sinica, Beijing, China

Introduction The study of life-mass extinction events during the earth history was given considerable impetus by the hypothesis of an asteroid impact at the end of the Cretaceous proposed by Alvarez et al.(1). This hypothesis has been challenged since Zoller et al.(2) found that air-borne particles collected from a recent eruption of a hot-spot volcano, Kilauea, Hawaii, were enriched in Ir with concentrations comparable to the concentrations associated with meteorites. Scientists also discovered that other hypotheses, e.g. geochemical enrichment, could also explain the iridium anomaly(3,4). Recent research on kerogen extracted from K-T boundary found that the concentrations of Ir in kerogen leached from two K-T boundary clays may reach 1100ppb(Stevns Klint, Denmark) and 1500ppb (Caravaca, Spain). Thus, the Authers proposed whether (5) the anomalous Ir is originated from biomass extinction. This proposition seems to shed some new light on this problem. Until now, Even though much succeeding research has been catalyzed, no imperative evidence either for or against any hypotheses has yet been given. We claim that the critical problem in identifying the sources of anomalous Ir is first to find a factor which could indicate the different characters of Ir in its various enrichment mechanisms, including extraterrestrial, volcanogenic. biogenic, and geochemical. We believe the chemical species of Ir could act as the finger to indicate its sources. So our research is focused on the chemical species of anomalous Ir in K-T boundary samples and their difference from those of meteorites and/or volcanic materials. We attempt to draw a conclusion from the different behaviours of Ir to reveal the true enrichment mechanism of the anomalous Ir in K-T boundary.

Results The geological samples were dissolved step by step by a selective chemical dissolution procedure newly-developed in our laboratory (6), eventually separated into six components: carbonate, metal, sulfide, oxide, silicate and HCl-HF resistant residue. We determined the contents of Ir and other elements in each component by radiochemical neutron activation analysis (7) and INAA. The detectiion errors for Ir and other elements are below 10% by NAA. The results were listed in Tables 1-2.

Table 1. Distribution of Ir in geological samples (in %)

sample	carbonate	metal	sulfide	oxide	silicate	residue
Baoxian meteorite LL4	6.1	43.4	22.8	11.8	4.9	—
Ningqiang meteorite CV3	6.6	27.8	18.0	11.5	8.6	27.6
K-T, Morgan Vreek, Canada	17.0	16.0	9.7	7.3	—	49.9
K-T, Montana, USA	32.1	—	—	—	24.1	43.8
K-T, Stevns Klint, Denmark	4.0	21.5	—	9.4	12.0	54.5
Lava, Kilauea, Hawaii	3.0	5.0	2.4	38.7	35.7	15.7
Ultrabasic rock, SRTH, Xinjiang	—	26.0	49.7	4.2	20.1	—

Table 2. Element distributions of sample L3S1 in Stevns Klint, Denmark (in %)

Element	carbonate	metal	sulfide	oxide	silicate	residue
Ir	4.0	21.5	—	9.4	12.0	54.5
Co	28.2	61.8	7.1	2.7	0.1	—
Ni	28.0	59.4	9.4	1.5	1.7	—
Fe	—	51.8		10.8	15.8	21.6
Sb	5.5	76.1	10.0	4.1	0.3	4.1
Sc	33.8	7.8	5.8	40.0	7.9	4.7
Th	73.3	23.1	0.6	2.0	1.0	—
Cr	24.2	4.6	10.2	48.4	12.6	—

Afterwards, we analyzed the composition of some light elements in the residue phase in the preceding samples as shown in Table 3.Finally we carried out microspherules analysis of the above residue by TEM and EDAX, see fig. 1.

Table 3. Concentrations of light elements in residue phase

sample		C, %	H,%	N,%
Fish Clay L1S1	1	34.98	2.56	3.78
	2	35.56	2.35	3.83
Montana, USA	1	3.34	1.96	0.3
	2	4.96	1.97	0.3
Ning qiang meteorite CV3	1	2.61	0.85	0
	2	3.65	1.06	0
Baoxian meteorite LL4	1	0.3	0.35	0
	2	0.3	0.51	0
Ultrabasic rock. SRTH	1	0.3	0	0
	2	0.3	0	0
Lava. Kilauea. Hawaii		3.82	0.31	0
Morgan Creek. Canada	1	33.71	2.79	1.24
	2	31.50	2.72	1.27

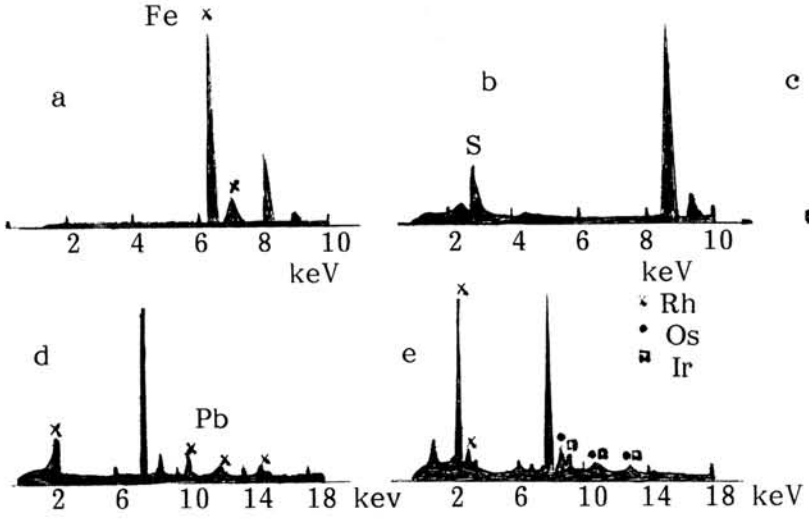

Fig.1. Particle graphs by EDAX. Some particle found in residue phases of geological samples

Discussion In the K-t boundary clays we analyzed, about 50% of Ir existed in each residue phase, but little in sulfide phase, regardless of their formation circumstances, either marine for sample Fish Clay L3S1, in Stevns Klint, or continental for samples in Montana, USA and Morgan Creek, Canada. This result objects to the hypothesis of geochemical enrichment of Ir proposed by Keith(3) who believed the Ir should be concentrated in sulfides and organometallic compounds. That means, most probably, that the anomalous Ir was not mainly caused by the geochemical enrichment. We can see also from table 2 that there is no correlation between Ir and other elements including siderophile, chalcophile or lithophile. This result also disfavors the mechanism of geochemical enrichment of Ir.

From table 3 we can see that the main component of Fish Clay L1S1, Stevns Klint, Denmark,is kerogen, whereas there is no kerogen in the residue of continental K-T sample, Montana, USA and this result we obtained in the different circumstances where the anomalous Ir formed showed that the Ir enrichment in boundary samples did not necessarily associate with kerogen, that is, the Ir enrichment is due to primitive sources and not particularly due to the existence of kerogen. Weproposed that the high content of Ir found in kerogen resulted from the primitively anomalous Ir remigration by kerogen physical adsorption. Whether the kerogen exists or not is related to the geological circumstances. Our further results demonstrated that the Ir in the residue is even more enriched after the kerogen has been removed. That means Ir is not combined with kerogen, that is, it is impossible that the anomalous Ir was originated from the organisms themselves.

Results of TEM and EDAX showed some particular spherules were existed in the residue phase of K-T boundary samples, e.g. some particles composed of iron were found in samples Fish Clay L3S1 and Morgan Creek, Canada.That showed one special event accompanied with high temperature or even high pressure in the boundary ages must have occurred. After that we found almost all spherules found in the volcano lava from kilauea were composed of bismuth, which was believed to be associated with gaseous-composed mineral from volcanic eruption, while in all K-T boundary samples we analyzed, the bismuth spherules were also found. Other particles such as Pb, Zn, and S exist in K-T boundary samples too. It has great possibility that these particles composed of Bi, Pb, Zn and S, respectively, came from condensation process of volcanic eruption and in fact, these particles had all been found in volatile components of volcano. Especially we found a spherule with 0.1 um diameter whose main components were Rh (90 %). Os (5%) and Ir (5%) in K-T boundary sample at Morgan Creek, Canada. We suggest that this spherule of noble nugget was formed in the process of impact material melting at the moment of contacting with target materials followed by recondensed mechanism after eruption to the atomsphere. On the basis of the above analyses, we propose: (1) It is impossible that the anomalous Ir was caused by geochemical enrichment; (2) The Ir enrichment in boundary did not necessarily associate with kerogen; (3) The volcanic activity must have participated in the extinction event at the end of the Cretaceous period; (4) Extraterrestrial impact was the trigger of K-T event.

Connecting all the results we listed above, we summarize a sequence which could perfectly explain the K-T extinction and its Ir anomaly. First, extraterrestrial material impacted the earth at the end of the Cretaceous. Because of the gigantic shockwave, world-wide volcano eruptions on a massive scale broke out. The violent eruptions are capable of injecting large amounts of sulfate aerosols into the lower stratosphere, with potentially devastating

atmospheric consequences, then, causing a massive catastrophe of biological history, ended the reign of dinosaurs with 95 % extinction. Along with mass extinction and geological enrichment, species of anomalous Ir from extraterrestrial impact and volcanic eruption were redistributed. Some were adsorbed by kerogen. That is why the Ir content was so high in kerogen leaching from some boundary samples. Thus, the species of Ir we found today are the mixed results of all the processes.

This work was financially supported by the National Natural Science Fundation of China (NSFC).

References 1. Alvarez L.W., Alvarez W., Asaro F., Michel H.V.,(1980) Science 208, 1095-1180. 2. Zoller W.H., Parrington J.R. and Phelan Kotra J.M. (1983) Science 222, 1118-1121. 3. Keith M.L.(1982) Geochim. Cosmochim. Acta46, 2621-2637. 4. Orth C.J., Gilmore J.S., Knight J.D., Pillmore C.L., Tschudy R.H., and Fassett J.E. (1982) Geol. Soc. Am. Spec. Pap. No.190. 5. Schmitz B., Andersson P., Dahl J.(1988) Geochim. Cosmochim. Acta.52 229.6.Kong P., Chai C.F.(1989) J.Radioanal. Nucl. Chem.130, 321-331. 7. Kong P. and Chai C.F. (1990) Chemical Geology 82, 51-56.

CHEMICAL COMPOSITIONS OF MICROTEKTITES IN LOESS

LI Chun-lai(李春来), OUYANG Zi-yuan (欧阳自远),
(Institute of Geochemistry, Chinese Academy of Sciences, Guiyang 550002, PRC)

I. INTRODUCTION

Different from macrotektites found on the ground, microtektites are microscopic tektite objects (less than 1 mm in diameter) found in sediments.

Loess, a fine, silt-size aeolian sediment, blankets large portions of Northwest China. Loess-palaeosol sequences have recorded the evolution of the earth surface. Its loess is loose and more or less uniform in composition, it is very convenient to sample. Loess may be the best continental sediment in which microtektites can be found.

Sperated from 8 meters thick loess samples which are taken from the top of L7 to the bottom of S8 on end, we found Australasian-Asian microtektites only in the upper layer of L8, a 40-70 cm horizon above the B/M boundry. The age of deposition is about 0.72 Ma.

Microtektites in loess are usually sphere, speroid, kidney-form, tear-drop and irrugular debris in shape. They are transparent and translucent, and some shade of green, amber and yellow in color. Their sizes range from 65 to 220 μm. Most of Microtektites were badly pitted and corroded, but there remain bubbles, cavities and scorious and flow microstructure in some ones.

II. CHEMICAL COMPOSITION

1. Major Elemental Compositions

Fourteen glassy microspherules from loess were analyzed with electron microprobe. On the basis of their major oxide compositions they may be divided into four chemical groups:

(1). Normal Microtektite. Studies of microtektites from deep-sea cores indicate that normal microtektites are lighter in color and larger in size, and they are similar in chemical composition to macro-tektites, but the contents of SiO_2, Al_2O_3, FeO and MgO are highly variable, Acoording to our data, the oxide compositions of this type of microtektites in loess falls within the compositions range of the same ones in deep-sea cores.

(2). Bottle-green Microtektite. This kind of microtektites is characterized by a lower SiO_2 and higher MgO. The highest contents of MgO is25% and the contents of SiO_2 in most of them are 48-54%. The heavier the color of the former, the higher the contents of MgO, Al_2O_3 and FeO, the lower the contents of SiO_2 in them. Our works show the major element compositions of bottle-green microtektites found in loess greatly extends the normal composition ranges of Ivory Coast and Australian ones in deep-sea

cores. They also overlap North American crystal - bearing microspherules in composition.

(3) . High -Aluminium Microtektite. They consist mainly of SiO2 and Al2O3, and distinctly differ in chemical composition from normal and bottle-green microtektites. Our data indicate this type of microtektites in loess is much similar in oxide composition to those found in deep -sea cores at Molino de Cobo, Spain.

2. Trace Elemetal Compositions

In our preliminary works, we obtained INAA data of only 3 H-Al microtektites in Loess, 4 normal Australasian microtektites in deep sea core and 1 glassy Si-Mg microspherules, although more than 8 microparticles were analyzed by instrumental neutron activation analysis.

According to our data, it is clear that glassy Si-Mg microspherule is heavily different from microtektite in the characteristics of trace elements, especially the former having very high Cr, Co contents. On the whole, the contents of refractory elements Ba, Cr, Co, Ta, etc. in microtektite tend to be higher than those in macro-tektite. Compared to normal microtektite, H-Al and bottle-green microtektites tend to contain higher refractory elements. For example, Ba content in H-Al microtektite from loess is 2-11 times higher than that in Australasian normal microtektite, and Sc, Th in the former are also more abundant than those in the latter. Cr, Co, Sc content in bottle - green microtektite are respectively 13, 3, 1. 4 times as high as that in nomal microtektite.

INAA data from Frey (1970, 1977) , which were from composites of microtektites with larger size, show microtektite is simmilar in the characteristics of rare-earth elements with macro-tektite, but the former is lightly lower in La, Ce, Yb, Lu and higher in Eu in some degree. Our INAA data of 7 individual microtektites support his conclusions, but microtektites in loess show the depletion of La, Ce, Yb, Lu and the excess of Eu more distinctly, and the smaller the size, the higher the abundance of Eu in microtektite from loess. The distinct positive anomaly of Eu in microtektite imply feldspar maybe is the predominant continent in its parent materials.

Since microtektites in loess are very small in size and very light in weight, the INAA analytical precise is so low that we cannot gain more information about the origin of (micro) tektite by means of its trace elements.

III. DISSCUSION

Walter et al. (1964, 1967) recognized that the compositional variation of macrotektites resulted from selective elemental vaporization. Cassidy (1969) pointed out that, because microtektite has a large relative surface aera, it could have suffered more loss of volatile oxides than tektite during a short melting period. This results in the compositional differences between microtektite and macro-tektite [8]. But their experiments didn't show the large compositional range enough to overlap the compositions of microtektites.

Geochemistry of trace elements in (micro) tektite indicates that, as constrasted to macro-tektite, microtektite, extraordinary H-Al and bottle-green microtektite, has more

refractory elements. This imply that microtektite may have suffered the loss of volatile elements, or it is made from selected constituents of parent materials that were abundant in refractory elements under the exceptional condition of impact. In microtektites from deep sea sediments and lunar impact glasses, some particles approximate to only a sort of mineral such as feldspar in chemical composition and the standard mineral composition. This indicates that selected melting of individual mineral may arise in the exceptional high flash - pressure - temperature resulted from impact.

The contents of K2O in macro-tektite is normally 2-4% , whereas that in microtektite from deep sea cores is normally 2-6%, some is as low as 0.001%, some is as high as 9. 31%.7 microtektites in 11 microtektites found in loess has rather high K2O (7. 34-9. 61%) . Their standard minerals consist mainly of feldspar and corundum, the content of the former is as high as 35. 3-73. 2%. This indicates that the parent material contains rather high feldspar. This is corresponded with the spectation that high positive anomaly of Eu may result from high content of feldspar.

we concluded that these differences are mainly due to target materials that microtektites and macrotektites derived from. thus parent materials of (micro)tektites are multiple -source constituents.

In addition, the preserving condition of microtektites may affect their composition to some extent. Lower MgO and CaO in microtektites in loess, in comparison with those in deep sea core, may attribute to the different composition, PH, EH and ionic strength of etching fluids through loess deposits and deep sea sediments.

IV. CONCLUSIONS

1. Examined 27 samples taken from L7 to L8 at Luochuan loess section, we found 16 microtektites in loess deposits.

2. Microtektites in loess occur only in the upper layer of L8, a 40-70 cm horizon above the B /M boundary. The age of deposition is about 0. 72 Ma. They are similar in occurence layer and age of deposition to other Australasian microtektites in deep sea cores, thus suggested to belong to Australia -Southeast Asian strewnfield.

3. Microtektites loess are micron light-colored tektite objects with 65 to 220 μ in size. They are of spheric bubbles and cavities, splashed and ablated forms, scorious and flow microstructure.

4. On the basis of their main oxide composition, microtektites in loess are divided into three chemical groups: normal, bottle-green and high-aluminium microtektite, each of which is similar in main composition to the same type of microtektites in deep sea sediments. Their compositional differences attribute to their parent materials and preserving condition.

5. Geochemistry of trace elements in microtektite and tektite indicates that their parent materials are multiple source contintuents. Higher content of refractory elements in microtektite maybe imply there are more refractory contintuents in the parent materials of microtektite than those in the parent materials of macro-tektite.

A Evidence for the Impact Origin of Tektites

Lin Wenzhu
Institute of Geochemistry, Academia Sinica, Guiyang,China

Barnes review tektite research career nearly sixty years, make one to belive that all tektites are impactites(1). A lot of the detailed geochemical studies and the isotopic studies for the tektite support this conclusion(2,3). Recent reviews have likewise favored terrestrial impact origin(2,4). Nevertheless, an endless debate has continued to the present about the origin of tektite. Somebody argues for an extraterrestrial (or lunar) volcanic origin(5). They thought that homogeneous glass isn't able to form while the time available in an impact(6). In reality, nuclear explosion, impact cratering and impact recovery experiment also occurs the glass which chemically is extremely homogeneous in short time duration (10^{-6}-10^{-1}s). The formational mechanism of the tektite is similar to the nuclear explosive and impact cratering melts (or glass)(7). So, these glasses we named " SHOCK GLASS ". Their melts were in non-linear oscillating, non-equilibrium dynamic, adiabatic expansive condition and fractales of the translational symmetry and cycle transformed a new phase - an amorphous solid state. In the extreme high-temperature turbulent flow occurrence the melt homogenize. Fig. 1 show the infrared spectra of shock glass. It is worth notice that shock glass. do not contain water and show an absorption band which it't probably C-H stretching vibration at 2916 CM^{-1}.

The volcanic glass is quenched by earth's interior magmas in the thermal equilibrium. Water is one of the most important volatiles in magmas(8). Water was " frozen " in volcanic glass while liquidus phase converts an amorphous solid state. So, the infrared spectra of the volcanic glass strikingly show bands of O-H stretching vibration, rangin in wavenumber from 3000 to 3700 Cm^{-1}, and at 1630 - 1640 CM^{-1} molecular H_2O dissolved in the glass(Fig. 2). The infrared spectra of tektite is similar to one of nuclear explosive glass, but strikingly differ with volcanic glass. This result suggest that a evidence for the impact origin of tektite.

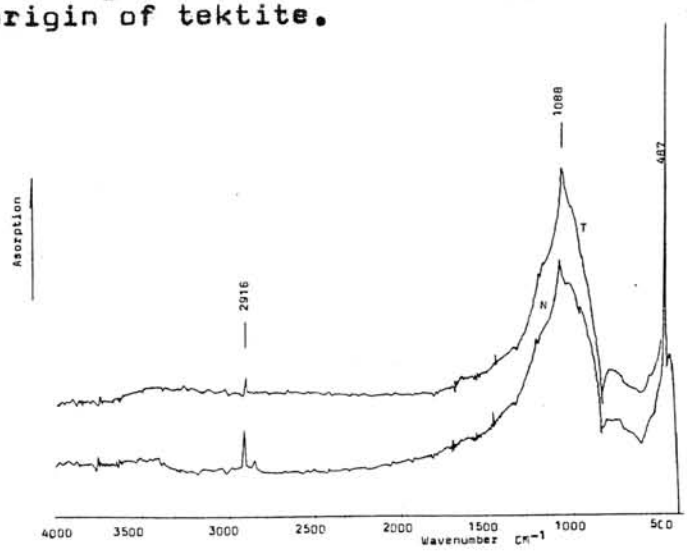

Fig. 1 Infrared spectra of the shock glass. N, nuclear explosion T, tektite

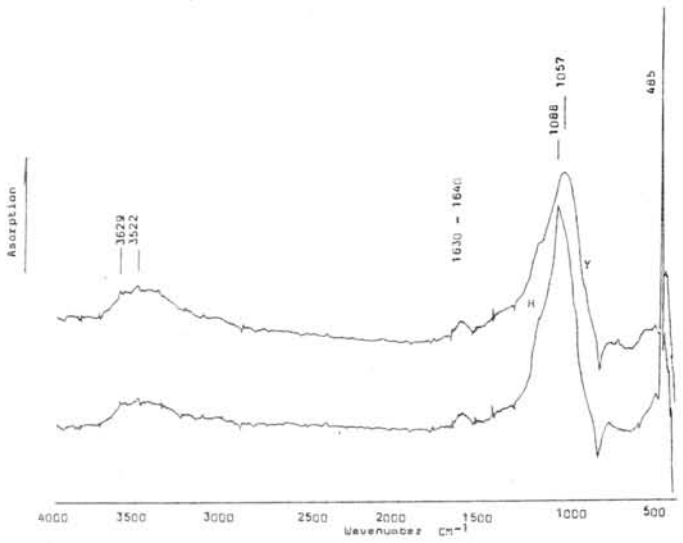

Fig. 2 The infrared spectra of volcanic glass
Y, obsidian (Zhejiang)
H, obsidian (Jilin)

References 1. Barnes V. E. (1990) Meteoritics 25, 149-159 2. Koeberl C. (1990) Tectonophysics 171,405-422. 3. Shaw H. F. and Wasserburg G. J. (1982) Earth Planet Sci. Lett. 60, 155-177. 4. Glass B. P. (1990) Tectonophysics 171, 393-404. 5. Futtrell D. S. (1991) Chem Erde 51, 72-80. 6. OKeefe J. A. (1986) 49th Ann. Meteoritical Society Meeting G-12. 7. Lin Wenzhu and Ouyang Ziyuan (1991) Scientia Geologica Sinica 2, 148-158. 8. Stolper E. (1982) Contrib Mineral Petrol 81, 1-17.

Special Session

Lunar Meteorites

MINERALOGICAL STUDIES OF LUNAR METEORITE Y-793169, A CRYSTALLINE BASALT. Hiroshi Takeda, Tomoko Arai and Kazuto Saiki. Mineralogical Institute, Faculty of Science, University of Tokyo, Hongo, Tokyo 113, Japan

Introduction Since 1989, four lunar meteorites, EET87521, Yamato (Y)-793274, Y-793169, and Asuka(A)-881757 have been proposed as derived from mare regions of the Moon [1,2,3,4]. EET87521 and Y-793274 are breccias rich in lunar mare components [5]. Y-793169 has been reported as a eucrite because it is composed of pigeonite and plagioclase [6]. However, its chemical trend of pyroxenes was different from that of eucrites [7]. As a part of the consortium studies, we studied Y-793169 and A-881757 by mineralogical techniques, including electron probe microanalysis, and compared them with basaltic components in mare breccias EET87521 and Y-793274 and with Apollo and Luna mare basalts [8] to elucidate their crystallization trends.

Delaney [1] and Warren and Kallemeyn [2,9] have proposed that some highland components are mixed in these two lunar meteorites. We also searched for slowly cooled plutonic pyroxenes common in lunar meteorites from the highlands on the basis of the mineralogical criteria, but we were unable to find such mineral components in them [5]. Boesenberg and Delaney [10] proposed now that Mg-rich components are basalts with different origin. We report detailed chemical trends of pyroxenes within Y-793169 and A-881757 and discuss the relationship among these lunar mare meteorites.

Samples and experimental techniques We investigated polished thin sections (PTS) A-881757,51-4 (Asuka-31) and Y-793169,51-3 supplied by the National Inst. of Polar Res. (NIPR) for the consortium studies. Mineral chemistries and textures of the PTSs were examined by an electron probe microanalyzer (EPMA) and scanning electron microscope (SEM), JEOL 840A with X-ray chemical map analysis (CMA) utilities of Kevex Super 8000. Chemical analyses were made with JEOL EPMA (8600 Super Probe) at the Geological Inst., and with a JEOL EPMA (JCXA-733) at Ocean Res. Inst., Univ. of Tokyo. We measured zoning profiles selected by the PYXQUAD system [11].

Results: Y-793169 Y-793169,51-3 PTS is a crystalline subophitic basalt with Fe-rich pyroxene, plagioclase and dark mesostasis portions. Fractures in pyroxene crystals and partly maskelinitized plagioclase crystals indicate shock effects, but the entire textures are not disturbed. Some of dark mesostasis materials are converted into dark glassy materials with Fe, Al, Mg, Na and K. The pyroxene crystals reach up to 3 X 1 mm in size and the plagioclase laths (up to 1.0 X 0.5 mm in size) often show rhombic sections, but in two areas, aggregates of plagioclase are formed. Both pyroxene and plagioclase crystals show extensive chemical zoning. The pyroxene-plagioclase ratio (volume) is about 2:1.

Chemical compositions of pyroxenes in the PTS are shown in the pyroxene quadrilateral (Fig. 1). The zoning trend distributes more at the Fe-rich side of the pyroxene quadrilateral toward Fe-rich Hd (hedenbergite). Pyroxenes in basaltic clasts of EET87521 and fragments in the matrix of Y-793274 show a similar chemical trend to Y-793169.

One trend of the typical chemical zonings (Fig. 1) is from Mg-rich core $Ca_{10}Mg_{55}Fe_{35}$ to Ca-rich mantle with nearly constant Mg/(Mg+Fe) ratios. Another trend is from Mg-rich core to about the middle of the pyroxene quadrilateral and shows Fe-enrichment with nearly constant Ca contents

towards the mesostasis portion. The most Fe-rich composition almost reaches the Ca-Fe join. Although very fine exsolution-like textures are found in some pyroxenes, the EPMA traverses did not show the chemical separation.

The An-contents of plagioclase crystals range from 96 to 85. There are mesostasis regions, in Ca-Fe-rich end of a pyroxene crystal near a plagioclase crystal. It consists of ilmenite, fayalite and a silica mineral. Chemical compositions of ilmenite in the mesostasis portion are Fe-rich. Although this basalt has been classified as a VLT basalt, the amount of ilmenite in the mesostasis is fairly large.

Asuka-881757 Mineralogy of A-881757 (Asuka-31) has been described previously in detail [3]. It is coarser-grained than Y-793169, but evidence of exsolution has not been detected by EPMA. The most Mg-rich core of the zoning trend is more Fe-rich than that of Y-793169. The symplectite texture reported by Yanai [3] is similar to the texture of the mesostasis portion in EET87521 [5].

Discussion The chemical trends of zoned pyroxenes in Y-793169 and A-881757 and those of only the basaltic clasts in EET87521 (BS1) and some pyroxene fragments in Y-793274 are similar and may represent those of initial crystallization from Fe-rich lavas. The trends are similar to those of pyroxenes such as those reported for rare mare-rock clasts (Ba-2 in 60019) found in Apollo 16 breccias and Luna 16 [5], and the VLT clasts in lunar meteorites from the highlands [12]. The Y-793169 trend represents more Mg-rich one than those of A-881757 and EET87521. A-881757 is coarse grained, but is not a cumulate rock as reported for Asuka-31 [3]. The Apollo 16 pyroxene zonation trends are more Mg-rich than EET87521, but are similar to the Y-793169 and Y-793274 trend. The most Fe- and Ca-rich trend of EET87521 goes to that of hedenbergite in the HPF clast in Y-791197 [13]. The presence of such Fe-rich pyroxene and fayalite fragments in EET87521 and Y-793274 suggests that these breccias sampled differentiated portions of the source lavas. The absence of exsolution lamellae observable by EPMA supports a rapid cooling in a shallow lava.

The discovery of a similar mesostasis portion in Y-793169 to that in the BS1 clast in EET87521 provides us with useful information on the final differentiation process of this lava. The presence of ilmenite in the mesostasis of all these VLT basalts indicates that the precipitation of Ti will take place even for a VLT basalt at the last stage of the small-scale differentiation. The coexistence of a silica mineral, fayalite and the ilmenite in Y-793169, implies that fayalite and silica were crystallized together at the final stage. A rock with fayalite, hedenbergite, silica, and Na-rich plagioclase has been reconstructed from the components in the matrix of EET87521 and Y-793274, but the compositions of plagioclase in Y-793169 are not as Na-rich as those in EET87521 and Y-793274.

The Cr-Ti spinel found in the mesostasis ilmenite in EET87521 is unique among lunar spinels because of its Cr-Fe-rich composition [5]. The chromian ulvöspinel reported in Asuka-31 [3] is poorer in Ca, but the symplectite in it may be related to the mesostasis in EET87521.

Boesenberg and Delaney [10] studied lithic clasts in EET87521 sample and recognized two VLT fractionation series. They proposed that among the VLT clasts, further subdivision is possible based on the correlation of Fe/(Fe+Mg) with Ti/(Ti+Cr) in the pyroxene (Fig. 2). Ti/(Ti+Cr) is a useful fractionation indicator as Ti is incompatible and Cr is compatible in pyroxene, and when coupled with Fe/(Fe+Mg), has been used to argue the

differentiation trends of VLT basalts [14]. Pyroxenes in the EET87521 VLT lithic clasts fall into two distinct groups [10]. Group A contains lithic clasts with low Fe/(Fe+Mg) ratios and varying Ti/(Ti+Cr) and Group B has higher Fe/(Fe+Mg) ratios and Ti/(Ti+Cr) higher than A (Fig. 2). The Luna 24 and Apollo 17 compositional data [15] show almost complete overlap with no clear split between the two groups. Y-793169 contains pyroxenes with low Fe/(Fe+Mg) ratios from 0.37 to 1.0 and Ti/(Ti+Cr) varying from 0.42 to 0.9. A-881757 has Fe/(Fe+Mg) between 0.48 and 0.91 and Ti/(Ti+Cr) between 0.53 and 0.92 (Fig. 2). The Y-793169 trend begins in the middle of the Group A trend of EET87521 and reaches the middle of the Group B trend and changes the dip of the slope to follow the general trend. A-881757 begins in between the Group A and B of EET87521 and the late stage trend is similar to that of Y-793169.

Two groups (A and B) may represent individual fractionating magma series, but these series may be linked to each other by derivation from magmas related by olivine fractionation in the source region [10]. The Mg-rich gabbroic clast with olivine has been found in Y793274 and Mg-rich pyroxenes are mainly found as an individual fragment with less zoning [5]. However, the zoning trend of Group B is mostly within one crystal or within lithic clasts.

The facts suggest that even within the VLT basalts, there are different fractionation trends depending on the bulk chemistry of magma and their crystal growth conditions. It should be remembered that the fractionation trends of Y-793169 and A-881757 and probably Group B of EET87521 are those of crystal growth during the solidification of the lavas. On the other hand Group A of EET87521 is too Fe-poor as a solidifing lava and may be fractionation trend of crystals separated by sinking from the main fractionating magma. Boesenberg and Delaney [10] mentioned that clasts in this group are small, while the more Fe-rich Group B are often larger and coarser grained. This observation is in line with our proposal that the Group A does not represent solidification of the lava.

In summary, general crystallization trends of their pyroxenes are similar, but the most Mg-rich core compositions and Ti/(Ti+Cr) vs. Fe/(Fe+Mg) trends are different. Y-793169 is a crystalline basalt similar to basaltic components in breccias EET87521 and Y793274. A mesostasis portion found in Y-793169 consists of ilmenite, fayalite and a silica mineral. Y793169 contains one of the most Mg-rich pigeonite core in the VLT basalts.

Acknowledgements. We are indebted to NIPR for the samples. We thank T. Ishii, E. Yoshida and O. Tachikawa for their help in microanalyses, K. Hashimoto, C. Akiyama for their technical assistance. This work was supported by funds from Cooperative Program (No. 84134) provided by Ocean Research Institute, University of Tokyo.

References 1. Delaney J. S. (1989) Nature 345, 889-890. 2. Warren P. H. and Kallemeyn G. W. (1989) GCA 53, 3323-3330. 3. Yanai K. (1991) Proc. Lunar Planet. Sci. Conf. 21, 317-324. 4. Takeda H., Saito J., Mori H., Yanai K., and Kojima H. (1991) Proc. NIPR Symp. Antarct. Meteorites, 4, 3-11. 5. Takeda H., Mori H., Saito J. and Miyamoto M. (1992) Proc. Lunar Planet. Sci. Conf. 22, 355-364. 6. Yanai K. and Kojima H. (1987) Photographic Catalog of the Antarctic Meteorites, p. 298, NIPR, Tokyo. 7. Takeda H. and Graham A. L. (1991) Meteoritics 26, 129-134. 8. Papike J. J., Hodges F. N., Bence A. E., Cameron M., and Rhodes J. M. (1976) Rev. Geophys. Space Phys., 14, 475-540. 9. Warren P. H. and Kallemeyn G. W.

(1991) Proc. NIPR Symp. Antarct. Meteorites, 4, 91-117. 10. Boesenberg J. S. and Delaney J. S. (1992) LPS XXIII, 127-128. 11. Saiki K., Yamaguchi A., and Takeda H. (1992) LPS XXIII, 1201-1202. 12. Treiman A. H. and Drake M. J. (1983) Geophys. Res. Lett., 10, 783-786. 13. Takeda H., Mori H., and Tagai T. (1986) Mem. Natl. Inst. Polar Res. Spec. Issue, 41, 45-57. 14. Nielsen R. L. and Drake M. J. (1978) Mare Crisium: The view from Lunar 24, 419-428, LPI. 15. Vaniman D. T. and Papike J. J. (1977) Proc. Lunar Planet. Sci. Conf. 8, 1443-1471.

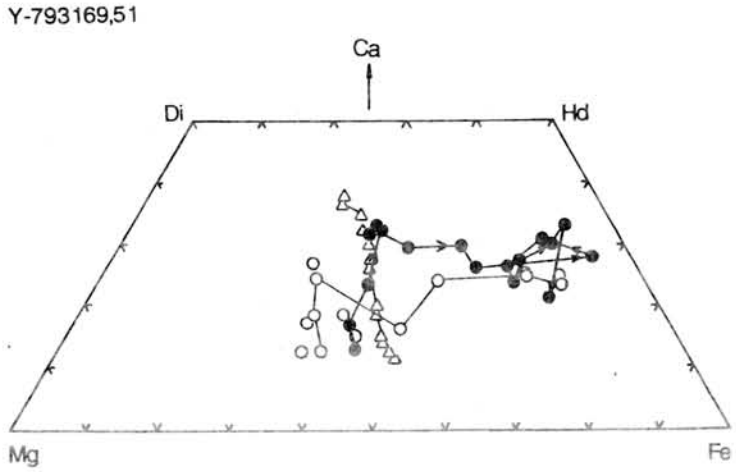

Fig. 1. Pyroxene quadrilateral of Y793169. Lines in zoned pyroxenes show zoning trend within one crystal. Solid and open circles and triangles represent different crystals.

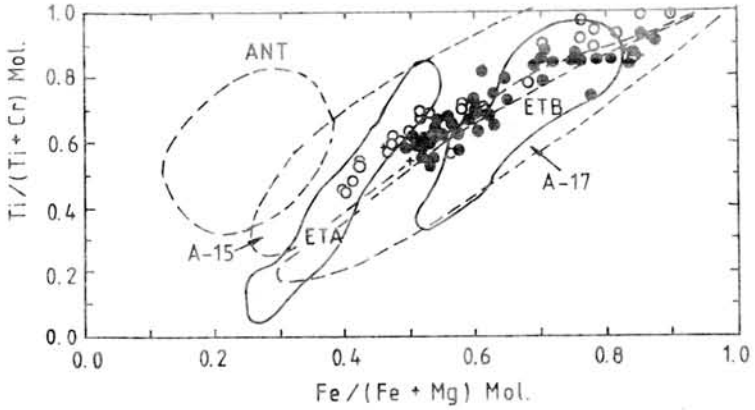

Fig. 2. Ti/(Ti+Cr) vs. Fe/(Fe+Mg) Mol ratios for pyroxenes in Y-793169. Data from A-15 mare basalts and A-17 VLT basalts are after Nielsen and Drake [14]. Open circles: Y-793169; solid circles: A-881757. ETA and ETB represent Group A and B of EET87521 [10].

Lithophile, Siderophile, and Volatile Geochemistry (Consortium Investigations) of Two Mare-basaltic Meteorites

Paul H. Warren and Gregory W. Kallemeyn
Institute of Geophysics and Planetary Physics, University of California, Los Angeles, CA 90024, USA

We have used INAA, RNAA and microprobe fused-bead analysis to determine the bulk compositions of two mare-basaltic meteorites from Antarctica: Yamato-793169, a 6.07-g diabase [Yanai and Kojima, 1990], and Asuka-881757, a 442- g gabbro, possibly a cumulate [Yanai, 1990]. Based on modes and pyroxene compositional data, both these meteorites appear similar to very-low-Ti (VLT) mare basalts.

The bulk composition of Y-793169 had not previously been studied. The only previous study of A-881757 [Lindstrom et al., 1991] was based on a small chip that was apparently not highly representative of this coarse-grained (typically 2-4 mm) rock. In this consortium investigation, we analyzed an aliquot of powder produced from a large mass of Asuka-881757, and from Y-793169 an aliquot of powder produced from a 0.119-g sample of stirred, sand-sized particles, in turn derived from an ~ 0.5-g chip.

The TiO_2 concentration we find for A-881757 is 2.5 wt%, significantly higher than the result (1.66 wt%) reported based on a wet-chemical analysis by Yanai [1990], but lower than the result (5.5 wt%) of Lindstrom et al. [1991]. Results for incompatible element concentrations, e.g., REE (see figure) are generally slightly higher than those of Lindstrom et al. [1991], and much higher than the typical concentrations of VLT mare basalts [data for Y-791197c are from Warren and Kallemeyn, 1991]. However, in both A-881757 and Y-793169 the heavy REE are enriched over La, to a degree seldom seen among low-Ti mare basalts (Apollo 12 ilmenite basalts are the nearest exception). The moderate incompatible element contents indicate that A-881757 is only moderately accumulative in origin.

Ratios such as Fe/Mn, Ga/Al and Co/Cr confirm the lunar provenance of Y-793169 (as well as A-881757). Our RNAA results indicate that in both cases the siderophile elements are extremely depleted, as is typical of "pristine" lunar igneous rocks. In most respects, these are quite ordinary lunar mare basalts. They might even be paired, despite the distinctive coarse-grained texture of A-881757.

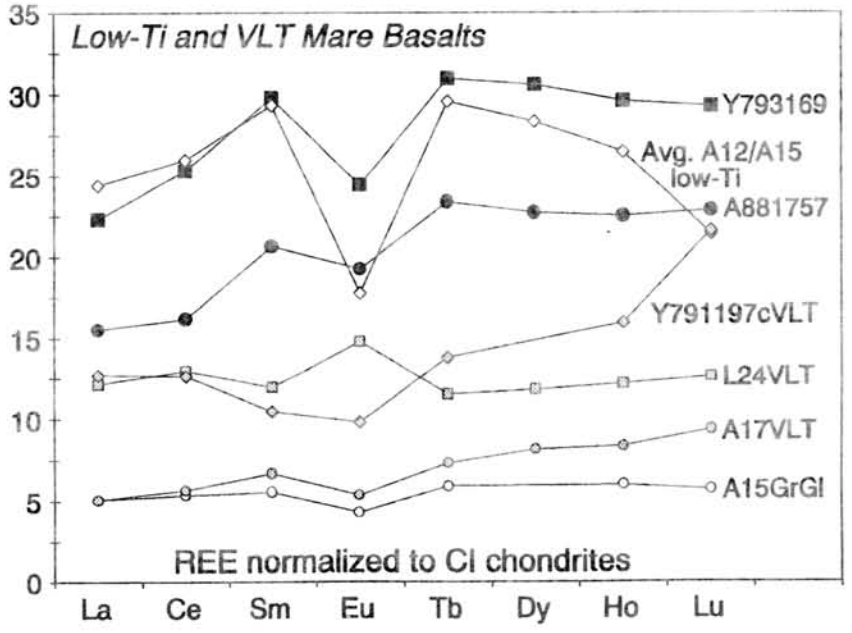

References

Lindstrom M. M., Mittlefehldt D. W. and Martinez R. R. (1991) *Abstracts 16th Symp. Antarctic Met.*, 102-105.

Warren P. H. and Kallemeyn G. W. (1991) *Proc. NIPR Symp. Antarctic Meteorites*, 4, 91-117.

Yanai K. (1990) *Abstracts 15th Symp. Antarctic Met.*, 119-121.

Yanai K. and Kojima H. (1990) *Abstracts 15th Symp. Antarctic Met.*, 129-130.

THE GENESIS AND EVOLUTION OF THE MOON'S MAGMA OCEAN AS SUPPORTED BY LUNAR ANTARCTIC METEORITES

Gregory A. SNYDER and Lawrence A. TAYLOR, Department of Geological Sciences, University of Tennessee, Knoxville, TN 37996, USA

The Moon is the only planetary body, outside the Earth, which we have sampled in a relatively systematic way. The Moon appears to have had a shorter and simpler history than the Earth. Though debate continues on the origin of the Moon and its relationship to Earth, we nonetheless have created a substantial base of geologic, physical, and chemical groundtruth upon which to test our hypotheses Whereas continuous cycles of weathering and subduction have inexorably altered the Earth and adulterated the composition of its primitive mantle, the Moon has retained a vestige of its beginning. Mare basalts in excess of 4.0 Ga and crustal rocks of even greater antiquity have remained unaltered since their creation on the surface of the Moon (except for weathering by massive meteorite impact). For this reason alone, the Moon is the type-planet against which hypotheses of the origins of other planets must be logically compared..

The lunar meteorites have been an unexpected addition to the once-considered static collection of lunar rocks. Meteorites of lunar origin, which have been collected on Antarctic ice fields, are the only new samples which have been added to the data base of lunar rocks over the past 15 years. However, these nine samples (including two paired samples and a triplet) have gone a long way in confirming various lunar hypotheses and yielding information on the global character of the Earth's moon. These meteorites include clasts of VLT mare basalts and ferroan anorthosite (Neal et al., 1991; Warren and Kallemeyn, 1991) which confirm the complementary negative and positive Eu anomalies, respectively, of these basic lunar rock types. These complementary clasts confirm that the crust and mantle of the Moon were formed from the same reservoir, the lunar magma ocean (LMO), early in its history.

Studies of lunar Antarctic meteorites have confirmed the high global Al_2O_3 signature of the upper crust of the Moon concluded from studies of the Apollo collections (Warren and Kallemeyn, 1991). This high global Al_2O_3 concentration (25-27 wt.%) is consistent with the presence of a lunar magma ocean (LMO) early in the Moon's history. This LMO would have precipitated olivine and pyroxene cumulates early, but would have reached saturation with respect to plagioclase after 53-78 % crystallization (Snyder et al., 1992). This plagioclase subsequently would have floated, yielding the Al-enriched crust of the Moon (Wood, 1970). After 93-95% crystallization, the LMO would have also become saturated with respect to ilmenite (Figure 1). These ilmenite-rich cumulates could have become gravitationally unstable on a local scale and led to small-scale overturning in the upper 30-40 km of the lunar mantle. This localized overturning would have modified the character of the source region(s) for high-Ti mare basalts.

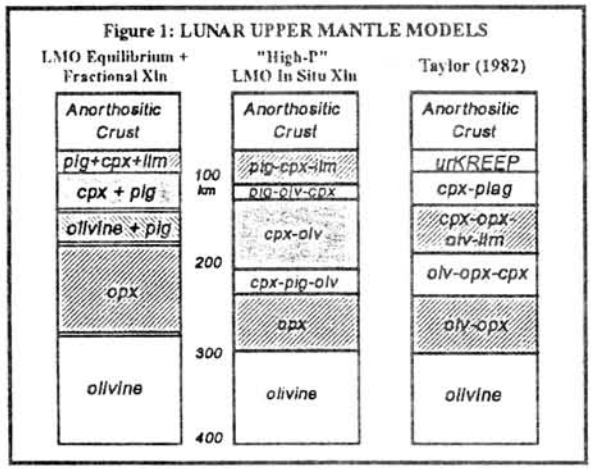

Figure 1: LUNAR UPPER MANTLE MODELS

Various workers have postulated a multitude of grossly similar bulk Moon and initial LMO compositions. The stratigraphy of the upper mantle of the Moon, as illustrated in Figure 1, is nonunique and based on an LMO starting composition similar to that of Buck and Toksoz (1980) and Ringwood et al. (1987). However, the modelling presented herein assumes that, once

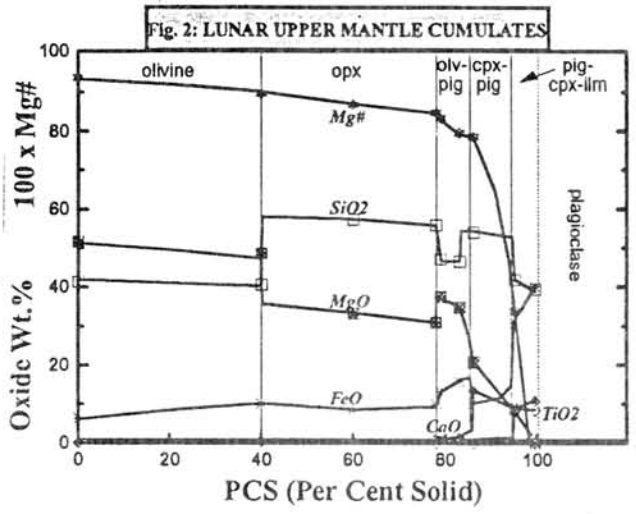

plagioclase becomes a liquidus phase, crystal-crystal separtions were not 100% efficient, leading to the entrainment of a small proportion of "floated" plagioclase.

The mineralogic layering of the lunar upper mantle naturally leads to chemical stratification. The major elements are controlled by these cumulus minerals and would be stratified in a manner like that illustrated in Figure 2. However, due to inefficient crystal-liquid separation, it is likely that these upper mantle cumulates also contain a small proportion of trapped intercumulus liquid. This 1-5% by volume trapped liquid contributed only a minute proportion to the major element balance of these cumulates. However, with continued crystallization incompatible trace-elements such as the LREE, K, and Th would have become increasingly enriched in the residual LMO liquid. This liquid, when trapped in the upper portions of the mantle cumulates, would have played an increasingly important role in the trace-element evolution of these cumulates as crystallization of the LMO reached its final stages (Figure 3).

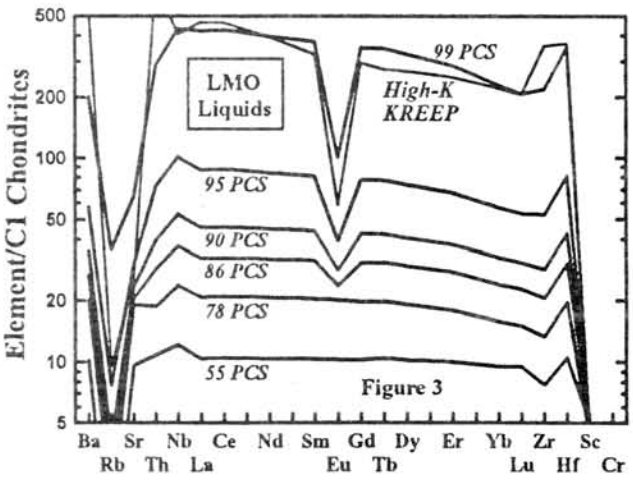

Figure 3

The trace-element chemistry of high-Ti basalts is readily explained by melting of a late-stage (after 95% crystallized) ilmenite-bearing LMO cumulate with 1-2% entrained plagioclase and 1-2% trapped residual liquid. In order to account for the high-Ti tenor of these basalts, ilmenite is required in the source. However, ilmenite does not precipitate from the LMO until late, when the Mg# of the mafic mantle cumulate is 34. High-Ti mare basalts exhibit a range of Mg#s; the most primitive samples have Mg#s of approximately 48. Therefore, any corresponding mafic source must have an Mg# above this value. In our model, the LMO precipitates a mafic solid with an Mg# of 79 at the 86% crystallized level. The radial distance between this layer and the ilmenite-bearing layer at 95% crystallized is only 30-40 km in a 300-400 km deep LMO. If small-scale convective overturn occurred during the formation of the mantle, then a proportion of the ilmenite-containing layer at the 95% crystallized level could have sunken to, and mixed with, the mafic cumulate from the 86% crystallized level. An 80:20 mixture of 86% crystallized level cumulate with 95% level cumulate yields a mafic cumulate with an Mg# of 73. The mineralogy of this mafic cumulate is: 46% pigeonite + 43% olivine + 7% clinopyroxene + 3% ilmenite + 1% trapped liquid (with 1-2% trapped KREEPy LMO liquid from the 95% crystallized level). Non-modal melting of such a source, whereby most of the liquid, plagioclase, and ilmenite were exhausted, is a likely scenario for generating the high-Ti mare basalts.

REE modelling of the source is consistent with this localized convective overturn. A residue from melting a mafic cumulate pile which would have lead to the high-Ti basalts can be calculated

by using bulk mineral/melt partition coefficients for the REE published in the literature and compiled by Snyder et al. (1992). This residue is shown in Figure 4 for 1-5% melting with only pigeonite, fayalite, and augite left in the residue. Based on experimental evidence, Green et al. (1975) have stated that ilmenite should be exhausted from the high-Ti source. This observation is not consistent with our modelling. In Figure 4, a field for these residue compositions is shown in reference to the 80:20 mixture of cumulates from the 86% crystallized level and the 95% crystallized level. Our model cumulate mixture can achieve a near perfect fit to the calculated 1-5% melting residues (Figure 4), both in terms of the shape of the LREE, HREE, and Eu anomaly, and the total REE abundances.

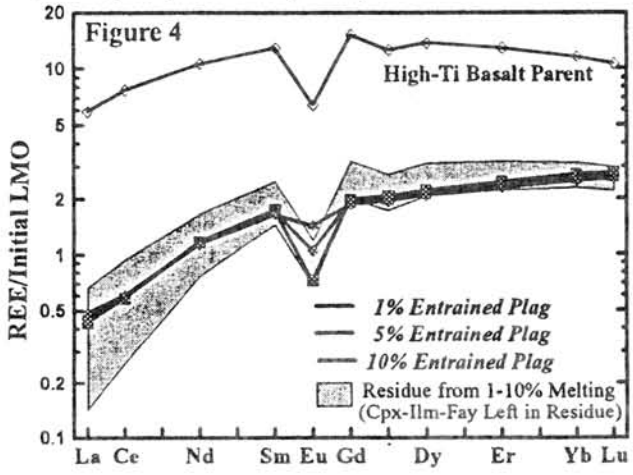

By varying the percentages of trapped liquid and entrained plagioclase, and the degree of fractional crystallization of the LMO, a wide range of sources which are LREE depleted to varying degrees, and exhibit a negative Eu anomaly, may be generated. This internal consistency lends credence to the plausibility of the model and points to the relative simplicity of the lunar upper mantle and its origin via a global magma ocean, an origin supported by data from the lunar meteorites.

REFERENCES: Buck, W.R. and Toksoz, M.N. (1980) *Proc. Lunar Planet. Sci. Conf. 11th*, 2043-2058; Green, D.H., Ringwood, A.E., Hibberson, W.O., and Ware, N.G. (1975) *Proc. Lunar Planet. Sci. Conf. 6th*, 871-893; Neal, C.R., Taylor, L.A., Liu, Y.-G., and Schmitt, R.A. (1991) *Geochim. Cosmochim. Acta 55*, 3037-3049; Ringwood, A.E. and Kesson, S.E. (1976) *Proc. Lunar Planet. Sci. Conf. 7th*, 1697-1722; Snyder, G.A., Taylor, L.A., Neal, C.R. (1992) *Geochim. Cosmochim. Acta 56*, in press; Warren, P.H. and Kallemeyn, G.W. (1991) *Geochim. Cosmochim. Acta 55*, 3123-3138; Wood, J.A., Dickey, J.S., Marvin, U.B., and Powell, B.N. (1970) *Proc. Apollo 11 Lunar Sci. Conf.*, 965-988.

GEOCHEMICAL AND CHRONOLOGICAL STUDIES FOR ASUKA-881757 LUNAR METEORITE. Kazuya Takahashi and Akimasa Masuda*. The Institute of Physical and Chemical Research Wako-shi, Saitama 351-01, Japan (*University of Electro-Communications, Chofu, Tokyo 182, Japan)

More than ten Antarctic meteorites have been recognized as the lunar meteorite. Many of them were classified anorthositic breccias and they are considered to have been originated from lunar highlands. Recently, several meteorites were identified as mare gabbros or basaltic breccias. Aska-31(Asuka-881757) is one of lunar meteorites with mare origin. According to Yanai and Kojima[1] and Lindstorm et al.[2], this meteorite is a new type of lunar sample (a very coarse-grained mare gabbro) and have the bulk chemical compositions and trace element abundances close to very-low-titanium mare basalt.

We were allocated Asuka-881757 SubNo.85 and SubNo.104 for REE (rare earth elements) measurements and Rb-Sr isotopic analyses. For SubNo.85, we analyzed REE abundances and Rb-Sr isotopic system as a whole rock sample and we separated SubNo.104 into mineral fractions by hand-picking under binocular. At present, we have analyzed whole rock sample and plagioclase fraction.

The REE abundance patterns of whole rock sample and plagioclase(maskelynite) fraction are shown in Fig.1. The whole rock sample is depleted in light-REE and shows clear convex curvature. Such pattern is also reported by Lindstorm et al.[2]. This pattern is consistent with the hypothesis that Asuka-881757 is mare origin. On the other hand, positive Eu anomaly is observed in the REE pattern of Asuka-881757. Neverthless, negative Eu anomalies have been observed in mare basalt. Asuka-881757 shows very coarse-grain feature (grain size is around 1-4 mm) and appears very heterogeneous. The positive Eu anomaly shown for Asuka-881757 should be due to the higher abundance of plagioclase in our sample than those for the other portions. It is also notable that no Ce anomalies are observed for Asuka-881757. For lunar highland samples and lunar meteorites with highland origin, various degrees of positive Ce anomalies have been found[3], [4]. The fact that Ce anomalies was not observed in Asuka-881757 could not become the evidence of mare origin, but it will give us suggestive data concerning the origin of Ce anomalies occurring in lunar highland samples.

Fig. 2 shows the results of Rb-Sr isotopic analyses. The samples from Asuka-881757 have very low Rb/Sr ratios and the expected age from two samples (whole rock and plagioclase) is around 3.7-3.8 Gyr. According to previous studies by many workers for lunar mare samples, low titanium basalt yielded Rb-Sr ages around 3.2-3.6 Gyr. The above age around 3.7-3.8 Gyr. is slightly older than the ages generally known for mare basalts.

In summary, all data, obtained at present, indicate that this lunar meteorite had originated from lunar mare region. Further Rb-Sr isotopic analyses and REE measurements for other mineral fractions will be discussed.

References

[1]Yanai, K. and Kojima, H. (1991): Proc. NIPR 15th Sym. Ant. Met., 118-130.

[2]Lindstrom, M.M., Mittlefehldt, D.W. and Martinez, R.R.(1991): NIPR 16th Sym. Ant. Met., 102-105(abstract).

[3]Masuda, A., Nakamura, N., Kurasawa, H. and Tanaka, T.(1972) Proc. Lunar Sci. Conf., 3rd 1307-1313.

[4]Takahashi, K., Masuda, A. and Shimizu, H. (1986) Proc. NIPR 10th Sym. Ant. Met., 96-105.

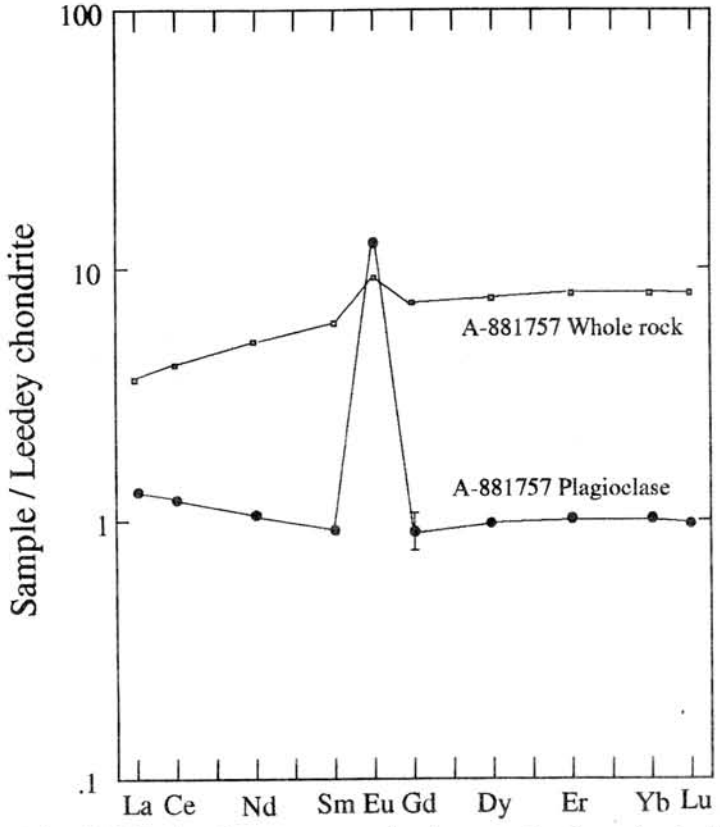

Fig. 1 REE abundance patterns for the samples from Asuka-881757

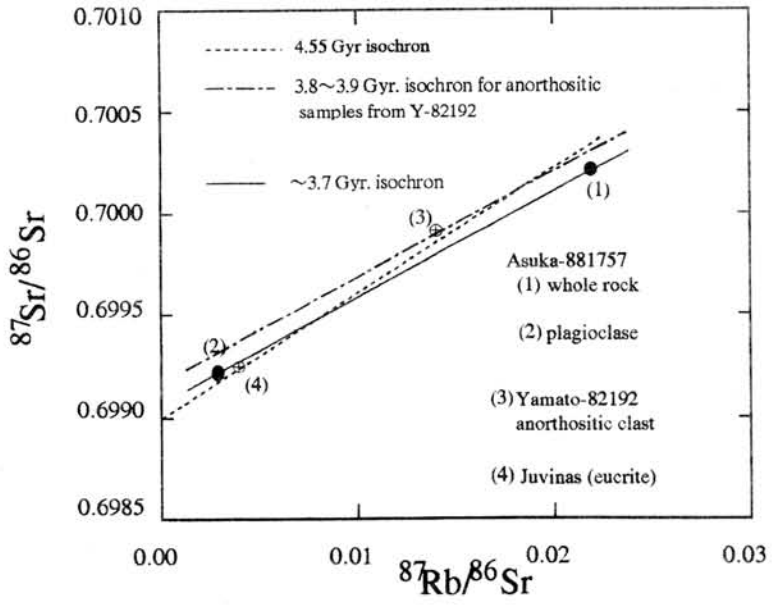

Fig. 2 ^{87}Rb-^{87}Sr diagram for several samples from lunar meteorites with the data of Juvinas eucrite
Data for Y-82192 are from Takahashi and Masuda[4]

U-Th-Pb, Sm-Nd, AND Rb-Sr ISOTOPIC SYSTEMATICS AND $^{40}Ar/^{39}Ar$ AGE OF LUNAR METEORITE ASUKA-881757; Keiji Misawa*, Mitsunobu Tatsumoto, U.S. Geological Survey, MS 963, Box 25046, Denver, CO 80225, U.S.A.; G. Brent Dalrymple, U.S. Geological Survey, MS 937, 345 Middlefield Rd., Menlo Park, CA 94025, U.S.A.; Keizo Yanai, National Institute of Polar Research, 9-10, Kaga 1-chome, Itabashi-ku, Tokyo 173, JAPAN; * Present address: National Institute of Polar Research.

Asuka-881757 is a new type of mare gabbro that is similar to Very-Low-Ti (VLT) basalts in bulk chemistry and mineral compositions [1-3]. We report the U-Th-Pb [4], Sm-Nd, and Rb-Sr isotopic systematics and the $^{40}Ar/^{39}Ar$ age of the meteorite, and discuss the genetic implications of this unique lunar meteorite. The meteorite is mainly composed of pyroxene, plagioclase, and ilmenite and contains brown-colored shock melt glass. Shock effects are also observed in plagioclase and pyroxene. Seven mineral separates and one whole-rock fraction were prepared for U-Th-Pb isotopic analysis. We carried out acid leaching on all separates using dilute HBr and HF to remove any terrestrial contamination and to strip the grain surface of any adsorbed Pb component. Along with these separates we also prepared two unleached fractions for Sm-Nd and Rb-Sr isotopic analyses. We measured $^{40}Ar/^{39}Ar$ age spectrum for fragments of shock melt glass and plagioclase using a continuous Ar-ion laser for heating, an infrared radiometer for measuring temperature, and a sensitive mass spectrometer for measuring isotope ratios [5]

In a $^{207}Pb/^{204}Pb$ *versus* $^{206}Pb/^{204}Pb$ diagram the whole-rock residue of Asuka-881757 does not plot on the data field of Apollo mare basalts and is less radiogenic. An observed $^{238}U/^{204}Pb$ (μ) value for the whole-rock residue is 96 and much smaller than that of Apollo mare basalts, which confirmed the previous suggestion that some portion of the Moon (*e.g.*, Crisium-Fecunditatis area) has evolved under a low-μ environment [6-8]. The Pb data from all residues define a Pb-Pb age of 3930 ± 52 Ma. However, plagioclase (PL1,R; PL2,R; and PL3,R) and whole-rock (WR,R) fractions do not plot on the line, suggesting open system behavior from a disturbance in the U-Pb system. Excluding these fractions the remaining four residues yield a Pb-Pb age of 3940 ± 28 Ma. During leaching preferential elemental fractionation occurred in the U-Pb and Th-Pb systems. Thus, the age calculation is made by combining the U, Th, and Pb in the leaches with those in the residues. Data points of the calculated values define U-Pb and Th-Pb isochron ages of 3920 ± 33 Ma and 3940 ± 14 Ma, respectively.

The Sm-Nd isochron diagram for the gabbro is shown in Figs. 1a and b. In order to check for low energy neutron capture effects on Sm isotopic composition in Asuka-881757, Sm was extracted from an unspiked pyroxene fraction. The Sm isotopic composition was found to be normal within errors and no neutron effect could be resolved (Table). The Sm-Nd data from residues and unleached fractions define an isochron age of 3830 ± 89 Ma. However, data points for "PL2,R", "PL3,R", and "MAG,R" slightly deviate from the isochron (Fig. 1a), indicating that the Sm-Nd system is also disturbed by post crystallization shock event(s). In these fractions significant amounts of Sm or Nd (35-50 % of total Sm or Nd) were leached out during the dilute HBr treatment. Excluding these three fractions the remaining five residues and two unleached fractions yield a Sm-Nd isochron age of 3850 ± 49 Ma with an initial ratio of 0.50799 ± 9. Except for "IL,R" the residues are more-radiogenic compared to the leaches, and the Sm/Nd ratios of leaches are smaller than chondritic (Fig. 1b), suggesting that LREE-enriched component(s) dissolved during the leaching. In Fig. 2, initial Nd isotopic compositions of mare basalts expressed in parts in 10^4 deviation (ε_{Nd}) from the average chondritic Sm-Nd parameters [9] are plotted against the age. A data point of Asuka-881757 plots along a growth curve defined by the Apollo 17 high-Ti basalts, the Apollo 12 ilmenite basalts, and the Apollo 15 basalt 15388,18 [10-14]. The high value of ~7 (T = 3.85 Ga) for ε_{Nd} is different from ε_{Nd} ~2 (T = 3.3 Ga) of the Luna 24 VLT basalt 24170 [19], suggesting that the source of Asuka-881757 differed significantly from that of 24170. Assuming Nd evolution from a *CH*ondritic *U*niform *R*eservoir at 4.4 Ga, the time-averaged $^{147}Sm/^{144}Nd$ ratio for the Asuka-881757 source could be larger than 0.3, more than 50% larger than chondritic and is somewhat higher than that for the Apollo 17 high-Ti basalts and the Apollo 12 ilmenite basalts. This is the most depleted source yet estimated for lunar rocks at 3.85 Ga. The similarity of LREE depletion in basalt source regions at least four different sampling sites is consistent with a global lunar magma ocean hypothesis. The Sm-Nd data are compatible with cumulate-remelting models for Asuka-881757 genesis and suggest that the source materials are deep in origin. This is also consistent with a low-μ source for Asuka-881757 estimated from the U-Pb data.

The Rb-Sr isochron diagram for the gabbro is shown in Figs. 3a, b, and c. The Rb-Sr data from residues and unleached fractions define an isochron age of 3810 ± 130 Ma. The data point for "IL,R" deviates from the isochron. In this fraction relatively large amounts of Rb or Sr (15% of total Rb or 24% of total Sr) were leached out during the 1*N* HF treatment. All leaches from the other fractions, however, contain less than 10% of total Rb or Sr. We thus considered that the deviation of the "IL,R" data point from the isochron might be due to the elemental fractionation during the leaching. Excluding this fraction the remaining seven residues and two unleached fractions yield a Rb-Sr isochron age of 3847 ± 31 Ma for $\lambda(^{87}Rb) = 1.42 \times 10^{-11}$ yr^{-1} (or 3923 ± 31 Ma for $\lambda = 1.39 \times 10^{-11}$ yr^{-1}) with an initial ratio of 0.69910 ± 2. A second calculation was made by combining the Rb and Sr in the leaches with those in the residues. The resultant data yield an age of 3838 ± 64 Ma with an initial ratio of 0.69910 ± 5, which is in good agreement with the Rb-Sr and Sm-Nd ages obtained from the residues' data. Initial Sr isotopic ratios for various mare basalts are plotted against the age (Fig. 4). Interlaboratory bias is adjusted for the NBS Sr standard value of 0.71026. The time-averaged $^{87}Rb/^{86}Sr$ in source materials of Asuka-881757 from LUNI [16] at 4.56 Ga is calculated to be

0.007. A comparison to the value of 0.019 for Asuka-881757 indicates that a Rb/Sr fractionation of ~3 x occurred during the formation of the gabbro at 3.84 Ga. The inferred Rb/Sr ratio of the Asuka-881757 source is very low and identical to the source materials estimated for the Apollo 11 low-K basalts, the Luna 16 basalt, and the Luna 24 VLT basalt [15, 17-19].

A 52-step $^{40}Ar/^{39}Ar$ incremental heating experiment on a single fragment (2.467 mg) of impact melt glass from Asuka-881757 yielded an age spectrum with a weighted mean plateau age of 3789 ± 16 Ma (2σ) (42 of 52 steps, 98 % of ^{39}Ar released; Fig. 5a). A plagioclase crystal (1.657 mg) from Asuka-881757 has a good plateau at 3808 ± 18 (2σ) Ma (Fig. 5b), which is within analytical error of the plateau age for the glass at the 95 % C. L. These results indicate that the meteorite was subjected to a shock event, which formed the melt glass and might be responsible for the disturbances in the U-Th-Pb, Sm-Nd, and Rb-Sr systems, at that time.

The age obtained here is somewhat older than those of low-Ti basalts (3.2-3.4 Ga) or VLT basalt (3.3 Ga) but similar to those of high-Ti basalts (3.6-3.9 Ga) and lunar basin-forming events at 3.8-4.0 Ga, which indicates that the gabbro was formed from a magma related to a basin excavation event(s), as were lunar basalts. However, it must be emphasized that the gabbro derived from a low-μ, low Rb/Sr, and high Sm/Nd source region.

References: [1] K. Yanai (1991) *Proc. 21st Lunar Planet. Sci. Conf.*, 317-324. [2] K. Yanai and H. Kojima (1991) *Proc. NIPR Symp. Antarc. Meteorites* 4, 70-90. [3] M.M. Lindstrom *et al.* (1991) *Papers presented to 16th Symp. Antarc. Meteorites* 102-105. [4] K. Misawa *et al.* (1992) *Proc. NIPR Symp. Antarc. Meteorites* 5, 3-22. [5] G.B. Dalrymple and G. Ryder (1991) *Geophys. Res. Lett.* **18**, 1163-1166. [6] F. Tera and G.J. Wasserburg (1972) *Earth Planet. Sci. Lett.* **13**, 457-466. [7] M. Tatsumoto (1973) *Geochim. Cosmochim. Acta* **37**, 1079-1086. [8] D.M. Unruh and M. Tatsumoto (1978) in *Mare Crisium: The View from Lunar 24* (eds. R.B. Merrill and J.J. Papike), pp. 679-694, Pergamon Press. [9] S.B. Jacobsen and G.J. Wasserburg (1980) *Earth Planet. Sci. Lett.* **50**, 139-155. [10] G.W. Lugmair *et al.* (1975) *Proc. 6th Lunar Sci. Conf.*, 1419-1429. [11] G.W. Lugmair and K. Marti (1978) *Earth Planet. Sci. Lett.* **39**,349-357. [12] L.E. Nyquist *et al.* (1979) *Proc. 10th Lunar Planet. Sci. Conf.*, 77-114. [13] D.M. Unruh *et al.* (1984) *Proc. 14th Lunar Planet. Sci. Conf.*, in *J. Geophys. Res.* **89**, B459-B477 [14] E.J. Dasch *et al.* (1989) *Lunar Planet. Sci.* XX, 218-219. [15] The Lunatic Asylum (1978) in *Mare Crisium: The View from Lunar 24* (eds. R.B. Merrill and J.J. Papike), pp. 657-678, Pergamon Press. [16] L.E. Nyquist *et al.* (1974) *Proc. 5th Lunar Sci. Conf.*, 1515-1539. [17] D.A. Papanastassiou *et al.* (1977) *Proc. 8th Lunar Sci. Conf.*, 1639-1672. [18] D.A. Papanastassiou and G.J. Wasserburg (1972) *Earth Planet. Sci. Lett.* **13**, 368-374. [19] L.E. Nyquist et al. (1978) in *Mare Crisium: The View from Lunar 24* (eds. R.B. Merrill and J.J. Papike), pp. 631-653, Pergamon Press. [20] G.P. Russ *et al.* (1971) *Earth Planet. Sci. Lett.* **13**, 53-60. [21] I.R. Fletcher and K.J.R. Losman (1982) *Geochim. Cosmochim. Acta* 46, 1983-1987. [22] L.E. Nyquist *et al.* (1981) *Earth Planet. Sci. Lett.* **55**, 335-355. [23] L.A. Taylor *et al.* (1983) *Earth Planet. Sci. Lett.* **66**, 33-47. [24] L.E. Nyquist *et al.* (1975) *Proc. 6th Lunar Sci. Conf.*, 1445-1465. [25] J.B. Paces *et al.* (1991) *Geochim. Cosmochim. Acta* **55**, 2025-2043.

Table. Results of Sm and Nd Analyses

Sm isotopes*	$^{144}Sm/^{152}Sm$	$^{148}Sm/^{152}Sm$	$^{149}Sm/^{152}Sm$	$^{150}Sm/^{152}Sm$	$^{154}Sm/^{152}Sm$
Normal (n=5)	0.11496 ± 1[¶]	0.42045 ± 2	0.51687 ± 2	0.27600 ± 2	0.85085 ± 4
Asuka-881757 PX	0.11496 ± 3	0.42041 ± 3	0.51685 ± 4	0.27596 ± 3	0.85081 ± 8
Nd isotopes**	$^{142}Nd/^{144}Nd$	$^{143}Nd/^{144}Nd$	$^{145}Nd/^{144}Nd$	$^{148}Nd/^{144}Nd$	$^{150}Nd/^{144}Nd$
La Jolla STD (n=9)	1.141870 ± 44	0.511865[§] ± 22[†]	0.348416 ± 6	0.241583 ± 11	0.236459 ± 5
Asuka-881757 PX	1.141830 ± 34	0.515201 ± 12	0.348420 ± 7	0.241583 ± 9	0.236457 ± 12

* Isotopic ratios are normalized to $^{144}Sm/^{152}Sm = 0.56081$ [20]. ** Nd was measured as the oxide. Calculated with $^{18}O/^{16}O = 0.00210$ and $^{17}O/^{16}O = 0.000374$ and normalized to $^{146}Nd/^{144}Nd = 0.7219$. ¶ Errors represent 95% C.L. of the mean. § Including Nd^+ runs (n=2). † Error limits are $2\sigma_p$

Fig. 1. Sm-Nd internal isochron. (a): Residues and unleached fractions. The inset shows the deviation of $^{143}Nd/^{144}Nd$ of measured values from the best fit isochron. (b): First (0.01*N* HBr or 1*N* HF) and second (0.1*N* HBr) leaches.

Fig. 2. ε_{Nd} *versus* T diagram. The initial ε_{Nd} value is calculated using the chondritic parameters [9] and the error limits are calculated following the optimized procedures by [21]. Lunar basalts data are from [13] and references therein.

Fig. 3. Rb-Sr internal isochron. (a and b): First (0.01*N* HBr or 1*N* HF) and second (0.1*N* HBr) leaches. (c): Residues and unleached fractions. The inset shows the deviation of $^{87}Sr/^{86}Sr$ of measured values from the best fit isochron.

Fig. 4. Initial Sr *versus* T diagram. Lunar basalts data are from[17, 18, 22-25].

Fig. 5. High resolution $^{40}Ar/^{39}Ar$ age spectrum for (a) shock-melt glass and (b) plagioclase from Asuka-881757 obtained by laser step heating.

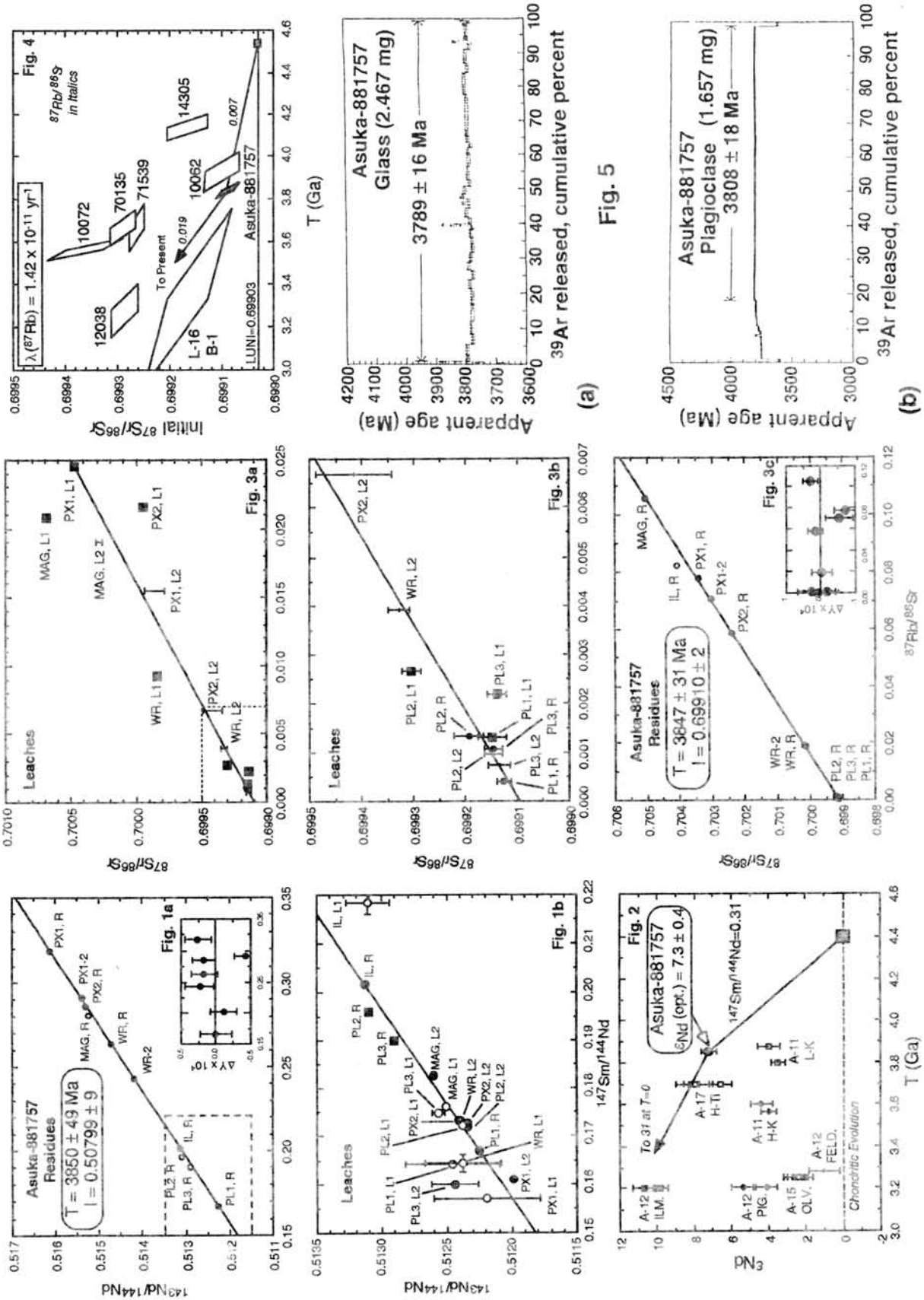
Fig. 4
λ(87Rb) = 1.42 x 10-11 yr-1
87Rb/86Sr in Italics
10072
70135
71539
14305
12038
10062
0.019
0.007
To Present
L-16
B-1
LUNI=0.69903
Asuka-881757
Initial 87Sr/86Sr
T (Ga)
Asuka-881757
Glass (2.467 mg)
3789 ± 16 Ma
Apparent age (Ma)
39Ar released, cumulative percent
(a)
Asuka-881757
Plagioclase (1.657 mg)
3808 ± 18 Ma
(b)
Fig. 5
Fig. 3a
Leaches
Fig. 3b
Fig. 3c
Asuka-881757
Residues
T = 3847 ± 31 Ma
I = 0.69910 ± 2
87Sr/86Sr
87Rb/86Sr
Fig. 1a
T = 3850 ± 49 Ma
I = 0.50799 ± 9
143Nd/144Nd
Fig. 1b
147Sm/144Nd
Fig. 2
Asuka-881757
εNd (opt.) = 7.3 ± 0.4
147Sm/144Nd=0.31
To 31 at T=0
Chondritic Evolution
εNd
T (Ga)

U-Th-Pb Chronology of Yamato 793169 Lunar Meteorite

N. Torigoye, K. Misawa*, and M. Tatsumoto
U.S. Geological Survey, MS 963, Box 25046, Denver, CO 80225, U.S.A.

Yamato 793169 is a medium- to coarse-grained unbrecciated, lunar diabase. It consists of mainly pyroxene and plagioclase, and the chemical composition is similar to those of the low-titanium and VLT lunar mare basalts [1]. As a part of the consortium study, we are studying the chronology of the meteorite using the U-Th-Pb, Sm-Nd, and Ar-Ar methods, and this report includes only the U-Th-Pb data obtained so far.

A sample weighing 104 mg was gently crushed and separated into two size fractions, <63 μm (Fines) and 63-150 μm, with nylon sieves. Pyroxene (PX1) and plagioclase (PL) separates were handpicked from the 63-150 μm fraction. The rest of the 63-150 μm fraction is enriched in pyroxene (PX2).

These four separates were first washed with distilled acetone and then ethanol. In order to remove any terrestrial Pb contamination or adsorbed surficial Pb components, the samples were further leached with 0.01N HBr and 0.1N HBr. The residues were then dissolved with concentrated HF and HNO_3. The U, Th, and Pb concentrations and Pb isotopic compositions of both leaches and residues were determined.

The $^{206}Pb/^{204}Pb$ values range from 83 (PL) to 125 (PX1) among the three handpicked separates. The Pb isotopic compositions are radiogenic compared to those of terrestrial basalts but less radiogenic compared to Apollo mare basalts. The less radiogenic feature is in accordance with Pb characteristics of brecciated VLT lunar meteorites [2]. The $^{206}Pb/^{204}Pb$ value of the fine fraction is much less radiogenic (25.2). We suspect this feature is probably due to incomplete removal of terrestrial Pb during leaching. The Pb data are plotted on a $^{207}Pb/^{206}Pb$ versus $^{204}Pb/^{206}Pb$ diagram in Fig. 1. The Pb-Pb age defined by the two pyroxene separates, PX1 and PX2 is 3920 ± 2 Ma (solid line). Fines and PL deviate from the line. The Pb data of PL was excluded in the calculation, since petrologic evidence suggested that the plagioclase was recrystallized due to shock events [1]. The Fines plot close to our blank Pb value, suggesting terrestrial contamination. The U-Pb data are plotted on a $^{207}Pb^*/^{206}Pb^*$ versus $^{238}U/^{206}Pb^*$ diagram (Fig. 2). Using the Pb isotopic composition of Cañon Diablo troilite for our initial Pb correction, the two PX fractions yield an concordia upper intercept age of 3980 Ma. Using more evolved initial Pb composition ($^{238}U/^{204}Pb$ = μ of 8 between 4.56 and 4.44 Ga and 10 between 4.44 to 3.92 Ga), the two PX fractions define concordia intercept ages of 3921 ± 1 Ma and 201 ± 67 Ma.

*Present address: National Institute of Polar Research, Itabashi-ku, Tokyo 173, Japan.

These ages, however, are only defined by the two PX fractions and verification by other methods is needed. If the age defined by the pyroxenes is meaningful, the Pb data indicates that the diabase was derived from a low U/Pb source; (μ value as low as 10). In order to clarify the U-Pb data, Sm-Nd and Ar-Ar analyses are in progress and the results will be discussed.

References:

[1] Yanai, K. and Kojima, H., Proc. NIPR Symp. Antarct. Meteorites, **4**, 70-90 (1991).

[2] Tatsumoto, M. and Premo, W.R. Proc. NIPR Symp. Antarctic Meteorites, 4, 56-69 (1991).

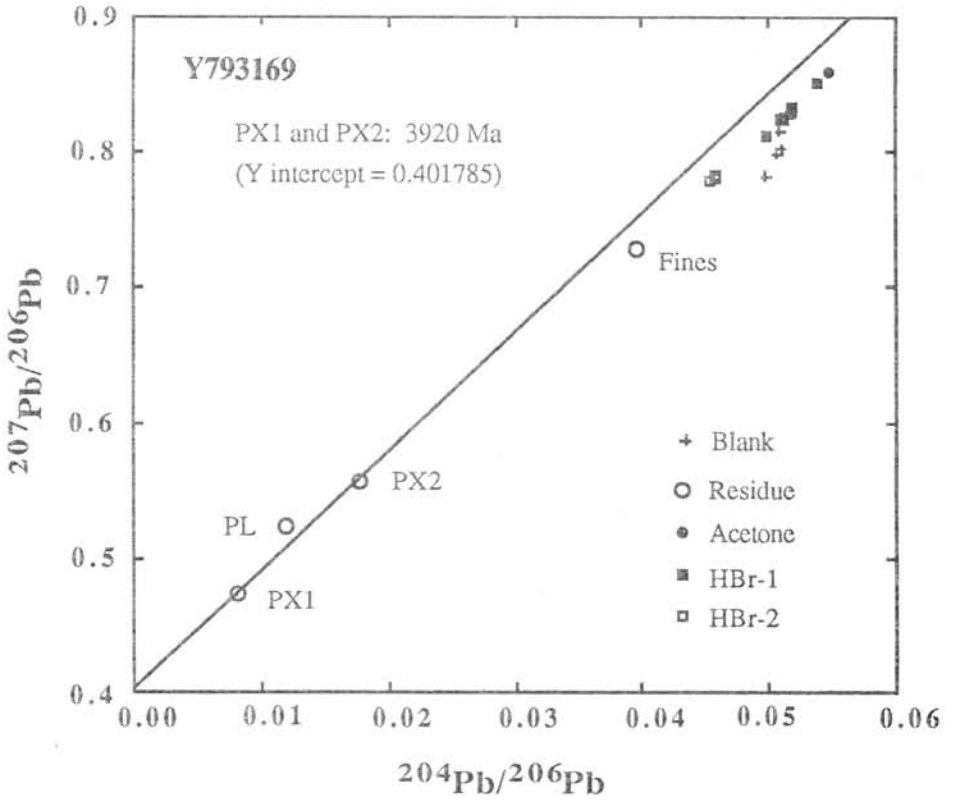

Fig. 1. $^{207}Pb/^{206}Pb$ vs. $^{204}Pb/^{206}Pb$ diagram for Y793169. Acetone indicates acetone and ethanol washed samples, HBr-1 and HBr-2 indicate 0.01N HBr leached and 0.1N HBr leached samples, respectively. The age obtained from the solid line, defined by PX1 and PX2, is 3920 Ma.

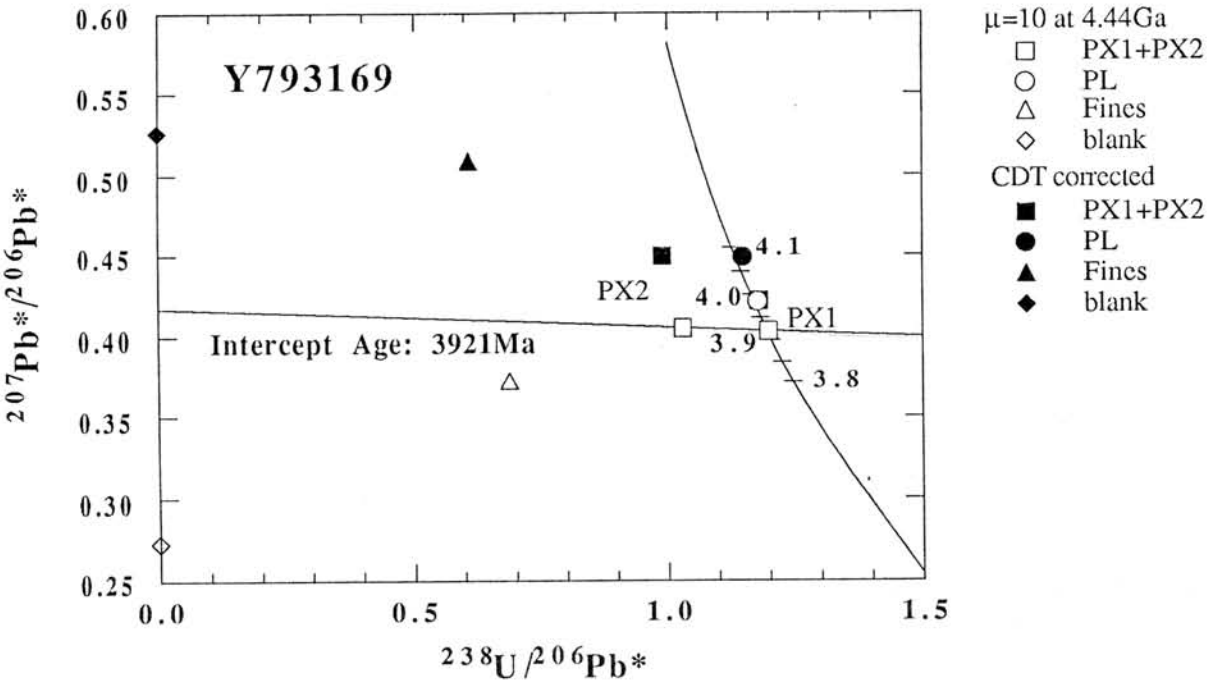

Fig. 2 Modified concordia diagram for Y793169. Filled symbols are data corrected for initial Pb using the Cañon Diablo troilite (CDT) Pb isotopic composition . Open symbols are data corrected using initial Pb isotopic compositions of a low μ source material. In this calculation, it is assumed that the source material evolved from CDT Pb with μ=8 between 4.56 Ga and 4.44 Ga and μ=10 between 4.44 Ga and 3.92 Ga.

NOBLE GASES AND ^{81}KR-TERRESTRIAL AGE OF ASUKA-31

Keisuke NAGAO[1] and Yayoi MIURA[2]
1)Institute for Study of the Earth's Interior, Okayama University, Misasa, Tottori 682-01, Japan.
2)Department of Earth and Planetary Physics, University of Tokyo, Bunkyo, Tokyo 113, Japan.

Introduction

Asuka-31 lunar meteorite was discovered by the Japanese Expedition Party in December 1988. This meteorite is a new type of lunar meteorite and is unbrecciated, coarse-grained gabbro retaining original texture after its consolidation. High Fe and low Ti concentrations are in the range of lunar mare basalt. These characteristic features of this meteorite have been summarized by Yanai (1991). We measured noble gases of the Asuka-31 to investigate the history of this meteorite on the moon and the transit to the earth using cosmogenic and radiogenic isotopes as well as trapped solar noble gases. Cosmogenic radionuclide ^{81}Kr was also measured to determine the terrestrial age.

Experimental method

Step heating noble gas extraction was applied for a small sample size of 10.2 mg (*SH-sample*). The temperatures were 600, 800, 1000, 1200, 1400 and 1700 °C. After that, 395.3 mg specimen was totally melted to measure ^{81}Kr as well as other all noble gas isotopes (*TM-sample*). Noble gas mass spectrometer used in this work was VG5400 which has been modified and improved in our laboratory. Low blank noble gas preparation line is connected to this mass spectrometer. Detection limit of noble gas isotopes using ion counting system was about 1×10^{-14} and 1×10^{-15} cm^{3}STP for He and Xe isotopes, respectively. Hot blank levels were $<1\times10^{-11}$, 2×10^{-11}, $<1\times10^{-9}$, $<1\times10^{-13}$, and $<1\times10^{-14}$ cm^{3}STP for ^{4}He, ^{20}Ne, ^{40}Ar, ^{84}Kr and ^{132}Xe, respectively.

For the calculation of ^{81}Kr-terrestrial age, an apparent exposure age based on the cosmogenic Kr isotopic compositions was calculated by,

$$T_a=(1/\lambda)(P_{81}/P_{83})(^{83}Kr/^{81}Kr)_c,$$

where λ ($=3.25\times10^{-6}y^{-1}$) is the decay constant of ^{81}Kr and P_m means a production rate for ^{m}Kr. Using the apparent exposure age T_a, the ^{81}Kr-terrestrial age T_t was calculated by,

$$T_t=(1/\lambda)\ln(T_a/T_e),$$

where T_e is a true exposure age (Freundel et al., 1986).

Results and discussion

The noble gas data are presented in Tables 1 and 2. Because of the small amounts of Ne isotopes extracted by the individual step heating, reliable isotopic compositions were difficult to be obtained until now by correcting $^{40}Ar^{++}$, CO_2^{++} and blank. From this reason, Ne isotopic ratios for step heating were not presented in the table.

Ne isotopes have cosmogenic composition indicating virtually no trapped Ne. Trapped He was also negligible. The very low ^{3}He/^{4}He ratios, $<7\times10^{-5}$, observed in 800, 1000 and 1200°C fractions of step heating show low abundances of both cosmogenic and trapped He in this meteorite. Although trace abundances of trapped Ar , Kr and Xe were found in this lunar meteorite, their relative abundances are not similar to that of solar gases but

to those of planetary or Earth's atmospheric noble gases. These low or negligible concentrations of trapped noble gases contrast strikingly with the high abundances of solar type noble gases trapped in other lunar meteorites previously reported by others (e.g. Bogard and Johnson, 1983; Takaoka, 1986; Takaoka, 1987; Eugster and Niedermann, 1988; Eugster et al., 1991). After the gabroic formation, this meteorite seems to be buried in the depth until its ejection from the moon.

Cosmogenic ^{38}Ar concentrations calculated are 1.83 and 1.87 $x10^{-9}$ cm^3STP/g for *TM-sample* and *SH-sample*, respectively. The concentrations are in good agreement with each other. Because ^{3}He concentrations of both *TM-* and *SH-samples* are also agree with each other, ^{3}He might be totally cosmogenic. Cosmogenic ^{21}Ne concentration of *TM-sample* is calculated to be $2.32x10^{-9}$ cm^3STP/g. Cosmic-ray exposure age of 1.16 ± 0.11 Ma was obtained based on the cosmogenic ^{38}Ar content and the production rate of $(0.158\pm0.013)x10^{-8}cm^3STP/gMa$ calculated using the formula by Freundel(1986) and the bulk chemical composition reported by Yanai (1991). Cosmogenic $^{131}Xe/^{126}Xe$ ratio is about 4.9, which indicates heavy shielding against cosmic-ray irradiation during its residence on the moon. However, it is difficult at present to estimate the shielding depth and the production rates of these nuclides because of a lack of data for trace elements. If an appreciable amount of cosmogenic ^{38}Ar produced under the heavy shielding condition contributes to the total amount of cosmogenic ^{38}Ar, the transit time from the moon to the earth should be shorter than the exposure age 1.16 Ma calculated above.

^{81}Kr was measured in *TM-sample* as shown in Table 2. The concentration was $2.1x10^{-13}cm^3STP/g$. For the terrestrial age estimation, the apparent exposure age was calculated to be 1.73 ± 0.24 Ma using the cosmogenic Kr isotopic ratios assuming the terrestrial atmospheric Kr isotopic ratios as the trapped Kr. The terrestrial age obtained by the formula presented above is 0.123 ± 0.052 Ma using the true exposure age of 1.16 ± 0.11 Ma. However, the ^{81}Kr concentration observed in this meteorite is as high as the saturation level of lunar anorthositic meteorite Y-82192 and Stannern eucrite (Michel et al., 1991) suggesting a short terrestrial age for Asuka-31. If we consider the exposure ages based on the other cosmogenic isotopes and the apparent exposure age calculated by $(^{78}Kr/^{83}Kr)_c$, the terrestrial age might be shortened to about 0.06 Ma.

Radiogenic ^{4}He and ^{40}Ar concentrations in *TM-sample* are about 60% of those in *SH-sample*. U, Th and K concentrations seem to be higher in *SH* than in *TM*. The ^{40}Ar concentration of $1.62x10^{-5}$ cm^3STP/g and the 0.04 wt.% K_2O content (Yanai, 1991) give K-Ar age of 3.8 ± 0.4 Ga assuming 10 and 20 % errors for Ar and K analyses, respectively. ^{134}Xe and ^{136}Xe show clear excesses relative to the trapped Xe composition and their relative abundances agree with those produced by ^{238}U spontaneous fission. U concentration in *TM-sample* can be estimated by the fissiogenic ^{136}Xe abundance of $6.6x10^{-13}cm^3STP/g$. The U concentration was calculated to be 260 ppb assuming the K-Ar age of 3.8 Ga. ^{4}He production from U and Th in this meteorite becomes $3x10^{-4}cm^3STP/g$ during the 3.8 Ga K-Ar age, which is almost an order of magnitude higher than the observed value. Most of radiogenic He might have been lost from this meteorite.

REFERENCES: Bogard and Johnson (1983), Geophys. Res. Lett., 10, 801-803; Eugster and Niedermann (1988), Earth Planet. Sci. Lett., 89, 15-27; Eugster et al. (1991), Geochim. Cosmochim. Acta, 55, 3139-3148; Freundel et al. (1986), Geochim. Cosmochim. Acta, 50, 2663-2673; Michel et al. (1991), Meteoritics, 26,

372-373 (abstract); Takaoka (1986), Mem. Natl Inst. Polar Res., Spec. Iss., 41, 124-132; Takaoka (1987), Mem. Natl Inst. Polar Res., Spec. Iss., 46, 96-104; Yanai (1991), Proc. Lunar Planet. Sci., 21, 317-324.

Table 1. Noble gas concentrations and He, Ne and Ar isotopic compositions of Asuka-31 lunar meteorite.

Sample	$^{3}He^{2)}$	$^{4}He^{2)}$	$^{3}He/^{4}He^{1)}$	$^{20}Ne^{2)}$	$^{21}Ne^{2)}$	$^{22}Ne^{2)}$	$^{20}Ne/^{22}Ne$	$^{21}Ne/^{22}Ne$	$^{36}Ar^{2)}$	$^{38}Ar^{2)}$	$^{40}Ar^{2)}$	$^{38}Ar/^{36}Ar$	$^{40}Ar/^{36}Ar$	$^{84}Kr^{3)}$	$^{132}Xe^{3)}$
Total melt using 395.3 mg (TM-sample)															
	1.02	3300	3.086 ±.015	0.289	0.257	0.331	0.8726 ±.0045	0.7765 ±.0023	0.152	0.188	1620	1.243 ±.012	10690 ± 88	22.4	10.1
Step heating using 10.2 mg (SH-sample)															
600°C	0.601	1060	5.669 ±.050						0.535	0.101	586	0.1894 ±.0012	1095 ± 7	125	8.35
800°C	0.135	2000	0.675 ±.010						0.225	0.0445	797	0.1979 ±.0025	3543 ± 65	76.1	4.47
1000°C	0.0754	1360	0.554 ±.011						0.0491	0.0152	307	0.309 ±.022	6260 ±550	23.4	3.04
1200°C	0.0644	878	0.733 ±.013						0.0766	0.0819	422	1.069 ±.097	5510 ±310	23.1	8.50
1400°C	0.0338	96.6	3.40 ±.20						0.0568	0.0784	273	1.38 ±.22	4800 ±360	15.0	3.82
1700°C	0.0023	1.3	17 ±7						0.0388	0.0266	122	0.68 ±.30	3100 ±2500	10.6	3.55
Total	0.912	5396	1.69						0.981	0.348	2510	0.355	2560	273	31.7

1) $^{3}He/^{4}He$ ratios in the unit of 10^{-4}.
2) He, Ne and Ar concentrations in the unit of 10^{-8} cm³STP/g.
3) Kr and Xe concentrations in the unit of 10^{-12} cm³STP/g.

Table 2. Kr and Xe isotopic compositions of Asuka-31 lunar meteorite.

Sample	[^{84}Kr]	^{78}Kr	^{80}Kr	^{81}Kr	^{82}Kr	^{83}Kr	^{84}Kr	^{86}Kr	[^{132}Xe]	^{124}Xe	^{126}Xe	^{128}Xe	^{129}Xe	^{130}Xe	^{131}Xe	^{132}Xe	^{134}Xe	^{136}Xe
Total melt using 395.3 mg (TM-sample)																		
	22.4	2.156 ±.034	9.10 ±.20	0.916 ±.061	24.82 ± .45	26.45 ± .45	=100	29.35 ± .42	10.1	1.28 ±.11	2.02 ±.16	9.49 ±.31	98.43 ±1.84	16.29 ±.47	84.6 ±1.6	=100	43.0 ±1.0	38.30 ±.77
Step heating using 10.2 mg (SH-sample)																		
600°C	125	0.52 ±.21	4.02 ±.42		20.7 ±1.2	19.1 ±1.4	=100	30.4 ±1.7	8.35			8.1 ±1.8	107 ±10	16.0 ±3.3	79 ±12	=100	41.7 ±5.4	33.6 ±2.3
800°C	76.1	0.41 ±.10	4.10 ±.65		19.4 ±1.5	20.3 ±1.1	=100	29.8 ±1.3	4.47	1.9 ±.9	1.4 ±.7	8.1 ±2.0	125 ±19	17.8 ±2.6	88 ±8	=100	40.7 ±5.5	38.2 ±5.5
1000°C	23.4	1.09 ±.41	4.28 ±.84		20.3 ±2.7	21.6 ±2.8	=100	30.9 ±4.3	3.04			9.0 ±2.8	95 ±13	14.8 ±5.7	82 ±19	=100	38.8 ±4.5	26.8 ±4.3
1200°C	23.1	1.25 ±.49	5.83 ±.51		21.3 ±1.9	21.7 ±1.8	=100	31.2 ±3.9	6.50	1.4 ±.9	1.8 ±1.2	10.6 ±3.4	95 ±10	16.2 ±3.2	84 ±10	=100	42.4 ±5.0	36.4 ±7.4
1400°C	15.0	1.77 ±.96	6.21 ±.07		23.6 ±3.5	22.2 ±2.1	=100	30.3 ±3.6	3.82			10.6 ±2.9	109 ±10	13.7 ±4.0	94 ±11	=100	39.8 ±7.7	37.4 ±6.7
1700°C	10.6	0.97 ±.38	4.19 ±.98		19.9 ±2.5	19.8 ±2.3	=100	30.0 ±1.9	3.55			7.6 ±2.1	104 ± 6	15.1 ±2.9	74 ±6	=100	38.1 ±5.8	33.6 ±5.2
AVCC		0.597	3.92		20.15	20.17	=100	30.98		0.464	0.409	8.25		16.26	82.00	=100	38.36	32.33
Air		0.609	3.96		20.22	20.14	=100	30.52		0.354	0.330	7.136	98.32	15.14	78.90	=100	38.79	32.94

[^{84}Kr] and [^{132}Xe] are concentrations in the unit of 10^{-12}cm^{3}STP/g.

COSMIC RAY EXPOSURE HISTORIES OF LUNAR METEORITES ASUKA 881757, YAMATO 793169, AND CALCALONG CREEK

K. Nishiizumi, J. R. Arnold, Department of Chemistry, University of California, San Diego, La Jolla, CA 92093-0317; M. W. Caffee, R. C. Finkel, J. Southon, CAMS, Lawrence Livermore National Lab, L-397, P.O. Box 808, Livermore, CA 94551; R. C. Reedy, Group SST-8, Los Alamos National Lab, Los Alamos, NM 87545

Most lunar meteorites have complex cosmic ray exposure histories [e.g. 1, 2]. They have been exposed both at some depth on the moon (2π irradiation) before their ejection and as small bodies in space (4π irradiation) during transportation from the moon to the earth. Their terrestrial ages can also be long, similar to many other meteorites found in Antarctica. Measurement of cosmogenic nuclides can provide essential constraints for these ages and help to unravel the complex histories of these objects. This complexity requires measurement of three or more cosmogenic nuclides in the same sample. We have measured three to five cosmogenic radionuclides in all 11 lunar meteorites (8 individual falls) from Antarctica and one from Australia [e. g. 2-4].

We report here cosmogenic ^{36}Cl ($t_{1/2}$ = 3.0x10^5 years), ^{26}Al (7.05x10^5 years), and ^{10}Be (1.5x10^6 years) results for lunar meteorites Asuka 881757 (recovered mass 442 g) and Yamato 793169 (6.1g) as well as ^{26}Al data for Calcalong Creek (recovered mass 19 g). The AMS measurements were performed at Lawrence Livermore National Lab [5]. The results are shown in Table 1 along with earlier results for Calcalong Creek [4]. Although three nuclides do not provide enough information to fully explain the complex histories of these meteorites, our results do constrain the system.

The production rates of cosmogenic nuclides for 2π and 4π exposure geometry are relatively well known. Depth profiles of ^{10}Be, ^{26}Al, ^{36}Cl, ^{41}Ca, and ^{53}Mn have been measured in the Apollo 15 deep drill core [6-8]. These observed profiles can be used to derive the exposure histories of lunar meteorites. Since the target compositions vary for each lunar meteorite and differ from that of the Apollo 15 drill core, the observed cosmogenic radionuclide concentrations must be normalized using the Reedy-Arnold model [9] except in the case of ^{53}Mn which is always normalized to Fe. In general, the production rate of ^{10}Be is also nearly independent of composition, since the concentration of O, the major target element for its production, is similar for all lunar samples.

Asuka 881757: Based on the ^{10}Be concentration, this meteorite was exposed to cosmic rays at a depth of ~160 g/cm^2 on the moon. However, normalized ^{36}Cl (15.8 ± 0.4 dpm/kg) and ^{26}Al (56 ± 3 dpm/kg) activities are too high to agree with expected activities at this depth according to the Apollo 15 core profile. If the meteorite was excavated from a greater depth on the moon (more

than several m) to a near surface location (~few g/cm^2) at a time ~2My ago and was ejected recently, all three radionuclide concentrations can be explained. The transition time from the moon to the earth in this scenario is shorter than ~0.1 My. A simpler scenario is that the meteorite was ejected from deeper than several m in the moon and all cosmogenic nuclides were produced in space (4π irradiation). Measured ^{36}Cl activities, in dpm/kg meteorite, were normalized to the target element concentration, dpm/kg (40K+8Ca+Fe), for comparison with the other meteorites. The expected ^{36}Cl saturation activity is ~23 ± 3 dpm/kg (40K+8Ca+Fe) for a 4π irradiation. Required exposure age (transition time) is 0.9 ± 0.1 My for all three nuclides. The terrestrial age is less than 0.05 My from the ^{36}Cl concentration.

Yamato 793169: Based on the high normalized activities of ^{26}Al (108 ± 3 dpm/kg) and ^{36}Cl (19.3 ± 0.3 dpm/kg) compared to the low ^{10}Be concentration, this meteorite can not be explained by a 2π irradiation model. The meteorite must have been ejected from deeper than several m in the moon and all cosmogenic nuclides were produced in space. The exposure age is 1.1 ± 0.2 My based on the ^{10}Be activity. The high saturation activity of ^{26}Al, 132 ± 14 dpm/kg, compared to the calculated value of 83 dpm/kg based on Fuse and Anders [10] can be explained by SCR (solar cosmic ray) production of the nuclide in space. The slightly high ^{36}Cl can also be explained by an SCR contribution. The terrestrial age is shorter than 0.05 My.

Calcalong Creek: We measured ^{26}Al in addition to our previous ^{10}Be and ^{36}Cl measurements [4]. The observed ^{26}Al activity is the highest value among all known meteorites. This high ^{26}Al is certainly due to SCR production. The existence of a large amount of SCR product suggests that the size of the recovered meteorite must be nearly the same as its preatmospheric size in either the 2π or the 4π exposure cases described below. In the 2π model the meteorite was ejected from the surface of the moon. Our sample had to have been exposed to cosmic rays at ~1 g/cm^2 depth where it accumulated the majority of its radionuclide signature. Since the recovered equivalent diameter of the meteorite is about 3 cm this lunar origin can be tested by measuring the side opposite our chip which should have much lower SCR production. Another possibility is that the meteorite was ejected from deep in the moon and acquired its cosmogenic radionuclides exposed to cosmic rays as a small body in space, the 4π case. The required 4π exposure time is 3 ± 1 My based on the measured ^{10}Be activity. The GCR (galactic cosmic ray) production rates in such a small meteorite are lower than in more ordinary sized meteorites and are difficult to estimate. The estimated depth of the sample we measured for this 4π case is ~2 g/cm^2 assuming a preatmospheric radius of 5 g/cm^2 based on the measured ^{26}Al activity. The production rate of ^{36}Cl can be calculated to be 15 ± 2 dpm/kg at the same depth. The terrestrial age is shorter than 0.03 My.

Although a variety of combinations of the 2π and 4π models are possible for these lunar meteorites, further useful discussions are not possible until other cosmogenic nuclides such as ^{41}Ca, ^{53}Mn, and noble gases have been determined.

The exposure histories of 12 lunar meteorites (9 independent cases) have been studied. Five or six out of nine lunar meteorites were ejected from relatively shallow depths (a few cm to about 3 m) and their transition times from the moon to the earth were all short (much shorter than 0.1 My). The impact events seem to have occurred within the last 0.1 My for four or five lunar meteorites and 0.3 My ago for one. Three or four lunar meteorites were ejected from deeper depths (more than several m), and transition times are 0.9 to 11 My from the moon to the earth. In earlier work, we found only one meteorite which had a transition time in the range of millions of years [2-4]. The statistics of 2π vs. 4π exposure are changed by the present work. In an early Monte Carlo model [11], the dynamics of meteorites of lunar origin were simulated. According to this analysis, on the assumption that objects ejected from the moon escape the earth's gravity field, roughly half of those reaching the earth have transit times less than 1 My. Nine cases are not enough to substantiate or refute the model calculation.

The atmospheric entry velocity and/or entry angle of lunar meteorites must have been much lower than ordinary meteorites since at least three out of nine lunar meteorites contain SCR produced nuclides. It interesting that we have found SCR effects in three lunar meteorites and one or two SNC meteorites but only two or three ordinary chondrites.

We wish to thank NIPR and R. A. Haag for providing meteorite samples. This work was supported by NASA grant NAG 9-33 and NSF grant DPP-8916036.

References

[1] Eugster O. (1989) *Science 245*, 1197-1202.

[2] Nishiizumi K. *et al.* (1991) *Geochim. Cosmochim. Acta 55*, 3149-3155.

[3] Nishiizumi K. *et al.* (1991) *16th Symposium on Antarctic Meteorites* 188-190 (National Inst. Polar Res., Tokyo).

[4] Nishiizumi K. *et al.* (1992) *54th Meteoritical Society Meeting*

[5] Southon, J.R. *et al.* (1990) *Nucl. Inst. Methods B52*, 301-305.

[6] Imamura M. *et al.* (1973) *Earth Planet. Sci. Lett. 20*, 107-112.

[7] Nishiizumi K. *et al.* (1984) *Earth Planet. Sci. Lett. 70*, 157-163; 164-168.

[8] Nishiizumi K. *et al.* (1990) *Lunar and Planetary Science XXI*, 893-894 (Lunar Planet. Inst., Houston).

[9] Reedy R.C. and Arnold J.R. (1972) *J. Geophys. Res. 77*, 537-555.

[10] Fuse K. and Anders E. (1969) *Geochim. Cosmochim. Acta 33*, 653-670.

[11] Arnold J.R. (1965) *Astrophys. J. 141*, 1536-1547.

Table 1. Measurements of cosmogenic nuclides in lunar meteorites

	Weight (mg)	^{36}Cl dpm/kg*	^{26}Al dpm/kg*	^{10}Be dpm/kg*	Ref
Asuka 881757,105	132.27	16.31 ± 0.38	48.8 ± 2.6	7.19 ± 0.12	
Yamato 793169,55	20.15	18.32 ± 0.24	87.4 ± 2.0	7.87 ± 0.14	
Calcalong Creek	45.99	16.51 ± 0.21	170.9 ± 5.3	12.98 ± 0.35	[4]

* dpm/kg meteorite

^{40}Ar-^{39}Ar ANALYSES OF A LUNAR METEORITE(Y-86032) AND A FEW LL3 AND LL4 CHONDRITES FROM ANTARCTICA

Kaneoka, I.* and Nagao, K.**

* Earthquake Research Institute, University of Tokyo, Bunkyo-ku, Tokyo 113

** Institute for Study of the Earth's Interior, Okayama University, Misasa, Tottori-ken 682-01.

In order to clarify the thermal history of each meteorite, ^{40}Ar-^{39}Ar analyses were performed for a lunar meteorite(Y-86032), two LL3 chondrites (Y-790448, ALH-764) and a LL4 chondrite(Y-7442) from Antarctica.

Y-86032 is a fragmental breccia, including abundant mineral and lithic clasts. A lithic clast was prepared for ^{40}Ar-^{39}Ar analyses. For this meteorite, results based on petrological and mineralogical studies(1, 2), geochemical studies(3) and isotope studies (4, 5) have been reported. The other three meteorites have been classified into the LL-type and un-equilibrated ones (6).

Samples were wrapped in Al-foil and irradiated with neutrons in the JMTR of Tohoku University. The lunar meteorite was irradiated at differnt period under different conditions from those of the other three LL-chondrites. The total fast neutron flux of $1x10^{19}nvt/cm^2$ was applied to the LL-chondrites, whereas the lunar meteorite received the total fast neutron flux of about $1x10^{18}nvt/cm^2$. The hornblende MMhb-I (K-Ar age: 519.5±2.5Ma) (7) was used as the age monitor. Ar gas was extracted and purified at the Isotope Center, University of Tokyo, and Ar isotopes were analysed on a VG-5400 mass spectrometer at Okayama University. Blanks and the effect of K-derived interfering isotopes were corrected to calculate an ^{40}Ar-^{39}Ar age. However, Ca-derived interfering isotopes could not be corrected due to the relatively long interval between the irradiation of samples and their Ar analyses. Hence, the calculated ^{40}Ar-^{39}Ar ages in some high temperature fractions should be regarded to show only rough estimates.

In the case of Y-86032, the obtained ^{40}Ar-^{39}Ar age spectum is rather scattered and no plateau age could be obtained. Since the amount of K-content in this sample might be rather low (100-200ppm) and Ca-content is rather high (12-13%) (3), the insufficient correction of Ca-derived interfering isotopes and blank corrections might have caused such effects.

Among three LL-chondrites analysed, only Y-790448 shows a plateau age of about 4500Ma in the lower temperature fractions(600-800°C) with much

younger ^{40}Ar-^{39}Ar ages in the higher temperature fractions. Systematically younger ^{40}Ar-^{39}Ar ages are observed in the higher temperature fractions for these LL-chondrites. Large amounts of trapped components such as ^{36}Ar are also observed in the higher temperature fractions. Although redistribution of radiogenic ^{40}Ar and/or recoil effect of ^{39}Ar are expected in these samples, they do not seem to affect the trapped components. It is inferred that the trapping sites of trapped components are different from those of radiogenic ^{40}Ar and K-derived ^{39}Ar. Fine phases contained in unequilibrated chondrites might play an important role to indicate an inversed stair-case pattern of ^{40}Ar-^{39}Ar age spectrum in the higher temperature fractions.

References

(1) Takeda, H., Kojima, H., Nishio, F., Yanai, K. and Lindstrom, M. M., Proc. NIPR Symp. Antarct. Meteorites, 2, 3-14 (1989).
(2) Takeda, H., Miyamoto, M., Mori, H., Wentworth, S. J. and McKay, D. S., Proc. Lunar Planet. Sci. Conf., 20th, 91-100 (1990).
(3) Lindstrom, M. M., Mittlefehldt, D. W., Martnetz, R. R., Lipschutz, M. E. and Wang, M-S., Proc. NIPR Symp. Antarct. Meteorites, 4, 12-32 (1991).
(4) Eugster, O., Niedermann, S., Burger, M., Krähenbühl, W., Weber, H., Clayton, R. N. and Mayeda, K. K., Proc. NIPR Symp. Antarct. Meteorites, 2, 25-35 (1989).
(5) Tatsumoto, M. and Premo, W. R., Proc. NIPR Symp. Antarct. Meteorites, 4, 56-69 (1991).
(6) Yanai, K. and Kojima, H. comp., Photographic Catalog of Antarctic Meteorites, Tokyo, Natl Inst. Polar Res., 298p. (1987).
(7) Alexander, E. C. Jr., Mickelson, G. M. and Lanphere, M. A., U. S. Geol. Survey Open-File Rep., 78-701, 6-9 (1978).

HEAVY NOBLE GAS CONSTRAINT ON THE ORIGIN OF TEKTITES.

Kayo MATSUBARA and Jun-ichi MATSUDA
Department of Earth and Space Science, Faculty of Science,
Osaka University, Toyonaka, Osaka 560, Japan.

Tektites are a kind of natural silica-rich glass and look like obsidians. Although some authors favor a lunar origin for tektites, they are thought to be produced during meteoritic collisions with the Earth as well as impact glasses. However, there are some differences between tektites and impact glasses; for example, tektites occur in geographically restricted areas and chemically homogeneous, on the other hand, impact glasses are found only at the location of a defined impact crater and are inhomogeneous.

As noble gases are chemically inert, the behavior of noble gases depends on physical conditions. Therefore, the study of noble gases gives us the important information about formation process of the materials. We measured noble gas concentrations in tektites [1] and impact glasses [2,3] and reported that Ne was enriched in these samples compared to the relative pattern of noble gases in air. The Ne concentrations in tektites and impact glasses were very similar and were on the order of 10^{-7} cm^3STP/g. Therefore, Ne (and also He) does not give us any information on the origins of these glasses. On the other hand, the concentrations of heavy noble gases (Ar, Kr and Xe) in impact glasses were quite variable and higher than those in tektites. Thus, heavy noble gases can still be used as tracers to study the origin of these glasses.

The concentrations of ^{84}Kr and ^{132}Xe in tektites and impact glasses were complied in figure. Impact glasses were Aouelloul, Zhamanshin, Libyan Desert glasses [3] and Darwin glass [2]. Tektites were splash-form type ones collected from three strewn fields [1,4]. We measured noble gas concentrations in five new tektites and added the data in the figure. "Air" and "Solar" in the figure shows the lines corresponding to the ratio of noble gases in terrestrial atmosphere and in solar wind on lunar soils, respectively. In this figure, it is clear that concentrations of Ar and Kr (and also Xe) in impact glasses are higher than those in tektites and are clearly separated from the latter. The data points of impact glasses plot directly on the air ratio line, suggesting that noble gases were trapped from terrestrial atmosphere with no elemental fractionation.

We calculated solubility of noble gases in silicate glasses equilibrated with air at 1350 °C based on Lux's equations [5] and showed with the short bar "0". Although, the data points of tektites are scattered and some of data show only upper limits, they lie on or near the terrestrial air line, suggesting a terrestrial origin of tektites. The concentrations of Ar and Kr in tektites are lower than those calculated from equilibrium solubility with air at a pressure of one atmosphere. These suggest that tektites are of terrestrial origin and were exposed to a low-pressure atmosphere by being carried up to high altitudes by the impact of meteorite. In the figure, we also show the solubility of noble gases in tektites at high altitudes using Lux's equation [5] with short bars. The assumption is that the total pressure of air decreases exponentially with the scale height of 8.4km and that the relative ratios of noble gases in air are not changed with the height. The numerical values in the figure represent the altitude (km). From the data points of tektites, they seem to be solidified at 20-40km altitude.

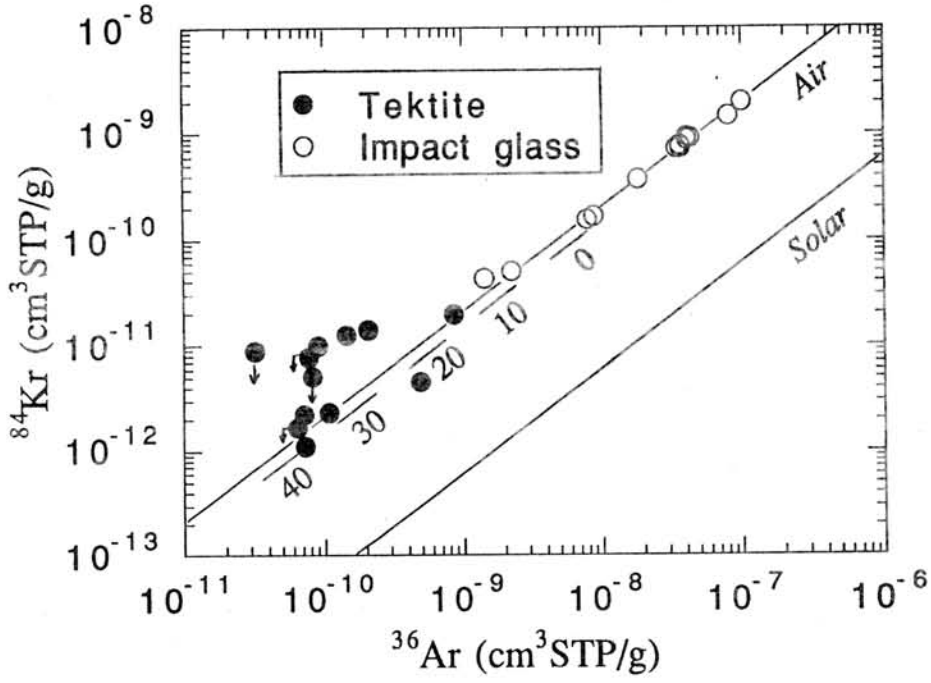

References

1. Matsubara K. and Matsuda J. (1991) *Meteoritics* **26**, 217-220.
2. Matsuda J., Matsubara K., Yajima H. and Yamamoto K. (1989) *Geochim. Cosmochim. Acta* **53**, 3025-3033.
3. Matsubara K., Matsuda J. and Koeberl C. (1991) *Geochim. Cosmochim. Acta* **55**, 2951-2955.
4. Hennecke E.W., Mannuel O.K. and Sabu D.D. (1975) *J. Geophys. Res.* **80**, 2931-2934.
5. Lux G. (1987) *Geochim. Cosmochim. Acta* **51**, 1549-1560.

NOBLE GASES IN SHOCK-PRODUCED DIAMONDS: THEIR RELATIONSHIP WITH SHOCK PRESSURE AND POROSITY.

J. Matsuda1), A. Kusumi2), H. Yajima2), K. Kusaba3), Y. Syono3).
1) Department of Earth and Space science, faculty of Science, Osaka University, Toyonaka, Osaka 560, Japan.
2) Department of Earth Sciences, Faculty of Science, Kobe University, Nada, Kobe 657, Japan.
3) The Research Institute for Iron, Steel and Other Metals, Tohoku University, Katahira, Sendai 980, Japan.

We synthesized the diamonds by shock transformation from natural graphite using a single- stage propellant gun, and examined the elemental abundances of noble gases. The shock produced diamonds we obtained were all cubic diamonds by x-ray diffraction. The diamonds yield increased with increasing shock pressure and also with increasing porosity of the starting material. The latter correlation should be due to the temperature increase at the shock. It is likely that the higher yield with the higher shock pressure is also due to the temperature increase rather than the pressure effect. It is conceivable that there are two possibilities for the transformation of graphite to diamonds. The first is the martensitic transformation of graphite. The second is the nucleation growth from the carbon melt. The correlation with the shock temperature suggests that the second mechanism is predominant in our experiments. The cubic diamonds were produced at the hot spot of the graphite neighboring the pore space in the starting material.

Considerable amounts of noble gases were trapped in the shock-produced diamonds when the raw material was sealed inside the container, but not trapped in diamond produced in an open system under vacuum. The elemental abundance pattern of noble gases in the former was similar to that in air, suggesting that noble gases in the pore within the pre-shock material were driven or dissolved into the diamonds when the container was tightly sealed. There was no correlation between the amounts of noble gases and the shock pressure at the syntheses (Fig. 1). The amount of noble gases in the diamonds had positive correlation with the porosity of the starting material, but are not exactly proportional to the latter (Fig. 2). However, when we take the diamond yield into account, we could good positive correlations between noble gas amounts and the pressure. These results may be well explained by the model we mentioned in the previous section that diamonds were produced only in the hot spot neighboring the pore.

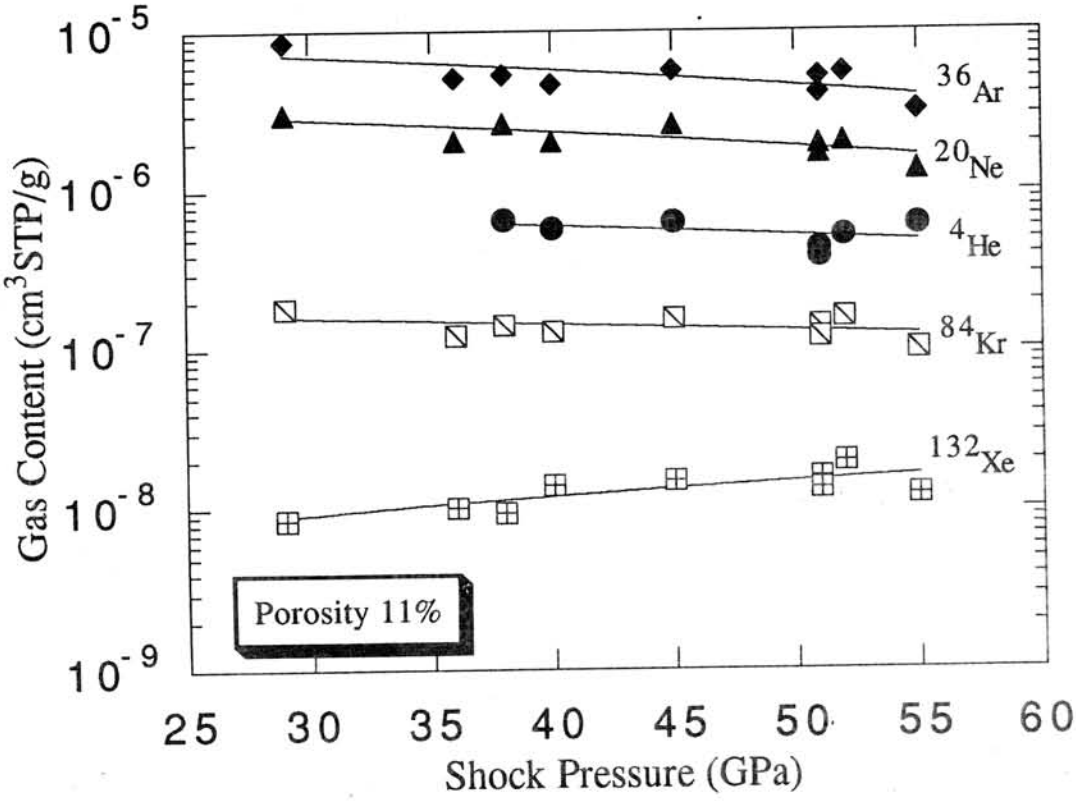
Gas Content (cm³STP/g)
10⁻⁵
10⁻⁶
10⁻⁷
10⁻⁸
10⁻⁹
36Ar
20Ne
4He
84Kr
132Xe
Porosity 11%
25 30 35 40 45 50 55 60
Shock Pressure (GPa)

Fig. 1

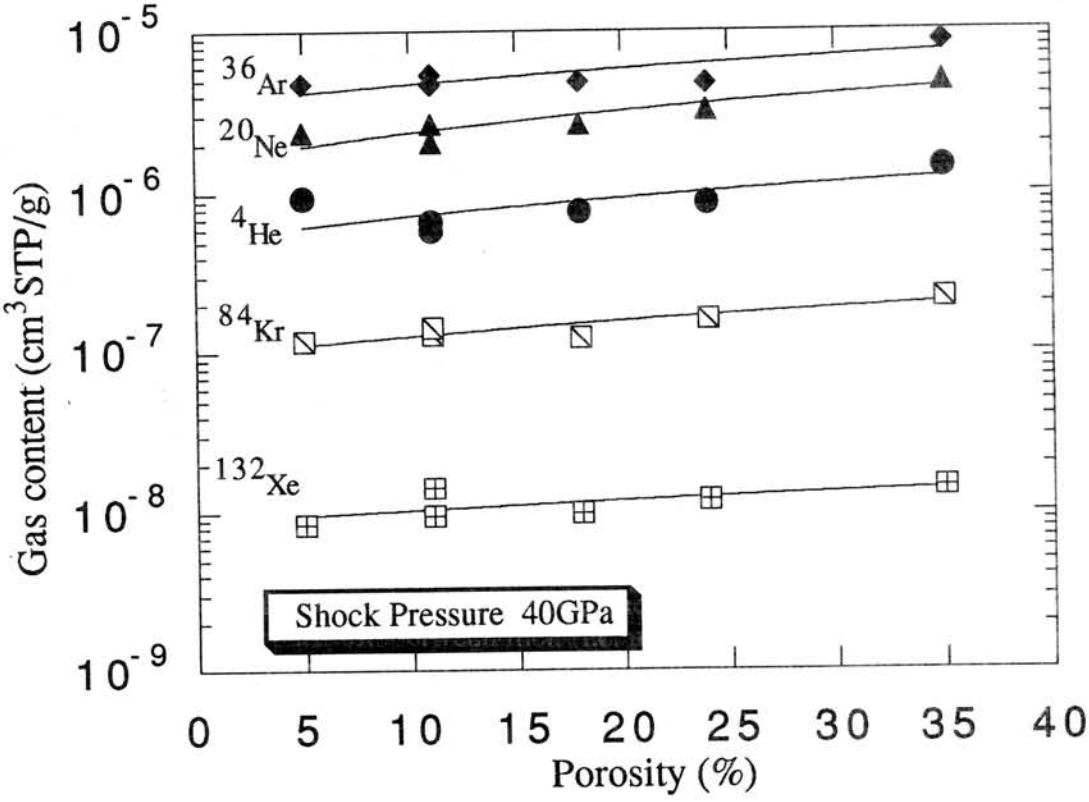
Gas content (cm³STP/g)
10⁻⁵
10⁻⁶
10⁻⁷
10⁻⁸
10⁻⁹
36Ar
20Ne
4He
84Kr
132Xe
Shock Pressure 40GPa
0 5 10 15 20 25 30 35 40
Porosity (%)

Fig. 2

EVOLUTION OF TERRESTRIAL NOBLE GAS

Minoru Ozima(1) and Kevin Zahnle(2). (1) Osaka University, Toyonaka City 560, Japan, (2) NASA-Ames, Moffet Field, CA94035-1000, USA

A number of authors have discussed mantle degassing on the basis of radiogenic noble gases such as ^{40}Ar, ^{129}Xe and ^{4}He and have obtained important conclusions about the atmospheric evolution, especially the timing of the mantle degassing. In comparison with these attempts, very little has been done to use stable noble gas isotopic composition in discussing earth evolution problems. We emphasize that while radiogenic noble gases give unique information on the chronology of mantle degassing, stable noble gas isotopic and elemental compositions impose crucial constraints on the physical processes governing the evolution of the atmosphere. We present a new unified model for the evolution of noble gas in the terrestrial atmosphere.

A model for terrestrial noble gas evolution: We assume that the primordial noble gas was solar[1]. We propose that the evolution of the terrestrial noble gas (except for radiogenic components) has proceeded in the following four stages.

Stage 1. Noble gas capture by earth-accreting planetesimals [2]. Throughout this process, the present xenon isotopic composition was established. The process also resulted in heavier noble gas enrichment relative to the primordial elemental abundance pattern.

Stage 2. Noble gas partition between melt and solid during a magma ocean period. The process resulted in the enrichment of lighter noble gases in the melt (magma ocean), but no isotopic fractionation took place.

Stage 3. Noble gas release from melt (magma ocean) into the atmosphere through bubbling. This resulted in the enrichment of heavier noble gases in the gas phase, i.e., in the atmosphere, but no isotopic fractionation.

Stage 4. Hydrodynamic escape of H_2 from the atmosphere[2]. The process resulted in the enrichment of heavier neon isotopes to establish the present atmospheric neon isotopic ratio $^{20}Ne/^{22}Ne$. The process also lead to an elemental fractionation.

Results. The above scenario leads to the following noble gas characteristics.

1. Overall noble gas elemental composition in the atmosphere was established through the above four processes. Consequently, heavier noble gases are enriched relative to the primordial solar composition. However, xenon enrichment is much less than in chondritic pattern. The pattern is generally akin to the chondritic pattern, but xenon is less enriched. This may partly answer the long-standing 'missing Xe' problem.
2. Xenon isotopic composition was established through the stage 1, and the atmospheric neon isotopic composition was established through the stage 3. Ar and Kr both in the mantle and in the atmosphere and neon in the mantle have retained the primordial solar type isotopic compositions.

Discussions.

The above scenario can explain major characteristics of terrestrial noble gases. These are, (1) similar isotopic composition of Xe, Kr and Ar ($^{38}Ar/^{36}Ar$) between the mantle and the atmosphere, (2) enrichment of heavier xenon isotopes relative to the solar xenon, (3) heavier $^{20}Ne/^{22}Ne$ in the atmosphere than in the mantle, (4) Similar enrichment of heavier noble gases in the atmosphere to the chondritic pattern, but with less enrichment in Xe (missing Xe ?).

Since noble gases are less incompatible[3] in contrary to a common supposition, noble gas partition between melt (i.e. magma) and crystal cannot be responsible to a major mantle degassing. Equilibrium partition of noble gas between melt and solid cannot give rise to an effective release of noble gas. More effective process would be bubbling in magma ocean.Impact degassing would be effective, but is not known if this process can explain the particular noble gas elemental abundance pattern.

Figure 1 A general scheme for the terrestrial noble gas evolution.

time (yr)	*Noble gas characteristics*	*Locale*	*Process*
0	Xe isotopic fractionation Enrichment of heavier noble gases	planetesimals	gravitational capture
10^7 - 10^8	Ne isotopic fractionation in the atmosphere Enrichment of heavier noble gases in the degassed mantle.	atmosphere	hydrodynamic escape of H_2
10^8 - 10^9	Noble gas degassing into the atmosphere Enrichment of lighter noble gases in the solid Earth Separation of Ar and Xe from K and I	magma ocean	bubble/melt partition
10^9 - present	Enrichment of heavier noble gases in the degassed Earth Continuous mantle outgassing	mantle	melt/crystal partition

References 1. Ozima,M. and K.Nakazawa (1980), Nature 284 313-6. 2. Zahnle,K.J., Pollack,J.B.and Kasting,J.F.(1990) GCA 84 502-27. 3. Hiyagon,H. and M.Ozima (1986) GCA 50 2045-57, Broadhurst,C.L., M.J.Drake, B.E.Hagee and T.J.Bernatowicz (1992) GCA 56 709-23

Noble gases in unique meteorites Yamato-74063 and -74357.

N. Takaoka[1], K. Nagao[2] and Y. Miura[2,3]

1) Dept. Earth and Planet. Sci., Kyushu Univ., Fukuoka 812,
2) Inst.Study the Earth's Inter., Okayama Univ., Tottori 682-01,
3) Present address, Geophys. Inst., Univ. Tokyo, Tokyo 113.

Yamato-74063 and -74357 are similar to Acapulco in mineralogy and in oxygen isotopic composition. However, Y-74063 which has been classified as a new type of chondrite of type 6 to 7 intermediate between E and H chondrite groups, is different from Acapulco-type meteorites and all known chondrite groups in bulk chemistry (Yanai and Kojima, 1991). Y-74063 contains large amounts of trapped Ar, Krand Xe, and enrichment of Xe overwhelms C and E chondrites, and even ureilites with a few exceptions. However, carrier phases of trapped gases are unkown (Takaoka and Yoshida, 1991; Takaoka et al., 1991).

Magnetic (Fe-Ni) and non-magnetic (silicates) separates of Y-74063, and a bulk sample of Y-74357 were analysed for abundances and isotopic compositions of five stable noble gases by stepwise heating. Noble gases in mineral grains of Y-74063 were also investigated by laser beam extraction (Takaoka et al., 1991).

The Fe-Ni separate, and the silicates separate which was treated in 0.05 M HCl for 3.5 hours still contain 24 and 34 % of trapped Ar respectively, compared to the bulk. This suggests that the trapped gases reside in Fe-Ni and silicates insoluble in dilute HCl as well as minerals soluble in dilute HCl, or that carrier phases are as fine as to disperse in the Fe-Ni and silicates grains. An isotopic feature to be noted is homogeneity in $^{129}Xe/^{132}Xe$, as found in Fig. 1. The $^{129}Xe/^{132}Xe$ ratio is same (1.093) for all temperature fractions of both separates except for the 750 C fraction of Fe-Ni which may be contaminated by atmospheric Xe. This indicates a negligible contribution of radiogenic ^{129}Xe produced by in-situ decay of ^{129}I. Release patterns of trapped gases are different between Fe-Ni and silicates (Fig. 1). The release pattern for the silicates is compatible with that from chondrites. The release pattern for the Fe-Ni separate is broad and sifts toward low tempeature, suggesting inclusions of low temperature minerals in Fe-Ni metal.

Abundances and isotopic ratios of noble gases released by the laser beam extraction were determined with a laser pulse of 75 mJ. Ejected melt was analysed with an EPMA to know the chemical composition. The

most gas-rich was a silicate portion bearing dusty inclusions.

Y-74357 is depleted in trapped gases. He and Ne are mixtures of cosmogenic and radiogenic gases, whereas Ar, Kr and Xe are mixtures of trapped, cosmogenic and radiogenic gases. Radiogenic ^{4}He and ^{40}Ar are less than 2.4×10^{-6} and 1.03×10^{-5} cc/g, respectively. No data are available for K, Th and U. Assuming K, Th and U contents typical of H chondrites, gas-retention ages are less than 0.8 and 1.9 Ga for ^{4}He and ^{40}Ar, respectively. This is very short compared to Y-74063 (Takaoka and Yoshida, 1991), Acapulco (Palme et al., 1981) and A-77081 (Schultz et al., 1982), and suggests that this meteorite was subjected to late metamorphism, whereas three meteorites above mentioned were not subjected to any major metamorphic event during the last 4.5 Ga.

Cosmogenic ^{21}Ne is as high as 4.59×10^{-8} cc/g with cosmogenic ^{22}Ne/^{21}Ne = 1.076 and ^{3}He/^{21}Ne = 1.8, whereas cosmogenic ^{38}Ar is as low as 1.33×10^{-9} cc/g. Assuming production rates of cosmogenic nuclides for the chondritic composition, cosmogenic ^{3}He, ^{21}Ne and ^{38}Ar give 5, 12 and 3 Ma for cosmic-ray exposure ages, respectively. The short ^{3}He age is attributable to diffusive loss of He. However, discrepancy between the ^{21}Ne and ^{38}Ar ages is abnormally large. The cosmogenic ^{22}Ne/^{21}Ne ratio indicates an intermediate preatmospheric size. Target chemistry enrich in Mg and depleted in Ca and Fe would be needed to produce such large difference. No data are available on target chemistry, however.

References: Palme et al.(1981) Geochim. Cosmochim. Acta, 45, 727-752 Schultz et al.(1982) Earth Planet. Sci. Lett., 61, 23-31. Takaoka and Yoshida (1991) Proc. NIPR Symp. Ant. Met. 4, 178-186. Takaoka et al.(1991) Meteoritics, 26, 400. Yanai and Kojima (1991) Proc. NIPR Symp. Ant. Met., 4, 118-130.

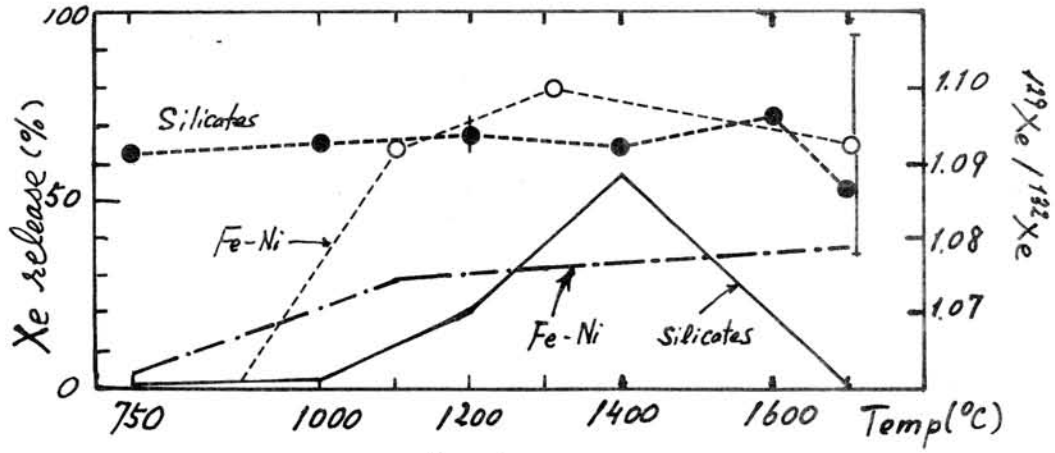

Fig. 1.

Special Lecture (II)

Prof. H. Wänke

ON THE MARTIAN VOLATILES AS INFERRED FROM SNC-METEORITES.

Heinrich Wänke and Gerlind Dreibus, Max-Planck-Institut für Chemie, Saarstrasse 23, D-6500 Mainz, F.R.Germany.

From the analytical data of SNC-meteorites and observed element correlations, it is evident that the ratios of moderately volatile to refractory elements like Na/Al and K/La as well as the ratios of volatile to refractory elements like Br/La are about a factor of 2 higher for Mars than for the Earth. With the well justified assumption that the abundance of refractory elements is identical on both planets within a much smaller factor, one finds that the abundance of moderately volatile and volatile elements on Mars is about twice as high as on Earth [1].

The abundance of sulphur on Mars cannot be directly estimated as most of it will reside in the core. However, we can assume that the abundance of sulphur on Mars is similar to the abundance of elements of similar volatility. In this way, we obtain a core mass of 22 % and a core composition of 14% S, 7.6% Ni, 0.4% Co and 78% Fe [1].

The abundance of elements in the Martian mantle as derived from SNC-meteorites [1] is plotted in the Figure. The depletion of elements with chalcophile character is obvious and indicates extraction of chalcophile elements into the core by segregation of FeS. From the abundance of chalcophile elements in the Martian mantle, one can quantitatively show that the extraction of these elements took place according to their sulphide-silicate partition coefficients.

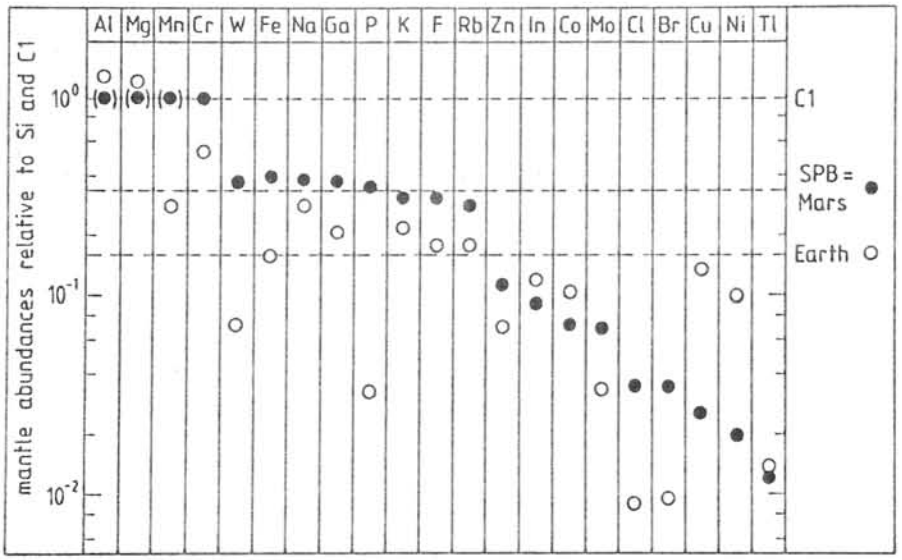

FIGURE

Normalized (Si = 1.00) elemental abundances in the (primitive) terrestrial and Martian mantle.

The sulphide-silicate equilibrium in the Martian mantle indicates its saturation with FeS. The FeO content of the Martian mantle is about a factor of 2 higher than that of the terrestrial mantle. Hence, the sulphur abundance in the Martian mantle is expected to be substantially above the S abundance in the Earth's mantle as the solubility of FeS in silicates increases with the FeO content. Hence, the observed high concentrations of sulphur in mantle derived magmas as represented by the shergottites (sulphur content between 600 and 2800 ppm) is not surprising.

In light of the two component model of planet formation [2,3], the high depletion of chalcophile elements in the Martian mantle indicates that on Mars the (volatile element depleted) reduced component A and the volatiles containing oxidized component B have been equilibrated with each other during the formation of this planet. In other words, an almost homogeneous accretion is inferred during which metallic iron from component A had the chance to equilibrate with component B containing sulphur in C1-abundance and to form FeS. In the same way, water added to the growing planet by component B reacted with the metallic Fe of component A, oxidizing it to FeO, while the generated hydrogen escaped. Hence, we should expect a very dry Martian mantle, because water although added in large quantities to the planet during accretion, was reduced to H_2 except for trace amounts.

To estimate the water content of the Martian mantle, we [4] have used data on the water content of Shergotty of 180 ppm measured by Yang and Epstein [5]. Shergotty is enriched in La by a factor of 5 relative to the Martian mantle. Assuming a similar enrichment for H_2O, a mantle concentration of 180 : 5 = 36 ppm was found. This is exactly the value obtained earlier by us [6], comparing the solubility of H_2O and HCl in silicate

melts and using the abundance of chlorine in the Martian mantle as deduced from SNC-meteorites. The exact match is, of course, purely fortuitous considering the uncertainties.

Over the years, the dry Martian mantle as proposed by us [4], has been questioned in light of water-rich inclusions observed in SNC-meteorites [7]. However, it was not known if the host phase of these inclusions have crystallized from mantle derived magmas or represent material from a water-rich Martian crust taken up by intrusions and overplating of mantle derived magmas. The contradictory evidence of a dry Martian mantle as indicated by the low water content of SNC-meteorites and the erosional Martian surface features, which seem to require large amounts of water has recently been discussed by Carr and Wänke [8].

In respect to the water content of SNC-meteorites most interesting results were recently obtained by Karlsson et al. [9], who measured the oxygen isotope composition of water degassed from SNC-meteorites at different temperatures. In this way, it was found that all SNC-meteorites contain aside the presence of terrestrial contamination a large fraction of the water, which, although Martian, is not derived from the Martian mantle. It obviously represents Martian surface water with an oxygen isotope composition up to three times further away from the terrestrial isotope fractionation line than the oxygen in the silicates of SNC-meteorites. At the high temperatures during magma generation in the Martian mantle isotopic equilibration between oxygen of the silicates and of water would certainly have been established. Hence, only a fraction of the water found in SNC-meteorites can be mantle derived and the other non-terrestrial part must come from a Martian surface reservoir. If the oxygen isotopes of the surface component were created by non-linear isotope fractionation processes the total amount of water of this composition cannot be large.

Even if we assume the 180 ppm H_2O in Shergotty to be fully mantle derived and compare it with the 1330 ppm S in Shergotty, it is evident that sulphur, respectively SO_2 (2660 ppm), is a much more abundant volatile compound in the Shergotty magma than water. Reflecting the similar abundances of H_2O, CO_2 and SO_2 in terrestrial magmas, these three compounds are also found in about equal abundances in terrestrial volcanic gases. On a planet with a mantle considerably poorer in water than the Earth's mantle, but similar or richer in sulphur, it is to be expected SO_2 (and CO_2) to dominate the exhalation gases although part of the sulphur might degas in form of H_2S and elemental S.

At presence, the mean surface temperature of Mars at low latitudes is -55°C, while on the poles the temperature drops to less than -140°C. Considering the lower solar luminosity 3.5 bys ago, the equatorial mean temperature would drop to about -73°C or close to the freezing point of SO_2. Thus without an appreciable greenhouse effect, H_2O should have been a solid at all latitudes, CO_2 a solid or gas depending on latitude and SO_2 a liquid or solid depending on latitude. On Mars, SO_2, CO_2 and H_2O from volcanic intrusions would migrate through the megaregolith towards the surface. Most of the CO_2 will be quickly transferred to the atmosphere, while SO_2 gas would feed solid, respectively liquid SO_2 tables at low depths. Local warming by a volcanic intrusion will liquefy the stored SO_2 and drive it to the surface as a liquid at temperatures close to the SO_2 triple point (16 mbar and -73°C). Water vapour would be trapped at greater depth in form of ice.

SO_2 is a very efficient greenhouse gas and its importance for heating of the Martian atmosphere was pointed out by Postawko and Kuhn [10]. The atmospheric lifetime of SO_2 is limited by photochemical oxidation to SO_3 and atmosphere-surface reactions. However larger discharges of SO_2 into the atmosphere would lead to a short term warmer climate which in turn can volatilize more SO_2 stored in the regolith and finally melt the water ice stored at greater depths.

The Martian soil contains about 3.5% S most probably in form of sulphates. As water is the most likely source of oxidation to transform FeS to SO_3, we have to ask what portion of water once present at the Martian surface was used up for this process.

In summary, we like to stress the importance of sulphur and SO_2 on Mars. In the case that water should have been supplied in sufficient quantities to the Martian surface by a late veneer and stored in the near surface layers in form of ice, temporary greenhouse warming by SO_2 after large SO_2 discharges may have been responsible for melting of ice and break-out of water in areas not directly connected to volcanic activity. Aside of water, liquid SO_2 could explain at least some of the erosion features on the Martian surface. It seems that on Mars the oxygen fugacity is governed by sulphur.

References: 1 Wänke H. and Dreibus G. (1988) Phil. Trans. R. Soc. Lond. A325, 545. 2 Ringwood A.E. (1979) On the Origin of the Earth and Moon, Springer Verlag, New York. 3 Wänke H. (1981) Phil. Trans. R. Soc. Lond. A303, 287. 4. Dreibus G. and Wänke H. (1989) In Origin and Evolution of Planetary and Satellite Atmospheres. U. Arizona Press, p. 268. 5. Yang J. and Epstein S. (1985) LPS XVI, Suppl. A, 25. 6. Dreibus G. and Wänke H. (1987) Icarus 71, 225. 7. Johnson M.C. et al. (1991) GCA 55, 349. 8. Carr M. and Wänke H. (1991) LPS XXII, 181. 9. Karlsson H.R. et al. (1992) Science 255, 1409. 10. Postawko S.E. and Kuhn W.R. (1986) JGR 91, no. B4, p. D431.

Friday, August 21, 1992

0900-1445 *Symposium, Auditorium*

1445-1545 *Special Lecture (III)*

Dr. H. Palme (Invited Speaker)
Max-Planck-Institut für Chemie
Mainz, F.R. Germany

On the Carriers of Anomalous Nitrogen Components in Primitive Meteorites

Kiyota, K. Sugiura, N. and Hashizume, K
Dept. of Earth and Planet. Phys., Faculty of Science, Univ. of Tokyo, Tokyo, Japan

Presolar grains such as diamond and SiC have been found in primitive meteorites. Because of their chemical stability, these are easily enriched by HF/HCl treatment. However, there may be other presolar grains, which are less stable against these reagents. Using nitrogen isotopic ratio as an indicator, we are searching for such presolar grains in primitive meteorites.

We have measured nitrogen isotopic ratios of many primitive chondrites, and some of them have abundant anomalous nitrogen in bulk samples. One of such chondrites, ALH77214 (L3.4) has nitrogen of $\delta^{15}N = -300‰$ in bulk sample. Diamonds and SiC which are known to contain isotopically light nitrogen are not abundant enough to explain this anomaly. In search of the carriers of the anomalous nitrogen, this meteorite was treated as follows; 1)the sample was crashed in an agate mortar, 2)magnetic materials were separated from the crashed sample with a hand magnet, 3)the magnetic fraction was treated by conc. NaOH aq. at 100°C for 19 days to separate a purely metallic sample, 4)by using a supersonic bath, very fine grains (less than 1μm in diameter) were separated from the non magnetic fraction, 5)coarse grains (sub mm in diameter), which are expected to be mostly fragments of chondrules, were picked up from non magnetic fraction. Samples were heated stepwisely from 200°C up to 1200°C in an oxygen atmosphere. The extracted nitrogen and argon gases were measured with a mass-spectrometer.

From the measurement of these samples, we obtained the information about the carriers of anomalous nitrogen in ALH77214 as follows;

1)metal is not the carrier,

2)some chondrules have light nitrogen,

3)very fine grains (less than 1μm) contain light nitrogen.

Since the fraction of very fine grains contains matrix abundantly, this chondrite seems to have carriers of isotopically anomalous nitrogen in both chondrules and matrix.

NITROGEN ISOTOPIC COMPOSITIONS IN EUCRITES

Yayoi MIURA and Naoji SUGIURA

Department of Earth and Planetary Physics, University of Tokyo, Bunkyo, Tokyo 113

Introduction Eucrites are well known as differentiated meteorite produced by igneous process on the HED parent body. The abundances of primordial noble gases in eucrites are too low compared with other components, e.g. cosmogenic and adsorption of earth's atmosphere, to determine their primordial compositions.

In this study, we try to obtain information concerning primordial component using nitrogen isotopes, whose behavior is expected to differ from those of noble gases. Nitrogen isotopic compositions of five eucrites have been measured by stepped combustion method and their trapped components were studied.

Analytical method Each sample weighing 80-300mg was wrapped in platinum foil and set into ultra high vacuum line connected to a quadrupole mass spectrometer. Nine analyses have been done for four eucrites, and five of nine samples were treated with H_2O_2 to remove organic contaminations. Nitrogen, Ne and Ar have been measured. The analytical procedure for mass spectrometry is same as standard one given in Hashizume and Sugiura (1990).

Results and discussion For three characteristic samples, the release profile of nitrogen and the delta values of extracted nitrogen isotopic compositions are shown in Fig.1. Since cosmogenic nitrogen is generally released at higher temperatures than about 900°C, delta values in high temperature fractions are significantly high. In the figure for Camel Donga eucrite, high delta values are also shown in lower temperature fractions. This is probably due to terrestrial organic material because this sample was not treated with H_2O_2. Nitrogen isotopic compositions in middle temperature fractions are expected to show the composition of primordial nitrogen. The minimum delta values, which are observed in 700-900°C fractions, rang from -39 permil of Y-792511 to 43 permil of Y-82066. Nitrogen abundances extracted in 700-1200°C fractions and minimum delta values for all samples we measured are plotted in Fig.2, and it seems that minimum delta value increases in inverse proportion to nitrogen abundance. We tentatively present two explanations for this trend; 1)this is a result of a mass-dependent isotope fractionation process, such as diffusive loss of nitrogen, in this case indigenous isotopic compositions of nitrogen are different for each sample, 2)the variation of delta value resulted from mixing between indigenous and cosmogenic nitrogen, in this case indigenous isotopic compositions may be constant in eucrites.

The contribution of cosmogenic nitrogen can be calculated. The production rate for ^{15}N of 5.6×10^{-12}g/g/my and exposure ages determined by cosmogenic noble gases for each samples are used for the cosmogenic correction. The corrected $^{15}N/^{14}N$ ratios are in the rage of $(3.45-3.75)\times10^{-3}$ (corresponding to -59.9 permil to 21.8 permil) with the mean value of $(3.60\pm0.12)\times10^{-3}$. The nitrogen isotopic ratios of Camel Donga, ALH-765 and Y-792510 are lower than the atmospheric ratio, and those in Juvinas and Y-

82066 are higher. This trend is similar to that of measured minimum delta value as shown in the figure. It implies that trapped nitrogen in eucrites are close to the isotopic ratio of atmospheric nitrogen. However it is slightly different from atmospheric nitrogen and different each other. Abundances of nitrogen taken from higher than 700°C fractions are less than 1 ppm except for Y-792510 and typically 0.1-0.3 ppm.

In summary, we found 1)primordial nitrogen abundance is from ten to hundred times less than those in chondrites, 2)isotopic compositions of indigenous nitrogen in eucrites are close to that of earth's atmosphere but show somewhat lower or higher ratios in each eucrite.

Reference: Hashizume and Sugiura (1990) Mass Spectroscopy 38, 269-286.

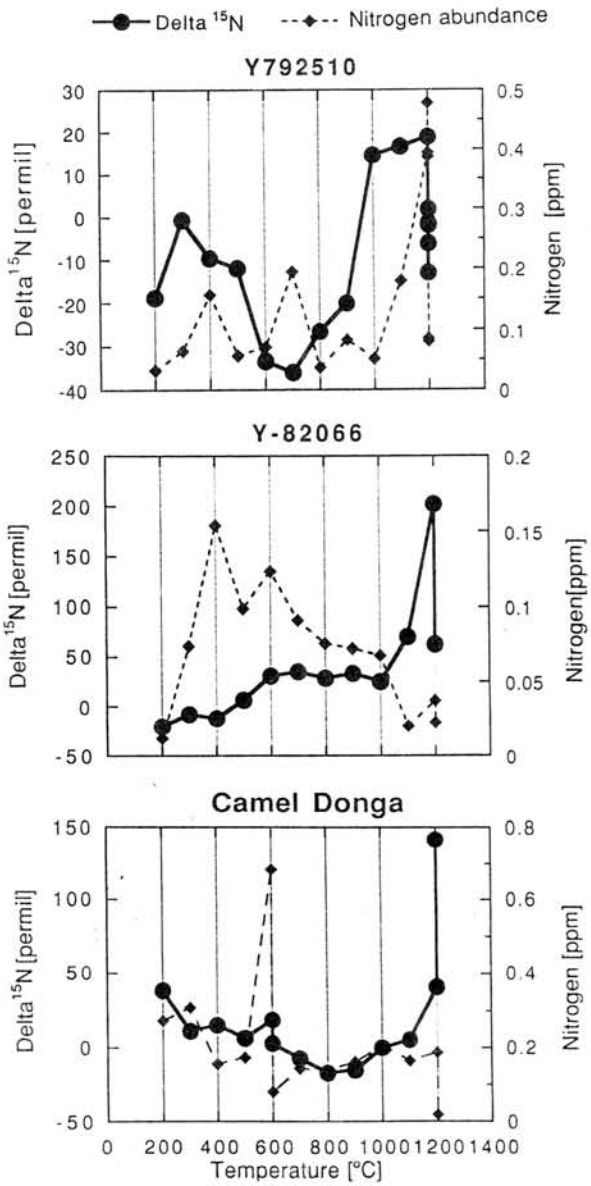

Fig.1
The release profile of the nitrogen and the delta value, which is defined by $\delta\,^{15}N=((^{15}N/^{14}N)_{sample}/(^{15}N/^{14}N)_{air}-1)$ x1000. Characteristic pattern in three eucrites, Y-792510, Y-82066 and Camel Donga are shown.

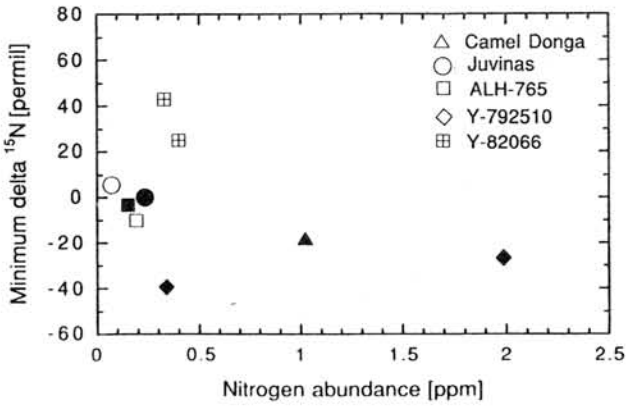

Fig.2
The plot between the amount of the extracted nitrogen taken from higher than 700°C fractions and the minimum delta value. Open and solid symbols show the samples treated with H_2O_2 and not treated, respectively.

Rb-Sr AGE OF AN IMPACT EVENT RECORDED IN THE YAMATO-791088 H-CHONDRITE

Hirokazu Fujimaki*, Ken-Ichiro Aoki*, Ken-ichi Ishikawa**, Hideyasu Kojima***, and Keizo Yanai***

*Institute of Mineralogy, Petrology, and Economic Geology, Tohoku Univ. Sendai, Miyagi 980, **College of General Education, Tohoku Univ., Sendai, Miyagi 980, ***National Institute of Polar Research, Itabashi, Tokyo 173

A giant asteroid impact have melted some parts of the surface of the parent bodies of the meteorites. Such intense impacts have been recorded especially in many L and LL chondrites. Abundant glass or glassy materials containing euhedral minerals have been frequently reported for those types of chondrites. Accordingly, many investigators have tried to date mainly L and LL chondrites (e.g., Minster and Allegre, 1979; Nakamura and Okano, 1985; Takigami and Kaneoka, 1986; Nakamura et al., 1990). In contrast, the age of the impact event has been scarcely dated for the H chondrites. The number of the impact-melted H chondrites may be small and/or the impact might not have been so intensive as to have melted an adequate amount for dating; both could be the reasons. The contrast may imply the difference of the mode of accretion between the H and L(LL) chondrite parent bodies. Chronological data accumulation of the impacts is essential to contribute to the study of the mode of accretion. We therefore attempted to date the impact event recorded in one of the H-chondrites.

Yamato-791088 is a rather large H chondrite (2138 g) and includes vesiculated glassy zone(s) from which the sample used in this experiment was cut (Yanai and Kojima, 1987). The sample consists of mainly cryptocrystalline materials and fine minerals. Abundant and circular vesicles are noticed. Although many chondrules can be recognized, their shape is highly deformed and some of them are hardly recognized as chondrules. It seems that nearly whole melting has been achieved but not complete. Metal grains seem also deformed and sulfide mineral is rarely present. Many of the metal grains are altered and probably lost during grinding.

The sample chip was cleaned in pure hot-water in an ultrasonic cleaner for approximately 3 hours and this procedure has been repeated three times to leach out water-soluble impurity. The sample was separated into eight fractions in alcohol using their magnetic properties. The fraction #1 is the most magnetic one and the #8 the least magnetic portions with non-magnetic mixtures.

The Rb and Sr concentrations were determined by isotope dilution method. The eluted HCl solution was collected for semi-quantitative analysis of some major elements. The analytical results of Rb and Sr concentrations and Sr isotopic compositions are shown in the Table with calculated $^{87}Rb/^{86}Sr$ ratio. The range of the Rb abundances are from 0.314 to 2.88 ppm. The Sr abundances range from 2.71 to 24.3 ppm. Excluding #1, 2, and 8, the variation range (0.3444-0.6023) of $^{87}Rb/^{86}Sr$ is wide, and so is that of the $^{87}Sr/^{86}Sr$ ratio.

Table. Rb and Sr concentrations and Sr isotopic compositions

Fraction#	Rb	Sr	$^{87}Rb/^{86}Sr$	$^{87}Sr/^{86}Sr$
1	0.314	2.71	0.3352	0.71389
2	1.06	5.95	0.5162	0.72471
3	2.46	14.2	0.5035	0.73151
4	2.57	13.9	0.5319	0.73204
5	2.15	12.1	0.5157	0.73147
6	2.88	24.3	0.3444	0.72905
7	1.95	9.39	0.6023	0.73275
8	2.49	12.33	0.5862	0.74148

Fraction #1 is metal-rich fraction with minor amounts of silicate minerals. #2 also contains metallic fragments but the amount is much less than #1. Both the fractions contain nearly no glass but mineral fragments according to the X-ray examination. #8 contains small amounts of graphite and reddish to white alteration products. Although glassy material is dominant in the other fractions as checked by the X-ray examination, olivine and pyroxene fragments are also major constituents. #1 and 2 fractions will not make isochron with the other fractions. #8 should not either.

Note the Figure; all the data were plotted. The solid circles are fraction #3 to 7, and open circles are #1, 2 and 8. The calculated age is 1027 +/- 47 Ma (2 sigma) and the initial ratio is 0.72402 +/- 0.00034 (2 sigma). The obtained age should indicate the time of an impact event on the parent body. The age indicates that not only the L and LL chondrite parent bodies have been impacted till "quite" recently, but the H chondrite parent body has been similarly impacted as well.

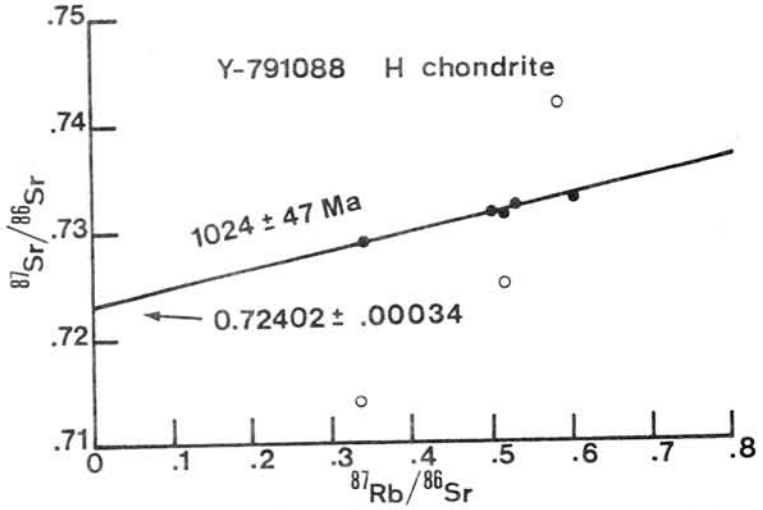

References

[1] Minster J. F. and Allegre C. J., (1979) Meteoritics, 14, 235-248.

[2] Nakamura N. and Okano O., (1985) Nature, 315, 563-565.

[3] Nakamura N., Fujiwara T., and Nohda S., (1990) Nature, 345, 51-52.

[4] Takigami Y. and Kaneoka I., (1986) Mem. Natl. Inst. Polar Res., Spec. Iss., 46, 133-143.

[5] Yanai K. and Kojima H., (1987) Photographic Catalog of the Antarctic Meteorites, pp. 298, Natl. Inst. Polar Res., Tokyo

Effects of total gas pressure on Mg isotopic mass fractionation in condensation experiments of Mg-silicates.

Akira TSUCHIYAMA and Chiaki UYEDA. *Institute of Earth and Planetary Sciences, College of General Education, Osaka University, Toyonaka 560, Japan.*

INTRODUCTION. Isotopic mass fractionation of refractory elements gives important information on condensation and vaporization processes in the primordial solar nebula. The isotopic fractionation have been studied by condensation and vaporization experiments (*e.g.*, [1-3]). Uyeda *et al.* [3] studied Mg isotopic mass fractionation in the condensation experiments, and showed that the condensed phases fractionate toward the heavy mass with respect to the gas phase as well as in vaporization processes. Based on the experimental results, they concluded that the evaluation of isotopic fractionation between the condensed phase and the residual gas phase is essential in primitive meteorites considered as originating from distillation processes. However, in the condensation experiments, origin of the isotopic fractionation by condensation was uncertain because the experiments were carried out at constant total pressure (1.4 Pa of H_2). The mean free path of the gas change with the total gas pressure, and thus behaviors of the isotopic fractionation may also change. In the present study, effect of the total pressure on the Mg isotopic fractionation has been investigated, and origin of the fractionation is discussed.

EXPERIMENTS. The condensation experiments were done with the similar method of the previous experiments [3,4]; a forsterite powder placed at the bottom of the cylindrical Mo crucible (16mmϕ x 146mm) was vaporized at T_{vap}=1580-1585°C in a vacuum furnace, and condensates were obtained along a temperature gradient of the crucible at 1400°C $\sim$ room temperature. Three different total pressures were adopted (2.4×10^{-4}, 1.4 and 70 Pa; Table 1). He gas was used for the ambient gas instead of H_2 gas which was used in the previous experiments. Run of EC22 was done in vacuum (2.4×10^{-4} Pa) without the ambient gas. In order to obtain a large amount of condensates in this high vacuum, smaller crucibles (5mmϕ) with Mo sponges placed on the vaporization source were used to obtain homogeneous angular components of the molecular velocities of the gas. In runs of EC23 and EC24, constant pressures were obtained by bleeding He gas during evacuation. $^{26}Mg/^{24}Mg$ ratios of the condensates were obtained by an ion microprobe analyzer (modified HITACHI IMA-2A) [3].

RESULTS. Congruent vaporization took place in the He atmosphere as well as in the H_2 atmosphere. The condensation sequences obtained in the experiments were follows; Mo+ forsterite (1500-1430°C), Mo+forsterite+MgO (1430-1140°C), Mo+forsterite+MgO+Mo_3Si (1140-860°C), forsterite+Si (860-500°C), and amorphous (500°C-Room temperature) at 2.4×10^{-4} Pa; Mo+forsterite (1500-1130°C), Mo+forsterite+Mo_3Si (1130-1060°C), Mo+forsterite+Mo_3Si +Si (1060-890°C), Mo+forsterite+Si (890-500°C), and amorphous (500°C-Room temperature) at 1.4 Pa; Mo+forsterite (1500-1250°C), forsterite (1250-500°C), and amorphous (500°C-Room temperature) at 70 Pa. The sequences at low pressures (2.4×10^{-4} and 1.4 Pa) are not explained by the equilibrium condensation model, and kinetic effects are considered to be very large. A large amount of Mo was condensed in the present experiments compared with the previous

experiments. Probably, O_2 molecules vaporized from forsterite reacted with the Mo crucible to form MoO_2 and MoO_3 molecules in He atmosphere (H_2O molecules were formed in H_2 atmosphere), and Mo metal was recondensed from these molecules at low temperatures.

Table 1 Summary of condensation experiments.

Run#	Pressure [Pa]	Atmosphere	T_{vap} [°C]	Time [hrs]	m_{res} [mg]	m_o [mg]	λ/d at 300-1800K	Δ^{26}Mg(residue) [per mill]
EC22	2.4×10^{-4}	-	1585	96.0	800	1244	2x103-1x104	+9.5
EC23	70	He	1580	107.2	1068	2515	0.02-0.1	+1.7
EC24	1.4	He	1585	61.5	1060	2510	0.88-5.3	+9.2
Previous	1.4	H_2	1510	41-72			0.55-3.3	

T_{vap} : Vaporization temperature
m_{res} : Amount of forsterite vaporization residue.
m_o : Initial amount of forsterite used as vaporization source.
λ : Mean free path of He or H_2.
d : Diameter of the sample crucible.

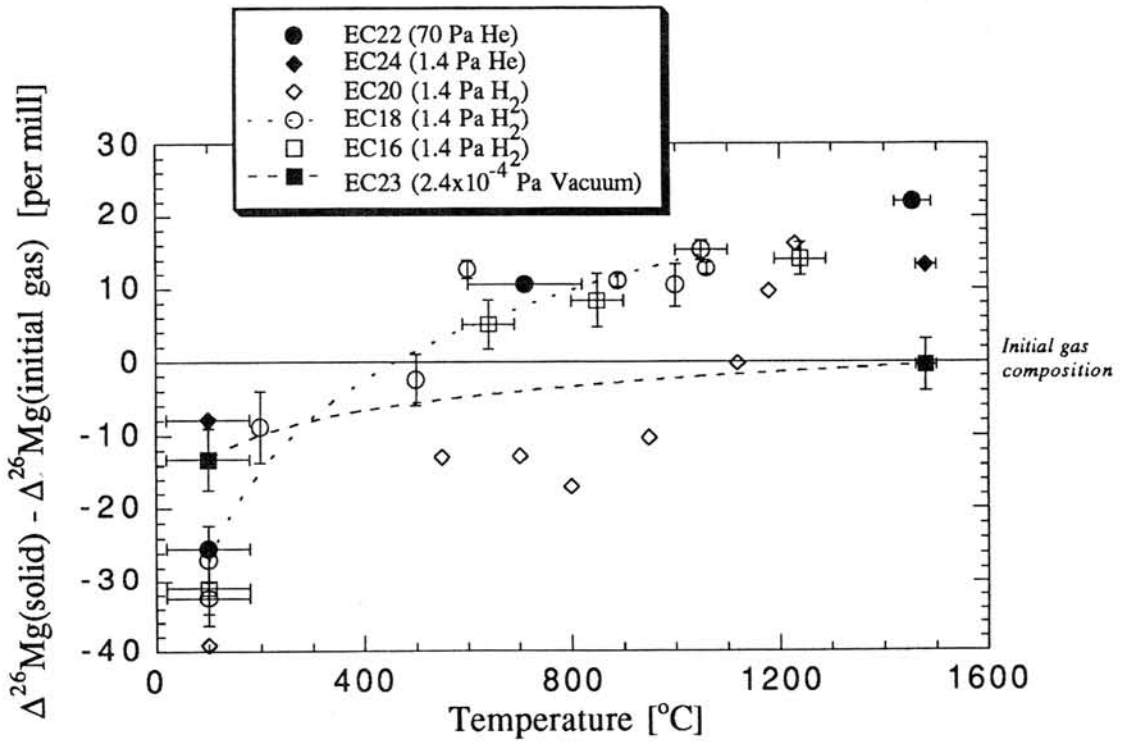

Figure 1. Change in the Mg isotopic ratios of the condensates as a function of condensation temperature.

Mg isotopic fractionation took place not only by condensation but also by vaporization. Averaged isotopic ratio of the vaporized gas was obtained from the isotopic ratio of the vaporization residue, Δ^{26}Mg(residue), and the amounts of initial vaporization source, m_o, and the vaporization residue, m_{res}. Fig.1 shows the isotopic ratio of the condensates, Δ^{26}Mg(solid), with respect to the averaged isotopic ratio of the vaporized gas, Δ^{26}Mg(initial gas), as a function of the condensation temperature, where Δ^{26}Mg is follows;

$$\Delta^{26}Mg = \{[^{26}Mg]/[^{24}Mg]_{sample}\}/\{[^{26}Mg]/[^{24}Mg]_{standard}-1\}x10^3. \quad (1)$$

Results of the previous experiments at 1.4 Pa H_2 (EC16, 18, 20) are also shown in Fig.1. In these previous experiments, condensates richer in ^{26}Mg by about 10-20 per mill than the vaporized gas start to be formed at the highest condensation temperature, T_c, and become poorer in ^{26}Mg, and finally the fractionation becomes -30～-40 per mill. This Δ^{26}Mg(solid) - temperature relation was explained in terms of the Rayleigh fractionation model in which isotopically heavier condensates are formed successively from isotopically lighter gas. The present experiments at low pressures ($2.4x10^{-4}$ and 1.4 Pa) give similar results to the previous experiments, while that at high pressure (70 Pa) gives different result in which only a small amount of fractionation takes place.

DISCUSSION. Fig.2 shows effective isotopic fractionation factor, α^*, at T_c plotted against the total pressure, where

$$\alpha^* = \{[^{26}Mg]/[^{24}Mg]_{solid}\}/\{[^{26}Mg]/[^{24}Mg]_{gas}\}. \quad (2)$$

It is seen from this diagram that the isotopic fractionation by the condensation is large at low pressures, and becomes small with increasing pressure.

The mean free paths of the ambient gas molecules, λ, are calculated to be about 9-50 m, 1.4-8.5 cm and 0.3-2 mm at $2.4x10^{-4}$, 1.4 and 70 Pa, respectively. These values are much larger than the diameter of the crucible, d, at $2.4x10^{-4}$, comparable to d at 1.4 Pa, and smaller than d at 70 Pa (Table 1). Accordingly, molecular condition holds at $2.4x10^{-4}$ Pa, in which the vaporized gas molecules do not collide with each other but only with the wall of the crucible. On the other hand, local equilibrium holds along the temperature gradient at 70 Pa, in which the vaporized gas molecules collide with He molecules. In fact, the condensation sequences at $2.4x10^{-4}$ and 1.4 Pa are inconsistent with the solid-gas equilibrium model, while that is consistent at 70 Pa.

It is also expected that isotopic exchange reaction between solid and gas is out of equilibrium at low pressures, while local equilibrium is held at high pressures. The present results on the isotopic fractionation (Fig.2) indicate that large isotopic fractionation ($\alpha^*>1.01$) takes place at low pressures under disequilibrium conditions, while only small fractionation (α^* ～1.00) takes place at high pressures near equilibrium conditions. At low pressures, molecules of smaller mass absorbed on the surfaces of condensed crystals might be selectively resorbed into the gas, and thus the large isotopic fractionation takes place. Theoretical consideration on Si isotopic fractionation shows that α=1.003 for silicates - gas equilibrium [5]. This is also consistent with the small fractionation at high pressures.

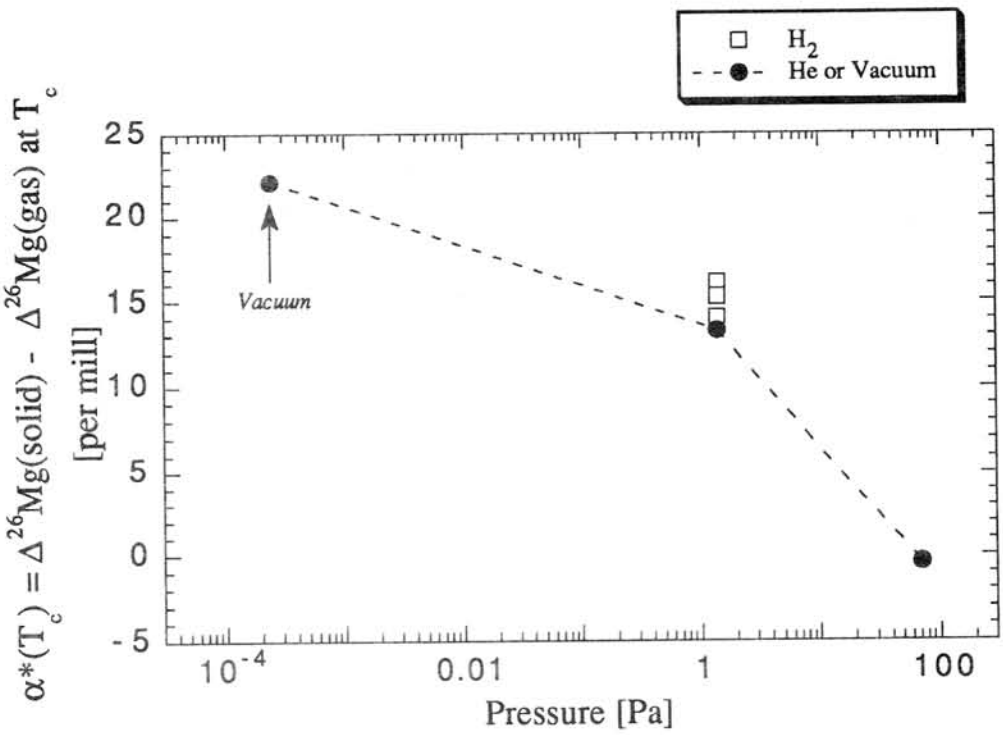

Figure. 2 Effective isotopic fractionation factor, α^*, at the maximum condensation temperature, T_c, plotted against the total pressure of He or H_2.

If gas molecules were collided sufficiently with each other in the primordial solar nebula, condensates would be isotopically in equilibrium with gas during condensation, and thus only small mass fractionation took place. Large isotopic fractionation of refractory elements has not been reported in chondrites even in the matrix except for CAI's. If the matrix with small isotopic fractionation was formed by condensation, isotopic equilibrium would be maintained in the cooling nebula. However, systematic study of isotopic fractionation of the matrix has not been done, and such study is required for understanding matrix formation.

References: [1] Esat T.M., Spear R.H. and Taylor S.R. (1986) Nature, 319, 576-578. [2] Davis A.M., Hashimoto A., Clayton R.N. and Mayeda T.K. (1990) Nature, 347, 655-657. [3] Uyeda C., Tsuchiyama A. and Okano J. (1991) Earth Planet. Sci. Lett., 107, 138-147. [4] Tsuchiyama A. (1991) In "Origin and Evolution of Interplanetary Dust" eds. A.C.Levasseur-Regourd and H.Hasegawa, 83-86. Kluwer Academic Press. [5] Clayton R.N., Mayeda T.K. and Epstein S. (1978) Proc. Lunar Sci. Conf. 9th, 1267-1278.

Isotope Line Analysis on Primitive Meteorites using Ion Microprobe.

Chiaki Uyeda & Akira Tsuchiyama
College of general Education, Osaka Univ. Toyonaka Osaka 560, Japan

It is well known that primitive meteorites such as carbonaceas chondrites are composed of micron-sized components with different chemical and isotopic compositions. Various techniques of micro-analysis has been introduced for its analytical studies. Amoung them, the ion microprobe method was considered to be effective for studying its isotopic and minor chemical profiles(eg.[1]), and the measuring techniques have been improved intensively during the last decade [2,3]. As a result, various types of isotopic anomaries were observed from the micron-sized inclusions which derives from the mixing of extra solar components[2-6], as well as from the mass fractionation due to evaporation and condensation processes[4,7-10].

However up to now, the technique has been applied mainly to analysing a single micron-sized grain separated from the bulk meteorite sample. So far, in situ profile measurements of the bulk section has not been carried out intensively. In general, the ion-microprobe isotopic analysis is accompanied by various types of instrumental mass fractionation, which are considered to derive from the ionization process at the sample surface. The major factors which may interfere the in situ analysis are, ① the matrix effect, ② the geometry of the primary and secondary beam with respect to the sputtered sample surfaces,③ kinetic processes of the secondary ions inside the sample, ④ variation of the charge potential due to the inhomogeniety of the sample conductivity. Usually the micron-sized grains are aggregated in the meteorites in various orientations, having various conductivities, chemical and isotopic compositions. Hence the intrinsic isotopic values of the individual micro-spots in an in situ line analysis, when measured by a ion-probe of 1-30 μ m in diameter, can be disturbed considerably by the instrumental mass fractionations mentioned above.

On the other hand, a large number of textures observed in the primitive meteorites, such as the the chondrules, the CAI's, or the amoeboid textures, have the size of more than several hundred microns. For these large-sized textures, isotope line-analysis data will provide sufficient infromation to estimate its formation history, even if the diameter of the ion-probe is wider than 80 μ m. The amount of instrumental fractionation mentioned above will be reduced, when the spatial resolution is lowered down to this size.

Considering this situation, we have developed a new method for Mg isotopes which realizes the in situ line analysis for non-conductive samples. Since the ion microprobe used at our laboratory

(modified Hitachi IMA-2A) has a low mass resolution of less than 200, it is difficult to divide the peak of the interfering molecular ion from the host peaks. In order to minimize the effect of the ^{24}MgH ion to the ^{25}Mg peak, the condition of the primary ion beam is chosen to be 40mA/cm² in current and 100 μm in diameter. Due to the large curret, charge build-up at the sample surface of the sample becomes a serious problem [10]. In the present study, the conductivity of the sample sufface is improved by attaching a considerable amount of induim metal on the sample surface.

The preliminary result of the line analysis are shown in Fig.1. The line analysis of the standard sample(Olivine, from San Carlos, New Mexico) over a range of 3mm is shown in the left portion of the figure. It is seen that the isotopically homogeneous profile is observed with the error of less than 3‰ . In the right portion, the central part(Ⅱ) of the olivine standard is substituded with a piece of ^{24}Mg enriched diopside glass [$CaMgSi_2O_6$]. The isotopic component of the enriched glass are calculated to beΔ 26 = +22.3‰ with respect to the terrestrial standard, according to the amount of doping fraction of^{24}Mg.

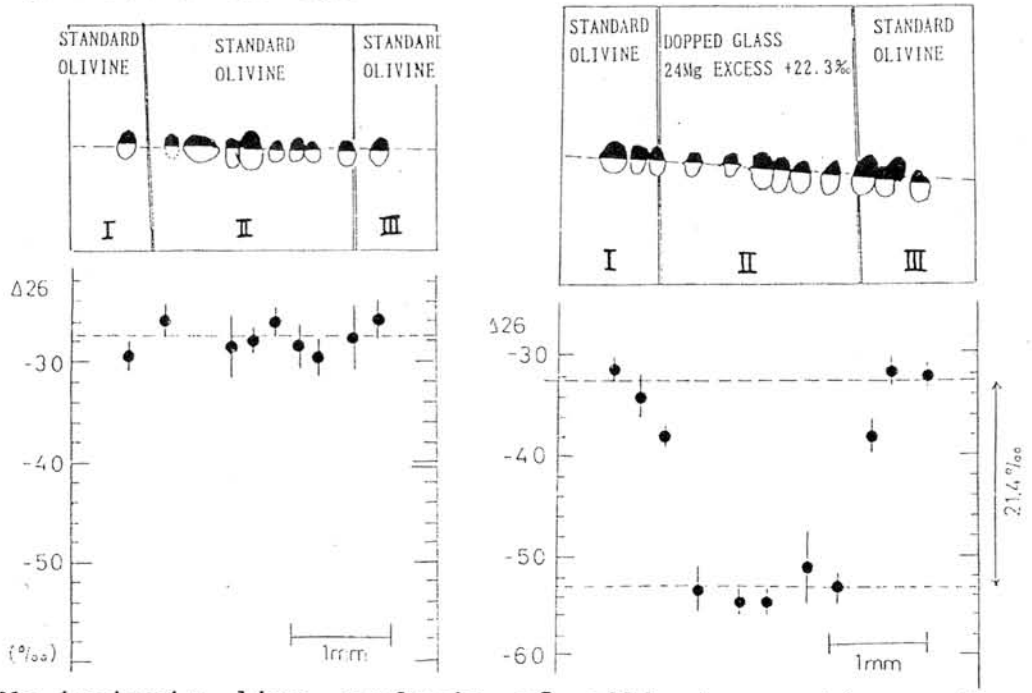

Fig.1 Mg-isotopic line analysis of silicate sections. The line analysis of the standard sample(Olivine from San Calros,New Mexico) is shown in the left portion of the figure. In the right portion, the intermediate position is substituded with a piece of ^{24}Mg enriched diopside glass.

The measured data shows a flat profile in the diopside resion with the average isotopic value to beΔ 26= +21.4 ‰ , which coinsides with the calculated value within an error of about ± 3 ‰ . Accordingly, it is concluded that line analysis of Mg isotopes can be performed for non-conductive samples over a range of 5mm on the sample surface. The isotopic variation of an unknown sample with respect to the standard sample may be evaluated precisely by placing the unknown sample in the position of the diopside glass in Fig.1, and performing the same line analysis described above. It is also noted that the sample preparation described above is effective to check the amount of instrumental mass fractionation. In general, the amount of instrumental mass fractionation changes considerably with the position of the primary ion at the sample surface, and it is necessary to evaluate this effect in the course of day-by- day measurements in the case of line analysis as mentioned above.

It is noted that the search of new isotopic anomaries in meteorites can be carried out far more effectively by performing an in situ line analysis than by separating the individual grain from the bulk samples as it is commomly done at the present moment. Esspecially, the mass fractionation data of individual components, which are considered to arrise from the evaporation and condensation process in the solar nebula, would be a subject of large significance using this method. Large mass fractionation has been observed in the CAI or in the POI inclusions of the CV chondrites, as well as in the hibonite inclusions of the CM chondrites. The results are compared in Fig.2. The correlation between isotopic fractionation, morphology, major chemicals or the REE patterns are considered to be weak. The whole nature of the evaporation and condensation process has not been explained consistently, because the number of fractionation data are limited, and also because the isotopic behavior of refractory elements in the evaporation-condensation process are poorly understood[7-10].

Recently, a number of experimental studys have been performed to understand the mechanism of isotopic behaviors in the evaporation-condensation processes [8-11]. Accordingly, it became clear that not only the residues but also the condensates were fractionnated in the heavy isotopes according to the fraction of the residual gas phase[10,11]. The evaluation of isotopic mass fractionation between the condensed phase and the residual gas phase is considered to be essential for the analysis of various isotopic data observed in the meteorites. It was also pointed out that the situation of the residual gas phase may be estimated form the isotopic data in the silicate condensation process[10]. It is noted that more systematic studies are required, changing the redox conditions, total pressure and so on, in order to understand the whole nature

of isotopic fractionation in the process[12].

As for the number of meteorite datas, so far the isotopic abundance of refractory elements has been measured mainly on refractory inclusions such as the CAI's, hibonite bearing grains or the SiC grains as mentioned above. However, evaporation and condensation are considered to be the major process in the course of grain formation in the early solar nebula, and in this sence, almost all the components in the meteorites may have experienced these processes. Therefore, it is desiable to carry out a systematic survey on all the components of the meteorites, in order to obtain the whole view of the evaporation-condensation process. The in situ isotope analysis will be a effective method in realizing this survey.

Finally, this method of line analysis is applicable also to the analysis of other major elements such as Si,O,S or Fe. Developments on measuring these elements are now in progress.

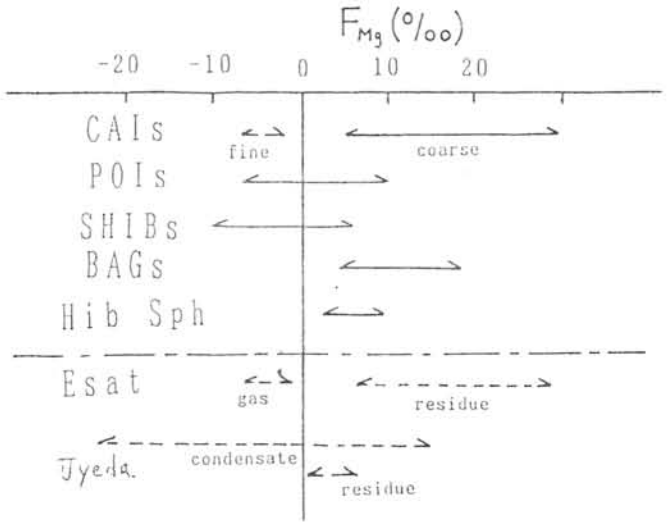

Fig.2 Mg mass fractionation of refractory inclusion observed in the primitive CV and CM chondrites[3-7]. The value of laboratory products by Esat[8] and Uyeda [10] are shown in broken lines.

References

[1]NISHIMURA.H & OKANO.J (1974) J.Appl.Phys.Suppl.2 Pt.1 339.
[2]McKEEGAN,J.& ZINNER,E. (1987) GCA 51 1468.
[3]HUNEKE,J.C.,ARMSTRONG,J.T. & WASSER BURG,G.J. (1983)GCA 47 1635
[4]LEE,T.,PAPANASTASSIOU,D.A.& WASSERBURG,G.J.(1977)Geophys.R.L3 109
[5]CLAYTON,R.N.,et al.(1988)Phil.Trans.R.Soc.Lond.A325,481 .
[6]ZINNER,R., MING,T. & ANDERS,E.(1989) GCA 53 3273.
[7]IRELAND,T.R.,COMPSTON,W. & ESAT,T.M.(1986) GCA 50 1413.
[8]ESAT,T.M.SPEAR,R.H. & TAYLOR,S.R.(1986)319,576.
[9]DAVIS.A., HASHIMOTO,A.,CLAYTON.R.N. MAYEDA,K.(1990) Nature 347
[10]UYEDA.C, TSUCHIYAMA,A.& OKANO,J.(1989b) EPSL 107 138
[11]TSUCHIYAMA,A(1988)Abst.13th Symp.Antarctic ,123.

ION MICROPROBE MEASUREMENTS OF Mg ISOTOPES IN TYPE-B1 CAI OF ALLENDE METEORITE.

Osamu Koike, Hisayoshi Yurimoto, Hiroshi Nagasawa* and Shigeho Sueno. Institute of Geoscience, University of Tsukuba, Tsukuba, Ibaraki, 305 Japan. *Department of Chemistry, Gakushuin University, Mejiro, Tokyo, 171 Japan.

Introduction Ca-Al rich inclusions (CAIs) from Allende (CV3) meteorite are known in which excesses of ^{26}Mg correlates well with the $^{26}Al/^{24}Mg$ ratio in the host phases. This isochrone relationship indicates the in situ decay of ^{26}Al, and an upper limit of $^{26}Al/^{27}Al$ ~$5x10^{-5}$ has been established for the early solar nebula [1, 2]. The difference of slopes of apparent isochrone could, in principal, reflect differences in the time at which the CAI attained isotopic closure. We have attempted to measure this ^{26}Mg excesses in Type B1 CAI of Allende meteorites by Secondary Ion Mass Spectrometry (SIMS). In this time, We report the analytical procedure and the results of Mg isotopic measurement.

Experimental Mineral separated samples for Allende HN-3 Type B1 CAI [3] have been prepared for Mg isotopic analysis. The spinel (low Al/Mg phase) and anorthite (high Al/Mg phase) grains were mounted in epoxy disks and were performed with the Tsukuba University CAMECA IMS 3F ion microprobe. Measurements were made at sufficiently high mass resolution ($M/\Delta M$~4,500) to exclude all significant interferences. Secondary ion signal were corrected for the counting system dead time, and then, for individual values, time interpolation was made. Measurements were made by cycling through the mass sequence 24, 25, 26, and 27 in electrostatic peak switching mode [4]. A run consisted of 100 cycles and a series of several runs were made on a single spot. The energy slit was set to select an energy window of 100 eV. Instrumental mass fractionations were corrected using terestrial spinel and anorthite.

Results The results of Mg-Al analysis are given in Fig 1. This isochrone lines were attained by combining spinel point with anorthite points. One isochrone slope has the same value ($4.47x10^{-5}$) to the canonical value (~$5x10^{-5}$) of Type B1 CAI. The other one has slightly gentle ($2.74x10^{-5}$). The difference may be caused by a multistage crystallization of anorthite grains in CAI formation.

References 1. Lee T., Papanastassiou D. A., and Wassrerburg G. J. (1976) *Geophys. Res. Lett., 16,* 775-778. 2. Hutcheon I. D. (1982) *Amer. Chem. Soc. Symposium Ser. 176,* 95-128. 3. Nagahara H. (1987). *In Overseas Scientific Research on Mexican Meteorite Nos. 59042011, 60041064, and 61034059.*(eds. H. Nagasawa, T. Matsui, H. Ohashi, K. Yamakoshi, G. Sanchez-rubio), 65-78. 4. G. Slodzian, J. C. Lorin, R. Dennebouy, and A. Havette. *In Secondary Ion Mass Spectrometry SIMS IV*, 153-157.

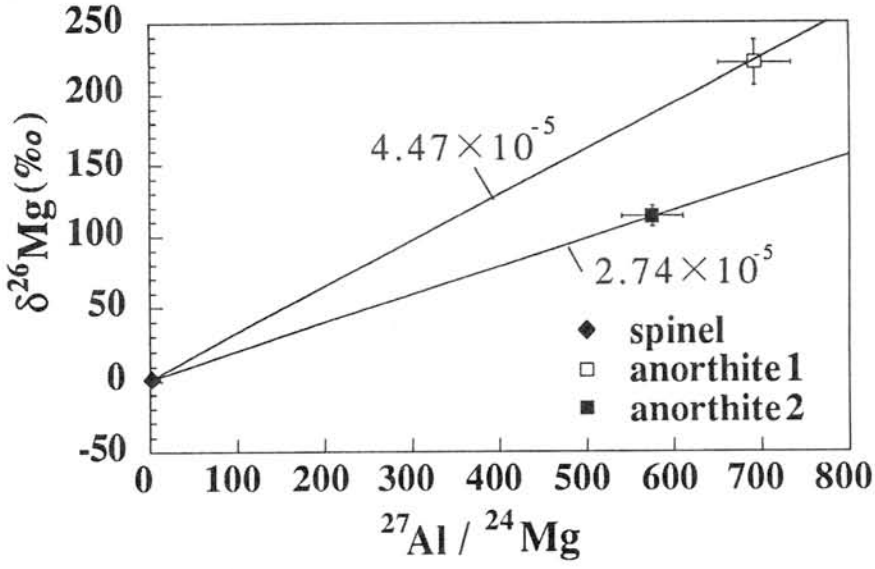

Fig 1. Al-Mg evolution diagram for Allende Type B1 CAI (HN-3).
Error bars are $2\sigma_{mean}$.

OXYGEN ISOTOPIC COMPOSITIONS OF ACHONDRITES

Robert N. Clayton and Toshiko K. Mayeda

Enrico Fermi Institute, University of Chicago, Chicago, IL 60637, USA

Eight achondrite groups are recognized on the basis of their oxygen isotopic compositions: (1) HED = howardites, eucrites, diogenites, mesosiderites, and main-group pallasites; (2) SNC = shergottites, nakhlites, and Chassigny; (3) aubrites; (4) winonaites and IAB irons; (5) ureilites; (6) lodranites and acapulcoites; (7) brachinites; and (8) lunar meteorites. Each of these groups occupies a unique field in the oxygen isotope graph (Fig. 1) with the exception that the aubrites and lunar meteorites are indistinguishable from the Earth (Clayton et al., 1976, 1984, 1992; Clayton and Mayeda, 1978a, 1978b, 1983, 1988; Mayeda and Clayton, 1980; Mayeda et al., 1983, 1984, 1987). The isotopic compositions will be discussed first in terms of the variations *within* each group, then in terms of the variations from one group to another.

Two of the achondrite groups, HED and SNC, are composed of several different meteorite types probably related to one another by igneous differentiation on a parent body which had undergone extensive melting (Hewins and Newsom, 1989; McSween, 1985). By analogy with igneous processes on the Earth and Moon, we anticipate that samples from such a parent body should have a constant $\Delta^{17}O$ (i.e., be related to one another by mass-dependent fractionation only) and ranges of $\delta^{18}O$ of 1–2‰, associated with the small mineral-mineral fractionation factors at igneous temperatures. All lithologies of the SNC group follow such a pattern, so that oxygen isotope data support the origin of all the SNC meteorites in the same parent body. (It was recognized on the basis of oxygen isotopes (Clayton and Mayeda, 1983) that the dunite Brachina was *not* a member of the SNC group.) Karlsson et al. (1992) have shown that water extracted from some SNC meteorites has even higher $\Delta^{17}O$ than the meteorites themselves, implying an extraplanetary source for the Martian atmosphere.

Many lines of evidence imply that eucrites and diogenites are related to one another through igneous differentiation processes (see Hewins and Newsom, 1989, and references therein). Howardites are breccias consisting primarily of eucritic and diogenitic clasts. Hence, there is general agreement that eucrites, diogenites, and howardites (HED) are from the same parent body. The association between HED and mesosiderites is less direct: bulk chemical compositions of mesosiderite silicates and howardites are very similar (Mittlefehldt et al., 1979) and eucritic clasts are observed in some mesosiderites (Rubin and Jerde, 1987). Similarities between mesosiderites and main-group pallasites are found in the chemical compositions of olivine (Mittlefehldt, 1980). Oxygen isotopic compositions of chromite suggest a genetic connection between the main-group pallasites and the IIIAB irons (Clayton et al., 1986). Chemical evidence for this association has been presented by Scott (1977) and Buseck (1977). Chemical similarity between metal in mesosiderites and the IIIAB iron meteorites was noted by Hassanzadeh et al. (1990). These and other authors propose that the metal and silicate parts of the mesosiderites represent the two partners of a collision. However, the oxygen isotopic composition of the IIIAB chromite suggests that it was derived from the same oxygen reservoir as the silicates in the pallasites, mesosiderites, and HED meteorites, implying that all of these meteorites may come from a single parent body. If all these rock-types are exposed at the surface of one parent body, it must have been previously disrupted and re-assembled, Miranda-like. The perennial problem of underrepresentation of dunites remains.

It should be noted that two non-main-group pallasites, Eagle Station and Itzawisis, have oxygen isotopic compositions far from the HED field, and must represent samples of a different parent body. Thus pallasites were formed in at least two bodies, which opens the possibility that the main-group pallasites and other members of the HED group may also come from several parent bodies with very similar materials and processes.

The aubrites (enstatite achondrites) are the only achondrites with oxygen isotopic compositions the same as a chondrite group (the enstatite chondrites) (Mayeda and Clayton, 1980; Clayton et al., 1984). Because of the strong chemical similarity between these two groups, a genetic association has generally been accepted (Watters and Prinz, 1979). Relative to the enstatite chondrites, the aubrites are depleted in a feldspathic component. Wilson and Keil (1991) have proposed an explosive volcanic mechanism for the removal of a basaltic liquid from the parent body, leaving an aubrite residue.

The ureilites have an oxygen isotope pattern totally unlike any other achondrite group (Clayton and Mayeda, 1988). Instead of being constant, the $\Delta^{17}O$ value ranges from –0.4 to –2.5‰. The data fall along a ^{16}O-mixing line which overlaps and extends the mixing line defined by CAI and dark inclusions from C3 chondrites. The mixing line must represent either the sampling of a very heterogeneous parent body or a series of intimate mixtures of two different bodies. The latter hypothesis would require that both bodies originally lay on the carbonaceous chondrite mixing line. Some of the ureilites are polymict breccias: Nilpena, for example, contains clasts spanning 8‰ in $\delta^{18}O$, which seems easier to reconcile with a single heterogeneous body (as CV3 parents are known to be), rather than mixing on a millimeter scale of two asteroidal bodies.

However the oxygen isotopic heterogeneity originated, it was clearly a nebular process rather than one of planetary differentiation. The same must be true of the principal chemical variation of the ureilites: the content of ferrous iron in the silicates, which correlates well with the oxygen isotopic composition. Thus both the chemical and isotopic compositions of the ureilties result from pre-parent-body nebular processes, with little disturbance resulting from subsequent igneous and metamorphic processes. Within this framework, the mineralogical and textural features of the ureilites are best accounted for by a catastrophic disruption of the hot interior of a parent body with overall carbonaceous chondrite composition (Takeda, 1987).

The lodranites and acapulcoites appear to belong to a distinct oxygen isotope group. The observed range of $\Delta^{17}O$, however, is about three times as great as the estimated analytical uncertainty, which implies an origin either on an isotopically heterogeneous parent body or on several different parent bodies. McCoy et al. (1992) proposed that the principal difference between lodranites and acapulcoites is in their thermal history, lodranites having melted and undergone some removal of metal, troilite, and feldspathic liquid, while acapulcoites were very little melted. The iron meteorite Sombrerete has albite + orthopyroxene inclusions with oxygen isotopic ratios at the lower end of this group, and might be complementary to the lodranites (Mayeda and Clayton, 1980).

The winonaites (Winona, Mt. Morris WI, Pontlyfni, Tierra Blanca, and Y-75300) have oxygen isotope ratios and chemical compositions indistinguishable from the silicate inclusions in IAB iron meteorites, and are therefore classified in the same group (Mayeda and Clayton, 1980; Clayton et al., 1984). Their $\Delta^{17}O$ value of -0.46 ± 0.05 is resolved from the value of -0.25 ± 0.08 for the HED group.

The brachinites (Brachina, Eagles Nest, Window Butte, and ALH 84025) are a group of primitive achondrites (dunites) which may form a separate oxygen isotope class with $\Delta^{17}O = -0.28 \pm 0.08$. This group is not resolvable from the HED group on the basis of $\Delta^{17}O$, but is consistently higher in $\delta^{18}O$ than the HED group, whereas the olivine-rich members of HED (the pallasites) are at the low-^{18}O end of that group.

Oxygen isotopic compositions of lunar meteorites are in agreement with measurements on Apollo lunar samples (Mayeda et al., 1983, 1986). The Moon is an excellent example of a differentiated parent body in which all primordial oxygen isotopic heterogeneities have been removed by igneous processes.

The distribution of the various achondrite groups on the three-isotope graph (Fig. 1) remains unexplained. The ureilites are a special case, and appear to reflect their origin in a carbonaceous-chondrite-like parent body. A rough ^{16}O-mixing line might be drawn to connect the aubrites, winonaite-IAB, and acapulcoite-lodranite groups, and another such line could relate the SNC and HED groups. Dispersion of data away from ^{16}O-mixing lines must result from contributions of mass-dependent isotopic fractionation in the gas-solid interactions in the nebula. At the very least, it should be possible to understand the relationship between Earth and Mars (SNC), since their relative locations in the solar system are known. However, no plausible mechanism has yet been proposed for the observed compositions.

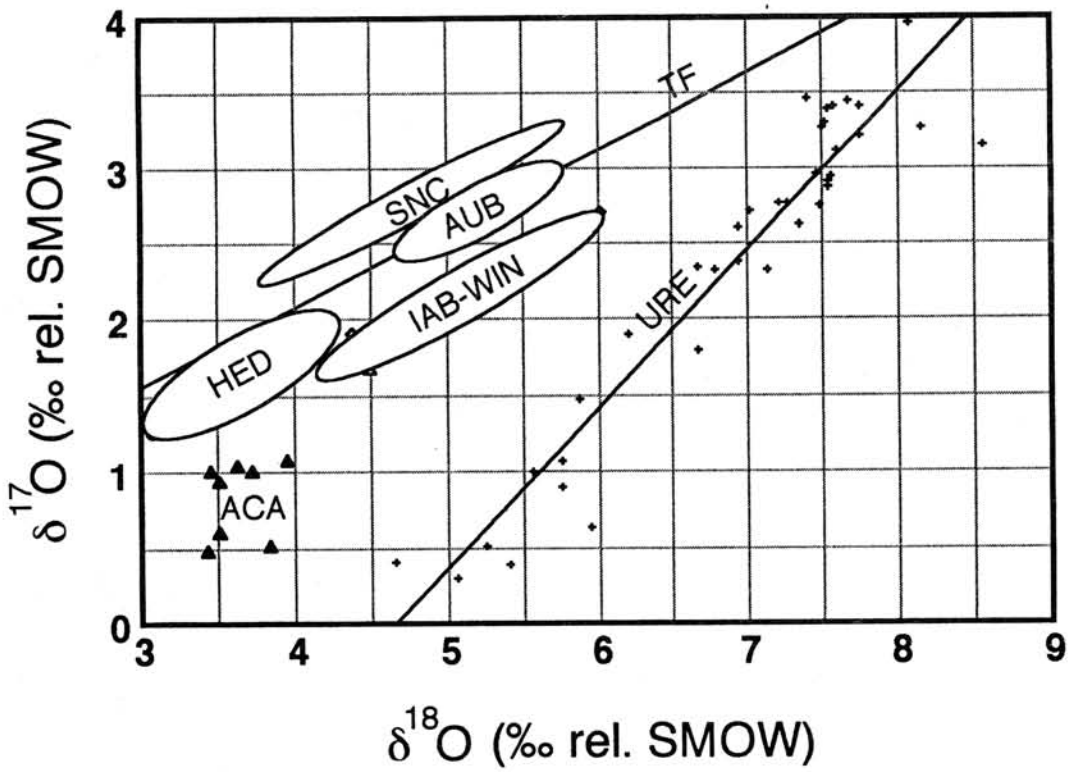

Fig. 1 Oxygen isotopic compositions of achondrites. Abbreviations: TF = terrestrial fractionation; SNC = shergottites, nakhlites, Chassigny; AUB = aubrites; HED = howardites, eucrites, diogenites; IAB-WIN = IAB irons and winonaites; ACA = acapulcoites and lodranites; URE = ureilites. Lunar meteorites (not shown) coincide with aubrites.

References. Buseck P.R. (1977) *GCA* **41**, 711–740. Clayton R.N. and Mayeda T.K. (1978a) *GCA* **42**, 325–327. Clayton R.N. and Mayeda T.K. (1978b) *EPSL* **40**, 168–174. Clayton R.N. and Mayeda T.K. (1983) *EPSL* **62**, 1–6. Clayton R.N. and Mayeda T.K. (1988) *GCA* **52**, 1313–1318. Clayton R.N., Onuma N., and Mayeda T.K. (1976) *EPSL* **30**, 10–12. Clayton R.N., Mayeda T.K., Prinz M., Nehru C.E., and Delaney J.S. (1986) *LPS XVII*, 141–142. Clayton R.N., Mayeda T.K., and Yanai K. (1984) *N.I.P.R. Spec. Issue No. 35*, 267–271, Tokyo. Clayton R.N., Mayeda T.K., and Nagahara H. (1992) *LPS XXIII*, 231–232. Hassanzadeh J., Rubin A.E., and Wasson J.T. (1990) *GCA* **54**, 3197–3208. Hewins R.H. and Newsom H.E. (1987) In *Meteorites and the Early Solar System*, J.F. Kerridge and M.S. Matthews, eds., pp. 73–101. University of Arizona Press, Tucson. Karlsson H.R., Clayton R.N., Gibson E.K. Jr., and Mayeda T.K. (1992) *Science* **255**, 1409–1411. Mayeda T.K. and Clayton R.N. (1980) *Proc. Lunar Planet Sci. Conf. 11*, 1145–1151. Pergamon. Mayeda T.K., Clayton R.N., and Molini-Velsko C.A. (1983) *Geophys. Res. Lett.* **10**, 799–800. Mayeda T.K., Clayton R.N., and Rubin A.E. (1984) *JGR* **89**, C245–C249. Mayeda T.K., Clayton R.N., and Yanai K. (1987) *N.I.P.R. Spec. Issue No. 46*, 144–150, Tokyo. McCoy T.J., Keil K., Mayeda T.K., and Clayton R.N. (1992) *LPS XXIII*, 871–872. McSween H.Y. Jr. (1985) *Rev. Geophys.* **23**, 391–416. Mittlefehldt D.W. (1980) *EPSL* **51**, 29–40. Mittlefehldt D.W., Chou C.-L., and Wasson J.T. (1979) *GCA* **43**, 673–688. Rubin A.E. and Jerde E.A. (1987) *EPSL* **84**, 1–14. Scott E.R.D. (1977) *GCA***41**, 349–360. Takeda H. (1987) *EPSL* **81**, 358–370. Watters T.R. and Prinz M. (1979) *Proc. Lunar Planet. Sci. Conf. 10th*, 1073–1093. Pergamon. Wilson L. and Keil K. (1991) *EPSL* **104**, 505–512.

CHEMICAL AND ISOTOPIC COMPOSITIONS IN ACID RESIDUES FROM VARIOUS METEORITES

Naoki Kano[1,2], Kazuo Yamakoshi[2], Ken'ichi Nogami[3]
1)Department of Earth & Planetary Physics, Faculty of Science, University of Tokyo, Bunkyo-ku, Tokyo 113, Japan.
2)Institute for Cosmic Ray Reserch, University of Tokyo, Tanashi, Tokyo 188, Japan.
3)Department of Physics, Dokkyo University School of Medicine, Tochigi 321-02, Japan.

1.Introduction

Acid residues and SiC therein from primitive meteorites are considered as one of the precusor materials which have survived pre-solar nebula. And in these samples, isotopic anomalies in noble gases, C, N, Si,etc. have been reported before [1,2,3,4,5]. And then, lately, Kumar and Goel reported that acid residues of Sikhote Allin iron meteorite have isotopically anomalous ratios for $^{190}Os/^{184}Os$ measured by RNA [6]. In this work, we are going to investigate Ru and/or Os isotopic compositions in acid residues of various meteorites systematically. So far, in the first stage, Ru isotopic abundance in acid soluble components from an iron meteorites, Canyon Diablo, is measured by a thermal ionization mass spectrometer (TIMS). At the same time, the determination of elemental composition in acid residues is carried out by instrumental neutron activation analysis(INAA). The texture and elemental distribution are investigated by using a scanning electron microscope (SEM) and an X-ray microanalyzer(XMA).

2.Experimental

The meteorites studied here are 1)Canyon Diablo #1,#2 (IA) from Arizona USA. 2)Allende (CV3) from Chihuahua Mexico 3)Nuevo Mercurio (H5) from Zacatecas Mexico. After removing fusion crusts by ceramics blade grinder, three types of meteorites were disaggregated by using freeze-thaw method and were melted by repeated alternating treatment with HCl,HF, aqua regia at room temperature. The acid resistant residues were gathered by centrifuging and then dried. In addition to these acid residues, iron and stony spherules and ^{3}He-rich component of deep sea magnetic components were used for analyses. Elemental analyses were carried out by INAA (TRIGA II; Inst. Atom. Energy Res.; Rikkyo Univ.) for mainly siderophile elements. The samples of 10-100mg were decomposed in sealed teflon vessels by the microwave dissolution method, and then Ru was extracted by distillation method [7]. In mass spectrometric technique of Ru, V shaped Re single filament with silica gel and phosphoric acid is employed. Ru isotopic analyses are performed by TIMS(VG #354). Ru ion beams in each samples are so faint, they are detected by Daly detector equipped with an ion counting assembly.

3.Results and Discussions

Preliminary results for siderophile elements by INAA are shown in Fig.1 and 2 (mainly for major elements in Fig.1 ;mainly for refractory trace elements in Fig.2). In Fig.1 and 2, the concentration of elements in acid residues are normalized to CI

chondrite, that is, the ordinate represents enrichment factors to CI. It was shown that refractory trace elements (W, Os, Re, Ir, Ru) are generally enriched in acid residues in contrast with major elements (Fe,Ni,Co,...). We are now working on analyses of the much refined samples.

Ru isotopic ratios in terrestrial standard (Aldrich $RuCl_3$) and the acid soluble component from Canyon Diablo are shown in Table 1. All isotope ratios shown in Table 1 are corrected for mass fractionation by normalization to $^{99}Ru/^{102}Ru=0.4042$(exponential law). In two acid soluble components from Canyon Diablo, all ratios were not found to be distinguishable from terrestrial values within the experimental errors. We are now measuring acid residues of various meteorites, iron spherule and so on.

Typical textures in acid residues from Canyon Diablo #1 are shown in Fig.3 and 4. The sample shown in Fig.3 looks conchoidal, and the sample shown in Fig.4 have fuzzy surfaces. In Fig.4, elemental concentrations obtained by XMA are shown by mapping illustlations simulaneously. Besides Fe,Ni,Al analyzed by INAA, Si and S are also seen in this grain. However, Fig.5 shows that no particular element is not maldistributed locally.

References

[1] Zinner E.,Tang M.,and Anders E. Nature 330, 730-732(1987)
[2] Zinner E.,Tang M.,and Anders E. GCA 53,3273-3290(1989)
[3] Zinner E.,Amari S.,Anders E.,and Lewis R.S. Nature 349, 51-54 (1991)
[4] Zinner E.,Amari S.,and Lewis R.S. Lunar Planet Sci.22, 1553-1554 (1991)
[5] Ott U.,Begemann F.,Yang J., and Epstein S. Nature 332,700-702 (1988)
[6] Kumar P. and Goel P.S.,Geochem. Journal 25,399-409 (1991)
[7] Terada K., Matsumoto K., and Kiba T., Bull.Chem.Soc.Jpn. 48, 2567-2571 (1975)

Table 1 Ru isotopic ratios for terrestrial standard and acid soluble components from Canyon Diablo

	96/102	98/102	100/102	101/102	104/102
terrestrial	0.175417	0.058987	0.398972	0.540826	0.591041
standard	± 515	± 292	± 326	± 242	± 358
(Aldrich	0.175284	0.058942	0.399104	0.540651	0.591140
reagent)	± 107	± 40	± 83	± 140	± 208
	0.175405	0.058971	0.399136	0.540766	0.591705
	± 709	± 252	± 340	± 458	± 510
	0.174920	0.058388	0.398763	0.540370	0.590989
	± 324	± 618	± 332	± 153	± 291
Canyon Diablo					
(Acid	0.173654	0.058533	0.398649	0.540909	0.592176
soluble	± 859	± 944	± 774	± 418	± 518
component)	0.174536	0.058921	0.398634	0.539574	0.590867
	± 3920	± 5735	± 2906	± 513	± 1710

All ratios are corrected by normalization to $^{99}Ru/^{102}Ru=0.4042$. Errors are two standard errors of the mean.

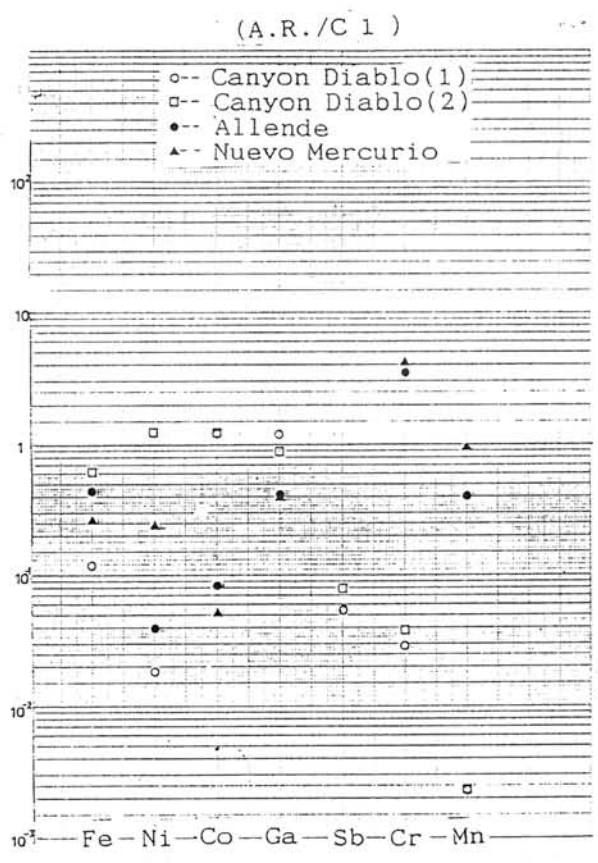

Fig.1.Major siderophile element abundances in acid residues relative to CI

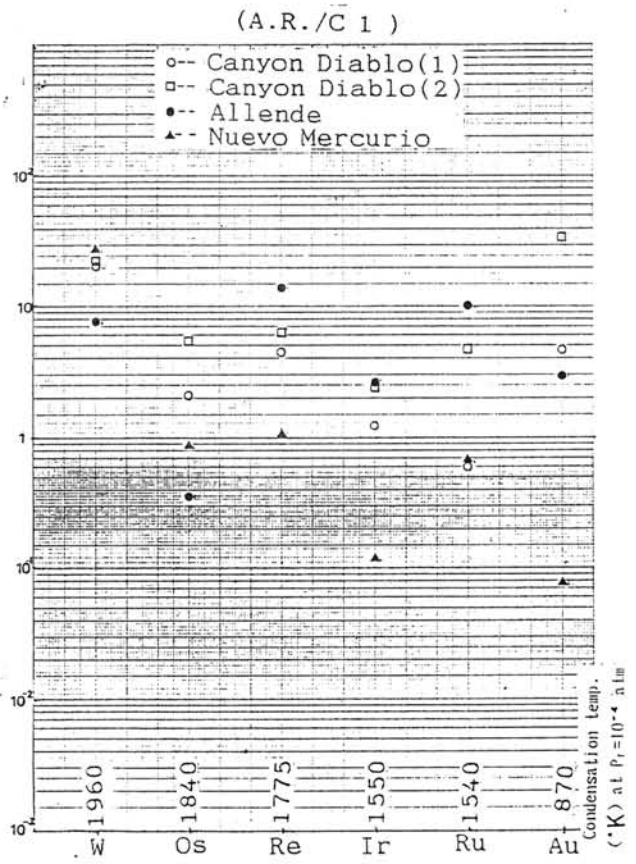

Fig.2. Refractory trace siderophile element abundances in acid residues relative to CI

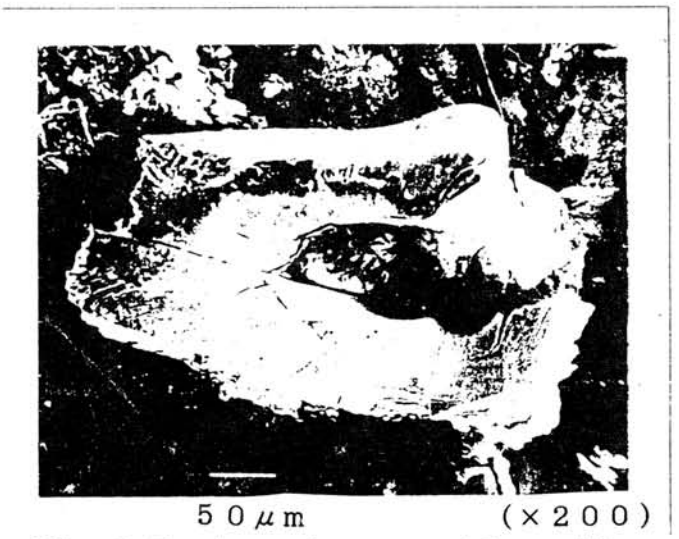

Fig.3.Texture in an acid residue from Canyon Diablo by SEM

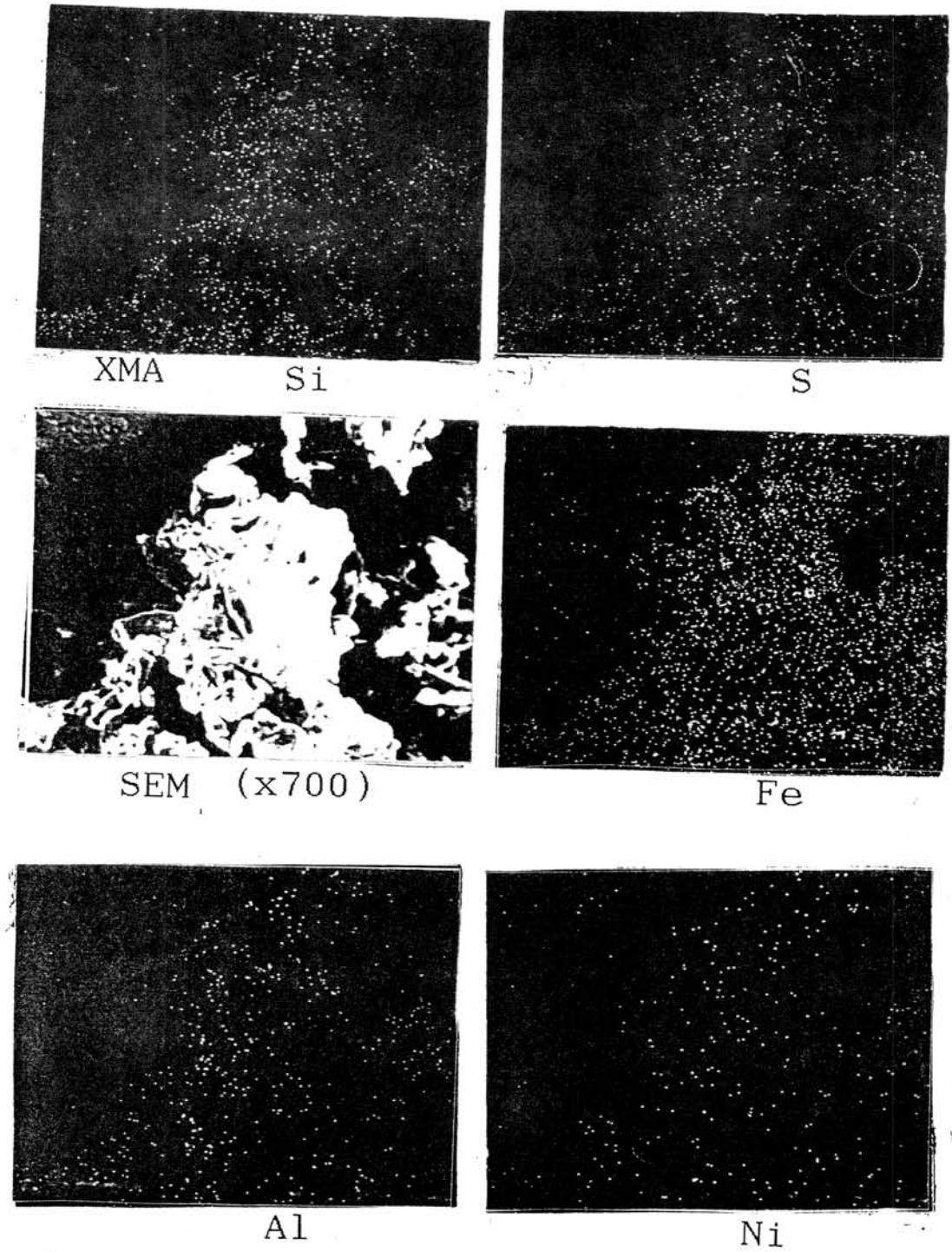

Fig.4. Texture in an acid residue from Canyon Diablo by SEM and elemental mapping illustlation by XMA

NON-CHEMICAL METHODS FOR THE ISOLATION AND STUDY OF INTERSTELLAR GRAINS IN PRIMITIVE METEORITES. Conel M. O'D. Alexander, Xia Gao, Patrick D. Swan, and Robert M. Walker, McDonnell Center for the Space Sciences and Physics Department, Campus Box 1105, Washington University, St. Louis, MO USA.

Chemical treatments that concentrate certain mineral phases in acid-resistant residues gives a powerful method for isolating interstellar grains from primitive meteorites [1]. Specifically, isotopic measurements of both major and minor elements, including noble gases, on individual grains of SiC and graphite found in acid residues have shown that many of these grains must have formed as stellar condensates around other stars prior to the formation of our solar system [2,3]. Detailed studies of many hundreds of individual grains are currently being used to test fundamental ideas of nucleosynthesis and stellar evolution. The results are consistent with the formation of most grains in the envelopes of rapidly evolving asymptotic giant branch (AGB) stars that have ended their lives on the main sequence [4]. However, isotopic patterns in certain grains show clear evidence for explosive nucleosynthesis and may well have formed in the remnants of supernova explosions [5].

The laboratory study of interstellar grains is a new field of research with many unanswered questions. We do not yet know how many stars have contributed dust, nor do we know the detailed histories of individual grains from the time they were formed, through the processes that led to their accumulation in a pre-nebular interstellar gas-dust cloud to their survival in the solar nebula and finally, their accumulation in meteorites. To address many outstanding questions it is essential to be able to study interstellar grains as they were incorporated in the meteorites prior to acid-etching treatment. We give here only one example of why this is necessary but many others are possible. Nichols *et al.* [3] have shown that certain grains of SiC are highly enriched in ^{22}Ne. This enrichment is associated with helium suggesting that both species may have been implanted as a stellar wind after the grains had formed. Moreover, it has been noted that the two etching series Murchison, K (0.1-5μm) and L (1-25μm), have very different noble gas concentrations in the SiC fractions and it is suggested that the different etching conditions used in the two series may be responsible for the effect [6]. Yet it is the grains from the Murchison K etching series that typically have highly pitted surfaces suggestive of chemical corrosion (Amari, pers. com.) while many of the larger L series grains are smooth and uncorroded. Clearly, if one wishes to learn about surface implanted species, it would be desirable to measure the noble gases in pristine interstellar grains that have not been exposed to strong laboratory reagents!

The ideal separation method would allow one to detect and select individual interstellar grains from samples of bulk meteorite. We have previously described an X-ray mapping technique that can be used to locate interstellar SiC grains *in situ* [7]. We have now located close to 100 SiC grains in polished sections of the CM meteorites Murchison and Cold Bokkeveld. Ion probe measurements on 18 of the grains show anomalous carbon isotopic ratios similar to those found in acid residues of Murchison. SEM stereo imagery of the remaining grains indicates that most of them are also indigenous to the meteorite. Although these *in situ* grains represent an important resource for future studies, most are too small (≤ 1 μm) to be useful for noble gas studies. In addition, the rate of discovery of grains is low, being only ~ 0.5/day under optimized mapping conditions. Moreover, the yield is much lower in certain areas of some of the sections suggesting that plucking of grains during polishing is a severe problem.

All of the SiC grains so far found *in situ* occur as isolated entities in the matrix and most are small (≤ 1 μm). This suggests that physical separation techniques, which sort the meteorite constituents by size and density, among other parameters, could concentrate the SiC considerably. Indeed, one of the key steps in the history of the discovery of interstellar grains was the use of physical separation techniques by the Bern group [8] to concentrate the carriers of anomalous noble gases in primitive meteorites. Using similar procedures, we have

succeeded in producing non-etched separates that are enriched several hundred fold in SiC grains as measured directly using X-ray mapping.

Details of the procedure are shown in the flow chart below. A sample of the Murchison meteorite was first disaggregated using a freeze-thaw technique. Following magnetic separation and organic solvent treatments, the resulting material was sieved into various size fractions. Aliquots of the < 5 μm fraction were further treated in a Franz magnetic separator. The least magnetic material was then density separated using an ultracentrifuge to produce a fraction $\rho \geq 2.9 g/cm^3$. High magnification images of the SiC grains found in this separate show surfaces that are remarkably smooth compared to those seen in the K-series acid residues but similar to those in the L series. Ion probe isotopic measurements of the SiC concentrates are currently in progress.

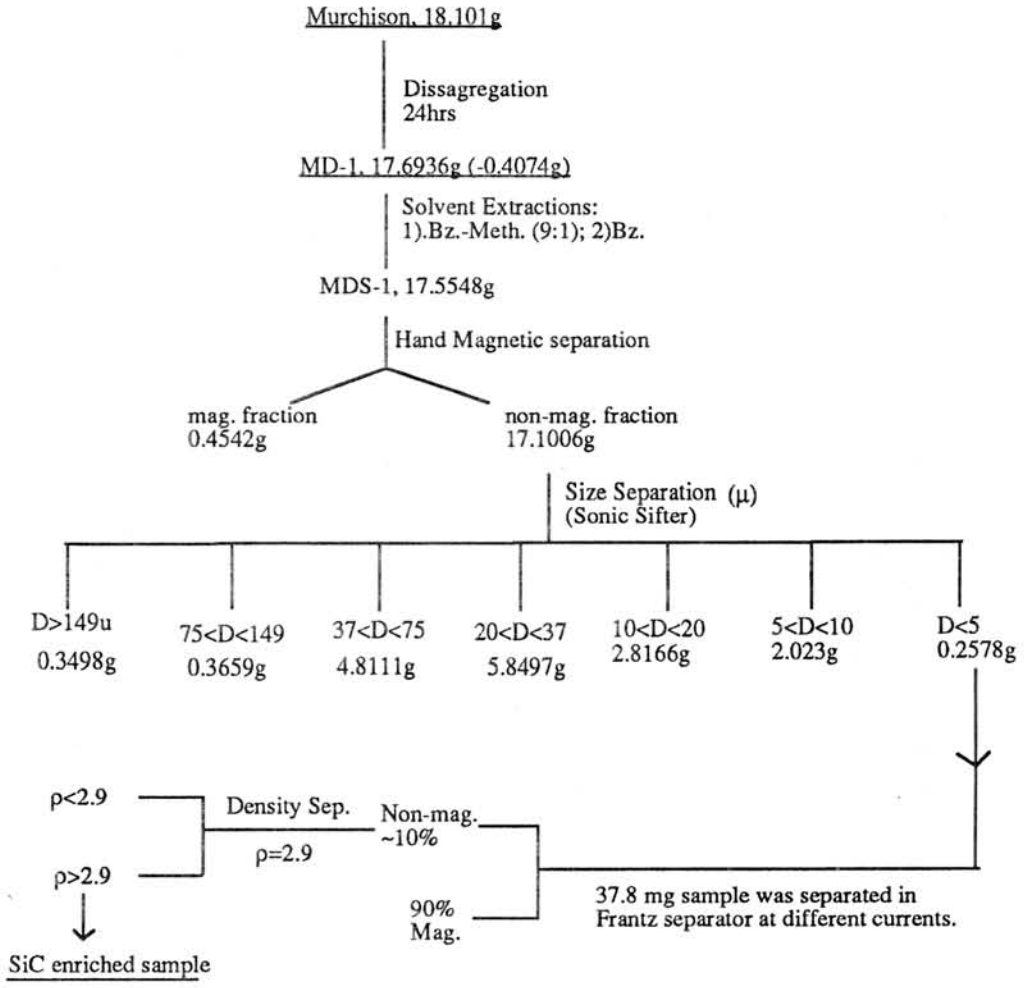

References 1. Tang M. and Anders E. (1988) GCA **52**, 1235-1254. 2. Zinner E. Tang M. and Anders E. (1989) GCA **53**, 3273-3290. 3. Nichols R. H. Jr., Hohenberg C. M., Hoppe P. Amari S. and Lewis R. S. (1992) LPS XXIII, 989-990. 4. Gallino, R. Busso M., Picchio G. and Raiteri C. M. (1990) Nature **348**, 298-302. 5. Amari, S., Hoppe P., Zinner E. and Lewis R. S. (1992a) LPS XXIII, 27-28. 6. Amari S., Lewis R. S. and Anders E. (1992b) GCA in press. 7. Alexander C. M. O'D., Swan P. and Walker R. M. (1990) Nature **348**, 715-717. 8. Eberhardt P. (1974) EPSL **24**, 182-187.

ISOTOPIC COMPOSITIONS OF CORUNDUM AND HIBONITE GRAINS FROM THE MURCHISON METEORITE. Sachiko Amari[1,2], Ernst Zinner[1], and Roy S. Lewis[2] [1]McDonnell Center for the Space Sciences and Physics Department, Washington University, One Brookings Dr., St. Louis MO 63130-4899 [2]Enrico Fermi Institute, The University of Chicago, 5640 S. Ellis Ave., Chicago, IL 60637-1433

INTRODUCTION Corundum and hibonite are refractory phases predicted to condense from a gas of solar composition [1]. Corundum is also predicted to condense in stellar atmospheres both under C>O and C<O conditions [2]. Therefore, analyses of these grains could provide important clues concerning both the early history and pre-history of the solar system. For example, in the Orgueil meteorite, Huss et al. [3] found that one out of 23 corundum grains has a significantly higher $(^{26}Al/^{27}Al)_0$ ratio ($9x10^{-4}$) than the "canonical" value of $5x10^{-5}$. This suggests an interstellar origin for this grain. Virag et al. [4] measured 26 corundum grains 3 to 15 μm in size from the Murchison meteorite. We have extended this study to smaller grains from the Murchison separate KJG (2.1-4.5μm). The procedure of the sample preparation is described elsewhere [5]. In this fraction most of the grains (73% in number) are SiC. We measured $^{18}O/^{16}O$ ratios in 92 hibonite and 41 corundum grains, $^{17}O/^{16}O$ ratios were measured in addition in 9 hibonite and 4 corundum grains; Mg isotopic ratios were measured in 17 hibonite and 37 corundum grains.

RESULTS AND DISCUSSIONS For most of the grains, $\delta^{18}O$ values range from -70 to +20 ‰. One hibonite and one corundum grain fall significantly above this range, having $\delta^{18}O$ values of 55±14‰ and 80±13‰, respectively. On an oxygen three isotope plot they fall close to the terrestrial fractionation line (Fig. 1). Mass fractionated (heavy) oxygen isotopic ratios have previously been found in FUN inclusions and HAL-type hibonite inclusions [6,7]. In the latter, Ca and Ti isotopic fractionations have also been observed and these objects have been interpreted to be distillation residues. To check this possibility, we measured $^{40}Ca/^{44}Ca$ in the hibonite grain. We obtained an isotopic fractionation of F_{Ca}=3.7±4.0 (‰). This is much smaller than what would be expected from the HAL-type hibonites and, if distillation was responsible for the oxygen fractionation of the hibonite grain, it must have occurred on a different precursor than in this object.

$Al/^{24}Mg$ ratios in hibonite range from 25 to 17600, in corundum from 6500 to 51900. Six of 17 hibonite grains have clear excesses of ^{26}Mg with $(^{26}Al/^{27}Al)_0$ ratios of about $5x10^{-5}$, for the others we obtain upper limits for $(^{26}Al/^{27}Al)_0$, the smallest limit being $2.3x10^{-6}$. Thirtytwo out of 37 corundum grains have significant excesses of ^{26}Mg (Fig. 2). Inferred $(^{26}Al/^{27}Al)_0$ ratios range from $<2.3x10^{-7}$ to about $5x10^{-5}$, similar to the result by Virag et al. [4]. None of these ratios exceeds the "canonical" ratio of $(^{26}Al/^{27}Al)_0=5x10^{-5}$ typical for Type B Allende inclusions. Compared to the 3 groups found in larger corundum grains by Virag et al. [4], the grains in the group with $(^{26}Al/^{27}Al)_0 > 10^{-5}$ are more abundant in the small grain size fraction of this study (76%) than in the larger grain size fraction (60%).

References 1. Grossman L. (1972) GCA **36**, 597-619. 2. Lattimer J., Schramm D. and Grossman L. (1978) Ap. J. **219**, 230-249. 3. Huss G.R., Hutchen I.D., Wasserburg G.J. and Stone J. (1992) LPSC **XIII**, 563-564. 4. Virag A., Zinner E., Amari S. and Anders E. (1991) GCA **55**, 2045-2062. 5. Amari S., Lewis R.S. and Anders E. (1992) GCA, submitted. 6. Wasserburg G.J., Lee T. and Papanastassiou D.A. (1977) Geophys. Res. Lett. **4**, 299-302. 7. Ireland T.R., Zinner E.K., Fahey A.J. and Esat T.M. (1992) GCA, in press.

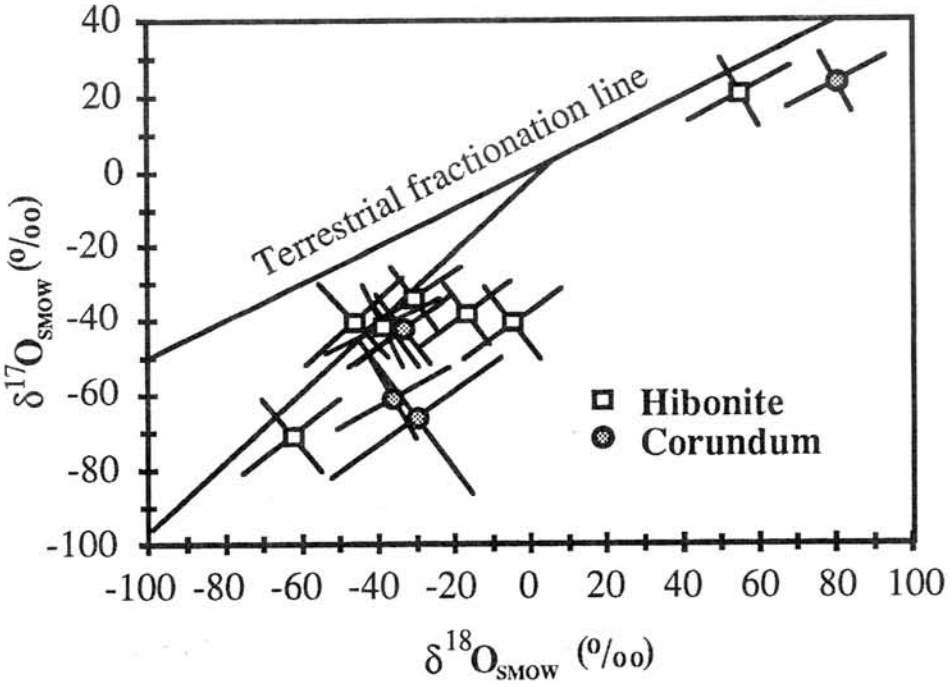
Terrestrial fractionation line
Hibonite
Corundum
$\delta^{17}O_{SMOW}$ (‰)
$\delta^{18}O_{SMOW}$ (‰)
40
20
0
-20
-40
-60
-80
-100
-100 -80 -60 -40 -20 0 20 40 60 80 100

Fig. 1

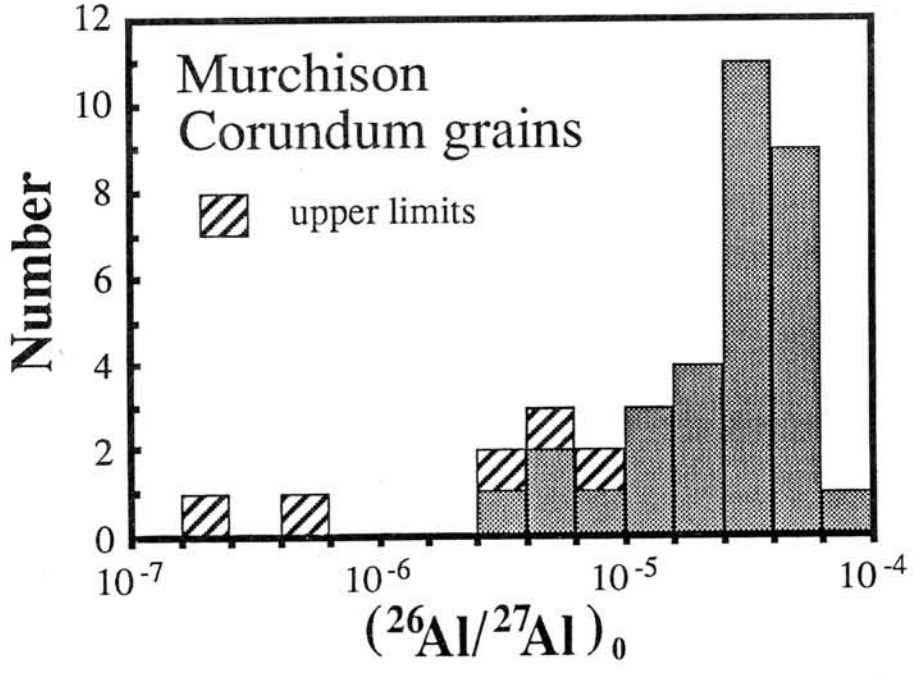
Murchison
Corundum grains
upper limits
Number
$(^{26}Al/^{27}Al)_0$
12
10
8
6
4
2
0
10^{-7}
10^{-6}
10^{-5}
10^{-4}

Fig. 2

Proposal for measuring the TL of Japanese Antarctic meteorites

K. NINAGAWA[1], A. MATOBA[1], I. YAMAMOTO[1], T. WADA[2], S. MATSUNAMI[3], N. TAKAOKA[4], D. W. G. SEARS[5], H. KOJIMA[6] and K. YANAI[6]

[1]*Okayama University of Science, 1-1, Ridai-cho, Okayama 700*
[2]*Okayama University, 1-1, Tsushimanaka 3-chome, Okayama 700*
[3]*Naruto University of Education, Takashima, Naruto, Tokushima 772*
[4]*Kyushu University, 10-1, Hakozaki 6-chome, Higashi-ku, Fukuoka 812*
[5]*University of Arkansas, Fayetteville, Arkansas 72701, USA*
[6]*National Institute of Polar Research, 9-10, Kaga 1-chome, Itabashi-ku, Tokyo 173*

Introduction The thermoluminescence [TL] of the meteorites is a useful tool to study the meteorite history. The induced TL, which depends on the mineral state, have a information of metamorphism. The natural TL, which is a consequence after accumulation of interplanetary radiation and thermal fading, have informations of meteorite orbits, shock heating and terrestrial ages. Cosmochemistry Group, Univ. of Arkansas supplies fundamental information of classification of unequilibrated ordinary chondrites and identification of paired fragments. The natural TL data have been reported in Antarctic meteorite newsletter of the U.S.A. and paired fragments were suggested on the basis of the natural TL data beside ^{26}Al. On the other hand Japanese collections of Antarctic meteorites has become about 8700 specimens since first gathering Yamato meteorites in the 1969. But systematic TL analysis has not been done for these collections. In Japan much effort of the TL measurement has been spent to determine the precise terrestrial ages.[1,2] But it have not been realized yet.

In this abstract we introduce the recent TL works and propose the TL analysis of Japanese Antarctic collections.

Finding shock heating and close solar passage meteorites Figure 1 is a plot of natural TL (LT/HT) against ^{26}Al activity for Antarctic meteorites.[3] Most of meteorites are concentrated on a regression line. The remaining samples plotted below this concentration presumably have been recently reheated. The low TL values of RKPA 79001 and 80202 are attributed to shock heating. Because the feldspar of them has been converted to maskelynite and there are extensive glassy veins. ALHA 77296/7 and META 78006 show no signs of shock reheating. Simplified TL theory indicates that passage within 0.7 A.U. at the sun would be sufficient to cause the observed levels of TL draining. [The low TL values of ALHA 77294 in Fig. 1 is caused by sampling near the fusion crust. Another TL measurement of this sample showed high natural TL.[4]]

Recent natural TL data of Antarctic meteorite newsletter are reported in the unit of equivalent dose [krad at 250 °C]. For samples with LT/HT ratios >0.5, the empirical calibration equation,

$$\log(\mathrm{LT/HT}) = 0.7306 \log(\text{equivalent dose}) - 0.8014 \quad (1)$$

is used to convert to equivalent dose. Values of < 5 krad are thought to be meteorites with small perihelia orbit (<0.85 A.U.); values of 5-30 krad are thought to be indicative of great terrestrial age (say, 400 ±150 ka); values 30-80 krad are thought to be indicative of more 'normal' terrestrial ages, 150±50 ka; high values > 80 krad are indicative of high dose rate. Recent natural TL study of observed falls suggested that meteorites with perihelia <0.85 A.U. should have very low levels of natural TL (<5 krad at 250°C in the glow curve), while meteorites with perihelia >0.85 A.U. should show a range of natural TL (>5 krad) with significant scatter as a result of slight variations in dose rate (shielding) and albedo.[5]

Pairing and ice movement

Benoit et al. measured the natural TL of a large number of ordinary chondrites, 302, from the Lewis Cliff ice field in Antarctica.[6] Weighty samples >20 g were selected to avoid measuring the samples suffered from heating during atmospheric passage and from wind-blown transport on the ice. They used a criterion for identifying paired fragments, the coincidence of natural TL dose [krad at 250 °C] within 10% as well as the following set of criteria, 1) the same chemical-petrologic class, 2) proximity of find location <1.5 km, 3) coincidence of induced TL [peak temperature within 10%, peak width within 20% and TL sensitivity within a factor of two], 4) cosmogenic isotopes,* 5) other petrographic data [shock veins, unusual inclusions and brecciation], 6) hand-specimen descriptions and field observations [weathering category, color, abundance of inclusions, appearance of TL powder before and after heating].

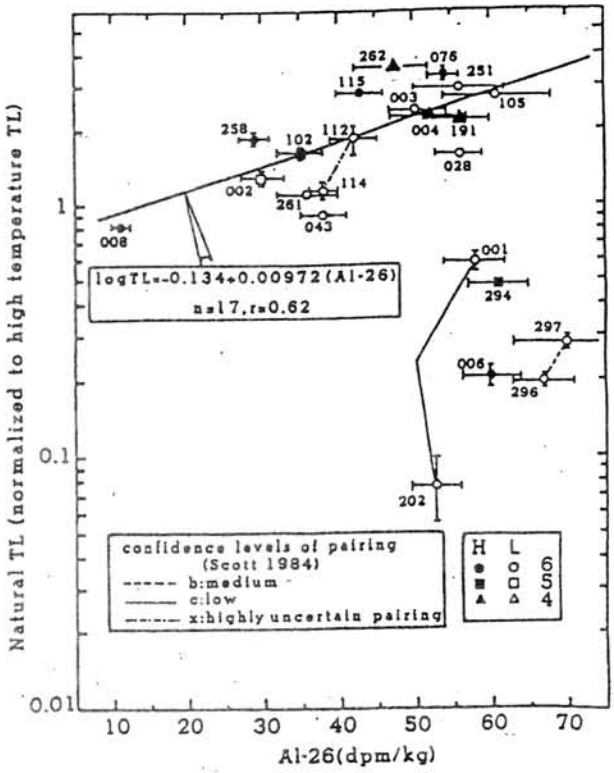

Fig.1 A plot of natural TL against ^{26}Al. (ref.3.)

Up to date 27 groups with 2~5 fragments have been assigned to 'paired' meteorites in the Lewis Cliff ice field. Paired meteorites in the Upper Ice Tongue tend to be found lying in a north-south relationship. The distribution of meteorites on the Lower Ice Tongue is random, boomerang-shaped, or east-west, and the distribution of pairing groups at Meteorite Moraine is not informative.

The distribution and population of natural TL levels were also investigated. On the Lower Tongue, there is a strong tendency for meteorites with low natural TL (say, 5-30 krad) to be found near the western edge of the field, while those in the central part of the tongue fairly uniformly high value of natural TL of approximately 30-80 krad. This trend indicate that there is a western component to the movement of the ice at this location, as well as the movement to the north. This western vector probably explains the concentration of meteorites along the western edge of the ice tongue. The population of low natural TL level, 5-30 krad, is higher at the Upper Ice Tongue (53%) than the Lower Ice Tongue (33%) and Meteorite Moraine (32%). Meteorites at the the Lower Ice Tongue and Meteorite Moraine have relatively high natural TL, and therefore young terrestrial ages, while those on the Upper Tongue show a broad range of ages including a great many large ages.

Unusual Antarctic H chondrites HAQ et al. found that the Antarctic H chondrites showed a different range of induced TL properties compared with those of H chondrites that was currently falling on the Earth.[6] Non-Antarctic H chondrites plot in a band in which peak temperature increases with peak width. But Antarctic H chondrites plot in a cluster above the non-Antarctic H chondrite band. The differences cannot be attributed to weathering or presence of a great many fragments of an unusual Antarctic meteorite. Sears et al. showed that for non-Antarctic H chondrites, there was no relationship between position on these plots and cosmic-ray exposure age, but for Antarctic H chondrites, those with cosmic-ray exposure ages < 20Ma, predominantly 8±2 Ma, are higher TL peak temperatures than those with ages > 20 Ma.[8] (Fig.2)

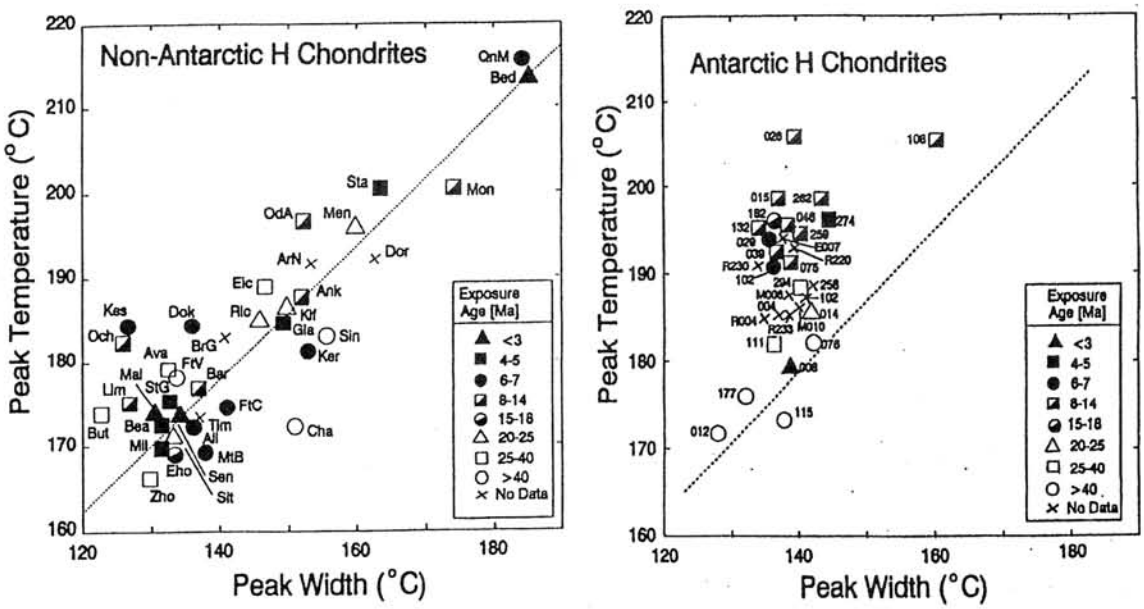

Fig.2 Plots of TL peak temperature against peak width. (ref.8.)

Benoit and Sears found that the unusual high peak temperature H chondrite experienced relatively little cosmic ray shielding from a plot of $^{3}He/^{21}Ne$ verses $^{22}Ne/^{21}Ne$, and suffered relatively rapid post-metamorphic cooling from central nickel content data for taenite grains.[9] They suggested that the break-up of the H chondrite parent body, 8Ma ago, produced two types of material with different size distributions and thermal histories, and the smaller objects reached Earth more rapidly through more rapid orbital evolution.

Conclusion We have summarised recent research on the TL properties of meteorites with particular emphasis on its value in preliminary screening of Antarctic meteorites. The technique provides information on petrologic type (thereby aqueous alteration and thermal metamorphism), break-up of parent bodies, terrestrial age, and paring, and it identifies those with unusual thermal and radiation histories. A program of systematic measurement of U.S. Antarctic meteorites has been in operation for six years. We are now initiating a program of measuring the TL properties of Japanese Antarctic meteorites.

References:

1) Ninagawa et al. (1983): Mem. Natl. Inst. Polar Res., Spec. Issue, **41**, 328-337.
2) Miono et al. (1990): Proc. NIPR Symp. Antarct. Meteorites, **3**, 240-243.
3) Hasan et al. (1987): Proc. Lunar Planet. Sci. Conf., **92**, E703-E709.
4) Ninagawa et al. (1990): Proc. NIPR Symp. Antarct. Meteorites, **3**, 244-253.
5) Benoit and Sears (1991): Icarus, **94**, 311-325.
6) Benoit et al. (1992): J. Geophys. Res., **97**, 4629-4648.
7) HAQ et al. (1988): Geochim. Cosmochim. Acta, **52**, 1679-1689.
8) Sears et al. (1991): Geochim. Cosmochim. Acta, **55**, 1193-1197.
9) Benoit and Sears (1992): Science, **255**, 1685-1687.

*; Data are largely undetermined for the Lewis Cliff meteorites.

DEPTH PROFILES OF COSMOGENIC ISOTOPES : IMPLICATIONS TO TERRESTRIAL AGES OF ANTARCTIC METEORITES. N. Bhandari, Earth Science and Solar System Division, Physical Research Laboratory, Navrangpura, Ahmedabad, 380009, India.

The dependence of production rates of cosmogenic radio- and stable isotopes on the size of the meteorites is now reasonably well understood as a result of measurements of depth profiles in many meteorites with simple exposure history and computations of nuclear cascade using High Energy Transport Code [1,2].Track density measurements in surface samples allows determination of pre-atmospheric size and shape of the meteorites and criteria have been developed to identify meteorites with simple exposure history which include (i) Correlation between track density and spallation neon isotope ratio $(^{22}Ne/^{21}Ne)_s$ and (ii) concordance of ^{21}Ne-^{26}Al and ^{21}Ne-^{53}Mn exposure ages [3].

Production Systematics : Measurements in radial cores taken from such meteorites having pre-atmospheric radius (under the assumption of spherical geometry) between 8 and 100 cm have yielded depth profiles expected in meteoroids in space [1]. These are found to be in good agreement with the computed profiles based on Monte Carlo calculations using the HERMES code [2]. The salient features of the production systematics are:

(1) Production rates are found not to change much with depth in small meteorites (8cm <R<15 cm). There is slight increase in production rates with size of the meteoroid in this size range.

(2) For larger bodies, (15cm <R <65 cm), the profiles show significant depth dependence, typically the production rate increases by about 30% from surface to the centre. The increase depends on the energetics of production of different isotopes from various target elements.

(3) For R>70 cm, the depth profiles are relatively flat with subdued transition maxima followed by a slow decrease towards the centre of the meteoroid.

The production profiles of ^{10}Be,^{22}Na,^{26}Al, and ^{53}Mn are given in [1].

Implications to Terrestrial Ages : These results show that there is considerable variation in isotope production depending on the size of the meteoroid and depth of the specimen. The uncertainties involved in calculated terrestrial ages computed from the extent of decay of radioisotopes on the earth since the fall of the meteorite can be minimized if the production rates corrected for size are used in each case. Thus a combination of track density measurements, which gives shielding depths and size of a meteoroid [6] and measurement of selected stable and radionuclide pairs [7,8] can lead to a more precise evaluation of terrestrial ages.This approach also enables identification of meteorites which have anomalous exposure to cosmic rays either due to complex exposure or due to variation in cosmic ray flux in the orbital space of the meteoroid or with time .

References : 1.Bhandari, N., Mathew, K.J., Rao, M.N., Herpers,U., Bremer, K., Vogt, S., Wölfli, W., Hofmann, H. J., Michel, R., Bodemann, R. and Lang, H. -J., (1992) Geochim. Cosmochim. Acta (submitted). 2. Michel, R., Dragovitsch P., Cloth P., Dagge, G. and Filges, D., (1991) Meteoritics, 26, 221-242. 3. Bhandari, N. (1986) Proc. Ind. Acad. Sci. 95, 183-191. 4.

Fireman, E.L. (1983) Mem. Natnl. Inst. Polar Res. Spec. Issue 30, 246-250. 5. Nishiizumi, K., Elmore, D. and Kubik, P.W. (1989) Earth planet. Sci. Lett. 93, 299-313. 6. Bhandari, N., Lal, D., Rajan, R.S., Arnold, J.R., Marti, K. and Moore, C.B. (1980) Nucl. Tracks 213-262. 7. Bhandari, N., Goswami, J.N. and Shukla, P.N. (1984) Papers presented at the 9th symposium on Antarctic Meteorites, NIPR, 44-1-44-3. 8. Bhandari, N., Proc. Workshop on Differences between Antarctic and Non Antarctic Meteorites, LPI Tech. Rep 90-01, 19-23.

CONCENTRATION OF ELECTRONIC PARAMAGNETIC CENTERS (EPC) IN CARBONACEOUS CHONDRITES. Eu. Osadchii (Inst. Experiment. Mineral, Russian Acad. Sc., Chernogolovka); Al. Kulikov (Inst. Chem. Phys., Russian Acad. Sc., Chernogolovka).

Fourteen carbonaceous chondrites of different groups were investigated using the method of electronic paramagnetic resonance (EPR) to determine EPC concentrations related to carbonaceous substance. Meteorite samplings with 10-25 mg in weight were chosen from fine-dispersive (0.2-1.5 mm) fractions of samples and thus were averaged. Measurements were performed at radiospectrometer EPR-3 "SIBIRIA" at liquid nitrogen temperature. By the value of g-factor (g=2.00) and width of the EPR line (ΔH/G) between first derivation peaks these signals can be related to carbonaceous substance.

The similar EPR-signals are observed in fossil coals. The absolute number (N) of EPC in the sample was determined by the comparison of the double integral of the EPR sample spectrum and solution of nitroxide radical. Vacuumed and nonvacuumed samples gave the similar results.

The results of the measurements are given in the Table 1.

The similar EPC concentrations in the limits of 4.10^{16}-9.10^{16} per gram are discovered in all the samples of meteorites of the CM group at the identical width of the EPR lines ΔH=20 Gauss.

In CV groups meteorites EPC are discovered only in Allende and Groznaia and their concentration is three orders higher than that in CM group. For these meteorites, broader of EPR lines (ΔH/G=136-276) are also typical. It is necessary to point out that in the meteorites Efremovka and Coolidge (both of them are finds), EPC are not detected.

Table 1. Concentration of EPC in different groups of carbonaceous chondrites.

Meteorite	No of sample	Group	Recovery	ΔH(G)	Number of EPC per gram (N)
Alais	15096	CI	1806	-	-
Orguel	2476	CI	1864	-	-
Kaidun	15415-30	CI	1980	-	-
Mighei	1856	CM	1889	20	9.10^{16}
Staroe Boriskino	198	CM	1930	20	5.10^{16}
Cold Bokkeveld	15098	CM	1838	20	4.10^{16}
Murray	2308	CM	1950	20	4.10^{16}
Nagoya	15092	CM	1879	20	7.10^{16}
Murchison	15044	CM	1969	20	5.10^{16}
Kainsaz	15265	CO	1937	-	-
Allende	15035	CV	1969	276	7.10^{19}
Groznaia	73	CV	1861	136	4.10^{19}
Efremovka	2349	CV	1962*	-	-
Coolidge	2566	CV	1937*	-	-

* Find

In the samples of meteorites of CI and CO groups EPC are not discovered or their concentration is lower than $n.10^{15}$.

EPC nature in carbonaceous chondrites is not quite clear at present and requires extra investigations. However, the obtained data can be used as a classification feature especially in difficult cases. A relative simplicity of the analysis and a small volume of sample without a special preparation contribute to all this.

CONCENTRATION OF ELECTRONIC PARAMAGNETIC CENTERS (EPC) IN CARBONACEOUS CHONDRITES. Eu. Osadchii (Inst. Experiment. Mineral, Russian Acad. Sc., Chernogolovka); Al. Kulikov (Inst. Chem. Phys., Russian Acad. Sc., Chernogolovka).

Fourteen carbonaceous chondrites of different groups were investigated using the method of electronic paramagnetic resonance (EPR) to determine EPC concentrations related to carbonaceous substance. Meteorite samplings with 10-25 mg in weight were chosen from fine-dispersive (0.2-1.5 mm) fractions of samples and thus were averaged. Measurements were performed at radiospectrometer EPR-3 "SIBIRIA" at liquid nitrogen temperature. By the value of g-factor (g=2.00) and width of the EPR line (ΔH/G) between first derivation peaks these signals can be related to carbonaceous substance.

The similar EPR-signals are observed in fossil coals. The absolute number (N) of EPC in the sample was determined by the comparison of the double integral of the EPR sample spectrum and solution of nitroxide radical. Vacuumed and nonvacuumed samples gave the similar results.

The results of the measurements are given in the Table 1.

The similar EPC concentrations in the limits of 4.10^{16}-9.10^{16} per gram are discovered in all the samples of meteorites of the CM group at the identical width of the EPR lines ΔH=20 Gauss.

In CV groups meteorites EPC are discovered only in Allende and Groznaia and their concentration is three orders higher than that in CM group. For these meteorites, broader of EPR lines (ΔH/G=136-276) are also typical. It is necessary to point out that in the meteorites Efremovka and Coolidge (both of them are finds), EPC are not detected.

Table 1. Concentration of EPC in different groups of carbonaceous chondrites.

Meteorite	No of sample	Group	Recovery	ΔH(G)	Number of EPC per gram (N)
Alais	15096	CI	1806	-	-
Orguel	2476	CI	1864	-	-
Kaidun	15415-30	CI	1980	-	-
Mighei	1856	CM	1889	20	9.10^{16}
Staroe Boriskino	198	CM	1930	20	5.10^{16}
Cold Bokkeveld	15098	CM	1838	20	4.10^{16}
Murray	2308	CM	1950	20	4.10^{16}
Nagoya	15092	CM	1879	20	7.10^{16}
Murchison	15044	CM	1969	20	5.10^{16}
Kainsaz	15265	CO	1937	-	-
Allende	15035	CV	1969	276	7.10^{19}
Groznaia	73	CV	1861	136	4.10^{19}
Efremovka	2349	CV	1962*	-	-
Coolidge	2566	CV	1937*	-	-

* Find

In the samples of meteorites of CI and CO groups EPC are not discovered or their concentration is lower than $n.10^{15}$.

EPC nature in carbonaceous chondrites is not quite clear at present and requires extra investigations. However, the obtained data can be used as a classification feature especially in difficult cases. A relative simplicity of the analysis and a small volume of sample without a special preparation contribute to all this.

PHYSICAL PROPERTIES OF 368 METEORITES - IMPLICATIONS OF EARLY SOLAR SYSTEM MAGNETIC FIELDS.

L.J. Pesonen, M. Terho and I.T. Kukkonen. Geophysics Department, Geological Survey of Finland, 02150 Espoo, FINLAND.

Introduction. Meteorites yield direct information about the geology, composition and physical properties of their parent bodies (asteroids, Moon, Mars). In particular the magnetic properties of meteorites provide valuable information about the magnetic field intensity during the formation and subsequent metamorphism of the meteorite parent bodies [1]. A more thorough understanding of the early planetary and interstellar magnetic fields would greatly benefit the construction of the evolutionary models of the solar system [2]. So far physical studies of meteorites have not received very much attention among meteorite investigators.

During the last ten years we have measured petrophysical properties (density, magnetic susceptibility and natural remanent magnetization, NRM) of 368 meteorites from Finnish collections [3, 4]. The petrophysical measurements have been substantiated with magnetic hysteresis determinations to study the magnetic grain size variations and simultaneously to classify the meteorites by using the magnetic hysteresis classification scheme of Sugiura [5]. In addition, Thellier paleointensity measurements on Finnish meteorites have been carried out.

There are three main branches of applications of the petrophysical database of meteorites: (i) classification of meteorites by their physical properties (a good correlation exists between standard chemical-petrological classification and petrophysical properties, see [3,4,6] for details); (ii) modelling of magnetic and gravity data to be measured during satellite fly-passes of small bodies (asteroids, comets, planetary satellites) and landings (Moon, Mars, planetary satellites); (iii) studies of the ancient magnetic fields (interplanetary or parental) during the accretion or during subsequent geological evolution of the meteorite parent bodies and planets and their moons [1,2].

In this paper we discuss the aspects of meteorite classification by petrophysical methods and the paleointensity results obtained with Thellier technique on sixteen chondrite and achondrite samples and with the Sonett technique [7], which uses the NRM-susceptibility plot for these meteorites to estimate the background magnetic field.

Results. The physical properties of 368 meteorite samples from the Finnish meteorite collections reveal definite trends when the data are shown on petrophysical relation diagrams, such as susceptibility vs. density (Fig.1a) or Koenigsberger Q-ratio vs. density. (Fig. 1b). The main reason for the increase in susceptibility, NRM and density is the systematic increase in the FeNi-content from achondrites→chondrites→stony irons→irons. The main chemical classes can thus be identified on these plots. In fact, this is often the case with the petrological groups as well (see e.g.,[4,6]) but the discrimination power is not sufficient to uniquely use the petrophysical technique to determine the group and the metamorphic type of a meteorite.

In spite of this we were able to estimate correctly the main chemical class, and in the majority of the cases (>60%), also the petrological group for 24 Czechoslowak, 3 Swedish and one Australian meteorites in a test study [6].

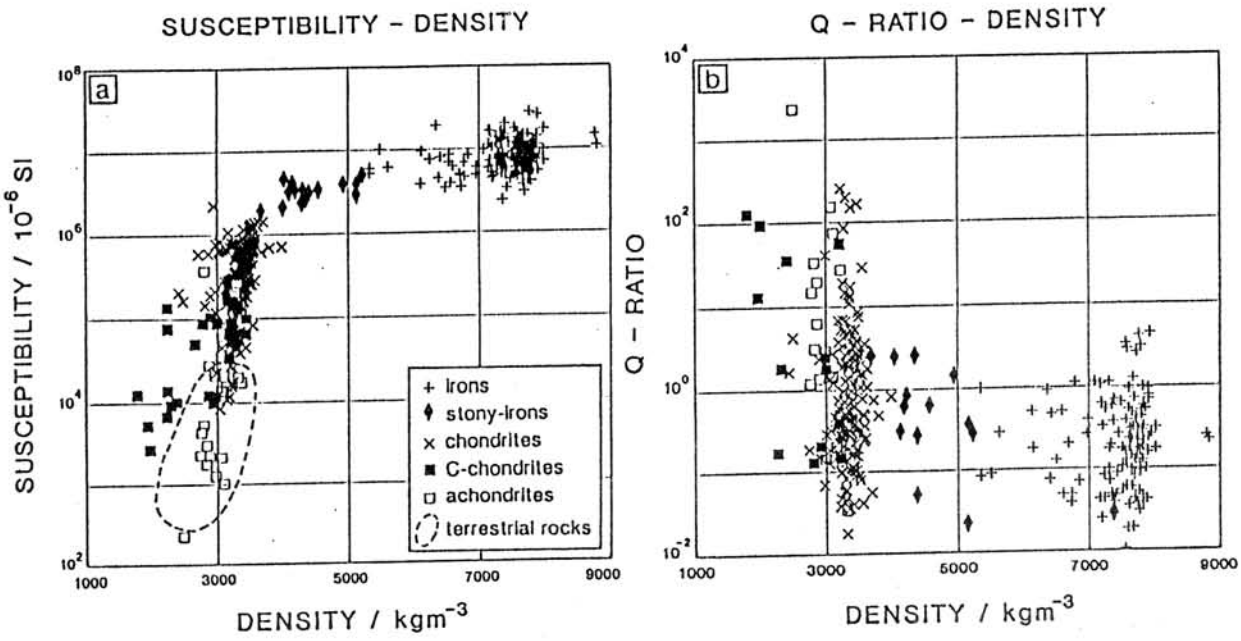

Fig. 1. Examples of the petrophysical relation diagrams used in classifying meteorites by their physical properties. (a) magnetic susceptibility vs. density. (b) Koenigsberger Q-ratio (~NRM/susceptibility) vs. density. Data on 368 meteorite samples from the Finnish meteorite collections. All data are on bulk samples. The susceptibility and NRM-data are not corrected for shape effects. The meteorite petrophysical database is listed in [4].

In addition to complex variations in metallic constituents (e.g., the variation in the Ni-content, presence of tetrataenite and magnetite, etc), the failures can be attributed to non-uniqueness problems (cluster plots overlaps), porosity, self-demagnetization, grain size and grain shape effects, electrical conductivity and frequency [see 4,6]

An example of the magnetic hysteresis data is shown in Fig. 2, where the Jr/Js (saturation remanence/saturation magnetization) is plotted against Hc (coercive force) for 50 achondrites and chondrites from Finnish meteorite collections. The roughly linear (log. scales) increase in Jr/Js and Hc in a serie from E→H→L→LL→C reflects the increase in the magnetic hardness of chondrites, respectively [5]. Note that the magnetically hardest samples (highest values for Jr/Js and for Hc; Fig.2) are found in the C- and LL-chondrites (see also [5]); these groups possesses the hardest NRM and IRM (isothermal remanent magnetization) characteristics as found by comparing the alternating field demagnetization curves of NRM and IRM [4].

Paleointensity was measured of 16 meteorite samples with the Thellier double heating technique [4]. The results show complex behaviours in most of the samples with no reliable paleointensity values, as often found for meteorites [5, 8]. The six magnetically hardest samples (representing C-,L-,LL-and H-chondrites) reveal very steep paleointensity plots (Arai-plots) indicating high paleofields ranging from 51 to728μT (0.51-7.28 oe) during the formation or during the last metamorphism of these meteorites or their parent bodies. Similar high paleofield values have been previously found by other groups for these meteorite types [1,2,5,7]. However, these values are suspect since they are not repeatable in laboratory experiments [8]. We are further investigating the causes for the high paleointensity data so often obtained of meteorites.

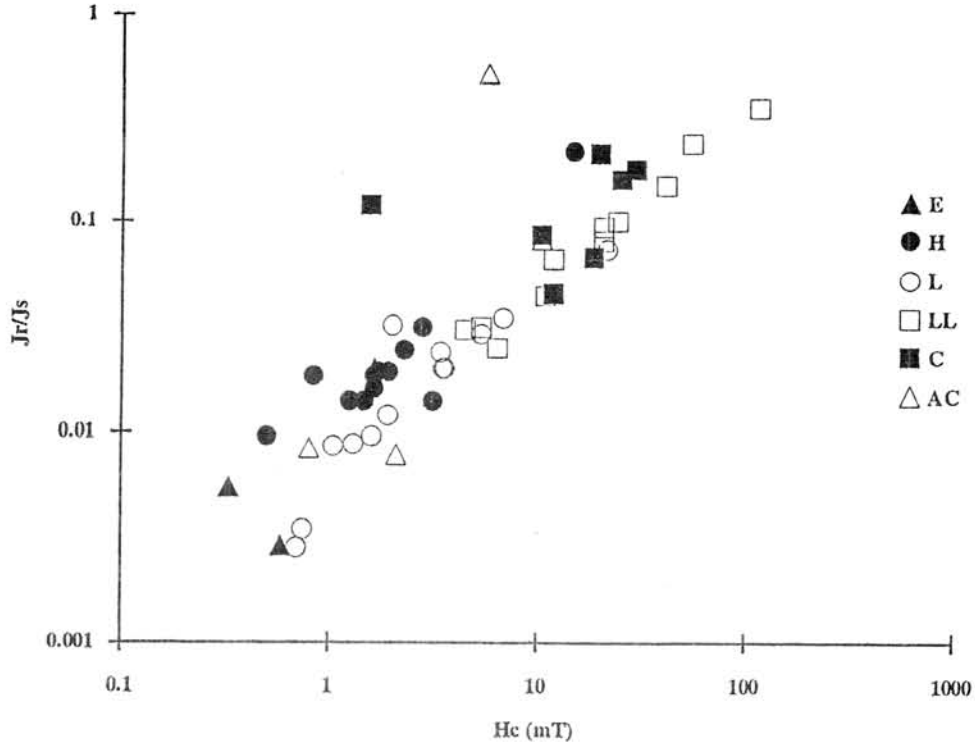

Fig.2. Magnetic hysteresis classification of 50 achondrites and chondrites from the Finnish collections. The Jr/Js is plotted against Hc, where Jr, Js are the saturation remanence and saturation magnetization, respectively, and Hc is the coercive force.

We also applied the Sonett-technique [7] to see whether our petrophysical database yields any evidence for the "common" background magnetic field which has probably affected all the meteorites. The NRM vs. susceptibilty data show a weak systematic overall trend from achondrites to chondrites when plotted on a log-log diagram giving some indications of the background field. The slope of this plot is ~0.36±0.08 which is slightly higher than that (0.18) found by Sonett (1978) of a large data set of magnetic properties of Russian meteorites. The difference in slopes is probably caused by calibration differences [4]. The roughly linear trend in NRM-susceptibility data is, however, not visible in the Q-values of chondrites (slope of NRM vs. susceptibility α Q, Fig.1b): a common background field would produce a constant Q-value, which is not the case for individual chondrites which show a large variation in Q-values. Moreover, the value for the background magnetic field, if real at all, is very difficult to estimate since the NRM and susceptibilty data are affected by many factors [4,6,7] and the method would require a knowledge of the average grain demagnetization factor for each sample, which can vary from 0 to 1(0 to 4π in cgs-units). An extreme lower limit for this field (with N = 1 SI) is ~2.8μT (0.028 oe) which is close to that (1-2 μT) found by Brecher and Ranganayki (1975) of ordinary chondrites for primeval interplanetary magnetic field.

References. 1. Cisowski S.M. (1987) In Geomagnetism 2 (ed. J.A. Jacobs), 525-560. 2. Levy E.H. and Sonett C.P. (1978) In Protostars and Planets (ed. T. Gehrels), 516-532. 3. Kukkonen I.T. and Pesonen L.J. (1983) Bull. Geol. Soc. Finl. 55, 157-177. 4. Terho M., Pesonen L.J. and Kukkonen I.T.(1992a) Rep.Q 29.1/91/1, Geoph.Dept. Geol.Surv.Finl., 40pp. 5. Sugiura N. (1977) J. Geomag. Geoelectr. 29, 519-539. 6. Terho M, Pesonen L.J. and Kukkonen I.T. (1992b) Stud. Geoph. Geod. 36 (in press). 7. Sonett C.P. (1978) Geop. Res. Letts. 5 (2), 151-154. 8. Westphal M. (1986) Phys. Earth. Plan. Int. 43, 300-306. 9. Brecher and Ranganayki (1975) Earth Plan. Sci. Letts. 25, 57-67.

Magnetic Properties of Willard L6 Chondrite and its NRM Record

A. YAMANAKA[1], M. FUNAKI[2] and H. NAGAI[1]

1: Shinshu University, Faculty of Science, 1-1 Asahi 3, Matsumoto 390

2: National Institute of Polar Research, 9-10 Kaga 1, Itabashi, Tokyo 173

Conventional wisdom suggests Willard (L6 chondrite) might have been heated to around 800°C or greater in its parent body during final metamorphism. If a sufficiently strong magnetic field was present in the body, the chondrite has the possibility to record the magnetic field, as a terrestrial igneous rocks might also. We have studied magnetic properties in order to elucidate whether the Willard chondrite possesses a reliable natural remanent magnetization (NRM).

The NRM stability against AF demagnetization in subsamples of the Willard chondrite was very different. Magnetization directions in some subsamples were stable at field in excess of 50 mT while some were very unstable. The NRM exhibited a gradual demagnetization with some zig-zag variation when thermally demagnetized. Its intensity decayed to 5% compared with original one at a temperature of 530°C. The NRM directions of the subsamples ranging from 0.1 to 2 g in weight, are widely scattered though their NRM stabilities can be high.

The magnetic hysteresis properties were measured, using a vibrating sample magnetometer, from room temperature to 770°C. The saturation magnetization curve suggests that the chondrite consists of kamacite and taenite; phase transition of kamacite at 730°C ($\alpha \rightarrow \gamma$) in the heating curve and 645°C ($\gamma \rightarrow \alpha$) in the cooling curve and the Curie point of taenite at 550°C in the heating curve. The coercivity (11 mT) decayed gradually and disappeared completely at 550°C in the heating curve. It appeared again from 550°C in the cooling curve and the value increased to 18 mT after heat treatment (Fig.1).

From these experimental results, we suggest taenite is the NRM carrier of this chondrite. Large amount of kamacite is presence, but its contribution to the NRM is quite low. Tetrataenite is considered to be absent in the coercivity record; if tetrataenite were present, the coercivity should be decreased after heat treatment at temperatures higher than 550°C. The high coercivity exhibited by some of the subsamples would suggest they are capable of high, long time, stability of acquired NRM's. We discuss some implications of the magnetic record.

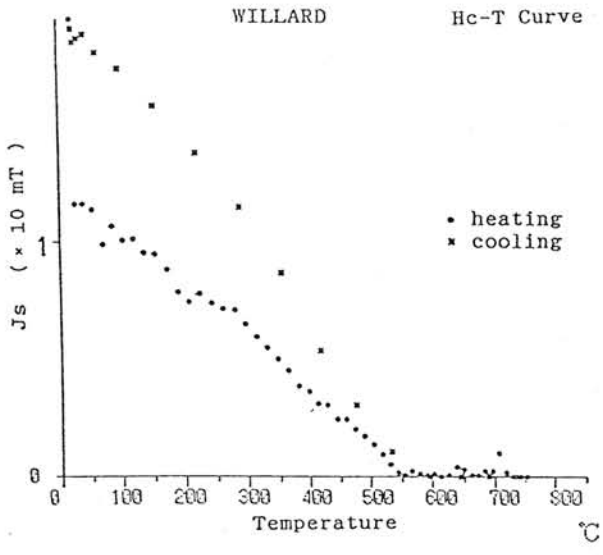

Fig. 1 Hc-T Curve of the Willard Chondrite

Temperature dependent changes in magnetic coercivity in some ordinary chondrites

Minoru Funaki
National Institute of Polar Research, 9–10 Kaga 1, Itabashi Tokyo 173

1. Introduction

Magnetic minerals in ordinary chondrites consist of iron–nickel (FeNi) alloys of various compositions. The principal component are kamacite and taenite. We have studied the temperature dependence of magnetic properties in order to discover the significant FeNi composition responsible for the natural remanet magnetization (NRM).

A vibrating sample magnetometer was assembled with a computer control for this study. Ordinary chondrites; St. Séverin (LL6), Olivenza (LL6), Y–75097 (L6), Y–75102 (L6), ALH–769 (L6) and other several samples, were obtained for this study.

The magnetic hysteresis loops were measured from room temperature to 780°C with temperature interval of about 15°C. These measurements were performed with a heating rate of 50°C/h, 10^{-4}Pa in pressure and the applied field intensity between +1.3 and −1.3 Tesla. The magnetic properties; saturation magnetization (J_S), saturation remanent magnetization (J_R), coercivity (H_C), remanent coercivity (H_{RC}) and initial susceptibility (Xi) were determined from the loops.

2. experimental results

Kamacite was clearly identified in the J_S–T curves in all the samples. Tetrataenite was clearly recognized in many samples (St. Séverin, Olivenza, ALH–769 etc.), but it could not be identified in some samples (Y–75097, Willard etc.). The indicator of NRM stability, J_R, H_C and H_{RC} values decreased gradually from room temperature to 550°C in the heating curve for all samples. Figure 1 shows the typical example of the behavior for the Y–75097 chondrite. The Xi–T curves were similar to the J_S–T curves, but a Curie point or a phase transition point around 500°C is more clearly identified than in the J_S–T curves.

3. Discussion

Previous results of thermal demagnetization of the chondrites have been clarified in that the significant fraction of the NRMs are demagnetized before 600°C, although their principal magnetic minerals were kamacite. The magnetic minerals with near equiatomic FeNi ordered tetrataenite (phase transition temperature 550°C) and/or taenite with Curie point around 550°C may be included in every chondrite. These minerals carry the NRMs for the chondrite. They are not observed clearly in every chondrite due to amount of them as observed in the J_S–T curve. However, they are clearly identified in the Xi–T curve. We propose that the most significant technique to identify the NRM carrier is the measurement of the temperature dependence of Xi.

Fig.1 Temperature dependent change of Y-75097 chondrite

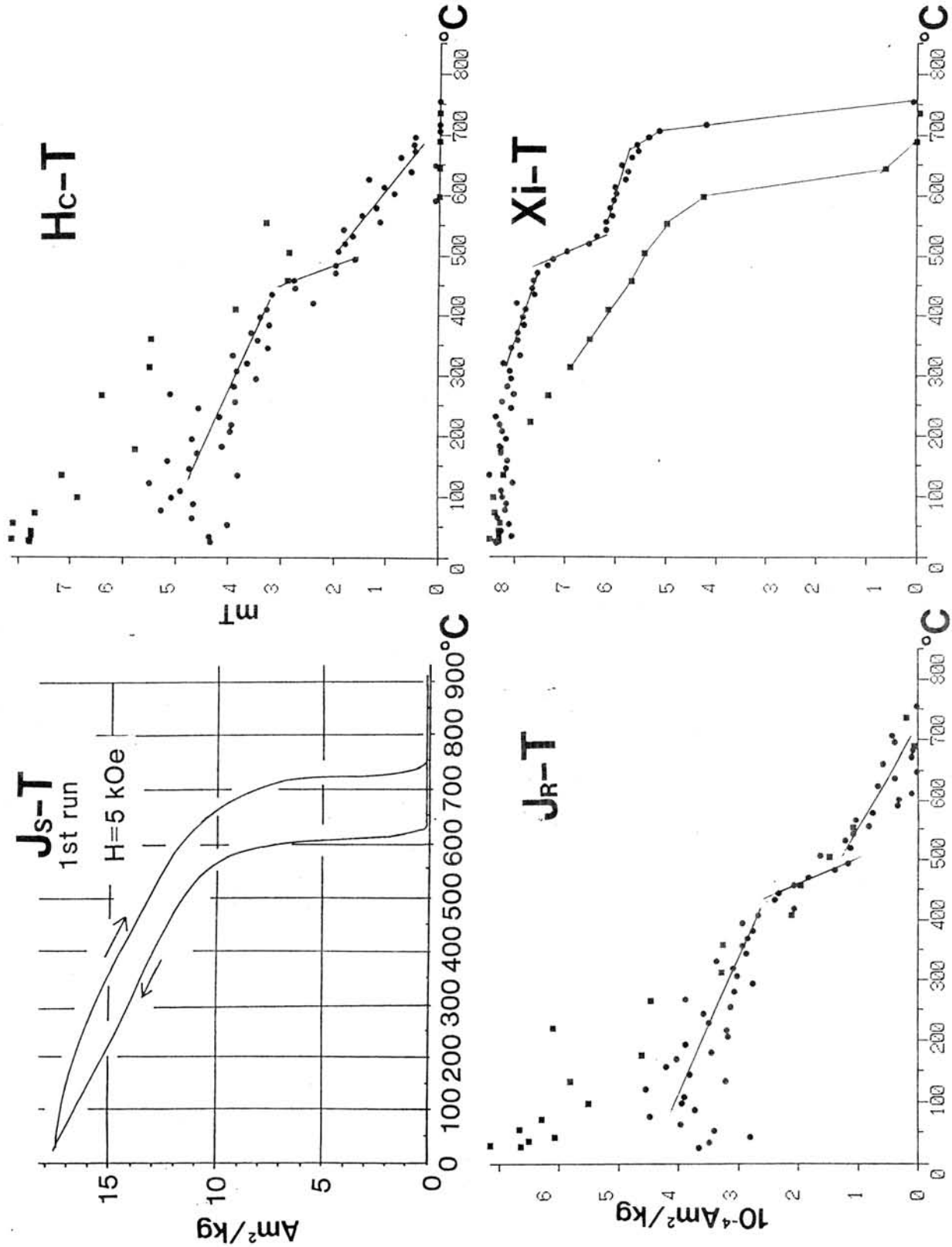

RADIOCARBON MEASUREMENTS ON METEORITES I: CO AND CO_2 SEPARATIONS FROM TEMPERATURE FRACTIONS.

Richard G. Cresswell[1], Yasunori Miura[2], Roelf P. Beukens[1] & John C. Rucklidge[1]

[1]IsoTrace Laboratory, University of Toronto, Toronto, Ontario, M5S 1A7, Canada
[2]Department of Mineralogical Sciences and Geology, Yamaguchi University, Yoshida, Yamaguchi 753

Introduction. In an attempt to resolve the disrepancies observed in saturation levels of radiocarbon in recently fallen meteorites, and thus better constrain the residence, or terrestrial ages of Antarctic samples, a new extraction, collection and processing line has been built at the IsoTrace Laboratory. Continuing the work previously reported at this conference (Beukens, et al., 1988), a further suite of Antarctic meteorites were analysed, following a procedure developed for the falls. As well as terrestrial ages, information on the weathering history of the samples may also be obtained.

Procedure. Samples of 300-500mg. are heated in a helium atmosphere ($\approx$500 torr) at temperatures determined from TGA-MS analysis of the Bruderheim meteorite. The helium is used as a carrier gas to cycle the gases first through a variable temperature trap, to trap CO_2, then over heated CuO to oxidize CO to CO_2, which is then frozen in liquid nitrogen-cooled traps. The separate fractions are doped with inert CO_2 carrier, converted to 'graphitic' carbon, and analyzed by accelerator mass spectrometry at IsoTrace.

Results and Discussion. Lower temperature ($<500°C$) fractions appear to be purely modern contaminants, provided extraction time is kept short (<2 hours). Carbonates will break down, evolving $>90\%$ of their carbon if the sample is then held at 880°C for 1 hour. By extracting for 1 hour at 880°C, negligible spallation carbon was released from analyzed falls, while a measure of any secondary carbonate, weathering components can be obtained. Spallation carbon is oxidized within silicates and diffuses to the surface, where it is released predominantly ($>70\%$) as CO. Previously, extractions run for 4 hours at 1000°C resulted in up to a 30% contribution from spallation carbon to this low-temperature fraction (Beukens, et al., 1988). Any graphite also reacts with the silicates as they break down, and is also released as CO.

While the total carbon from CO and CO_2 give a true measure of a sample's activity, in practice, the CO_2 released from the melt fraction gives an activity close to background, so only the CO measurement is used for terrestrial age estimates. Terrestrial ages are measured by comparing the ^{14}C content of this fration with that from the Bruderheim, a recent L6 fall. CO_2 is the dominant species ($>80\%$) released from carbonates at 880°C; we use this fraction for weathering activity determinations on the Antarctic meteorites. In this case the $^{14}C/^{12}C$ of this fraction is compared to a modern standard. This measurement gives a total activity averaged over all weathering episodes of the meteorite. Thus, an activity equivalent to the calculated terrestrial age of the sample suggests a long residence beneath the ice surface, with only a short recent exposure, while a high activity indicates a longer recent development of weathering minerals, or exchange with modern carbon. An idea of the

proportion of time spent at the original fall site relative to the time exposed at the stranding site may thus be obtained.

Analysis of a suite of Antarctic meteorites (5 L6 chondrites, an L3 chondrite and 2 H4 chondrites) using this new procedure give results that are consistent with measurements of other cosmogenic nuclides (Nishiizumi, 1987) and TL studies (Miono, et al., 1990), and may be compared to the earlier results of Beukens, et al. (1988) and those of other methods (e.g. Jull, et al., 1989).

Acknowledgements. We thank NIPR for the meteorite samples, and the support of the IsoTrace Laboratory and staff. This work is supported in part by National Science and Engineering Research Council Grant to A.E. Litherland, whose support is gratefully acknowledged.

References:

Beukens, R.P., Rucklidge, J.C. & Miura, Y., 1988. Proc. NIPR Symp. Antarct. Meteorites, 1, 224-230.

Jull, A.J.T., Donahue, D.L. & Linick, T.W., 1989. Geochim. Cosmochim. Acta, 53, 2095-2100.

Miono, S., Ono, H., Kujirai, H., Yoshida, M. & Nakanashi, A., 1990. Proc. NIPR Symp. Antarct. Meteorites, 3, 240-243.

Nishiizumi, K., 1987. Nucl. Tracks. Radiat. Meas., 13, 209-273.

COMETS, ASTEROIDS AND METEORITES: RELATIONSHIPS WITNESSED BY FIREBALLS.

Petr **Jakeš**(1,2) and Vladimír **Padevět**(3). (1)Lunar and Planetary Institute, 3600 Bay Area Boulevard, Houston TX 77058, (2) Department of Geosciences University of Houston, Houston TX, 77004, (3) Astronomical Institute Czech Academy of Sciences, 251 65 Ondrejov, Czechoslovakia

The orbital pre-fall characteristics of meteorites and petrologic arguments suggest that meteorites (with the exception of lunar and martian meteorites) come from a small number (20) of bodies in the asteroid belt, predominantly from AAA type (Athene, Apollo, Amor Earth-crossing) asteroids(1). The compositionally zoned asteroid belt(2) is source of both differentiated and primitive meteorites (chondrites) and hence the understanding of the asteroid belt is essential for an adequate interpretation of meteorites and vice versa. Opik(3) suggested that inactive comets may masquerade as Earth-crossing asteroids and that the meteorites may come from the comets. The idea has been almost abandoned(1), though revived by Wetherill's Monte Carlo simulations(4), suggesting that extinct comets may provide a significant fraction of Earth-crossing populations.

The composition of interplanetary dust particles (IDPs) (5), the composition of dust in Halley's comet(6) (grains with mass around 10^-12 g), composition of primitive meteorites (7), and cosmochemical arguments suggest they have similar chemical composition. The existence of "superchondritic" (i.e., compared to carbonaceous chondrite volatile-rich) material in the solar system has been suggested(8). Such material is often designated as "cometary" and with the exception of highly volatile elements (H,C,N,O) corresponds to the cosmic abundances(7). The existence and soft delivery of cometary material (dark material containing the macromolecular carbon(9)) to the Earth are of prime interest in the formation of the hydrosphere, biosphere, and generally the outermost layer of the Earth(10).

A few fascinating observations relating to the dark materials within the solar system were recently made. The observations revived some older ideas, for example:

a. Hartmann et al. and other authors(11) have advocated a relationship between dark asteroids of type C and cometary nuclei, and it has been observed(12) that comets could turn into dark asteroids through devolatilization and perturbation by large planets.

b. Dark asteroids (types C,D if indigenous to asteroid belt) that are presently on Earth-crossing orbits(13) may have been formed in the outer (i.e., colder) part of an asteroid belt, i.e., the region where carbon-rich material can supposedly condense (9).

c. Some of the dark bodies of the solar system that were earlier considered to be asteroids show cometary behavior. 2060 Chiron, which displays a sublimation of highly volatile gasses(16) that produces a coma(15), is indeed a comet with the largest known nucleus (180km)(16).

d. The place of origin of comets has been reconsidered since the last century several times(17). Using model calculations based on the observation that numerous short-period comets are in the plane of ecliptic, Duncan et al.(18) have shown the possibility of the existence of two sources for comets: Kuiper's belt (at 40 - 100 AU) and Oort's cloud (> 1000 AU). The double-track theory attributes the short-period comets to Kuiper's belt and the long-period comets to the Oort's cloud(18).

Understanding the relations between the composition of dark bodies (e.g., parent bodies of carbonaceous chondrites (CC), asteroids of F,P,D,C, and T types), the IDPs, and comets may change our thinking about the solar system and especially about the inventory of volatile and nonvolatile elements and thermal and /or chemical gradients. If the double-track theory for the origin of comets holds(19), the asteroid belt contains "captured" materials of Kuiper's belt, i.e., material of not so distant part of solar system as Oort's cloud, in the form of dark asteroids (e.g., type C), whereas other dark type asteroids (e.g., types F,P,D, and T) could be indigenous to the asteroid belt. The observation that F,D,P, and T asteroids have very low volatile contents(20) contradicts the generally accepted view that the outer part of the asteroid belt is "primitive", i.e., volatile rich. The interpretation of asteroid belt relationships asks for steep thermal and hence compositional gradients within the asteroid belt(27): silicate melt temperatures in the vicinity of Mars and extremely cold conditions allowing the carbon compounds to condense in the outer asteroid belt. The contention is difficult to accommodate for a gradient picture of the solar nebula disk.

In this contribution we add some observations on the relationship of meteorites, bolides, (fireballs) and meteor showers based on bolide network photography.

Bolide multistation photographic tracking allows the determination of the orbital pre-encounter parameters of solid bodies (0.01 - 100,000 kg in mass) with the Earth, and allows us to classify them according to their

ablation coefficient( ), penetration depth into the atmosphere(PE), theoretical densities( ), and terminal velocities(V). Four groups are recognized (Table 1). Three of the type I bolides were recovered as ordinary chondrites (Pribram, Lost City, and Innisfree).

Ceplecha(21) has shown that 38% of bolides come from cometary orbits (11% from highly eccentric orbits typical of new comets), but most of the bolides (62%) originate at asteroidal orbits. Seven of the 14 known meteoric showers could be attributed to known comets: N,S Taurids to 1970 P/Encke, Lyrids to 1861 I Thatcher-Beaker, Perseids to 1862 III Swift-Tuttle-Simons, Orionids to 1835 III P/Halley, Draconids to 1946 V P/Giacobini-Zinner, Leonids to 1966 I Tempel-Tuttle, and Leo Minorids to 1739 Zanotti. Geminids were related to asteroid 3200 Phaeton, considered to be an "extinct comet." Following the Whipple's(15) suggestion Spurný (22), using ablation coefficient and penetration depth criteria, found that Geminids (frequently) and Taurids (rarely) contain bolides of types I and II. This may indicate that meteoric showers from "comets" on AAA orbits contain some portion of "rocky" material comparable to chondrites.

We have studied the records of 292 bolides (Prairie and European networks) with measured terminal velocities and attempt to use the terminal velocity, calculated density, estimated terminal mass, and mechanical strength to correlate with the meteorite fall statistics(23). Two extreme hypotheses (Table 1) are examined: (A) bolides of types IIIa and IIIb do not have equivalents among the meteorites and (B) all four bolide types have meteoritic equivalents, and only IDPs (with low masses and densities) do not produce bolides.

If the entry parameters of meteoroids are similar, bodies with lower density should reach terminal velocity at higher altitudes than those with higher density. If it is assumed that fragmentation is the same for dense (I and II) and less dense (IIIa and IIIb) bodies, the calculated terminal altitudes show that among the bolides exist materials with lower densities than those of recovered meteorites and that model A of the correlation between meteorite falls and bolide observations is likely. If, however, the less dense bodies were more easily fragmented than denser bodies, the correlation is better for hypothesis B.

Table 1. Fireball observations

Fireball group		I	II	IIIa	IIIb
%of fireball	<1%	29%	33%	29%	9%
PE **		-4.6	(-5.25) to(-4.60)	(-5.70) to(-5.25)	-5.70
ablation coeff.[s^2/km^2]		0.007-0.028	0.028-0.056	0.08-0.13	0.17-0.26
type of orbit		asteroidal and cometary		cometary	

A hypothesis						
correlated meteorites	irons?	chondrites			none	none
density*	8.0 - 4.3	3.8-2.6		2.3-2.2	0.75	0.27
S_c[MPa]		100		0.10		0.001
%of falls	9%	79%	12%	0.7%	0%	0.5%

B hypothesis					
correlated meteorites	irons	ordinary chondrites		CV	CI
density*	8.0 - 4.3	3.8-3.6	3.6-3.5	2.9-2.6	2.3-2.2
S_c[MPa]		100	100	0.6	0.1
%of falls	9%	88%		2 %	0.7%

*Recovered meteorites Pribram, Lost City, and Innisfree were photographed as bolides of type I and only their densities (gm/cm ^3) are real, the other bolide densities are derived. ** PE penetration depth into the atmosphere. Sc denotes the mechanical strength.

Using the value of terminal velocities and the average value of ablation coefficients, the terminal (residual) masses (mE) can be calculated. Among the bodies studied, 99 were heavier than 0.1 kg and 153 heavier than 0.01 kg. The parameter(mE) indicates the end of ablation in the atmosphere, but it cannot distinguish between meteoroids that were totally disintegrated and those genuinely decelerated. Similarly the calculated terminal altitudes and mechanical strength values do not provide an unequivocal interpretation.

Correlation of bolide properties with meteorite falls could well be accommodated by hypothesis B in which each bolide type has a meteorite equivalent. This has, however, some "outrageous" implications: comets may carry chondrites an idea excercised many times in past (lately e.g., by Kitamura and Tsutchiyama(24)); icy dust balls

do not produce fireballs; the extremely primitive carbon-rich particles represented by the IDPs do not form larger discrete bodies of "meteorite" size; and the asteroid belt is a mixture of "native fractionated old bodies" with the captured comets. Hypothesis B therefore contradicts the "established" scheme of the asteroid belt in which the non-differentiated meteorites (CI, CM, and CV) form the outer part of the asteroid belt, whereas the fractionated metamorphosed and igneous meteorites characterize the inner asteroids. Though the varition of asteroid types with heliocentric distance is observed(2), the assignment of meteorite classes to asteroidal types could be disputed, e.g., using new data on low-albedo asteroids and their water contents(20).

In our B-hypothesis all observed fireballs have their meteorite equivalents. The fireballs associated with dark asteroids i.e., short-period comets, provide the fireballs of II, IIIA, and IIIB types (22). These can be assigned to large pieces of carbonaceous chondrites or chondrites in general. The IDPs of small mass(10^-12 g) do not cause the fireball effects and apparently arrive in the Earth's environment as discretely small grains at relatively low velocities (25).

Gombosi and Houpis(26) presented a two-component (raisin bread) model of comets in which a volatile and dusty component glues together the rocky material.In his "comet" review Whipple(15) indicated similar model. Such a model (with its "flaws") nicely relates comets and dark asteroids. The loss of the volatiles causes "darkening" of the body and ultimately its extinction. The transformation of comet to asteroid is the transformation of superchondritic (volatile-rich) to chondritic (volatile-depleted) compositions. We believe that chondrites and carbonaceous chondrites do come from the dark Earth-crossing asteroids, which are devolatlized materials of Kuiper's belt, whereas the IDPs may either represent dust particles of cometary ices (matrix) of two-component comets(26) or may be derived from long-period comets of distant origin (Oort's cloud).

The temperature (chemical) gradient in the early solar system did not probably suddenly change within the asteroid belt (the gradient of approximately 1500 K for distance of 3.5 AU) as commonly shown(27). The sudden change of gradients is an observation-intepretation-related artifact arbitrarily attributing the dark objects to primitive carbon-bearing volatile rich-materials. If Kuiper's belt contains 10^13 bodies(19) of approximately 1km^3 size then the total mass exceeds the 10^27 g. An another missing planet should be searched for at the center of Kuiper's belt (i.e., about 70 AU) not far from the spot where Titius-Bode's law suggests a planet.

References:

(1)Wetherill G.W. and Chapman C.R., 1988 in Meteorites and the early solar system, Kerridge J. ed., Univ.Arizona Press, 35 - 67. (2)Gradie J.C., and Tedesco E.F., 1982, Science, 216, 1404 - 1407. (3)Opik E.J., 1963, Adv.Astr.Astrophys., 2, 219. (4)Wetherill G.W., 1988, Icarus, 76, 1 - 18. Yeomans D.K., 1991, Astron.J., 101, 1920 - 1928. (5)Gibson E.K., 1992, J. Geophys.Res., 97, E3, 3865 - 3875. (6)Dikov Yu.P. et al., 1991, Geochemistry International, 29, 33-38. Kissel J., et al. 1986, Nature, 321, 326. (7)Anders E. and Grevesse N., 1989, Geochim. Cosmochim.Acta, 53, 197 - 214. (8)Oro J. and Mills T., 1989, Adv. Space Res. 9 , No 2, 105 - 120. Anders E., 1991, Space Science Rev. 56, 157 - 166. (9)Cruikshank D.P., 1989, Adv.Space Res., 9, No.2, 65 - 71. (10)Chyba Ch.F., 1990, Nature, 343, 129 - 133. (11)Hartmann, W.K., 1990, Astronomy, 18 (8), 44 - 48. (12)Ramadurai S., 1987, Adv. Space Res., 7, No.5, 121 - 124. (13)Whipple F.L., 1987, Phil.Trans.R.Soc.Lond. A323, 339 - 347. (15)Jewitt D.C and Meech K.J., 1988, Astrophys.Journ., 328, 974 - 986. (16)Hartmann W.K. et al., 1990, Icarus, 83, 1 - 15. Buratti B.J. and Dunbar R.S., 1991, Astroph.Journ., 366, L47-L49. (17)Edelman C., 1991, Astron. Astrophys., 244, 228-235. (18)Duncan M., Quinn T., and Tremaine S., 1988, Astrophys.J., 328, L69 - L73. (19)Dyson F.J.,(1992) Q.J.R.Astr.Soc., 33, 45 - 57. (20)Lebovsky L.A. et al., 1990, Icarus, 83, 16 - 26. (21)Ceplecha Z., 1988, Bull. Astr. Inst. Czech., 39, 221. Ceplecha Z. and McCrosky R.E., 1976, J. Geophys. Res., 81, 6257. (22)Spurný P., 1991, doc. diss., Astr.Inst.Czechosl. (23)Hutchison R. et al., 1977, Appendix to the Catalogue of meteorites, British Museum, London. Graham A.L. et al., 1986, Catalogue of meteorites, Univ. Arizona Press, Tucson, 460p. (24)Kitamura M. and Tsuchiyama A., 1990, Abstr.15. Symp. Ant. Meteorites, NIPR Tokyo, 38 - 39. (25)Brownlee D.E., 1989, Nature, 339, 13. (26)Gombosi T.I. and Houpis H.L.F., 1986, Nature, 324, 43 - 44. (27)Binzel R. et al., 1991, Sci.Amer., 88 - 94.

SHOCKED AND UNSHOCKED BASALT FRAGMENTS AND IMPACTITE GLASSES IN MONOMICT BRECCIA FROM THE LONAR IMPACT CRATER, INDIA

V. K. NAYAK
Department of Applied Geology, Indian School of Mines, Dhanbad, India

Shocked and unshocked basalt fragments and impactite glasses of various shapes and sizes embedded in pulverized clayey-rock material are recognized in monomict breccia from the ejecta blanket on the eastern side of the Indian Impact Crater at Lonar ($19^{\circ}58'N$: $76^{\circ}31'E$) which is in the Deccan Trap Basalts of the Cretaceous-Eocene age. A variety of shapes of shocked basalt fragments are rounded (Fig. 1), subrounded, squarish, ellipsoidal and irregular and impactite glasses are also spherical and ellipsoidal (Fig. 2). The shocked basalts are coarse grained while unshocked and weakly shocked basalts are generally fine grained. The mineralogy of the shocked ones consist of maskelynite, pyroxene (sometimes granulated) and opaques including pseudobrookite (Nayak, 1991) and preserve ophitic and sub-ophitic texture. These observations in the monomict breccia from the ejecta corroborate with those first described by Fredriksson et al. (1973) in impact breccia from the center of the Lonar crater ~265 meters below the rim. Such type of features have also been recognized in the lunar regolith (King et al. 1972).

The rounded shape of shocked basalt simulates chondrule of a meteorite, however, this is not chondrule which as defined by Fredriksson et al. (1973) is, "once wholly or partly liquid, individual bodies which cooled, solidified or crystallized rapidly". Mechanisms of development of chondrule-like rounded and other shapes of shocked basalt fragments are discussed. The observations indicate that various shapes are due to varying degree of mechanical process of abrasion which operated during ejection and fallout of basaltic material and surge immediately after the meteorite impact on the target basalts. The roundness of shocked basalt is ascribed to degree of abrasion while impactite glass spheres are considered due to shock-induced basalt melt droplets.

On the whole, the monomict breccia consists of an extraordinary assorted components of immense value and records the history of significant events in an impact environment on the Earth and perhaps implies similar processes on the Moon and other planets

Fig. 1. A photomicrograph of monomict breccia showing chondrule-like rounded shocked basalt with laths of maskelynite (white) and pyroxene and opaques(black) X.32

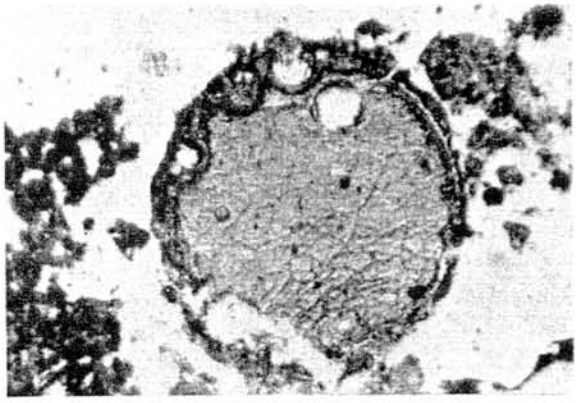

Fig. 2. A photomicrograph of monomict breccia showing impactite glass sphere. X.56

References

Fredriksson, K., Noonan, A. and Nelen, J. (1973). The Moon, 7, 475-482.

King, E. A., Butler, J. C. and Carman, M. F. (1972). Planetology Sec., 24th Inter. Geol. Congr., Montreal, Canada, 58-63.

Nayak, V. K. (1991). 16th Symposium on Antarctic Meteorites, National Institute of Polar Research, Tokyo, Japan, 23.

Special Lecture (III)

Dr. H. Palme

FORMATION OF ALLENDE CHONDRULES AND MATRIX

H.Palme, Max-Planck-Institut für Chemie, Saarstrasse 23, 6500 Mainz, Germany.

The two major components of Allende and other carbonaceous chondrites are matrix and chondrules. For Allende, McSween has estimated 35.9% matrix and 43% chondrules [1]. An important clue for understanding the formation of matrix and chondrules is that chondrules and matrix are to some extent chemically complementary. Allende chondrules are, on the average, higher in refractory lithophile elements (Ca, Al, REE etc.) than matrix. Chondrules are, on the other hand, lower than the bulk meteorite in Fe, Ni, Co and related elements; matrix is higher. This has been demonstrated by a new set of chondrule data obtained in Mainz [2,3] and by earlier analyses of Allende chondrules [4].
Fig. 1 shows a Cr-Ni plot for chondrules and matrix samples, including dark inclusions which are related to Allende matrix. The complementary character is obvious. Only a combination of chondrules and matrix yields the chondritic ratio of Ni/Cr that characterizes Allende and other carbonaceous chondrites. The solar photospheric ratio is also indicated to demonstrate that the bulk Allende ratio is a well defined ratio. Both, chondrules and matrix are required to contribute in the right proportions to produce the solar ratio in the mix. This is most easily achieved if both components come from the same reservoir containg Ni and Cr in solar proportions. A similar, although more subtle effect can be seen in the Ca/Al-ratio (Fig. 2). Chondrules have on the average higher ratios than the bulk, with the CI- ratio of 1.08, matrix and dark inclusions are lower.
This complementary relationship is not the result of metamorphic reactions on the Allende parent body but is a primary feature established at the time of formation of chondrules and matrix. Exchange of Ca and/or Al between matrix and chondrules on the Allende parent body by solid state diffusion is virtually impossible. The FeO-rich rims of chondrules and isolated forsterite grains and their steep compositional gradient to forsterite could not survive under conditions that would allow Ca-diffusion in pyroxene (e.g., [5,6]).
Another possible argument against the significance of the complementary Ca,Al-relationship is mass balance. There is an additional reservoir for Ca and Al, the Ca,Al-rich inclusions, and it may be thought that the bulk Allende Ca/Al-ratio is dominated by these inclusions. The complementary Ca/Al relationship between chondrules and matrix could then be accidental and would have no significance. However, it can be easily shown that the contribution of CAIs to the bulk inventory of Ca and Al is at most 30 %. [7]. Dark inclusions and matrix are not depleted in refractory elements [8]. They have approximately the CI-level. In addition, grain size fractions from Allende demonstrated that fine grained residues produced by removal of coarse grained material i.e., chondrules mineral grains and coarse grained CAIs still have chondritic refractory element abundances.
The variability in the chemical composition of chondrules requires heterogeneous i.e., coarse grained precursors. However, coarse grained precursors cannot be the result of melting processes, since there is no indication of crystal-liquid fractionation. For example, large radiating pyroxene chondrules consisting almost entirely of pyroxene have no excess of elements that prefer pyroxenes such as Sc. The uniform pattern of CI-normalized abundances of refractory elements is shown in Fig. 3. The opx/melt partition coefficients are indicated for comparison. If pyroxene or a pyroxene precursor in these chondrules ever formed by crystallisation from a larger melt pool it shoud record a pattern consistent with these partition coefficients. This is evidently not the case. Therefore, the pyroxene chondrules must have crystallized from a melt that had approximately the chemical composition of pyroxene but they were not produced by precipitation from an earlier melt. Lack of igneous REE-patterns in Allende chondrules was demonstrated earlier [9]. All this leads to the conclusion that chondrules are made by closed system melting of aggregates that are compositionally variable.
This compositional variability of aggregates may be produced by mixing variable fractions of previously condensed mineral grains such as olivine or pyroxene. Refractory elements (e. g., REE and Sc) would have condensed separately, i.e. earlier, in different phases. REE-patterns in chondrules sometimes carry a signature of volatility related fractionation [9].
The same reservoir that produced coarse mineral grains by condensation must also be capable of producing fine grained matrix. Condensation in a region of rapid temperature decrease may lead to formation of matrix. Fine-grained matrix is not monomineralic but an intimate mixture of olivine,

Fig. 1

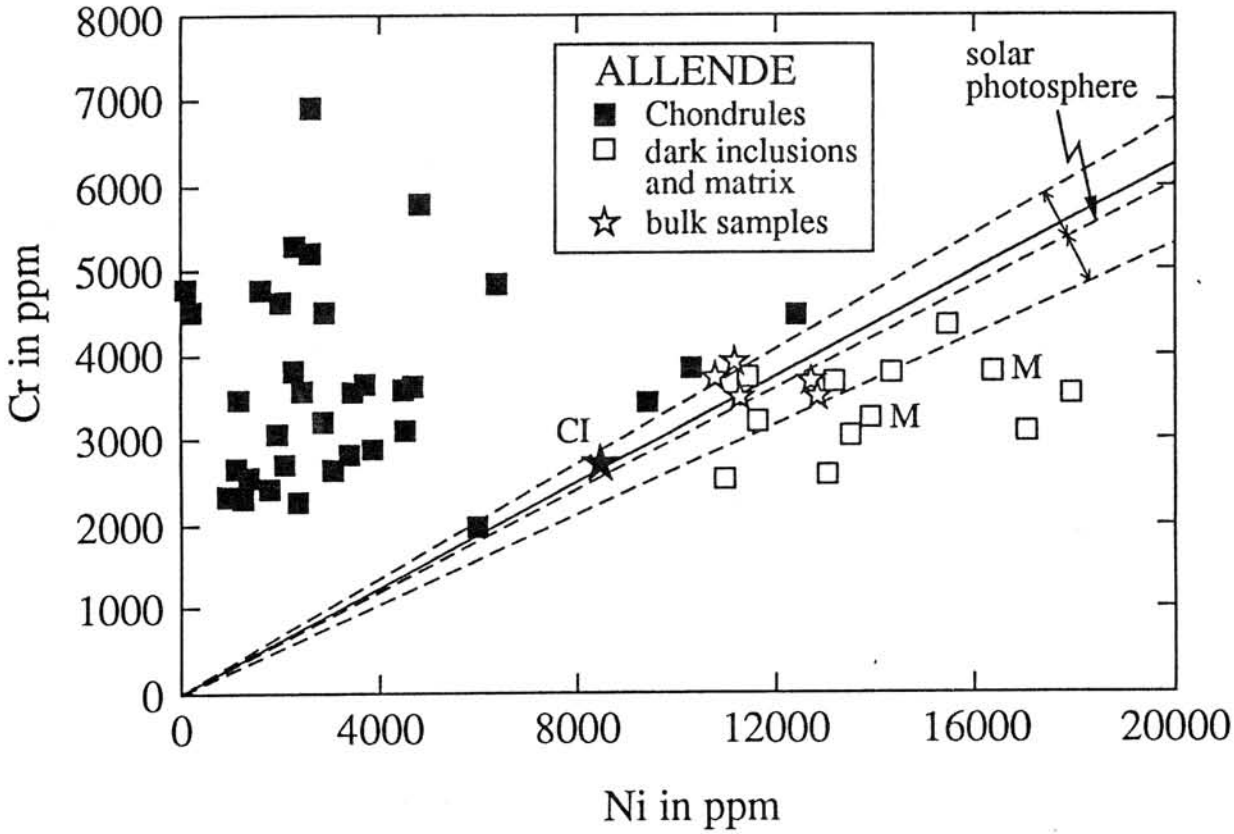
ALLENDE
Chondrules
dark inclusions and matrix
bulk samples
solar photosphere
CI
M
M
Cr in ppm
Ni in ppm
0
1000
2000
3000
4000
5000
6000
7000
8000
0
4000
8000
12000
16000
20000

Fig. 2

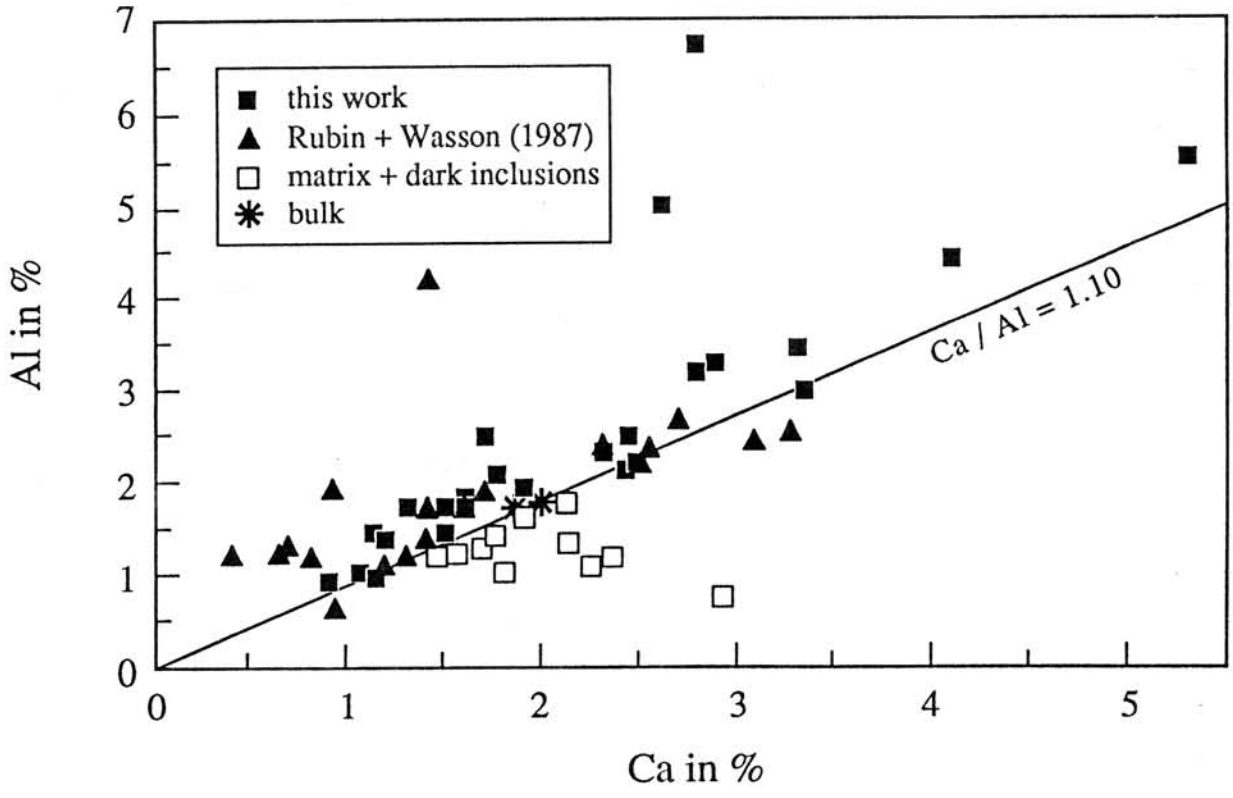
this work
Rubin + Wasson (1987)
matrix + dark inclusions
bulk
Ca / Al = 1.10
Al in %
Ca in %
0
1
2
3
4
5
6
7
0
1
2
3
4
5

Fig. 3. Refractory Elements in Radial Pyroxene Chondrules from Allende

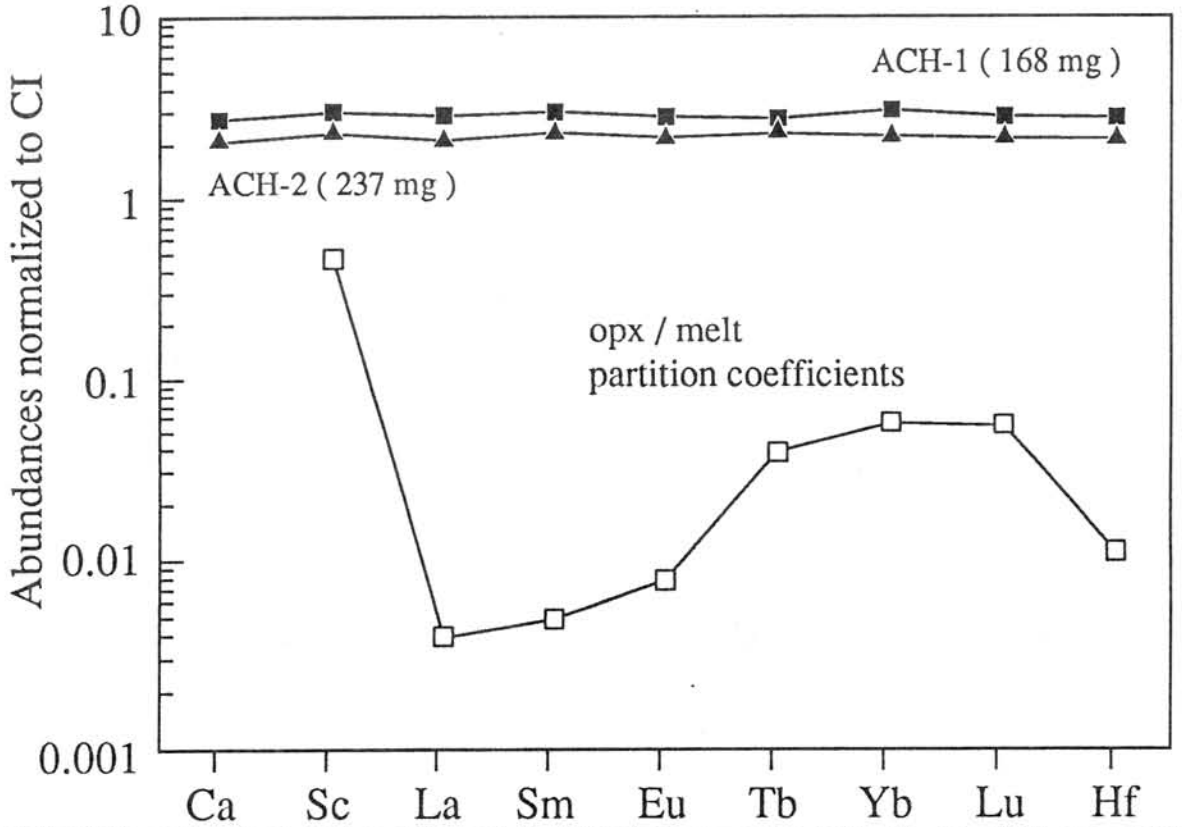

metal+sulfide and phases which also contain refractory elements such Al, Ca, REE etc. possibly reflecting rapid condensation.

To satisfy the complementary aspect and at the same time produce coarse and fine grained nebular objects requires large variations in local environments with respect to temperature, cooling rate and oxygen fugacity. Such variations are indeed recorded in the components of Allende: a variety of oxygen fugacities, large grains of forsterite formed by slow condensation, small grains of olivine that formed by rapid condensation etc.

Before the Allende components finally assembled to form a parent body they suffered a short heating event that redistributed volatile and moderately volatile elements and affected, as one might expect, fine grained materials much more effective than coarse grained [10, 11]. This event produced small FeO-rich rims around chondrules, isolated olivine grains and Ca, Al-inclusions and created an oxidized atmosphere. This last event before accretion has only affected members of the oxidized subgroup of CV-chondrites.

It thus appears that the early solar nebula must have provided a large variety of conditions required to produce the variability in chemical and mineralogical properties of components of primitive meteorites. However, the chondritic bulk chemical composition demonstrates the necessity of closed system evolution. All meteorite componets are derived from one reservoir. Minor amounts of exotic material may be added as it would not show up in bulk compositions.

Lit.: [1] McSween H.Y. Geochim. Cosmochim. Acta (1977) 41, 1777. [2] Spettel B. et al. (1989) Meteoritics 24, 326. [3] Palme H. et al. (1992) Lunar Planet. Sci. Conf. XXIII, 1021. [4] Rubin A. and Wasson J.T. (1987) Geochim. Cosmochim. Acta 51, 1923. [5] Weinbruch S. (1990) Meteoritics 25, 115. [6] Palme H. and Fegley B.F. (1990) Earth Planet. Sci. Lett. 101, 180. [7] Ireland T.R. et al. (1990) Lunar Planet. Sci. Conf. XXI, 546. [8] Bischoff A. et al. (1988) Lunar Planet. Sci. Conf. XIX, 88. [9] Misawa K. & Nakamura N. Geochim. Cosmochim. Acta 52, 1699. [10] Palme, H. & Wark, D. (1988) Lunar Planet. Sci. Conf. XIX, 897. [11] Palme H. et al. (1991) Meteoritics 91, 383.

Poster Session

and

Abstract Only

Identification of the fine magnetic structures in chondrites by magnetotactic bacterial technique

Minoru FUNAKI

National Institute of Polar Research, 9-10 Kaga 1, Itabashi Tokyo 173

Magnetotactic bacteria (cocci type) in the northern (southern) hemisphere migrate toward the S (N) pole along magnetic field lines. Since the size of bacteria is less than 2μm in diameter, they are a useful sensor to identify the magnetic poles on fine magnetic grains (larger than 10μm in diameter) in rocks. We have established and refined this technique and have applied the technique to ordinary chondrites.

The bacteria, collected from a pond near Tokyo, were cultivated for the S pole determination. The polarity of northern hemisphere bacteria was reversed using a 0.2 Tesla pulsed field. The purpose of this procedure was to provide migratory properties to sense the N poles. St. Séverin, Y-75097, ALH-769 and other chondrites were prepared for this observation after polishing.

The bacteria make dense clusters on the tetrataenite phase and on the kamacite phase. Domain walls are sometimes located and a pattern of sparsely distributed individual bacteria can be seen. It is difficult to estimate a dipole field on each magnetic grain based on the N and S poles distribution from the bacterial pattern. We will introduce this technique by the magnetotactic bacteria using video TV.

VAPOUR PHASE CRYSTALLIZATION OF Fe_3S_4 IN SEVERELY SHOCKED YANZHUANG CHONDRITE

CHEN Ming, XIE Xiande (Institute of Geochemistry,Academia Sinica, Guangzhou Branch, Guangzhou,510640,China)

Yanzhuang(H_6) had been subjected to a strong impact in space, it consists of the heavily deformed chondritic mass and black melt veins(0.1-15 mm in width)[1]. Shock effects in chondritic mass include deformation, phase transformation, melting and recrystallization of silicates and metal minerals. Black melt veins are composed of some shock molten and recrystallized materials of chondrite. Besides these, we found some thin veins of sulfide in chondritic mass. Optical microscope, scanning electron microscope (SEM) and energy disperse X-ray analysis (EDX) have been used to study the sulfide. Our studies show this sulfide is very unique in mineralogical characteristics and has a close relationship with impact process of the meteorite.

RESULTS:

(1) **Occurrence:**

The veins of sulfide (0.1-0.5 mm in width) are located in chondritic mass (Photo 1 A), especially in the area near the black melt veins. It shows that the sulfide came from the chondritic mass by migration, enrichment and recrystallization in the cracks during shock process.

(2) **Crystal morphological characteristics:**

The veins of sulfide are composed of the aggregates of euhedral and semi-euhedral crystals (0.02-0.20 mm in size). Most of crystals have monoclinic and cubic forms (Fig 1; Photo 1,B,C). In addition, there are a lot

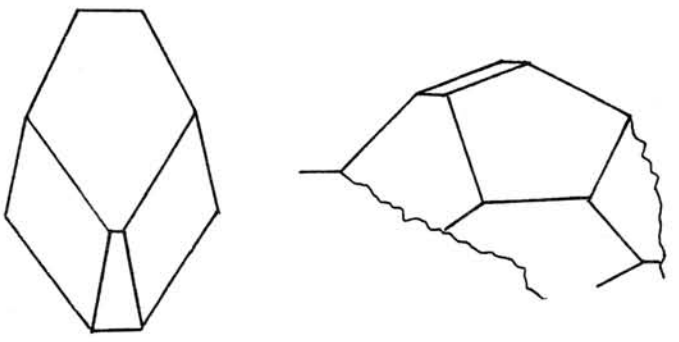

Fig. 1 cystal forms in the veins of sulfide

of holes and grooves (1-3 μm in diameter or width) in crystals, they are embodied as inclusions in round, sub-round, irregular and wormprint forms (Photo 1,D,E,F). Some of inclusions are semi-closed and usually link up to crystal faces.

428 μm

A

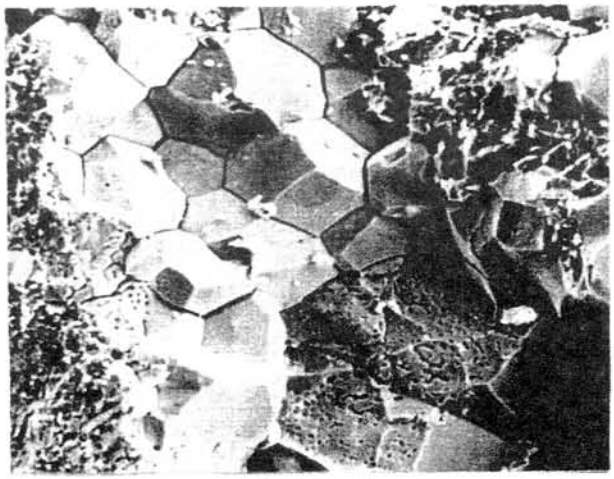

100 μm

B

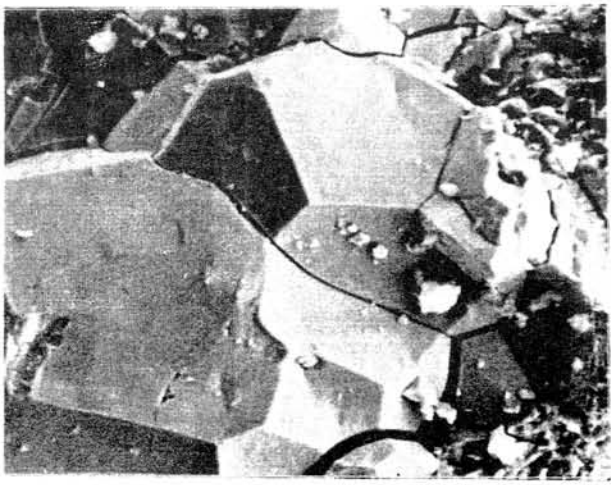

65 μm

C

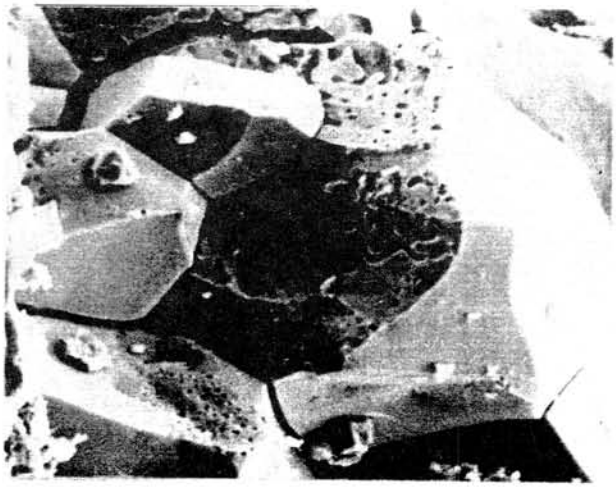

50 μm

D

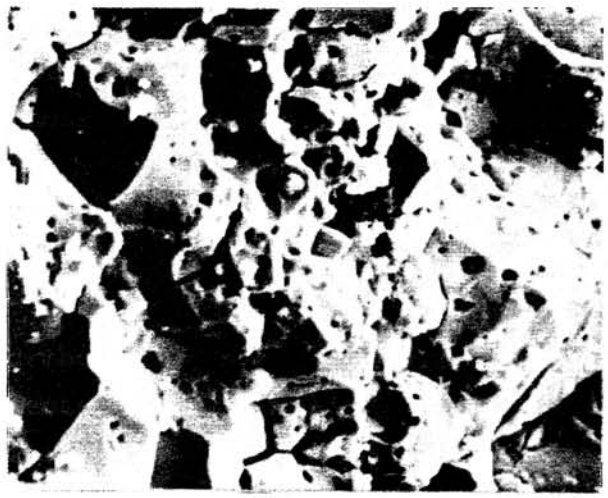

E

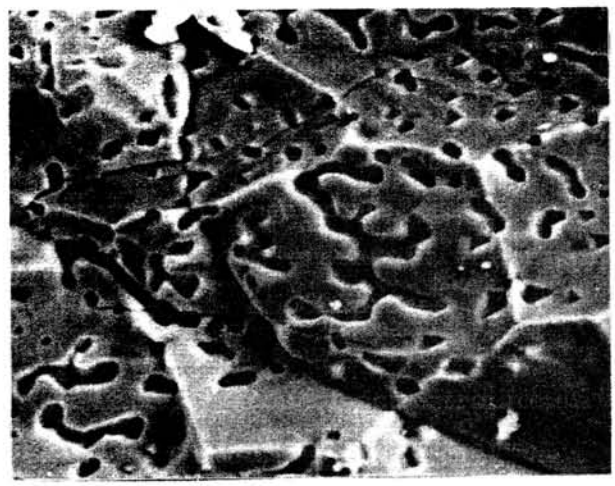

F

Photo 1 SEM images showing the occurrence of sulfides and crystal morphological chracteristics. (A) occurrence of sulfides; (B, C) Forms of sulfides ; (D,E,F) Holes and grooves in sulfides

(3) **Composition**

EDX analyses of the sulfide have given a chemical composition (at %) : S 55.18--58.54, Fe 44.82--41.46; mean: S 56.89 ± 1.71, Fe 43.11 ± 1.71 (Table 1). In contrast, the chemical composition of troilite in Yanzhuang is : S 50 ± 2 (at %), Fe 50 ± 2 (at %). The S content in the sulfide is higer than that of troilite. The chemical formula of this sulfide can be considered as Fe_3S_4.

Table 1 Composition of sulfide

(at %)

Num.	1	2	3	4	5	6	7
S	55.97	55.48	55.18	56.29	56.19	58.24	58.06
Fe	44.03	44.52	44.82	43.71	43.81	41.76	41.94
Num.	8	9	10	11	12	13	mean
S	57.44	57.45	58.54	56.81	55.67	58.26	56.89±1.71
Fe	42.56	42.55	41.46	43.19	44.33	41.74	43.11±1.71

DISCUSSIONS:

The sulfides with an approximate chemical composition of Fe_3S_4 have been found in terrestrial rocks [2,3] and were synthesized in laboratory [4] . These sulfides are monoclinic pyrrhotite, greigite (cubic) and smythite (hexagonal). It is seldom seen that Fe_3S_4 occur in meteorite.

The formation of crystal Fe_3S_4 in cracks in Yanzhuang shows the close relationship between the sulfide and shock process:

(1) The impact-generated high pressure and high temperature caused the melting, decomposition and vapourization of some troilite in the area of intense stress in chondrite. The decomposed S and Fe were migrated, enriched and lastly recrystallied in some cracks.

(2)The sulfide is relatively S-rich due to a S-rich crystallizing environment . Under the high pressure and high temperature, some sulfur were changed into vapour and liquid phases, this caused the specific form features of S inclusions in the crystallized sulfide. As soon as pressure was released, sulfur in vapour-liquid phases would expand quickly and escaped from some inclusions.

(3)Those Fe_3S_4 found in terrestrial rocks and synthesized in laboratory, are formed under the low pressure and low temperature. But, the sulfide in Yanzhuang crystallized in an environment of high temperature and high pressure according to the fact that vapour-liquid phase of sulfur coexisted with the crystallization of Fe_3S_4.

REFERENCES: [1] XIE Xiande et al. (1991) Abstracts 54th. Annual Meeting Meteorite Soc. p 254; [2] B.J. Skinner et al. (1964) Am. Mineral. 49(5,6) 543-555; [3] L.A. Taylor et al. (1972) Am. Mineral. 57(11,12) 1571-1577; [4] S.A. Kissin et al. (1982) Economic Geology 77(7) 1739 -1755

RADIOCARBON MEASUREMENTS ON METEORITES II: TERRESTRIAL AGES AND WEATHERING ACTIVITIES IN SOME ANTARCTIC CHONDRITES.

Yasunori Miura[1], Richard G. Cresswell[2], Roelf P. Beukens[2] & John C. Rucklidge[2]

[1]Department of Mineralogical Sciences and Geology, Yamaguchi University, Yoshida, Yamaguchi 753
[2]IsoTrace Laboratory, Universtiy of Toronto, Toronto, Ontario, M5S 1A7, Canada

Introduction. Radiocarbon measurements of Yamato and Allan Hills meteorites, and individual samples from Meteorite Hills, Reckling Peak and Bates Nunatak have been carried out as a continuation of a previous study, aimed at determining and disciminating the spallation and weathering components of radiocarbon in Antarctic meteorites (Beukens, et al., 1988), and providing a meteorite terrestrial history framework for glacier dynamics and meteorite stranding surface studies.

Samples are first heated to 500°C to remove surficial contamination. In the previous study, the sample was then heated to 1000°C for 4 hours, sealed, but under vacuum. For the last 30 minutes, carrier CO_2 was added and this plus the evolved gases were cycled over the sample, a heated CuO furnace and liquid nitrogen-cooled traps. The frozen CO_2 was subsequently converted to 'graphitic' carbon for analysis at IsoTrace (Beukens, et al., 1988). This procedure was repeated at melt temperature, and for a re-melt, to check extraction efficiencies. A significant component (up to 30%) of spallation carbon was shown to be evolved at 1000°C, based on studies of the Bruderheim meteorite, a recent fall. Thus, while a comparison of the melt component to that of Bruderheim afforded a measure of the terrestrial age, corrections to the lower temperature ('weathering') fraction results were required to estimate weathering activities. For the latest set of results (see the companion paper by Cresswell, et al. (this volume) for details), the low temperature fraction was held at ≈880°C for 1 hour, while the melt was held for 7 hours to ensure complete diffusion of the carbon, and transport to the traps. The evolved gases were separated into two components by a variable temperature trap that froze out the CO_2, while allowing the CO (and any CH_4) to be cycled over heated CuO and trapped as CO_2 in liquid nitrogen-cooled traps. Extraction backgrounds were measured on crucible blanks and determined to be less than 0.0007 dpm for each fraction.

Results and Discussion. Terrestrial ages have been determined on five L6 chondrites, one L3 chondrite and two H4 chondrites by comparing the CO component from the melt fraction of the sample with that of Bruderheim. Data appears to be consistent for L chondrites, but other classes require further examination before confidence in the dates can be given. The recent results support the previous observations that while both young and old terrestrial ages are observed from Yamato meteorites, there are still no reported young (<5,000a) samples from Allan Hills and its vicinity. This is in accord with collection sites associated with large, rapidly moving ice sheets in the Yamato region, but small ice sheets with slow to stagnant dynamics in the vicinity of the Trans-Antarctic Mountains.

Weathering activities are measured from the CO_2 component of the 880°C fraction, compared to the modern Oxalic Acid I standard. The new extraction procedure may give a clearer picture of the weathering history of the samples, indicating that recent weathering plays a more dominant role than previously assumed, and suggesting a rapid equilibration with modern atmospheric carbon.

Acknowledgements. We thank NIPR for the meteorite samples, and the support of the IsoTrace Laboratory and staff. This work is supported in part by a Natural Science and Engineering Research Council Grant to A.E. Litherland, whose support is gratefully acknowledged.

Reference:

Beukens, R.P., Rucklidge, J.C. & Miura, Y., 1988. Proc. NIPR Symp. Antarct. Meteorites, 1, 224-230.

75 — 1

Electron Microscopic observation of shocked minerals from Siljan crater , central Sweden and from some reference specimens

Junji Akai[*1] and Kenzo Yagi[*2] : *1 Departm. Geol. Mineral., Fac. Sci. Niigata Univ., Ikarashi 2-nocho, Niigata 950-21, Japan ; *2 Moiwasita 2-5-10, Minami- ku, Sapporo 061-21, Japan

Siljan structure is composed of a circular dome of Pre-Cambrian granite and has a diameter of ca.30 km.. Many characteristic tectonic features of Pre-Cambrian rocks in the Siljan structure , such as blocks tilted inwards , blockfaulting and a number of small overthrusts accompanying the faults have been found (Rutten, 1966). Steeply tilted blocks are found in the inner part of the structure. This Siljan ring structure has been estimated to be meteoritic impact crater or similar origin (Wickman, et al.,1963, Rutten, 1966) . The age of the tectonic movements could not be fixed beyond the fact that they are post- Silurian and pre-Quaternary.

Minerals which suffered intense shock by meteorite impact have, in general, permanent physical , chemical , mineralogical and morphological changes (ex. Beals et al.,1963; Dence,1964; Short, 1965 etc) . Both microscopic and macroscopic features are known; lattice-deformation effects and planar features (shock lamellae) are the example of the former , and shatter cones are the latter example. Shocked minerals from Siljan crater have been examined by Svensson (1973). According to him, the $\{10\ \bar{1}\ 3\}$ or $\{10\ \bar{1}\ 2\}$ crystallographic planes of the lammelae in quartz crystal in granitic rocks are by far the most common. This fact suggested peak shock pressure above 100 kb, based on previous laboratory experiments. However, detailed observation of fine textures of Electron Microscopic level (μm - nm scale) has not been carried out. In this study , textural features of electron microscopic level in shocked minerals from Siljan crater were examined by High Resolution Transmission Electron Microscopy (HRTEM) and Ansalytical Electron Microscopy (AEM) and described.

Specimens from Siljan crater were sampled by one of the authors (K.Y.). Specimens mainly from three localities in the Siljan crater were used for examination; the three localities are Hättberg which is located neraly in the centre of the crater, Tammeråsen and Stamsnös which is located nearly inner border of the crater. The examined specimens are as follows; [Hättberg,Specimen No. S8 (shatter cones, aplitic rock), S9 (impact breccia), S10 (shatter cones , finely brreciated) and S11 (aplitic rock)], [Tammeråsen S6 (shatter cones, aplitic rock)] and [Stamsnös (S4 and S5 (granitic rock, brecciated)]. Other reference specimens such as Ries and Manicouagan specimens were also partly used.

Specimens were examined mainly by HRTEM and AEM , and also by optical microscope and X-ray diffraction method.

Under the optical microscope, characteristic planar features of quartz were often found on some specimens (S6, S8 and S11) although fine-grained specimens were difficult to be observed. X-ray peak broadening was not clearly found.

Under the electron microscope, various fine textures were observed ; dislocations, linear features or linear microcracks, aggregates of fragmented grains, voids structures, textures related to formations of amorphous substances and transformed minerals, kink band ..... Among them, dislocations and short linear cracks (Fig.1) were most predominantly found on many rock forming mineral species in some samples. The linear features or cracks in TEM observation may correspond to optical microscopic linear or planar features ; that is, crack line observed in optical microscope may not be composed of single planar crack but composed of a bundle of the planar cracks.

Fragmentation was also found in very small scales in some specimens. In the process of fragmentation, Electron Diffraction (ED) pattern clearly changed from ordered type to diffuse complex type of ED pattern (Fig.2). Voids structures (Fig.3) were also found and they may be produced by shock event-related vaporization or some defect. Intermediate process of formation of amorphous substances from crystalline rock forming minerals was also found . In some specimens, some changes related to mineral transformation were observed. Kink band structure in biotite (Fig.4), which may be probably due to shock effects was rarely found in TEM observation. Thus, various fine textures of EM levels in shocked rock forming minerals in the Siljan crater rocks were found and briefly described.

One of the authors (J.A.) reported the possibility of small crater in Japan (Akai, 1989) but no additional positive data for confirmation for meteoritic impact crater could not be obtained ; so, this structure should be reinvestiagated also with other possibilities.

More detailed and systematic examinations of the mineral textures of EM levels may be necessary for these specimens.

References

Akai,J. (1989) Pap.to 14th Symp.Ant.Met. Natl.Inst.Pol.Res.150 ; Dence,M.R. (1964) Meteoritics, 2,249 ;Short (1965) Ann.N.Y.Acad.Sci.123,573; Svenssen (1973) Geol.Foren. i Stockh.Forhand.95, 139.; Wickman, F.E. et al. (1963) Arr. Min. Stockholm, 3, 193.

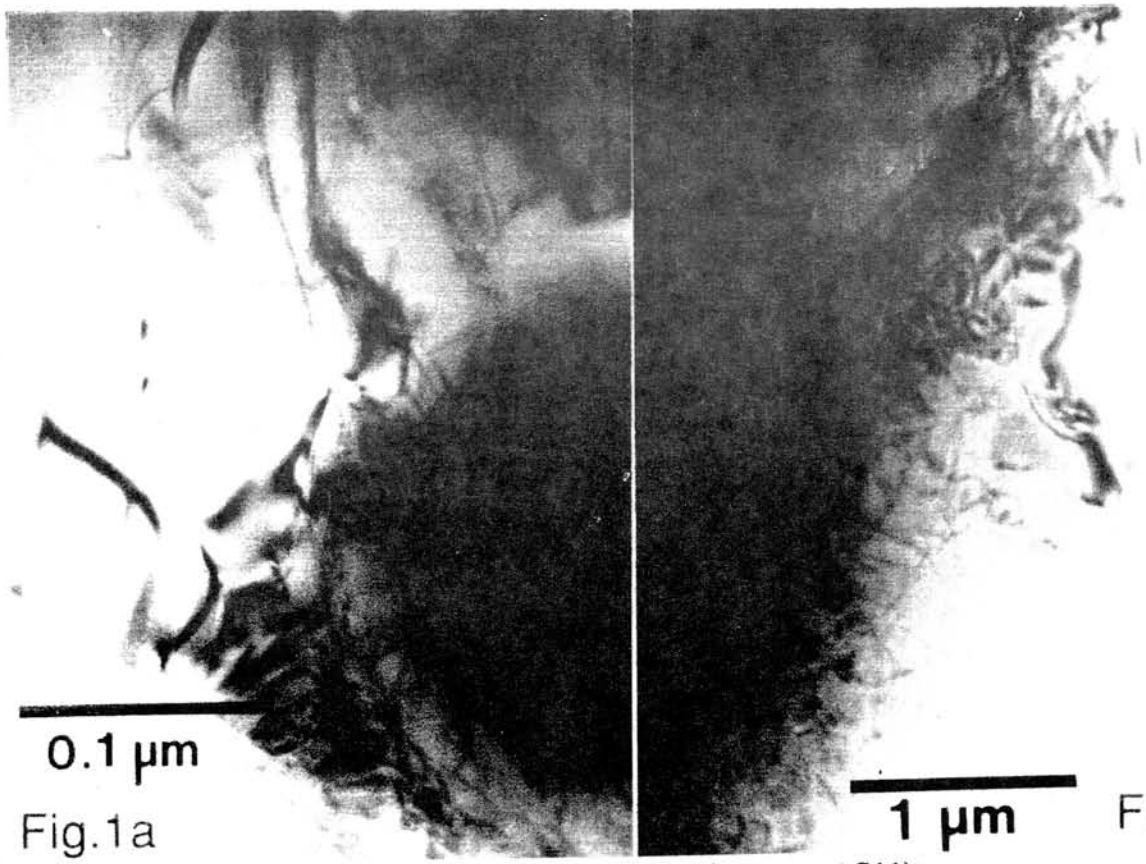

Fig.1a EM image of high density of dislocations in quartz (S11)

Fig.1b EM image of mica in S11, suggesting many dislocations.

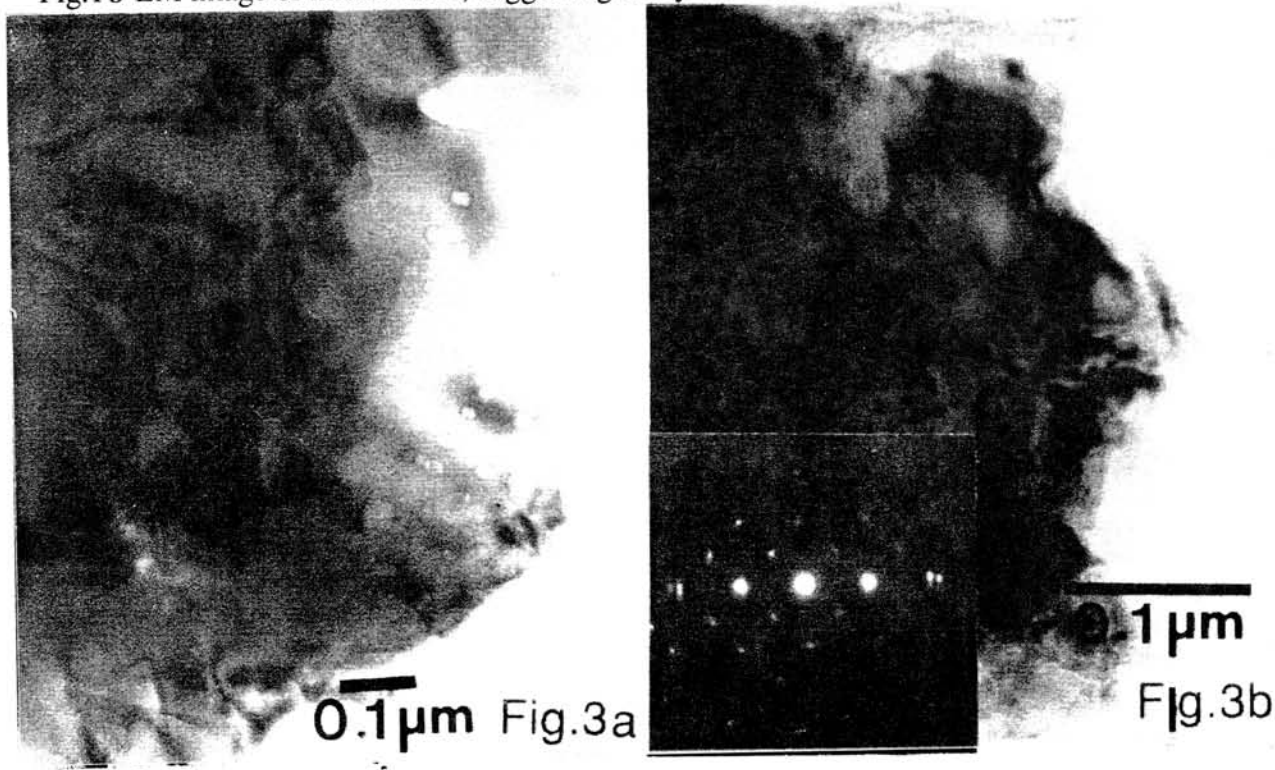

Fig.3a EM image of voids structure in magnetite (S11).

Fig.3b EM image of fragmented magnetite in S6

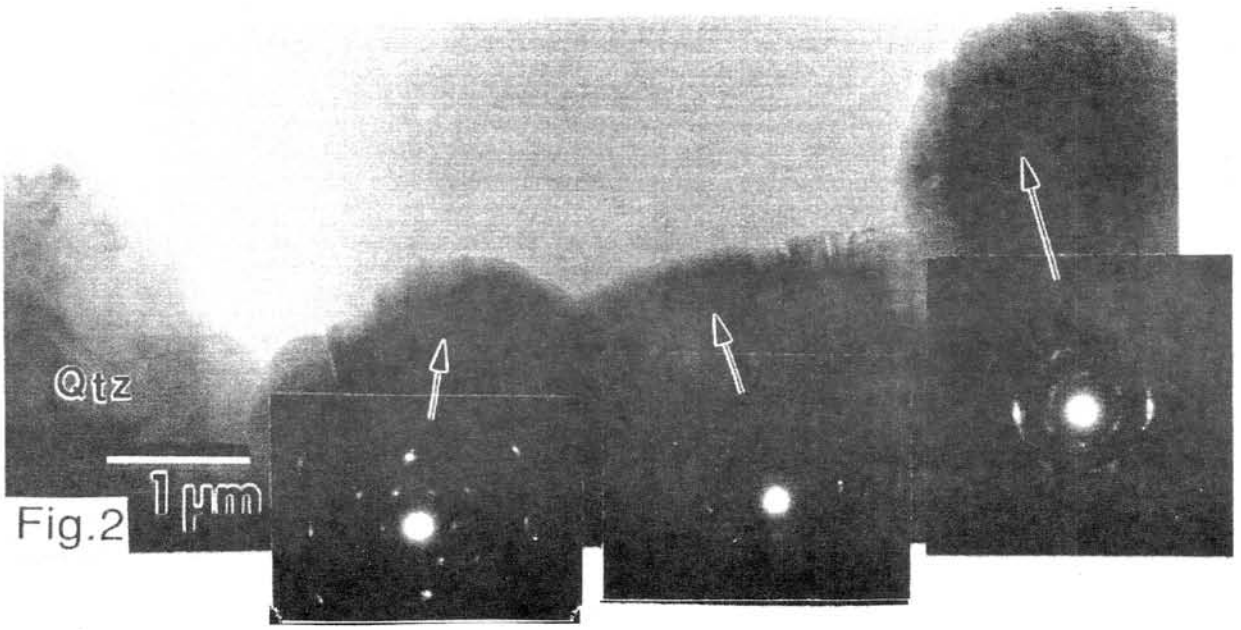

Fig.2 EM image of S 11 indicating structural decomposition process of mica.Chlorite is associated. ED pattern changes to disordered type. Adjacent quartz crystal has voids.

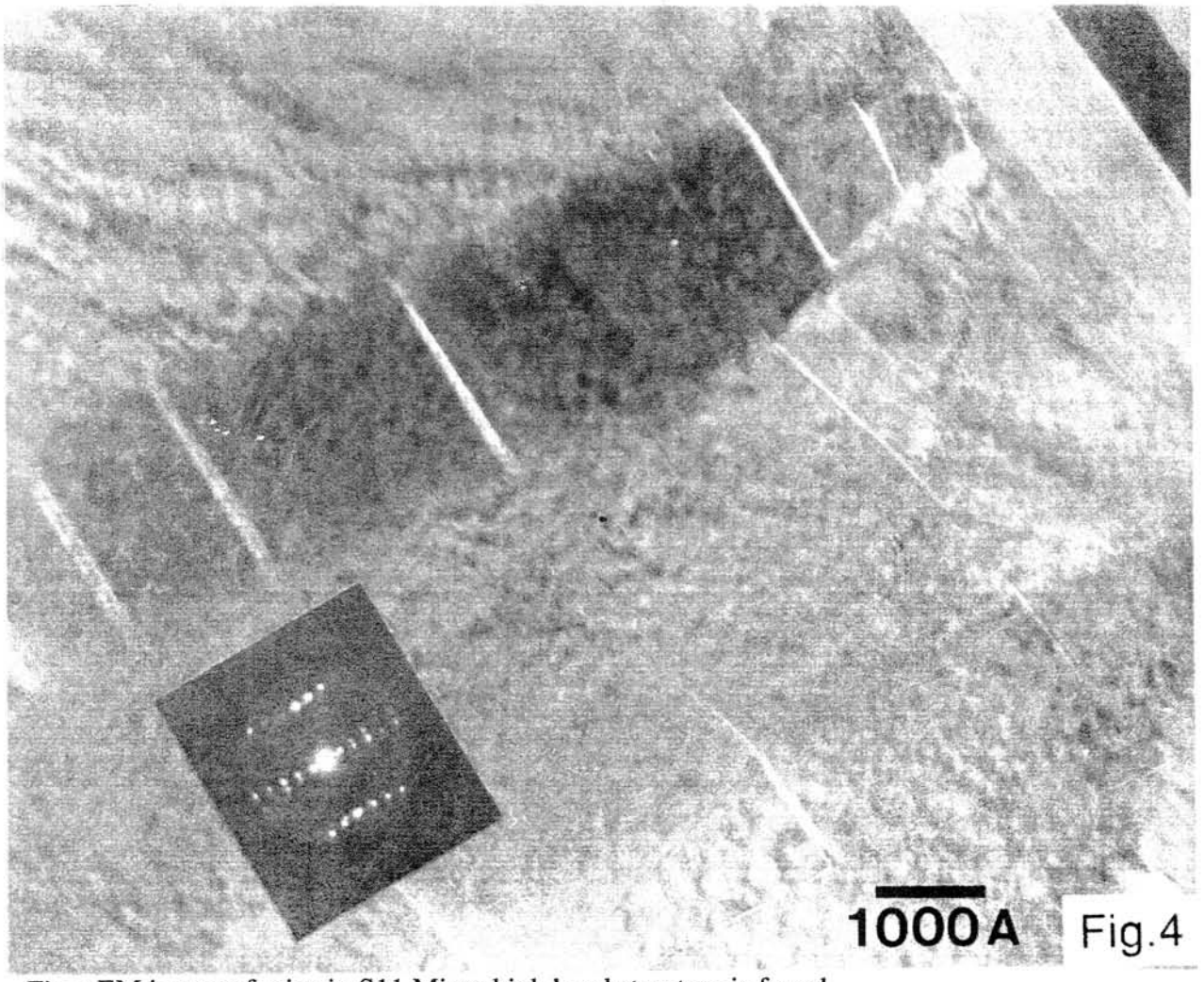

Fig.4 EM image of mica in S11.Micro kink band structure is found.

BASALTIC LUNAR METEORITES ASUKA-881757 AND YAMATO-793169; COMPARISON WITH EET87521 AND YAMATO-793274. Otto Eugster, Physikalisches Institut, University of Bern, CH-3012 Bern, Switzerland.

Asuka-881757 and Yamato-793169 are coarse-grained lunar gabbros [1, 2] whose chemistry is similar to very-low-titanium mare basalt. We obtained 0.503 g of Asuka-881757 and 0.024 g of Y-793169 for the determination of the exposure ages and the K-^{40}Ar gas retention ages and for the characterization of the solar-wind derived noble gases.

Table 1 gives the analytical results. The noble gas components (Table 2) were calculated using the assumptions given by Eugster et al. [3]. For the calculation of the exposure ages we used the same production rates as for the EET87521 basaltic lunar meteorite (10^{-8}cm^{3}STP/g Ma): P_3=0.8, P_{21}=0.0626, P_{38}=0.0764. Except for P_3 these production rates were calculated based on the data given by Hohenberg et al. [4] for a 2π-exposure geometry for the lunar surface inserting the chemical abundances given for Asuka-881757 by Yanai [2] and Lindstrom et al. [5]. Of course, we do not know whether Asuka-881757 and Y-793169 were exposed to cosmic rays mainly in the lunar regolith or in space after ejection from the moon. The determination of radionuclide activities, such as those of ^{10}Be, ^{26}Al, ^{36}Cl, ^{53}Mn and ^{81}Kr, will answer this question. The chemical composition of Asuka-881757 is quite similar to that of EET87521 [6], and Y-793169 is mineralogically similar to Asuka-881757. For comparison, Tables 2 and 3 also give the data for the two other basaltic lunar meteorites EET87521 and Y-793274, the latter one being a mixture of about two third mare material and one third highland component.

Table 1. Results of He, Ne, and Ar measurements of lunar meteorites Asuka-881757 and Yamato-793169

	^{4}He	^{20}Ne	^{40}Ar	^{4}He	^{20}Ne	^{22}Ne	^{36}Ar	^{40}Ar
	10^{-8}cm^{3}STP/g			^{3}He	^{22}Ne	^{21}Ne	^{38}Ar	^{36}Ar
Asuka-881757,106	1325	0.207	931	1082	0.864	1.212	0.899	5390
0.00786 g	± 50	± 0.010	± 60	± 30	± 0.040	± 0.030	± 0.030	± 500
Asuka-881757,106	1032	0.236	614	1029	0.886	1.227	1.42	1678
0.02935 g	± 30	± 0.010	± 40	± 40	± 0.040	± 0.030	± 0.04	± 20
Yamato-793169,46	228	0.697	697	182.3	1.147	1.235	0.672	1313
0.00826 g	± 10	± 0.030	± 30	± 5.0	± 0.050	± 0.030	± 0.020	± 20

Cosmic-ray exposure histories. Asuka-881757 shows the lowest cosmic-ray exposure of all lunar meteorites studied till now. If the exposure occurred on the moon and if the moon-Earth transfer time was negligibly brief the total exposure to cosmic rays lasted 3 Ma. However, if the cosmic-ray exposure occurred in space t(transfer) lasted about 1.3 Ma. For Y-793169 the lunar residence time t(moon) is 9.1 Ma assuming t(transfer)=0, and t(transfer)=4.2 Ma if t(moon)=0. Table 3 shows that the durations of exposure to cosmic rays for Y-793169 and EET87521 are about the same. Y-793274 yields a totally different exposure history with a lunar regolith residence time of 700 Ma.

Table 2. Cosmic-ray produced, radiogenic, and trapped noble gases (10^{-8}cm^{3}STP/g)

	Cosmogenic				Radiogenic	Trapped	
	^{3}He	^{21}Ne	^{38}Ar	^{22}Ne/^{21}Ne	^{40}Ar	^{20}Ne	^{36}Ar
Asuka-881757,106 0.00786 g	1.22 ± 0.06	0.198 ± 0.020	0.182 ± 0.020	1.202 ± 0.030	931 ± 60	< 0.04	0.054 ± 0.008
Asuka-881757,106 0.02935 g	1.00 ± 0.05	0.217 ± 0.020	0.215 ± 0.020	1.214 ± 0.030	614 ± 40	< 0.05	0.226 ± 0.016
Yamato-793169,46	1.25 ± 0.06	0.492 ± 0.030	0.786 ± 0.050	1.203 ± 0.030	697 ± 30	0.22 ± 0.02	< 0.04
For comparison							
EET87521,38[1] bulk	0.43 ± 0.04	0.40 ± 0.10	0.52 ± 0.16	-	870 ± 60	108 ± 6	118 ± 5
EET87521,39 bulk	< 0.8	0.30 ± 0.03	0.70 ± 0.35	-	1392 ± 40	65 ± 20	63 ± 15
Yamato-793274[2] bulk	27.5 ± 4.7	39.3 ± 2.3	57.6 ± 18.0	-	1440 ± 150	28700 1300	14000 ± 600

[1] See also Vogt et al. [9]. [2] Eugster et al. [3].

Solar wind exposure. Trapped solar wind noble gases in Asuka-881757 and Y-793169 are extremely low abundant or not present, whereas all other lunar meteorites studied so far contain solar wind derived noble gases. Considering the small sample sizes the origin of trapped ^{36}Ar in Asuka and of trapped ^{20}Ne in Y-793169 could be atmospheric contamination. We conclude that the Asuka-881757 and Y-793169 material never resided on the very lunar surface. In contrast to these lunar gabbros EET87521 is a brecciated lunar basalt containing some breccia fragments that were exposed to the solar wind. The high solar wind content of Y-793274 is typical for lunar regolith breccias with high cosmic-ray exposure age.

K-^{40}Ar gas retention ages. The K-^{40}Ar ages of 3670 Ma for Asuka-881757 and of 3510 Ma for Y-793169 are typical for mare regions on the moon such as Mare Tranquillitatis (Apollo 11) and Mare Serenitatis (Apollo 17) [7]. It appears that these mare gabbros retained most of their radiogenic ^{40}Ar. The crystallization ages obtained for Asuka-881757 based on the U-Th-Pb, Sm-Nd, and Rb-Sr methods are somewhat higher (3847-3940 Ma [8]).

Thermal history. Upper limits for the U/Th-^{4}He gas retention ages were estimated based on the U and Th concentrations and assuming that all ^{4}He is of radiogenic origin except for Y-793274. For Asuka-881757 and Y-793169 we adopted 0.1 ppm U and 0.33 ppm Th [5] and for EET87521 0.2 ppm U and 0.8 ppm Th [6]. For Y-793274 ^{4}He(rad) could not be determined because ^{4}He(tr) is too high. Asuka-881757, Y-793169, and EET87521 show losses of ^{4}He(rad) relative to ^{40}Ar(rad). T_3 is also lower than T_{21} (Table 3) due to ^{3}He(c) loss. Asuka-881757 suffered the lowest ^{3}He(c) and ^{4}He(rad) losses and its cosmic-ray exposure age is lower than that of the other three meteorites. This indicates that diffusion loss of He occurred in the lunar regolith.

Table 3. Cosmic-ray exposure ages for lunar surface exposure (2π) and K-^{40}Ar ages of basaltic lunar meteorites.

	Cosmic-ray exposure ages (Ma)				K-^{40}Ar age (Ma)
	T_3	T_{21}	T_{38}	T_{av}	T_{40}
Asuka-881757	1.4	3.3	2.6	3.0[1]	3670
Yamato-793169	1.6	7.9	10.3	9.1[1]	3510
For comparison					
EET87521[3]	<0.6	5.6	8.0	8.0[2]	3300
Yamato-793274[4]	34	340	740	700[2]	2800

[1] Av. of T_{21} and T_{38}. [2] Av. of T_{38}, T_{83}, and T_{126}. [3] See also Vogt et al., [9]. [4] Eugster et al. [3].

Acknowledgements. We are grateful to the Natl Inst. of Polar Research in Tokyo and to the Meteorite Working Group of NASA for providing the meteorite samples. We thank B. Balsiger, P. Guggisberg, and M. Zuber for assistance at various stages of this investigation. This work was supported by the Swiss National Science Foundation.

References. [1] Yanai K. and Kojima H. (1990), Abstracts, 15th Symp. A.M., 129-130. [2] Yanai K. (1991), Proc. Lunar Planet. Sci. Conf. 21, 317-324. [3] Eugster O., Michel Th., and Niedermann S. (1992), Proc. NIPR Symp. Antarct. Meteorites 5, 21-33. Natl Inst. Polar Res., Tokyo. [4] Hohenberg C.M., Marti K., Podosek F.A., Reedy R.C., and Shirck J.R. (1978), Proc. Lunar Planet. Sci. Conf. 9th, p. 2311-2344. [5] Lindstrom M.M., Mittlefehldt D.W., and Martinez R.R. (1991), papers pres. to NIPR Symp. Antarct. Meteorites, 102-105. [6] Koeberl Ch., Kurat G., and Brandstätter F. (1991), Proc. NIPR Symp. Antarct. Meteorites 4, 33-55. [7] Basaltic Volcanism Study Project (1981), Pergamon Press, Inc., New York, 1286 pp. [8] Misawa K., Tasumoto M., and Yanai K. (1992), Lunar Planet. Sci. 23, 917-918, Lunar Planet. Inst., Houston. [9] Vogt S.K., Herzog G.F., Eugster O., Michel Th., Niedermann S., Krähenbühl U., Middleton R., Dezfouly-Arjomandy B., Fink D., and Klein J. (1992), in preparation.

Gas-Liquid Condensation Evidences in Meteorites and Solar Nebular Condensation Model.

Hou Wei, Xie Hong-sen, Institute of Geochemistry, Academia Sinica, Guiyang 550002, China

I. Introduction

Except C1 chondrite, most meteorites contain some minerals that being from melt. Despite origin of the melt no clear, this fact shows there were liquid phases in formation process of most meteorites,so following questions are put before us: were these liquid phases directly relative to solar nebular condensation? Besides gas-solid condensation, was there gas-liquid condensation in nebular condensation process? In this paper we will try to use the reduction to absurdity for answering these questions. If some liquid phenomena in meteorites can not been explained by solid-liquid melt, we will inferred the liquid phases is from gas-liquid condensation.

II. The evidences of condensation origin of chondrules

1. The chondrules in chondrites are generally acknowledged to be solidefyed silicate melt-drops that were remelted gas-solid condensates. According to this hypothesis, this remelting would occur after gas-solid condensation of nebula, as remelting happened,the temperature of nebula would be lower than 700°C that was the lowest gas-solid condensation temperature of mineral-troilite in chondrule. The melting point of silicate mineral in chondrule is over 1800°C. The average diameter of chondrules is about 1mm. Therefore the melt-drops would have high subcool degree and high cooling rate,and the solidifyed drops must possess cryptocrystalline or glassy texture. However in chondrite the most chondrules possess porphyritic and granular texture that formed in slowly cooling,so these chondrules could not be results of remelting.

2. Thermodynamics calculation shows the temperature of gas-solid condensation of metal Fe-Ni is close to that of Mg-Fe silicate minerals and higher than that of troilite,so content of metal Fe-Ni in chondrules would be same with the matrix. In fact the content of metal Fe-Ni in chondrules is far lower than that

of matrix. Above these phenomena can not be explained by remelting hypothesis. They could be from gas-liquid condensation.

III. No differentiation origin evidences in "differentiated meteorites"

1. Some chondritic inclusions were observed in some iron meteorites and the abundence of their rare gas is higher to be close to chondrite. The measures of oxygen isotope of some pallasites show their feature to be similar to CV chondrite.

2. The melting experiments of chondrites show at high temperature the metal Fe-Ni and troilite of chondrite would melt and form no divisional Fe-Ni-S melt,then separated from silicate melt. The products that crystallizated from Fe-Ni-S melt would contain same rate of troilite/(troilite+metal Fe-Ni) with chondrite, and a part of product would possesses eutectic texture of Fe-Ni and (Fe,Ni)S. However the content of troilite in iron and stone-iron meteorites are far lower than that of chondrites, in them no eutectic texture were observed. Their troilite contains lower Ni than (Fe,Ni)S of products. These feature show iron and stone-iron meteorite were not from Fe-Ni-S melt. In stone-iron meteorite silicate minerals and metal Fe-Ni appear including each other,that contradicts the condition of having gravity in chondritic body.

3. Iron and stone-iron meteorites contain some minerals for example tridymite, christobalite, whitlockite that are not stable under high pressure. Based on cooling rate of metal Fe-Ni in these meteorites,calculated radiuses of their body are over 300km. In such big body's the core or core-mantle boundary above minerals could not be stable.

4. Up to now three types of achondrite(SNC) have been inferred to be from Mars, and other three types of achondrite(HED) have been considered to be from a body with basaltic mantle, but following fact will show not all achondrites were melt-differentiation origin: ① Ureilites possess igneous texture, euhedral olivine and orthopyroxene crystals embed in rich-C dark ground mass. The oxygen isotope anomaly and rare gas content of ground mass are similar to C group chondrites. ② Enstatite achondrites are composed of big crystals of enstatite,that show they would

occur in deep mantle of body. But they also have brecciated texture that would be due to shock,that shows they would be from the upper mantle of body. Above features can not be explained by differentiation hypothesis. Therefore we inferred most "differentiated meteorites" could be from gas-liquid condensation.

IV. The formation condition of meteorites and solar nebular condensation model

1. The formation condition of chondrite. The texture of chondrite shows after the melt-drops formed from gas-liquid condensation,the drop was immediately wrapped by fine grained gas-solid condensates(dusts). We think above process could occur near "triple point" of minerals contained in this chondrite. Because the bulk composition of a chondrite can not be represented by the composition of one mineral, this "triple point" could not be a point,but could be a broader range of temperature and pressure. The change tendency on the condition of formation of all group chondrites is: from E to H-L-LL-C, the T,P gradually decreased. Thus in sametime, the place of "triple point" of chondrite, from E to H-L-LL-C, were from near to far for sun, and for same place,the time that "triple point" appeared from E to H-L-LL-C, was from early to late.

2. The formation condition of "differentiated meteorites" These meteorites' texture shows they formed in a condition of high temperature and cooling slowly, thus the T,P of nebula would be higher than range "triple point" of these meteorites' minerals. At sametime the place formed these meteorites was nearer from sun than chondrite, and at same place these meteorites formed would be earlier than chondrite.

3. Solar nebular condensation model. The model is shown in Fig.1. In Fig.1 from the left of "a" boundary to right, the rock-matter's condensation is from no occuring to occuring. The "a" was between Mercury region and sun. From the left of "b" boundary to right, the H_2O's condensation was from no occuring to occuring. The "b" was between Venus region and Earth region. In the left of "c" boundary, all matter had gas-liquid(G-L) or gas-solid(G-S) condensations, but in right of "c", only matter's G-S condensation occured. The "c" was between Jupiter region and

Asteroid region. The GLS(R) and GLS(W) represent seats of time-space of "triple point" of rock-matter and H_2O respectively. Only rock-matter G-L condensation occured in (1) area of Fig.1; only rock-matter G-S condensation occured in (2); rock-matter G-S and H_2O G-L condensations occured in (3) area; rock-matter G-S and H_2O G-S condensations occured in (4) area. It is seen that in Mercury region and Venus region, rock-matter's G-L condensates (to be similar to iron,stone-iron meteorites and achondrite), the mixture of rock-matter's G-L and G-S condensates(to be similar to E,H,L,LL,C_3,C_2 group chondrites), and rock-matter's G-S condensates(to be similar to the matrix of chondrite) formed. In Earth region and Mars region, besides above three types of condensates, the mixture of rock-matter's G-S, H_2O's G-L, G-S condensates(to be similar to C1 chondrite) formed. Therefore, regardless of H_2O content, all types of meteorite can be seen as original matter of terrestrial planets, just the content of every type of meteorite varied for various planets.

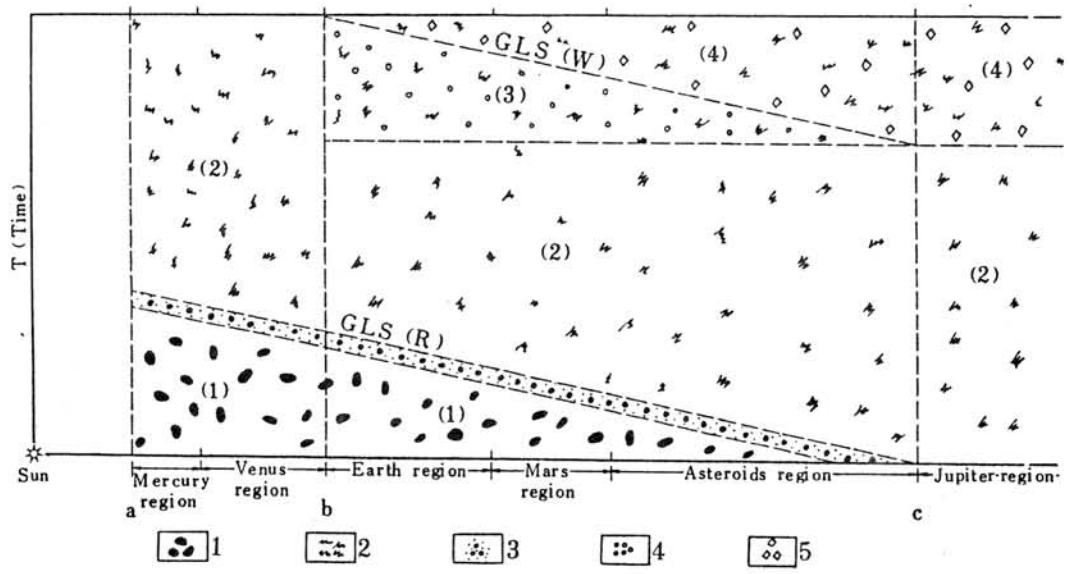

Fig.1 Solar nebular condensation model

1. G-L condensates of rock-matter
2. G-S condensated of rock-matter
3. Mixture of G-L and G-S condensates of rock-matter
4. G-L condensates of H_2O
5. G-S condensates of H_2O

SPINELS IN UNEQUILIBRATED ORDINARY CHONDRITES: CORRELATION BETWEEN THEIR AL/AL+CR RATIOS AND PETROLOGIC TYPES. KIMURA M.[1], YABUKI H.[2], IKEDA Y.[1] and EL GORESY A.[3]. 1) Ibaraki University, Mito, 2) The Institute of Physical and Chemical Research, Wako, and 3) Max-Planck-Institut, Heidelberg, Germany.

Spinels in 8 unequilibrated ordinary chondrites with type 3.3-3.9 in H, L and LL groups were analyzed to clarify the correlation between their chemistry, occurrence and petrologic type of chondrite. Spinels in 18 equilibrated chondrites were also analyzed for comparison.

Chemistry of spinel is correlated to its occurrence in unequilibrated chondrites. Mg-Al-spinel (atomic Al/Al+Cr ratio >0.2) mainly occurs in chondrules. Chromite (≤0.2) occurs in chondrules and matrix as isolated minerals, very often in association with Fe-Ni metal and troilite.

Figure 1 shows distribution of atomic Al/Al+Cr ratios of spinels in L-chondrites. Table 1 gives range, average and standard deviation (1σ) of Al/Al+Cr ratios of spinels in H, L and LL-chondrites. Spinels in unequilibrated chondrites have a very wide compositional range; atomic Al/Al+Cr ratios from 0.00-1.00. They also have a wide range of Mg/Mg+Fe ratios from 0.01-0.99. A remarkable feature is that Al_2O_3-free chromite occurs only in unequilibrated chondrites of type 3.3-3.4. On the other hand, chromites in type 3.7-3.9 chondrites of H, L and LL-groups always have Al_2O_3. Average Al/Al+Cr ratio of chromite increases from 0.004 for type 3.3-3.4, through 0.09 for type 3.6-3.8 to 0.12 for type 3.9. Standard deviation of Al/Al+Cr ratio of all spinels decreases with increasing types from 3.3 to 3.7 in L and LL-chondrites.

Spinels in type 4 and 5 chondrites are still heterogeneous in composition, as reported by Yabuki et al. [1]. Spinels even in type 6 chondrites are not always homogeneous. Nevertheless, compositional range of spinels in equilibrated chondrites become smaller with increasing petrologic type in general, and their standard deviations of Al/Al+Cr ratio are smaller than those in unequilibrated chondrites (Table 1).

The observed correlation between the compositions of spinel and petrologic types suggests that Al/Al+Cr ratio of spinel could be a sensitive indicator of petrologic type of ordinary chondrites, especially in unequilibrated chondrites. Such a correlation may result from exchange of Al_2O_3 and Cr_2O_3 within spinels during metamorphism. Standard deviation of atomic Mg/Mg+Fe ratio of spinel in a chondrite is usually smaller than that of Al/Al+Cr (Table 1), suggesting that divalent cations can diffuse faster than trivalent cations in spinel structure.

References: [1] Yabuki H., El Goresy A. and Ramdohr P. (1983) Meteoritics, 18, 426.

Table 1. Compositional variation of spinels.

Group	Type	No.	Al/Al+Cr				Mg/Mg+Fe	
			Min.	Max.	Average	1σ	Average	1σ
H	3.7	21	0.043	0.798	0.211	0.201	0.164	0.140
	3.8	43	0.010	0.996	0.448	0.395	0.336	0.233
	3.9	72	0.107	0.915	0.274	0.307	0.229	0.206
	4	137	0.106	0.773	0.285	0.248	0.236	0.172
	5	120	0.118	0.632	0.229	0.147	0.225	0.099
	6	130	0.118	0.244	0.158	0.034	0.164	0.044
L	3.4	26	0.000	0.998	0.317	0.388	0.175	0.167
	3.7	69	0.063	1.000	0.583	0.368	0.446	0.339
	4	199	0.078	0.983	0.421	0.346	0.274	0.202
	5	128	0.072	0.989	0.628	0.355	0.439	0.171
	6	44	0.122	0.439	0.207	0.089	0.180	0.066
LL	3.3	24	0.000	1.000	0.230	0.273	0.208	0.229
	3.6	25	0.025	0.998	0.192	0.267	0.202	0.262
	3.7	19	0.051	0.520	0.121	0.112	0.099	0.047
	4	6	0.145	0.276	0.187	0.047	0.164	0.199
	5	56	0.104	0.982	0.179	0.163	0.102	0.094
	6	51	0.115	0.473	0.214	0.082	0.165	0.074

Fig.1. Al/Al+Cr ratio of spinel group minerals in L-chondrites.

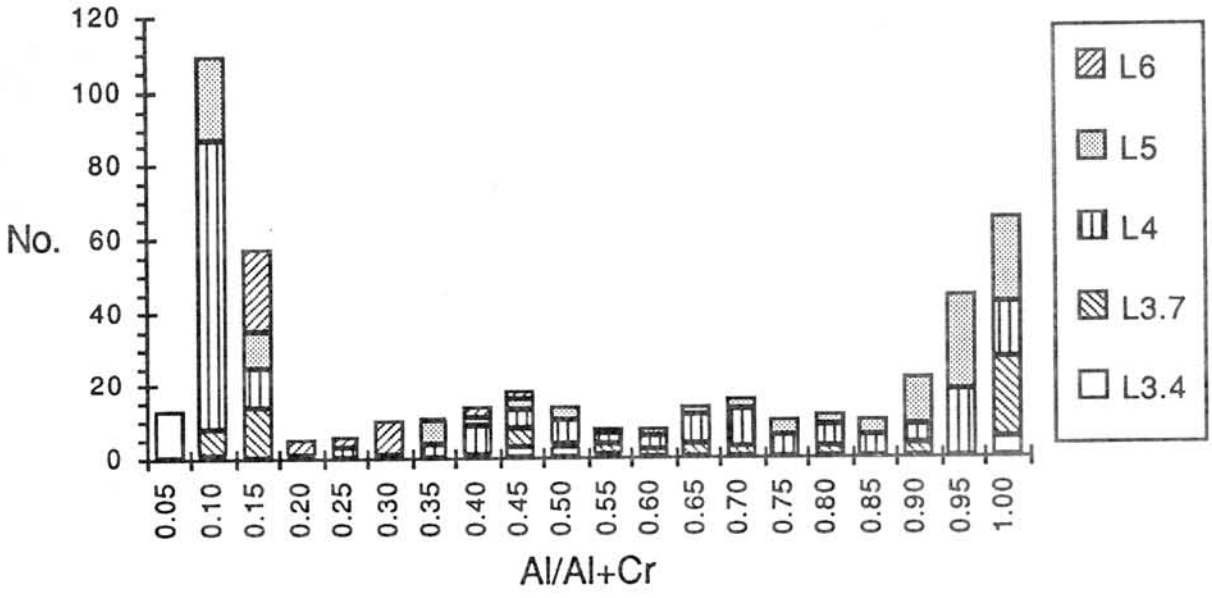

PETROLOGY AND MINERALOGY OF ANTARCTIC AUBRITES, Y-793592 AND ALH-78113, IN COMPARISON WITH NON-ANTARCTIC AUBRITES AND E-CHONDRITES.

KIMURA M.[1], LIN Y-T.[2], IKEDA Y.[1], EL GORESY A.[3], YANAI K.[4] and KOJIMA H.[4]. 1) Ibaraki University, Mito, 2) Institute of Geochemistry, Guanzhou, China, 3) Max-Planck Institut, Germany, Heidelberg, and 4) Natil. Inst. Polar Res., Tokyo.

The first Yamato aubrite Y-793592 [1] and ALH-78113 were mineralogically and petrologically studied. Some minerals in non-Antarctic aubrites and EH-chondrites were also analyzed for comparison. Y-793592 and ALH-78113 are breccias consisting of medium to coarse-grained fragments of orthoenstatite, up to 5mm, with fine-grained matrix. Matrices of both aubrites consist of enstatite fragment with minor diopside, olivine, feldspar, a silica mineral, glass, kamacite, taenite, schreibersite, troilite, alabandite, djerfisherite and daubreelite. All these phases are ≤ 200μ in size.

Enstatite ($En_{97.8\text{-}99.8}$ $Fs_{0.0\text{-}0.2}$ $Wo_{0.2\text{-}2.2}$) is the predominant mineral in Y-793592. Diopside ($En_{51.8\text{-}56.6}$ $Fs_{0.0\text{-}0.1}$ $Wo_{43.3\text{-}48.2}$) occurs in matrix. Most of plagioclase in Y-793592 are sodic ($Ab_{88.9\text{-}97.4}$ $An_{0.0\text{-}4.1}$ $Or_{2.2\text{-}4.8}$), but some plagioclases are rich in CaO ($An_{7.2\text{-}23.1}$). Y-793592 commonly has roedderite. This is the first discovery from aubrites. They always occur in matrix, and have 71.3-72.6% SiO_2, 0.4-0.9 Al_2O_3, 0.0-0.1 FeO, 19.1-19.9 MgO, 0.0-0.2 CaO, 3.1-3.4 Na_2O and 4.2-4.9 K_2O. Kamacite in Y-793592 has 0.0-0.6% Si and 2.4-5.3 Ni. Taenite has 0.2% Si and 34.5 Ni. Schreibersite has 16.7% Ni. Troilite contains 0.1-8.5% Ti. A few grains of Na-Cr-sulfide, which have 0.7-3.2% Na, 0.4-0.8 K, 35.4-42.3 S and 25.3-34.3 Cr, occur in matrix. Y-793592 contains alabandite and djerfisherite. Both minerals suffered severe terrestrial weathering.

Compositional range of most of enstatite in ALH-78113 is $En_{97.8\text{-}99.8}$ $Fs_{0.0\text{-}0.6}$ $Wo_{0.1\text{-}2.2}$. Coarse-grained enstatite has thin lamellae of diopside up to 5μ in thickness. Diopside ($En_{51.5\text{-}59.4}$ $Fs_{0.0\text{-}0.5}$ $Wo_{44.2\text{-}48.0}$) has often lamellae of enstatite. Plagioclase is heterogeneous in composition ($Ab_{28.4\text{-}97.6}$ $An_{0.0\text{-}70.6}$ $Or_{0.2\text{-}5.2}$). Kamacite has 0.0-0.4% Si and 1.5-5.8 Ni. Taenite has 0.1-0.3% Si and 38.8-51.4 Ni. Schreibersite contains 22.1-58.8% Ni. Djerfisherite in ALH-78113 has 0.1-0.7% Na, 8.1-9.2 K, 48.6-50.3 Fe, 3.5-4.4 Ni and 0.9-1.5 Cu. Some alabandites in matrix have thin lamellae, 1-2μ in thickness, probably of troilite. Alabandite has 0.3-0.6% Mg, 47.2-54.3 Mn and 7.0-14.4 Fe. Troilite is frequently accompanied with daubreelite as lamellae, 2-10μ in thickness, and has 0.4-1.7% Ti.

ALH-78113 has 200-300μ dark-colored and irregular-shaped pockets, which are aggregates of low-Ca pyroxene, olivine, diopside, plagioclase and glass with abundant opaque minerals (mainly kamacite and troilite) (hereafter, dark pocket). Olivine and low-Ca pyroxene usually have euhedral forms in the dark pockets. FeO-bearing low-Ca pyroxene (up to $Fs_{20.7}$), which has higher FeO than reported before from aubrites [e.g., 2], occur only in the dark pockets. Some of them show normal zoning toward the FeO-rich rims. A dark pocket has a K-feldspar ($Ab_{11.5}An_{0.1}Or_{88.4}$). This is also the first discovery from aubrites. The texture of the dark pocket is dissimilar

to microporphyritic clasts in Norton County [2]. The dark pockets may have formed during *in situ* melting, probably by shock-induced heating.

Djerfisherite occurs in Y-793592, ALH-78113, Bustee, Peña Blanca Spring, Cumberland Falls, Khor Temiki and Aubres. They are characterized by the low contents of Cu (0.9-2.3%) and Na (<0.7), and high content of Ni (0.4-5.5), relative to those in EH3-5 chondrites (1.3-7.4% Cu, 0.05-1.9 Na and 0.2-3.1 Ni). Y-793592 and Bustee have a few grains of Na-Cr-sulfide, and all of them are similar in composition to Na-Cr-sulfides in EH-chondrites, 1.1-2.1 Na, 0.2-0.7 K, 32.7-39.3 Cr and 40.6-48.3 S in ALH-77295 (EH3), and not to schöllhornite in Norton County [3].

Daubreelites in Y-793592, ALH-78113, Bustee and Khor Temiki are characterized by the lower contents of Zn (0.0-0.3%, 0.0-0.3, 0.05> and 0.1) than those in EH chondrites (0.7-8.1) except for those in South Oman (0.0-0.3). Zn prefers daubreelite to the other phases, except for rare sphalerite, in enstatite meteorites. Wolf et al. [4] reported the depletion of volatile elements such as Zn and In in aubrite, and suggested that a parent body of aubrite is depleted in volatile elements. The low content of Zn in daubreelite may reflect the depletion of volatile elements in aubrite precursor materials.

Roedderite may have formed under an Al_2O_3-depleted condition. For example, Indarch (EH4) seems to have a higher amount of roedderite than the other EH-chondrites, and it has the lowest bulk ratio of atomic Al/Al+Na+K (0.46) among EH-chondrites [5]. Fractionation of some Al_2O_3-phase may have resulted in the depletion of Al_2O_3 relative to alkali elements, leading to formation of roedderite in EH-chondrite [6]. Thus, the presence of roedderite in Y-793592 suggests that Al_2O_3 may have also fractionated in the precursor material of aubrites during nebular condensation process or magmatism.

Equilibrium temperature obtained by coexisting kamacite and taenite in ALH-78113 is ~500°C using the method of Afiattalab and Wasson [7]. Equilibrium temperature for coexisting kamacite and schreibersite in ALH-78113 is 400-500°C after the Fe-Ni-P phase diagram [8]. These low equilibration temperatures suggest that ALH-78113 may have cooled slowly, which is consistent with the presence of lamellae in enstatite, diopside, troilite and alabandite. Y-793592 has no mineral pairs for such geothermometers. However, rare occurrence of lamellae in pyroxenes and sulfides suggests more rapid cooling than ALH-78113.

References: [1] Yanai K. (1992) Proc. NIPR Symp. Antarc. Meteorites (in press). [2] Okada A., Keil K., Taylor G.J. and Newsom H. (1988) Meteoritics, 23, 59. [3] Okada A., Keil K., Leonard B.F. and Hutcheon I.D. (1985) Am. Mineral., 70, 638. [4] Wolf R., Ebihara M., Richter G.R. and Anders E. (1983) GCA, 47, 2257. [5] Kallemeyn G.W. and Wasson J.T. (1986) GCA, 50, 2153. [6] Ikeda Y. (1989) Proc. NIPR Symp. Antarc. Meteorites, 2, 109. [7] Afiattalab F. and Wasson J.T. (1980) GCA, 44, 431. [8] Romig A.D.and Goldstein J.I. (1980) Met. Trans., 11A, 1151.

GEOCHEMICAL AND MINERALOGICAL STUDY OF GABBROIC LUNAR MARE METEORITES ASUKA-881757 (Asuka-31) AND YAMATO-793169.

Christian KOEBERL[1], Gero KURAT[2] and Franz BRANDSTÄTTER[2]

[1]*Institute of Geochemistry, University of Vienna, Dr.-Karl-Lueger-Ring 1, A-1010 Vienna, Austria;*
[2]*Naturhistorisches Museum, Postfach 417, A-1014 Vienna, Austria.*

1. INTRODUCTION

The collection of lunar meteorites in Antarctica continues to yield more samples every year, and is growing in importance augmenting the presently available lunar sample collection. Eleven lunar meteorites have been recovered so far by Japanese and American expeditions to Antarctica, one more was found in Australia. Samples have been recovered from several geographically quite different locations in Antarctica. The first samples recovered have all originated from the lunar highlands, and are of anorthositic composition. The question regarding the number of individual source regions on the moon that are represented by the known lunar meteorites is of great importance. Recently, two new lunar meteorites were recovered from the MacAlpine Hills (MAC88104/88105; paired). These samples are very similar to other highlands meteorites, such as ALHA81005, Y-791187, and Y-82192/3 (LINDSTROM et al., 1991b,c; KOEBERL et al., 1991a; PALME et al., 1991), but the different finding location and exposure histories preclude pairing with the other samples (e.g., EUGSTER et al., 1991).

Elephant Moraine (EET) 87521 turned out to be the first lunar meteorite predominantly composed of mare components (WARREN and KALLEMEYN, 1989; DELANEY, 1989). Previous to this discovery, anorthositic highland rocks (which are believed not to be a predominant rock type on the lunar surface) dominated the lunar meteorite collection. This has now changed: after the identification of EET87521, Y-793274, a very small sample (8.66 g), was first thought to be of anorthositic (highlands) provenance as well (YANAI and KOJIMA, 1987), but more detailed consortium studies (KOEBERL et al., 1991b; LINDSTROM et al., 1991a) found that it is a mixture of mare and highlands components at a ratio of about 2:1. It may have originated from an impact that occurred at a mare/highlands boundary, or penetrated through a thin mare layer to underlying highlands.

Furthermore, Y-793169 and Asuka-31, have recently been preliminarily classified as mare rocks, possibly of VLT heritage. The first descriptions of Asuka-31, a gabbroic lunar meteorite, were provided by YANAI (1990a,b,c). Y-793169 was first reported to be of lunar origin by YANAI et al. (1987). Thus there are now four samples of predominantly mare provenance. These meteorites were the subject of recent studies (started in 1991/2), initiated by the National Institute of Polar Research (leaders: H. Takeda and K. Yanai). A consortium study of Asuka-881757 (Asuka-31) and Yamato Y-793169 has recently been organized. Due to the small size and preciousness of the samples, only a very limited amount of material was available, and only a small number of consortium members received samples. Samples became available in early 1992.

Asuka-881757 (Asuka-31) was discovered on December 20, 1989, on the northeastern end of the Nansen Ice Field, about 130 km south of the Japanese Asuka Station (YANAI, 1991c). It weighed 442.12 g and measured 8.0x8.0x5.8 cm and seems to be half of the original stone, partly covered by a smooth black fusion crust. In this abstract we describe first results of our geochemical, petrological, and mineralogical studies of samples of the lunar meteorites Asuka-881757 (Asuka-31) and Yamato Y-793169.

2. SAMPLES AND ANALYTICAL METHODS

We have received sample Asuka-881757 (Asuka-31) in two forms, first (,81) as a homogeneous powder, which cannot be used for any petrological or mineralogical studies, and later split ,111, a coarse-grained sample remaining from crushing the original samples, intended to allow some petrological analyses. Unfortunately, Y-793169 was received only as a homogeneous powder, prepared at the NIPR in Tokyo, thus not enabling us to do any mineralogical and petrological studies.

Nine individual samples of Asuka-881757 (Asuka-31) were analyzed by neutron activation analysis. Two splits of sample Asuka-881757,81 were used for bulk trace element analyses by instrumental neutron activation analysis (INAA). Most of the INAA methods have been described previously (see., e.g., KOEBERL et al., 1991a,b). The sample bulk1 weighed 108.30 mg, sample bulk2 126.25 mg. Our allocation of Y-793169 was split in two subsamples of 8.39 and 10.42 mg, which were used for bulk trace element analysis. From

the sample Asuka-881757,111, a number of crystals and fragments have been selected under the stereo microscope. We selected two batches of clear crystals (CL, CL2), one of yellowish crystals (YC), two black samples (BL, BL2), and one greyish lithology (LH). Sample weights are given in table 1. One additional sample, a small orange fragment (OY), which was obviously unique, was also found. Because it was so small (31 μg), this sample was irradiated separately at a high flux reactor (Forschungszentrum Seibersdorf) at a neutron flux of 6.10^{13} n/cm²s for about 120 hours.

After the INAA measurements and several months cooling time, polished sections of samples CL, CL2, BL, BL2, YC, LH, and OY were prepared and studied by optical microscopy, electron microscopy, and electron probe microanalysis. The crystals, fragments, and lithologies were analyzed with an ARL-SEMQ electron microprobe following routine procedures. SEM studies and BSE images were obtained with a Jeol JSM-6400 scanning electron microscope.

3. RESULTS AND DISCUSSION

The broken interior of Asuka-881757 is very coarse grained, consisting of brownish pyroxenes, translucent plagioclase, and black ilmenites. Some adhering brownish and greenish glassy melts (impact derived?) were observed in the hand specimen when one of the authors (CK) examined it at the NIPR. Unfortunately, the impact glasses were not available for analysis.

The results of the analyses for selected major elements, and the complete trace element data, are given in Table 1. Fig. 1 shows the provenance of the sample from bulk Fe/Mn contents, clearly confirming a lunar origin for A-881757. According to YANAI (1991c), the whole rock petrography shows that A-881757 consists mainly of plagioclase (maskelynitized) and pyroxene, and some ilmenite and troilite, with traces of olivine, apatite, and Ni-Fe metal; it shows gabbroic texture. The petrology and bulk chemical data support this view; A-881757 is clearly an unusual lunar mare basalt, unlike most samples retrieved by the Apollo and Luna missions. Its bulk Fe content is higher than that of any other lunar meteorites; the bulk chemical composition is somehow compatible with that of a VLT mare basalt. This is demonstrated in Fig. 2, where A-881757 is compared with Y-793274. The two samples differ mainly in Fe content.

Table 1 also gives the trace element composition of the subsamples selected from A-881757,111. The mineralogical studies of these samples are still in progress, but preliminary results can be given as follows.

Sample A31-CL. This sample consists of 3 translucent (clear) fragments of shocked plagioclase (maskelynite). It is highly anorthitic and contains a few small grains of heterogeneous, Fe-rich pyroxene and some patches of mesostasis (very Fe-rich pyroxene with about 39 wt% FeO, ilmenite, fayalite, and silica).
Sample A31-CL2. Very similar to A31-CL; this sample consists of 4 highly anorthitic maskelynites with similar inclusions of pyroxene, fayalite, ilmenite, and silica. Na_2O contents of maskelynite range from 0.4 - 1.8 wt%.
Sample A31-BL. This sample consists of 2 irregular black fragments of which one is mainly ilmenite with some pyroxene, Na-rich maskelynite, fayalite, and troilite attached. The second fragment consists of medium-grained mesostasis (with meta-igneous texture) consisting of fayalite, ilmenite, silica, and FeO-rich pyroxene with small inclusions of troilite.
Sample A31-BL2. This batch consists of 7 black, irregular fragments of up to 1.5 mm longest dimension. They are very similar to sample BL and consist mainly of fayalite, ilmenite, maskelynite (1.5 - 2.2 wt% Na_2O), silica, and a coarse-grained Ca-phosphate (probably apatite).
Sample A31-LH. It consists of two irregular, reddish-brown translucent fragments of 1-1.5 mm size; the fragments are similar to those of sample BL but consist mostly of Fe-rich pyroxene with few troilite and some metal inclusions. A small batch of melt, presumably of local origin, is attached to one of the fragments. There are some metal droplets in this melt.
Sample A31-YC. This sample consists of 3 mostly clear to yellowish transparent maskelynite fragments which contain a few pyroxenes. The yellow color stems from colored cracks (one fragment may be glass).
Sample A31-OY. This unusual orange fragment, which turned dark under irradiation, is of reddish-brown color under the microscope; it is optically isotropic and soft. EDX analyses show that is composed predominantly of carbon. The trace element data are very puzzling: high selenium, but rare earth elements near chondritic values. The origin of this object is not clear, but we cannot exclude contamination from the sample preparation at the NIPR. However, this does not readily explain the trace element composition.

The mineralogy and mineral chemistry of the separates from A-881757,111 is that of a coarse-grained gabbroic rock of VLT composition as described by YANAI (1991c). The texture of the mesostases suggests mild metamorphic (autometamorphic?) recrystallization. Mineral compositions are therefore still

highly unequilibrated. Compositional ranges found by us correspond to those found by YANAI (1991c). The trace element contents found in the mineral separates and fragments correspond closely to the mineralogical findings. Fig. 3 shows some of the chondrite normalized REE patterns; the bulk REE pattern is relatively flat with no clear Eu anomaly. The samples CL, CL2, and YC are, however, dominated by a distinct positive Eu anomaly, in agreement with their plagioclase mineralogy.

The results for Y-793169 are still preliminary; the trace element compositions are somewhat similar to those of A-881757. Some results are: Na: 0.22 wt%, K: 0.045 wt%, Hf 2.8 ppm, REE about 20% higher than in A-881757. Counting is still in progress. The study of lunar meteorites continues to contribute essential details towards a better understanding of the composition and history of the lunar surface.

Acknowledgements: We are grateful to the NIPR, particularly Dr. K. Yanai, and to Prof. H. Takeda, for samples and discussion.

REFERENCES

DELANEY, J.S. (1989) Lunar basalt breccia identified among Antarctic meteorites. Nature, **342,** *889-890.*

EUGSTER, O., BEER, J., BURGER, M., FINKEL, R.C., HOFMANN, H.J., KRÄHENBÜHL, U., MICHEL, T., SYNAL, H.A., and WÖLFLI, W. (1991) History of paired lunar meteorites MAC88104 and MAC88105 derived from noble gas isotopes, radionuclides, and some chemical abundances. Geochim. Cosmochim. Acta **55,** *3139-3148.*

KOEBERL, C., KURAT, G., and BRANDSTÄTTER, F. (1991a) MAC88105 - A regolith breccia from the lunar highlands: Mineralogical, petrological, and geochemical studies. Geochim. Cosmochim. Acta **55,** *3073-3087.*

KOEBERL, C., KURAT, G., and BRANDSTÄTTER, F. (1991b) Lunar meteorite Yamato-793274: Mixture of mare and highland components, and barringerite from the moon. Proc. NIPR Symp. Antarct. Meteorites **4,** *33-55.*

LINDSTROM, M.M., MITTLEFEHLDT, D.W., MARTINEZ, R.R., LIPSCHUTZ, M.E., and WANG, M.-S. (1991a) Geochemistry of Yamato 82192, 86032 and 793274 lunar meteorites. Proc. NIPR Symp. Antarct. Meteorites, **4,** *12-32.*

LINDSTROM, M.M., SCHWARZ, C., SCORE, R., and MASON, B. (1991b) Lunar meteorites MAC88104/5: General description and consortium overview. Geochim. Cosmochim. Acta **55,** *2999-3007.*

LINDSTROM, M.M., WENTWORTH, S., MARTINEZ, R.R., McKAY, D., WANG, M.-S., and LIPSCHUTZ, M.E. (1991c) Geochemistry and petrology of MAC88104/5 lunar meteorite. Geochim. Cosmochim. Acta **55,** *3089-3103.*

PALME, H., SPETTEL, B., JOCHUM, K.P., DREIBUS, G., WEBER, H., WECKWERTH, G., WÄNKE, H., BISCHOFF, A., and STÖFFLER, D. (1991) Lunar highland meteorites and the composition of the lunar crust. Geochim. Cosmochim. Acta. **55,** *3105-3122.*

WARREN, P.H., and KALLEMEYN, G.W. (1989) Elephant Moraine 87521: The first lunar meteorite composed of predominantly mare material. Geochim. Cosmochim. Acta, **53,** *3323-3330.*

YANAI, K. (1990a) Anorthositic gabbro: Cumulate meteorite from Antarctica. Lunar and Planetary Science XXI. Houston, Lunar Planet. Inst., 1365-66.

YANAI, K. (1990b) Asuka-31: Gabbroic cumulate originated from lunar mare region. Papers presented to the Fifteenth Symposium on Antarctic Meteorites, May 30-June 1 1990. Tokyo, Natl. Inst. Polar Res., 119-121.

YANAI, K. (1990c) Gabbroic meteorite Asuka-31: Preliminary examination of a new type of lunar meteorite in the Japanese collection of Antarctic meteorites. Proc. Lunar Planet. Sci. **21,** *317-324.*

YANAI, K., and KOJIMA, H. (1987) New lunar meteorite: Yamato-793274. Papers presented to the Twelfth Symposium on Antarctic Meteorites, June 8-10, 1987. Tokyo, Natl. Inst. Polar Res., 17-18.

YANAI, K., KOJIMA, H., KOEBERL, C., GRAHAM, A., and PRINZ, M. (1987) Photographic Catalog of Antarctic Meteorites. Tokyo, Natl. Inst. Polar Res., 298 pp.

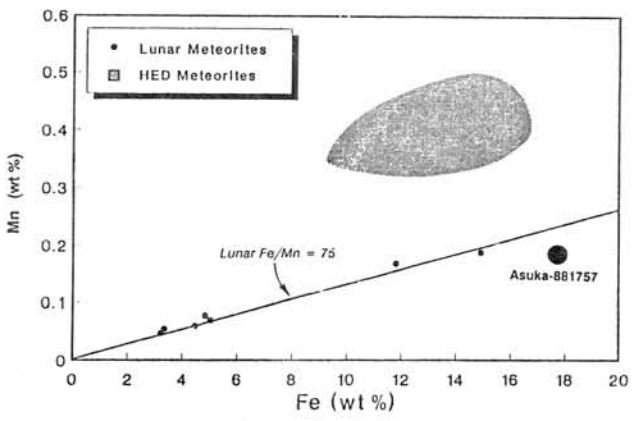

Fig. 1. *Fe-Mn ratio in lunar meteorites compared to basaltic meteorites. The group of lunar meteorites plotting between about 3-5 wt% Fe are highland meteorites.*

Table 1. *Major and trace element contents of 2 bulk and 7 mineral samples of A-881757. All data in ppm, except as noted.*

	Bulk1	Bulk2	A31-BL	A31-BL2	A31-CL	A31-CL2	A31-LH	A31-YC	A31-OY
Weight (mg)	108.3	126.25	0.56	2.87	2.09	4.01	2.81	0.75	0.031
Na (%)	0.22	0.21	0.14	0.018	0.73	0.073	0.032	0.78	0.001
K (%)	0.031	0.03	0.53	0.01	0.01	0.02	0.02	0.01	<0.04
Sc	101	98	141	46.3	3.89	3.15	156	11.7	1.05
Cr	1930	1850	1270	36800	62	63	3890	163	19.8
Fe (%)	18.1	17.6	41.1	50.7	1.68	0.96	23.4	2.69	0.27
Co	27.9	27.9	53.8	48.6	65.1	3.31	83.3	16.2	1.84
Ni	60	45	400	150	<100	20	150	150	13
Zn	3	2	<50	30	17	15	28	20	638
Ga	2.5	3	7.5	8	<2	<1.5	3.5	<2	0.04
As	0.065	0.06	0.22	0.14	0.07	0.02	0.03	0.13	<0.4
Se	<0.7	<0.5	<1.5	0.8	<0.6	<0.6	<3	0.6	219
Br	0.1	0.12	0.05	0.06	0.03	0.02	0.02	0.09	0.6
Rb	2.3	2.8	6	4	<6	0.95	7	<10	0.26
Sr	110	120	<200	120	730	750	140	600	<10
Zr	40	50	<600	260	110	65	<50	280	<10
Ag	<0.2	<0.2	<1	<0.4	<1	0.09	<0.8	<0.2	<0.1
Sb	<0.04	<0.03	0.065	0.028	0.01	0.01	0.046	0.01	0.25
Cs	0.038	0.037	<0.2	<0.1	0.018	0.012	<0.1	<0.1	n.d.
Ba	30	25	<20	15	31	20	84	40	11
La	3.75	3.64	2.57	2.94	0.49	0.25	1.47	0.65	0.22
Ce	11.5	10.3	11.9	7.2	1.38	0.85	4.95	2.2	0.51
Nd	8.9	7.8	11	5.7	1	0.57	4.6	<2	0.3
Sm	2.96	2.81	4.15	1.78	0.23	0.13	1.79	0.58	0.079
Eu	1.07	1.12	0.82	0.37	2.29	2.17	0.12	2.57	0.066
Gd	3.86	3.35	7.3	1.8	<0.4	0.2	2.4	<1	0.12
Tb	0.81	0.72	1.58	0.38	0.07	0.048	0.51	0.13	0.025
Dy	5.3	4.5	11.4	3.4	0.35	0.25	3.7	0.8	n.d.
Tm	0.49	0.36	1.09	0.52	<0.1	<0.05	0.38	<0.1	<0.03
Yb	3.64	2.94	8.15	3.93	0.18	0.13	2.65	0.49	0.07
Lu	0.56	0.49	1.24	0.61	0.012	0.013	0.41	0.062	0.009
Hf	2.37	2.05	5.41	5.74	0.13	0.045	0.92	0.19	0.02
Ta	0.23	0.22	1.61	0.78	0.09	0.06	0.21	0.16	0.02
W	0.084	0.073	0.2	0.1	0.07	0.06	0.21	0.38	n.d.
Ir (ppb)	<1	0.3	31	15	<4	<2	<3	<5	0.4
Au (ppb)	0.3	0.2	1.4	0.8	0.4	0.6	1.5	0.2	0.8
Hg	<2	<2	<8	<4	<9	<3	<10	<12	n.d.
Th	0.43	0.42	2.93	2.64	0.3	0.21	0.21	0.28	0.029
U	0.21	0.11	0.55	0.095	0.09	0.03	0.09	0.11	<0.05
K/U	1476	2909	9636	642	733	5000	1889	909	
Zr/Hf	16.88	24.39		45.30	846	1444		1474	
La/Th	8.72	8.67	0.88	1.11	1.63	1.19	7.00	2.32	7.59
Hf/Ta	10.30	9.32	3.36	7.36	1.44	0.75	4.38	1.19	1.00
Th/U	2.05	3.82	5.33	27.79	3.33	7.00	2.33	2.55	
LaN/YbN	0.70	0.84	0.21	0.51	1.84	1.30	0.37	0.90	2.12
Eu/Eu*	0.97	1.12	0.46	0.63		41.13	0.18		2.07

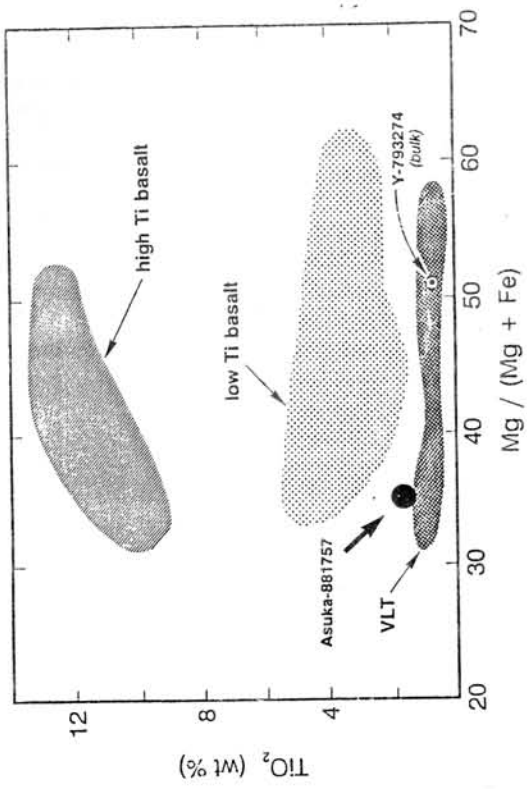

Fig. 2. *Bulk characterization of Asuka-881757 as a VLT mare meteorite.*

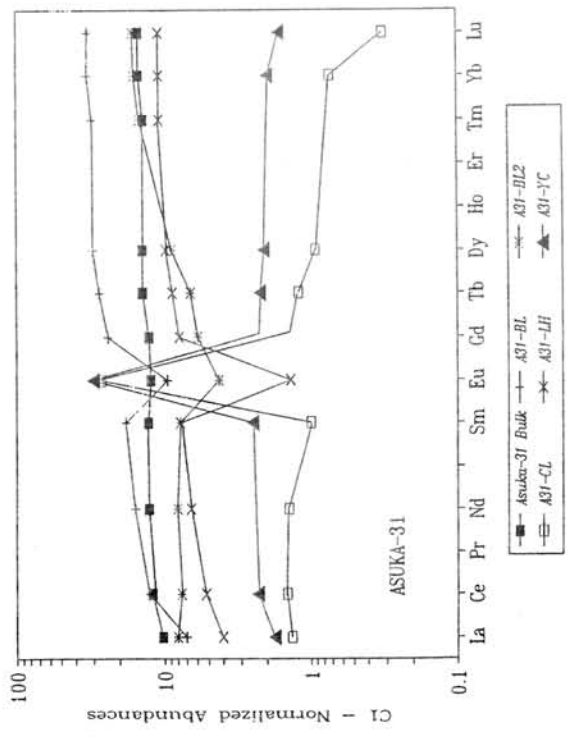

Fig. 3. *Chondrite-normalized REE abundance patterns for A-881757: bulk sample and selected mineral fragments.*

THE FORMATION AND EVOLUTION OF THE CONCENTRIC-RING GROWTH PATTERN OF FeNi METAL CRYSTALLIZATION FROM SHOCK MELT IN SPACE

LI Zhaohui [1], XIE Xiande [1], and ZHANG Datong [2]

1) Institute of Geochemistry, Academia Sinica, Guangzhou Branch, Wushan, Guangzhou, 510640 China
2) South China University of Technology, Guangzhou, 510641 China

INTRODUCTION We have, for the first time, discovered the tetra-concentric-ring growth pattern of FeNi metal crystallization from shock melt in the severely shocked and partly melted Yanzhuang H6 chondrite [1]. The black melt phase contains round and elliptic FeNi-FeS blobs of various sizes ranging from 5 μm to 7mm. Since the melting, cooling and recrystallization of FeNi metal occured in the environment of microgravity, high vacuum and superlow temperature of the space, the Yanzhuang chondrite serves as a valuable specimen for studing the mechanism of crystallization of FeNi metal in space.

The purposes of the present study are: 1) characterization of the microstructures of the surface of FeNi metal blobs and grains, and 2) characterization of the formation and evolution of the tetra-concentric-ring growth pattern of FeNi metal crystallization under microgravity condition.

EXPERIMENT The sample under study is a FeNi-FeS grain Y-1 which is collected from the black melt vein in Yanzhuang No.3 meterorite by hand picking after the sample was mechanically crushed. The grain Y-1 is 0.420 g in weight and 6 mm in length (Fig.1). The surface microstructures for the grain Y-1 wre studied by a Hitach S-550 scanning electron microscope system.

RESULTS AND DISCUSSION

1) Characterizatics of the metal in the FeNi-FeS grain Y-1.

The characteristics of the metal in the FeNi-FeS grain Y-1 is partly shown in Figures from No.2 to No.5 (except Fig.4 which is from grain Y-2). From these micrographs we can see that the grain Y-1 is constructed by numerous tiny(30-100 μm) dendritic crystallites of various forms, mainly rounded, elliptic, pea-shaped, needle-shaped, spear-like and stalagmite-shaped. These dendritic crystallites build up some typical structures on the surface of grain Y-1. They are dendritic, bears-shaped, cross-shaped and network-like structures.

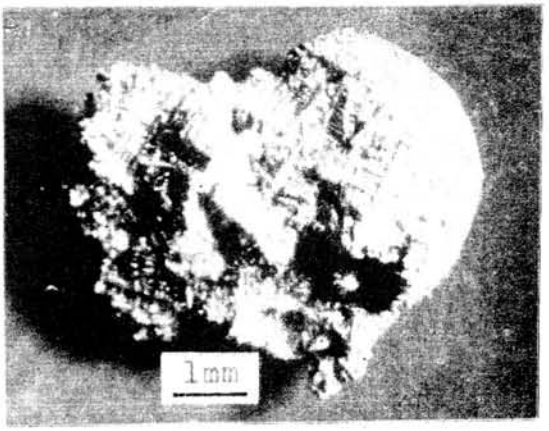

Fig.1 *Micrograph of FeNi-FeS grain Y-1, collected from a black melt vein in Yanzhuang No.3 meteorite.*

For the bears- and cross-shaped structures there exists a tendency of decrease of the grain size from 200μm at the head or at the intersection point of these structures to 5μm at their tails. The dendritic structure in

Y-1 looks quite similar to that in succiononitrile crystallized from supercooled melt [2]. The presence of above mentioned structures reflect fast cooling of the FeNi melt.

2) The formation and evolution of the tetra-concentric-ring growth pattern of FeNi metal crystallization from shock melt.

In order to study the formation and evolution of the growth pattern of FeNi metal crystallization from shock melt, we have systematically observed the surface microstructures on the tips of series of dendritic crystallites, and found very unique growth lines in the form of four concentric rings. On the basis of our SEM study, a five-stage model for the formation and evolution of the tetra-concentric-ring growth pattern of FeNi metal crystallization has been proposed as follows:

a) Initial stage of growing: a cross-shaped shallow groove of 3-5um wide and arc growth lines are formed at this stage, but no concentric rings are observed (Fig. 6, upper right corner).

b) Begining stage of concentric-ring-growing: only two concentric-ring growth lines (~5um wide) are observed on the tips of a dendritic crystallite (Fig.6, in the center). These two lines are seperated by a cross-shaped groove of 2.2-3.0 um in the width.

c) Developing stage of tetra-concentric-ring growth pattern: Fig.7 and Fig.8 show the well developed tetra-concentric-ring growth pattern on the tips of a elongated and a rounded dendritic crystallites respectively. The four concentric rings are also seperated by a 4-5 um wide cross-shaped groove.

d) Two-layer stage of growing: Fig.9 and Fig.10 show the tetra-concentric-ring growth lines on the tips of two layers, e.g., the smaller and younger upper layer grew up out of the elder lower layer, and both they have a common cross-shaped groove which controls the direction and orientation of crystal growth.

e) Multi-layer stage of dendritic crystal growing: As the crystallization from shock melt proceeds, the dendritic crystallite grows up layer by layer rapidly, thus led to the formation of bears-like, cross-shaped and other dendritic structures (Fig.2 and Fig.3).

In the conclusion, we deduce that tetra-concentric-ring growth pattern is a possible fundamental mode of FeNi metal crystallization from shock melt under the environment of microgravity of space and during the process of fast cooling.

Fig.6 SEM image showing the initial (upper right corner) and beginning stage (in the center).

Fig.2 close-up of the surface of the FeNi metal grain Y-1 showing various forms of microcrystallites and surface structures.

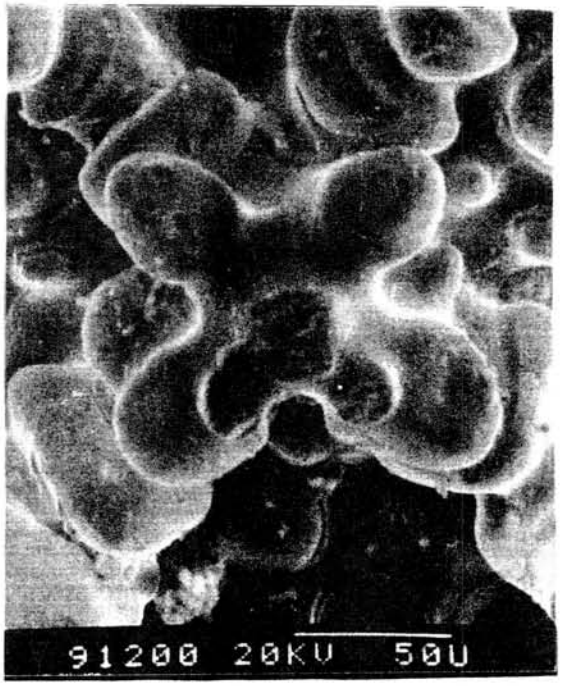

Fig.3 The petal-like microcrystallites developed from the intersection point of a cross-shaped structure.

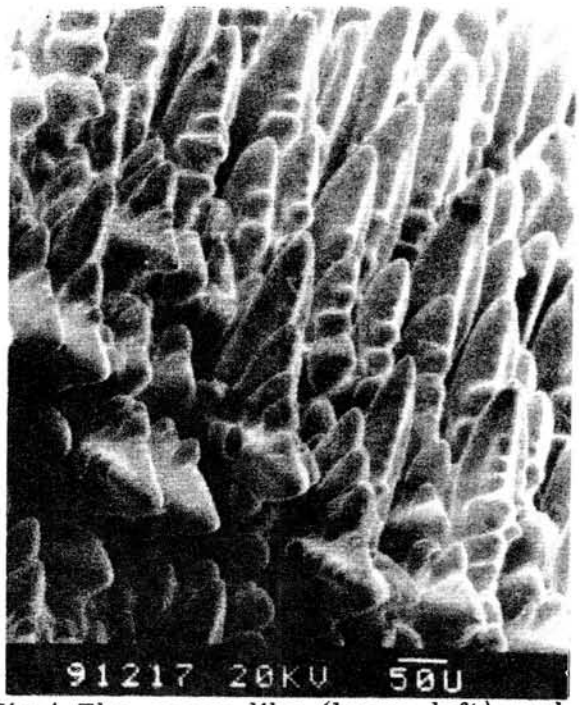

Fig.4 The spear-like (lower left) and stalagmite-shaped microcrystallites of FeNi metal.

Fig.5 The dendritic crystal growing of FeNi metal in grain Y-1.

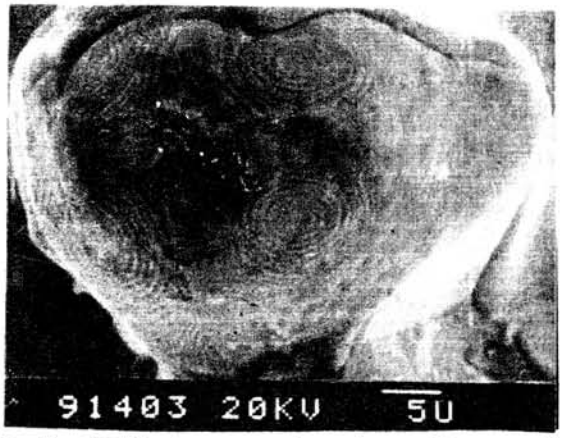

Fig.7 SEM image showing the well developed tetra-concentric-ring growth pattern on the tip of a elongated FeNi crystallite.

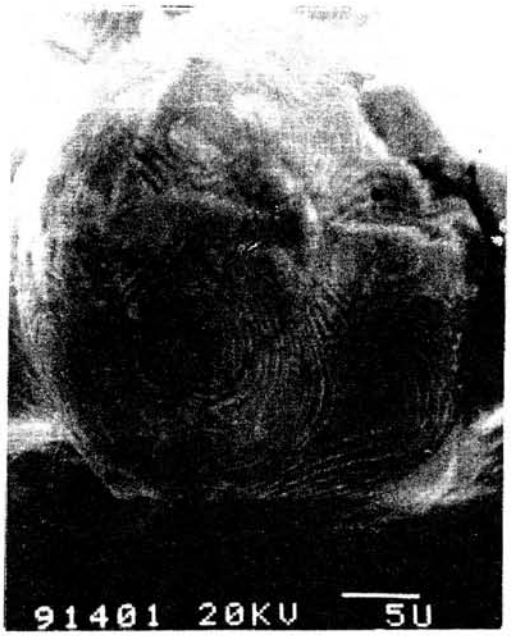

Fig.9 SEM image showing the two-layer stage of growing. the small younger upper layer grows up out of the lower layer.

Fig.8 SEM image showing the well developed tetra-concentric-ring growth pattern on the tip of a round FeNi crystallite.

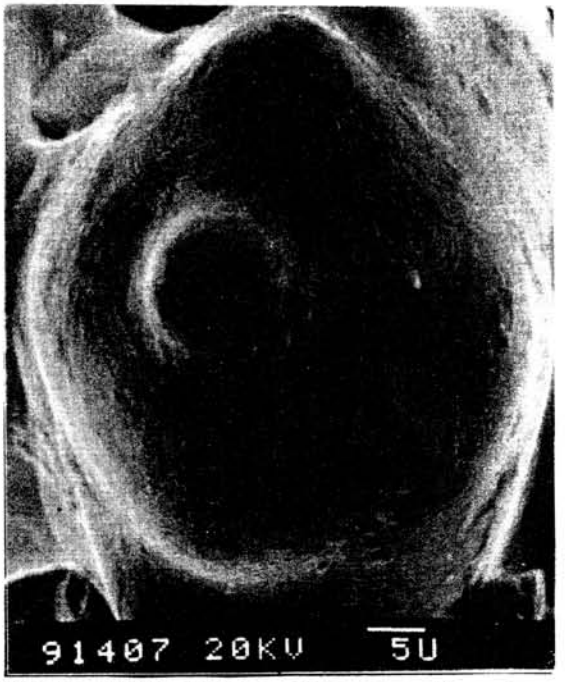

Fig.10 SEM image showing the two-layer stage of growing. the small younger upper layer grows up out of the lower layer.

REFERENCES

[1] *LI Zhaohui, XIE Xiande and ZHANG Datong (1991), Abstracts of the 54th Annual Meeting of Meteorite. Soc., 134-135.*

[2] *Glicksman, M.E. et al (1988), Metallurgical Tran-sactions A, Vol. 19A, 1945-1953.*

CRYSTALLIZATION TYPES OF THE ANTARCTIC METEORITES

Alexey A.Marakushev and Leonid L.Perchuk
Department of Petrology, Moscow State University, Russia

Using the two-pyroxene and olivine-pyroxene parageneses, four mineral types (I-IV) along with the solidus of chondrite meteorite are considered. Type I of the highest temperature reflects mineral assemblages of cosmic objects, such as lunar rocks and similar Antarktic meteorites. Composition of pigeonite reflects quite strong effect of fractionation of Fe during the rapid crystallization of a common volcanic melt. Meteorites of this type are characterized by relatively slow rate of the melt cooling; accumulation of iron is not recorded along with fractionation path. As the result, the $CaSiO_3$ content of pigeonites from the type II meteorites increases while the Fe/Mg ratio decreases during magmatic crystallization. Antarctic ureilites, evcrites, diogenites, howardites belong to this crystallization type. Two- pyroxene types of antarctic meteorites, III and IV, are widely spread among Antarctic meteorites (for example, ordinary chondrites). Their textures and mineral compositions reflect difference in temperature for the type III and type (1V). Relatively low temperatures for ordinary chondrites IV are resulted in high Mg/Fe distribution coefficients for coexisting olivine and orthopyroxene. Fluid inclusion data from ZAREV and other Russia meteorites are discussed in respect of origin of Antarctic meteorites. Intratelluric stage of crystallization is resulted in chondrites of non-equilibrated type III. A model for splitting the chondrite melts into the silicate chondrules and Fe-rich matrix under high fluid pressure is proposed. The temperature regimes of equilibrium crystallization for all four types are considered.

Thus, plutonic (under a fluid pressure) magmatism is resulted in chondrite meteorites, while other cosmic objects including some lunar rocks reflect volcanic facies om magmatism.

GEOCHEMISTRY AND PETROLOGY OF YAMATO HED METEORITES

David W. Mittlefehldt, C23, Lockheed Engineering & Sciences Co., 2400 Nasa Rd. 1, Houston, TX 77058, USA.
Marilyn M. Lindstrom, SN2/Office of the Curator, NASA Johnson Space Center, Houston, TX 77058, USA.

Howardite, eucrite (monomict and polymict) and diogenite (HED) meteorites represent the most extensive suite of crustal magmatic rocks from differentiated asteroids. The basalts, cumulate gabbros and cumulate orthopyroxenites that make up these meteorites or occur as clasts within them provide the most detailed view of igneous processes on the small bodies of the solar system during its earliest epoch. We have initiated petrological characterization and geochemical studies by instrumental neutron activation analysis (INAA) of representative set of Yamato HED samples. The purposes of our studies are to broaden the range of well characterized HED samples, and to further define igneous processes on the HED parent body. The samples we have studied are: diogenites Y-74013, Y-74097, Y-74136, Y-75032 and Y-791199; eucrites Y-793164 and Y-82066; cumulate eucrite Y-791195; polymict eucrites Y-791192 and Y-82049. We report here on our completed INAA work and the preliminary results of our petrologic study.

Diogenites. Yamato diogenites have been divided into two petrologic categories; Types A and B (Takeda *et al.*, 1981; Takeda, 1991). Type A diogenites are granular, recrystallized orthopyroxenites as typified by the first diogenite recovered from Antarctica, Y-6902 (Okada, 1975). Type B diogenites are brecciated pigeonite-plagioclase rocks petrologically intermediate between normal diogenites and cumulate eucrites, and are typified by Y-75032 (Takeda and Mori, 1985). The matrix of the Type B diogenites is black, glassy material composed of devitrified shock melt plus small clastic debris. Pyroxene compositions for the diogenites are displayed in Fig. 1.

We performed INAA on whole rock samples of 3 Type A diogenites, Y-74013, Y-74097 and Y-74136, and 2 Type B diogenites, Y-75032 and Y-791199. In addition, our samples of Y-74013 and Y-74136 contained large (mm-sized) chromite grains, and we separated a few for INAA. For Y-75032, we prepared a lithic clast sample free of glassy matrix, and a sample hand picked to be enriched in the glassy matrix.

The 3 Type A diogenites, Y-74013, Y-74097 and Y-74136, are essentially identical in composition except for slight differences in Cr, Co, Se, which are likely due to inhomogeneous distribution of the minor phases chromite, metal and troilite. Y-74013 has a slightly higher La content, which is probably caused by small differences in the amount of crystallized, interstitial liquid trapped in the sample. The REE data for the Type A diogenites are shown in Fig. 2, compared with a range for samples of the EETA79002 diogenite (Mittlefehldt and Meyers, 1991). Our REE analyses of Type A diogenites agree well with those of Masuda and Tanaka (1978) and Masuda *et al.* (1979) except that our samples have lower La contents. Our La data range from 6.5-14.2 ng/g, while those of Masuda and Tanaka (1978) and Masuda *et al.* (1979) range from 16 to 74.1 ng/g. This difference is likely due to differences in the amount of crystallized, interstitial liquid trapped in the samples. The Type A Yamato diogenites are geochemically indistinguishable from other Antarctic and non-Antarctic diogenites.

The Type B diogenites, Y-75032 and Y-791199, are richer in incompatible trace elements than the Type A diogenites, as illustrated in Fig. 2. The matrix-rich sample of Y-75032 has higher concentrations in the most incompatible elements than does the lithic clast sample; La and Hf are about 2 times higher in the matrix-rich sample compared to the lithic clast. The less incompatible elements Yb and Lu are only about 15% higher in the former, and Sc, which is compatible in pyroxene, is identical in the matrix and lithic clast samples. This suggests that either there is a larger interstitial melt component in the glassy matrix, or that foreign contaminants were introduced into the glassy matrix by impacts.

Our REE data for the Type B diogenites are systematically lower than those of Shimizu and Masuda (1981) for Y-75032. Compared to our Y-75032 clast REE data, Shimizu and Masuda's (1981) REE data are 3.4 times higher for La and 1.4 times higher for Lu. Our Eu datum agree well with that of Shimizu and Masuda (1981). The differences between the samples may be due to inhomogeneous distribution of a trapped, interstitial melt component, as discussed below.

The Type B diogenites are believed to be cumulates intermediate in composition between normal diogenites and cumulate eucrites, possibly forming a single fractional crystallization trend (Takeda and Mori, 1985). The REE pattern for Type B diogenites shows that these samples are not adcumulate rocks, however. Fig. 2 shows the REE pattern for a model pyroxene-plagioclase adcumulate compared to the

Type B diogenites. We calculated the model adcumulate as follows: From the compositions of our bulk samples and mineral compositions determined by electron microprobe (our data for pyroxene, plagioclase compositions from Takeda *et al.*, 1978), we estimated that our samples of Type B diogenites contain between 9-12% plagioclase. We used 10% plagioclase and 90% pyroxene for the model. We used the pyroxene and plagioclase partition coefficients of McKay *et al.* (1986) and Weill and McKay (1975), respectively. We assumed the parent melt had a flat REE pattern at ~25 times CI chondrites in order to approximate the Yb and Lu contents of the Type B diogenites. As can be seen, an adcumulate composed of 90% pigeonite and 10% plagioclase would have a light REE content an order of magnitude lower than measured, and should have a large positive Eu anomaly. The difference between the type B diogenite samples and the model cumulate indicates that either the parent melt of the Type B diogenites was LREE-enriched and had a negative Eu anomaly, or, more likely, that the diogenites contain substantial interstitial liquid trapped in the sample. For comparison, the REE pattern for Binda (Mittlefehldt, 1979), the cumulate eucrite closest in composition to the Type B diogenites (Takeda and Mori, 1985), is shown.

Cumulate Eucrite. Cumulate eucrite Y-791195 is most similar to Serra de Magé among the cumulate eucrites, but is slightly more ferroan, and incompatible trace element rich than the latter. The mean pyroxene in Y-791195 has an mg# (100 * molar MgO/(MgO+FeO)) of 45.4 *vs.* 56.3 for Serra de Magé (Harlow *et al.*, 1979). Pyroxene compositions for Y-791195 are shown in Fig. 1. The REE data for Y-791195 are shown in Fig. 3 and compared to other cumulate eucrites.

Eucrites. Eucrite Y-82066 is similar in composition to Sioux County. Fig. 4 shows the composition of Y-82066 normalized to mean Sioux County for a range of elements. As can be seen, many elements in Y-82066 are within analytical error of mean Sioux County (horizontal line). Note, however, that eucrites can vary considerably, as illustrated by the range observed for analyses of individual samples of Sioux County (stippled field, Fig. 4). Hence, in composition, Y-82066 appears to be a normal, unevolved eucrite of the Juvinas group.

Y-793164 is a more unusual eucrite. This eucrite is more FeO-rich than Juvinas type eucrites, but less ferroan than Lakangaon or Nuevo Laredo. Similarly, Y-793164 is intermediate between the Juvinas group and Lakangaon and Nuevo Laredo in Cr, Sc and REE. This indicates that Y-793164 is an intermediate member of the Nuevo Laredo trend eucrites, and fills an important gap in the eucrite sample suite. On a plot of Sc *vs.* La for eucrites (Fig. 5), Y-793164 is intermediate between Juvinas type eucrites and Lakangaon and Nuevo Laredo, and plots closest to Lakangaon. Vetluga is also a possible member of the Nuevo Laredo trend eucrites (Lindstrom and Mittlefehldt, 1992). Y-82066 plots with the Juvinas group eucrites.

Polymict Eucrites. We have analyzed two HED samples that are classified as polymict eucrites. Polymict eucrites are eucritic breccias containing up to 10% diogenitic component (Delaney *et al.* 1983). Among the elements we determine, Ca and Eu are sensitive indicators of the relative amounts of eucritic and diogenitic material in the polymict breccias because Ca is about 10 times and Eu about 100 times more abundant in eucrites than in diogenites. Fig. 6 is a plot of Ca *vs.* Eu for mean eucrites, polymict eucrites and howardites (compiled by Mittlefehldt), diogenites (Mittlefehldt, 1992) and the Yamato HED samples from this study. The two polymict eucrite samples, Y-791192 and Y-82049, contain substantially more than 10% diogenitic component: Y-791192 contains between 61-67% diogenitic material, while Y-82049 contains between 50-54%. These estimates are based on the Ca and Eu concentrations of the samples compared with those of average basaltic eucrites and diogenites. These samples plot in the field for howardites, and based on the samples we received, Y-791192 and Y-82049 should be classified as howardites. However, polymict eucrites can be inhomogeneous on the scale of the 370-450 milligram samples we received, and additional analyses of several different splits of these meteorites are required before they can be firmly classified.

Pyroxene analyses for Y-791192 and Y-82049 are shown in Fig. 1. Y-82049 contains a wide range of pyroxene compositions from magnesian orthopyroxene similar to Type A diogenite pyroxenes, to ferroan pigeonite similar to basaltic eucrite pyroxenes. Y-791192 has a more limited range in pyroxene composition. Almost all of the large pyroxene clasts we measured are identical in major element composition to Type B diogenite pyroxenes. The ferroan pigeonites from Y-791192 are all from basaltic clasts. Our pyroxene distributions are generally similar to those shown in Yanai and Kojima (1987).

Summary. The Type B diogenites are enriched in the most incompatible elements compared to a model adcumulate, indicating that they contain substantial trapped liquid component. The cumulate eucrite Y-791195 is intermediate in composition between Serra de Magé and Moore County in bulk composition and

pyroxene composition. Eucrite Y-82066 is a Juvinas group eucrite similar in composition to Sioux County, while Y-793164 is an intermediate member of the Nuevo Laredo trend eucrites. The polymict eucrites Y-791192 and Y-82049 contain a large fraction of diogenitic material, and, if our samples are representative, should be classified as howardites. The diogenitic component in Y-791192 appears to be similar to Type B diogenites.

References:

Delaney J.S., Takeda H., Prinz M., Nehru C.E. and Harlow G.E. (1983) The nomenclature of polymict basaltic achondrites. *Meteoritics* **18,** 103-111.

Harlow G.E., Nehru C.E., Prinz M., Taylor G.J. and Keil K. (1979) Pyroxenes in Serra de Magé: Cooling history in comparison with Moama and Moore County. *Earth Planet. Sci. Lett.* **43,** 173-181.

Lindstrom M.M. and Mittlefehldt D.W. (1992) A geochemical study of Russian eucrites and howardites (abstract). *Meteoritics*, submitted.

Masuda A. and Tanaka T. (1978) REE, Ba, Sr and Rb in the Yamato meteorites, with special reference to Yamato-691(a), -692(b) and -693(c). *Mem. Natl. Inst. Polar Res. Spec. Issue No. 8,* 229-232.

Masuda A., Tanaka T., Shimizu H., Wakisaka T. and Nakamura N. (1979) Rare-earth geochemistry of Antarctic diogenites. *Mem. Natl. Inst. Polar Res. Spec. Issue No. 15,* 177-188.

McKay G.A., Wagstaff J. and Yang S.-R. (1986) Clinopyroxene REE distribution coefficients for shergottites: The REE content of the Shergotty melt. *Geochim. Cosmochim. Acta* **50,** 927-937.

Mittlefehldt D.W. (1979) Petrographic and chemical characterization of igneous lithic clasts from mesosiderites and howardites and comparison with eucrites and diogenites. *Geochim. Cosmochim. Acta* **43,** 1917-1935.

Mittlefehldt D.W. and Meyers B. (1991) Petrology and geochemistry of the EETA79002 diogenite (abstract). *Meteoritics* **26,** 373.

Okada A. (1975) Petrologic studies of the Yamato meteorites part 1. Mineralogy of the Yamato meteorites. *Mem. Natl. Inst. Polar Res. Spec. Issue No. 5,* 14-66.

Shimizu H. and Masuda A. (1981) REE, Ba, Sr and Rb abundances in some unique Antarctic achondrites. *Mem. Natl. Inst. Polar Res. Spec. Issue No. 20,* 211-220.

Takeda H. (1991) Comparisons of Antarctic and non-Antarctic achondrites and possible origin of the differences. *Geochim. Cosmochim. Acta* **55,** 35-47.

Takeda H., Miyamoto M., Yanai K. and Haramura H. (1978) A preliminary mineralogical examination of the Yamato-74 achondrites. *Mem. Natl. Inst. Polar Res. Spec. Issue No. 8,* 170-184.

Takeda H. and Mori H. (1985) The diogenite-eucrite links and the crystallization history of a crust of their parent body. *Proc. Lunar Planet. Sci. Conf. 15th, Part 2; J. Geophys. Res.* **90,** C636-C648.

Takeda H., Mori H. and Yanai K. (1981) Mineralogy of the Yamato diogenites as possible pieces of a single fall. *Mem. Natl. Inst. Polar Res. Spec. Issue No. 20,* 81-99.

Weill D.F. and McKay G.A. (1975) The partitioning of Mg, Fe, Sr, Ce, Sm, Eu and Yb in lunar igneous systems and a possible origin of KREEP by equilibrium partial melting. *Proc. Lunar Sci. Conf. 6th,* 1143-1158.

Yanai K. and Kojima H. (1987) *Photographic Catalog of the Antarctic Meteorites.* Natl Inst. Polar Res., 298 pp.

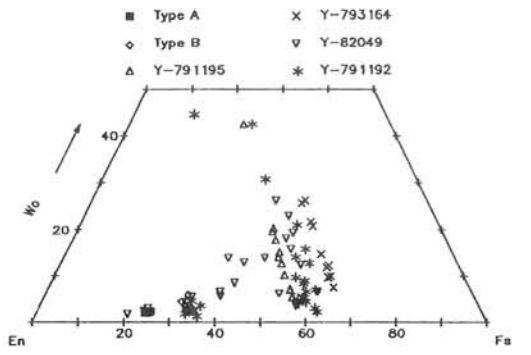

Fig. 1. Pyroxene quadrilateral for Yamato HED meteorites.

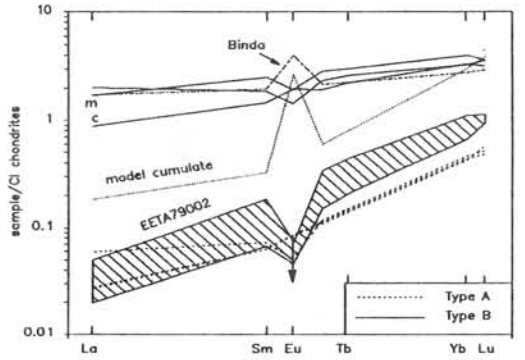

Fig. 2. REE diagram for Yamato diogenites. Lines labeled c and m refer to Y-75032 clast and matrix, respectively. The Binda eucrite (Mittlefehldt, 1979) and a field for 16 samples of EETA79002 (Mittlefehldt and Meyers, 1991) are shown for comparison, as is a calculated model Type B diogenite adcumulate.

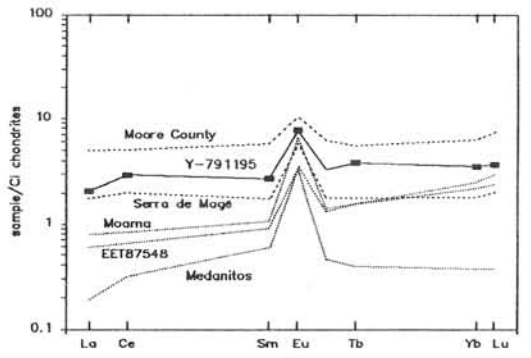

Fig. 3. REE diagram for Y-791195 compared to cumulate eucrites.

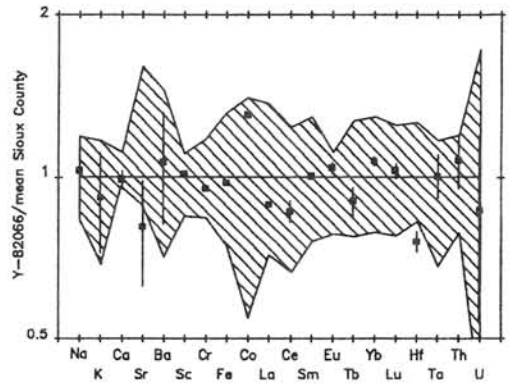

Fig. 4. Y-82066 normalized to mean Sioux County for various elements. The diagonally ruled field represent the range of analyses for Sioux County samples, compiled by Mittlefehldt.

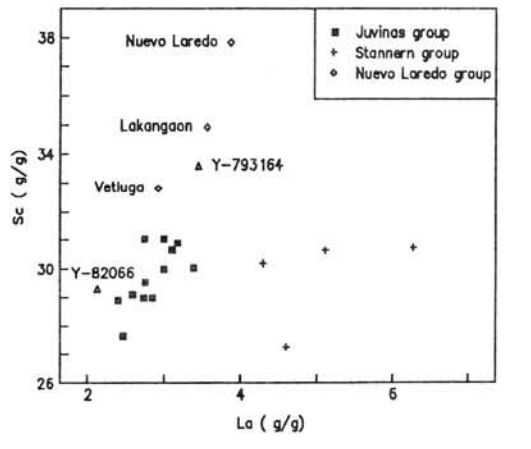

Fig. 5. Sc vs. La for eucrites showing Y-82066 and Y-793164. Eucrite data from a compilation of literature data, except for Vetluga (Lindstrom and Mittlefehldt, 1992).

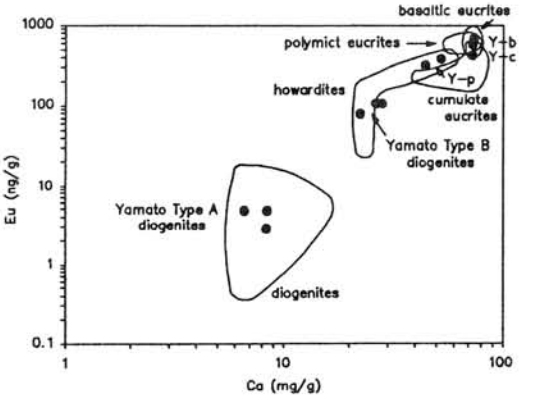

Fig. 6. Ca vs. Eu for HED samples comparing Yamato HEDs from this study with fields for basaltic eucrites, cumulate eucrites, polymict eucrites, howardites (compiled by Mittlefehldt), and diogenites (Mittlefehldt, unpublished). Y-p are polymict eucrites Y-791192 and Y-82049, Y-b are basaltic eucrites Y-793164 and Y-82066, Y-c is cumulate eucrite Y-791195.

SHOCKED QUARTZ, SILICA AND CARBON MATERIALS OF METEORITES, IMPACT CRATERS AND K/T BOUNDARY.

Yasunori MIURA, Toshio KATO and Masashi IMAI
Faculty of Science, Yamaguchi University, Yoshida, Yamaguchi, 753, Japan.

Shocked quartz silica and carbon minerals have been found from meteorites, impact craters and Cretaceous-Tertiary (K/T) boundary, where shocked quartz materials have been discussed by optical directions, mean optical refractive index and X-ray data [1]. The purpose of the present study is presentation of the detailed analytical data of shocked quartz, coesite, stishovite, graphite, lonsdaleite and diamond phases found in meteorites, the K/T boundaries and/or terrestrial impact craters [2,3,4,5].

1. Refractive index data

The previous reported data of optical mean refractive index drop from the normal value down to diaplectic glass value with increasing shock pressure. The similar values of "low" refractive index have been obtained in the K/T boundary and terrestrial impact crater samples.

The discrepancy between optical refractive index and X-ray density with high-precision lies in the fact that "optical bulk data" are produced from "two phases" of shocked quartz crystal and glass phases. Thus "crystal part" of shocked quartz shows "high" X-ray density, whereas mean bulk refractive index of shocked quartz reveals still "low" mixing value with crystal (SQ) and glass (SG) parts. Mean refractive index of mixing crystal and glass is obtained from the following equation:

$$\text{Mean refractive index: } R(m) = R(SQ) + R(SG)$$

2. X-ray power diffraction pattern

X-ray powder diffraction pettern of shocked quartz aggregate reveals that all X-ray peaks are splitted into major "three peaks" composed of low-density quartz (LQ), normal quartz (Q), and shocked quartz with high density (SQ). X-ray peaks of (110), (200), (201), (202) and (211) in the hexagonal cell which have not been observed in optical refractional data are splitted into many peaks.

The X-ray intensity among LQ, Q and SQ phases indicates that the SQ phase shows 36 % to 53 % in six K/T boundary samples [5]. The relative X-ray intensity ratio of shocked quartz to standard rock crystal decreases into 13 % to 37 %, which suggests that shocked quartz materials contain major parts of diaplectic amorphous phases (Gl) in the K/T boundary and impact crater.

3. Density of shocked quartz

The higher values of density-deviation obtained from diaplectic quartz grains are $+0.7\pm0.2\%$ in the Barringer Meteorite crater, $+0.8\pm0.2\%$ in the K/T boundary sample from Clear Creek North (CCN), Colorado, $+0.3\pm0.2\%$ in artificial sandstone crater, $+1.7\pm0.5\%$ in the Zagami achondritic meteorite [4], as shown in Table 1.

Experimental error of density-deviation ρ/ρ_0 is $\pm0.11\%$ at 15 times the measurements of standard rock crystal or CCN K/T shocked quartz. Thus the density-deviation exceeds 0.1% has significant meanings.

4. Atomic structure of shocked quartz

X-ray structure analyses of shocked quartz grains have been carried out on the terrestrial impact craters and CCN K/T boundary samples. Although the peak numbers are limited due to its diaplectic feature, the following results have been obtained:

1) Weakly shocked quartz (ρ / ρ_0=+0.2%) shows largely-deviated O - O atomic distance of -0.87% (compared with that of standard rock crystal) and weakly-deviated Si - O atomic distance of -0.31%.
2) Strongly shocked quartz (ρ / ρ_0=+0.7%) reveals both largely-deviated O - O and Si - O atomic distances of -0.61% and -0.62%, respectively.
3) Main cause of "high" density of shocked quartz is considered to be "shrinkage" of atomic structure.

5. Chemical composition

Chemical composition of shocked quartz phase (SQ) from electron and ion microprobe analyzers shows almost pure silica without Al element, though amorphous silica glassy phases (G2) contain Al contamination (ca.0.5 wt.% Al_2O_3).

6. Characterization of shocked quartz materials

Four major parts of shocked quartz silica aggregates from the K/T boundary and impact crater are divided into amorphous silica glasses (G1), low-density quartz (LQ), normal standard quartz (Q) and high-density shocked quartz (SQ) which have been formed by artificial impact experiments [2,3,4,5,6] in the powder state, as follows:

Shocked quartz aggregate (SQA) = SQ + Q + LQ + G1.

Single grain of SQ type shocked quartz phases consists of crystalline phase (SQ) and diaplectic amorphous regions (G2), as follows:

Shocked quartz grain (SQG) = SQ + G2.

Diaplectic amorphous phases (G2) reveal from coarse-grained silica (as multiple sets of lamellae) to submicroscopic fine-grained silica phases throughout SQG grains. Anomalous experimental data of shocked quartz with high density and shrinkages of atomic arrangements [2,3,4,5,6] are observed only the SQ crystalline phase. Shocked quartz as crystalline mineral means only crystalline SQ phase, whereas mixed shocked silica materials are considered to be "shocked quartz grain (SQG)" or "shocked quartz aggregate (SQA)". The experimental values of mean refractive index and bulk density of shocked quartz materials (i.e. SQA powder of LQ+Q+SQ+G1 phases, and SQG single grain of SQ+G phases), therefore, show bulk data with lower values.

7. Shocked silica phases

Chondritic meteorites from primordial parent body have no silica minerals formed by magmatic evolution. However Zagami SNC achondrites contain higher density shocked quartz (i.e. +1.6% of density-deviation) [7].

Density of fine-grained coesite from the Barringer crater has been obtained in this study. Shocked coesite from Barringer crater shows +0.5% of density-deviation, as listed in Table 1.

Stishovite found at K/T boundary shows high density-deviation of +0.2%, as shown in Table 1 [8].

It is found in this study that fine shocked grains with high density show different size and formation condition with coarse-grained normal standard silica minerals. The high density will be useful indicator of shocked phases.

Table 1. Density data of shocked silica minerals with high density.

Mineral	Density(ρ)	Density-deviation(ρ/ρ_0)	Remarks
1. Shocked quartz			
	2.689(12)*	+1.5(5)	Zagami achondrite
	2.667(4)	+0.8(2)	CCN K/T (U.S.A.)
	2.664(6)	+0.7(2)	Barringer crater
2. Shocked coesite	2.920(10)	+0.5(3)	Barringer(B2W)
3. Shocked stishovite	4.292(2)	+0.2(1)	K/T boundary [7]

* Numbers in parentheses are standard deviations in units of the last decimal place of the data used.

8. Carbon phases

The similar relic phases with high density crystal and amorphous phases formed by impact processes can be found in shocked carbon phases of graphite and diamond.

Shocked graphite with high density can be found in the Barringer craters. The density-deviation is +0.9(%).

Lonsdaleite has been considered to be hexagonal diamond. Shocked lonsdaleite [9] with high-density can be found in Allende (CV3) as intersteller diamond, about +5(%) of density-deviation.

Shocked diamond [10] with high density can be found in ion-beam sputtered diamond, about +2.9(%) of the density-deviation.

Acknowledgements

The present research is supported by the Grant-in-Aid for Scientific Researches of the Japanese Ministry of Education and Science, 1990-1992 of the senior author.

Main references

[1] Bohor B.F., Foord E.E., Modreski P.J. and Triplehorn D.W. (1987) Science, 224, 867-869.
[2] Miura Y. (1991): Shock Waves (Springer-Verlag), 1, 35-41.
[3] Miura Y. (1991): Lunar Planet. Sci. (U.S.A.), 22, 905-908.
[4] Miura Y. and T.Kato (1992): Celestial Mechanics (July issue), 5 pp. (in press).
[5] Imai M. (1992): Master Sci. Thesis, Yamaguchi University, 89 pp.
[6] Miura Y. et al.(1992): Proc. 18th Intern. Symp. of Shock Wave (Springer), 7 pp. (in press).
[7] Miura Y. et al. (1992): Shock Waves, Japan(Tokyo), 255-270; 503-510.
[8] McHone J.F., Niema R.A., Lewis C.F., Yates A.M. (1989): Science, 243, 776-779.
[9] Kitabakake M. and Wada K. (1985): Am. Inst. Physics, 58, 1693-1695.
[10] Lewis R.S., Ming T., Wacker J.F., Anders E. and Steel E. (1987): Nature, 326, 160-162.

AMS C-14 AGES OF YAMATO ACHONDRITIC METEORITES

Y. MIURA[1], A. J. T. JULL[2], D. J. DONAHUE[2], and K. YANAI[3]
[1] Faculty of science, Yamaguchi University, Yoshida, Yamaguchi 753, Japan.
[2] NSF Arizona AMS Facility, University of Arizona, Tucson, AZ 85721, USA.
[3] National Institute of Polar Research, Kaga 1-9-10, Itabashi, Tokyo 173, Japan.

In order to discuss pairing problem and terrestrial history of Antarctic meteorites, ^{14}C terrestrial and weathering ages of Antarctic achondrites will be reported in the 17th NIPR Symposium.

1. Experimental

Samples as small as 0.2 g can be measured using the ^{14}C sensitivity of the accelerator mass spectrometry (AMS) in Tucson. For heavily weathered samples, the carbonates are removed with an acid etch. For cosmogenic ^{14}C, the sample is melted with iron, in a flow of oxygen. The blank is $5\pm1\times10^{5}$ ^{14}C atoms.

The zero age is determined from saturated activity of ^{14}C in the Bruderheim L-6 chondrite, of 51.1 ± 1.5 dpm/kg. Data from Knyahinya confirm this value.

2. Samples

The samples used in this study are seven eucrites: Y-791186,51; Y-791960,52; Y-791962,50; Y-790260,90; Y-792510,95 and Y-74037,88; two diogenites: Y-74097,66 and ALH-77256,93. Three chondrite samples were also determined for cross-check.

3. Discussion

We will discuss the following questions in the 17th NIPR meeting, and compared with our results to earlier measurements of Antactic achondrites.

1) Do the ^{14}C ages measured on 7 eucrites and 2 diogenites show any differences?
2) Do two eucrites Y-791960 and Y-791962 show the same ^{14}C age?
3) Are there any different results from Y-790260, Y-792510 and Y-74037?
4) Do the two diogenites Y-74097 and ALH-77256 show the same ^{14}C age?

NOBLE GASES AND NITROGEN IN LAHRAULI UREILITE.

S.V.S.Murty and N.Bhandari, Physical Research Laboratory, Navrangpura, Ahmedabad 380009, India.

Introduction : Ureilites are carbon rich achondrites, supposedly derived from carbonaceous chrondrites. Trace element data of ureilites suggest a multistage igneous process for their origin (Goodrich et al. 1987) while oxygen isotopes clearly speak of heterogenous accretion (Clayton and Mayeda, 1988). Ureilites contain large amounts of trapped Ar, Kr and Xe similar to those found in carbonaceous chondrites. The carrier phases of the noble gases and the machanisms by which they have been incorporated into the ureilites are still not properly understood. Nitrogen studies in ureilites have revealed $\delta^{15}N$ ranging from 19.7‰ to -83.1‰ in the main group ureilites (Grady et al. 1985 and Grady and Pillinger, 1986) while a ^{15}N rich component with $\delta^{15}N \geq 540$‰ has been observed in polymict ureilites (Grady and Pillinger, 1988). We analysed nitrogen and noble gases in Lahrauli ureilite which fell in 1955 (Bhandari et al. 1981), in an effort to understand their origin and carrier phases that will in turn help in understanding the origin of ureilites. Here we report our results from a bulk sample of Lahrauli.

Experimental : Nitrogen and noble gases have been extracted by step wise pyrolysis at the temperatures (°C) 800, 1000, 1200, 1300, 1400, 1500 and 1700. Prior to pyrolysis, a combustion step in 100 m Torr O_2 is carried out at 400°C, to get rid of surficial contaminants. In each fraction, nitrogen and all the noble gases have been analysed by standard procedures (Murty and Goswami, 1992).

Noble Gases : He and Ne are dominated by spallation component. Using the chemical composition (Bhandari et al. 1981), and production rates of Hohenberg et al. 1978, and measured $^{3}He_{c}=32.1\times10^{-8}$ ccSTP/g and $^{21}Ne_{c}=6.58\times10^{-8}$ ccSTP/g, cosmic ray exposure ages of T_3=12.2 Ma and T_{21}=15.6 Ma are obtained. Ar, Kr and Xe are dominated by trapped component. The ratios ($^{36}Ar/^{132}Xe$)=140 and ($^{84}Kr/^{132}Xe$)=1.02 of

Lahrauli are in the range observed for ureilites (Wacker, 1986). The ($^{40}Ar/^{36}Ar$) ratio decreases with increasing temperature of extraction and reaches a minimum at 1500°C to 2.18×10^{-3}. The isotopic composition of Kr and Xe is constant in all temperature fractions and matches that of Kenna (Wilkening and Marti, 1976).

Nitrogen : The total N in Lahrauli amounts to 11.3 ppm with $\delta^{15}N$ = -72‰. The $\delta^{15}N$ of 800°C fraction is 5.5‰ and progressively decreases to -107‰ in the 1400°C fraction and subsequently increases to -89‰ in the 1700°C fraction. The $\delta^{15}N$ trend is most likely due to mixing between a heavy N-component ($\delta^{15}N \geq 5.5$‰) that has a low temperature release and a light N-component ($\delta^{15}N \leq -107$‰) that is more retentively sited. Increase in the $\delta^{15}N$, beyond 1400°C is most likely due to release of spallation nitrogen. The spallogenic ^{15}N needed to cause such an increase is consistent with the spallation ^{21}Ne present in Lahrauli. This is the lightest N-component, yet observed in a bulk ureilite. The unusual stony meteorite Acapulco also exhibits a similar N isotopic pattern (Sturgeon and Marti, 1991).

Discussion : In the diamond-free ureilite ALHA 78019, the ratio $^{36}Ar/^{132}Xe$ has been found to be 600. The value of 140 for the same ratio in Lahrauli probably reflects the partial loss of Ar and Kr in the shock that produced the diamonds. The lower ratios of $^{36}Ar/^{132}Xe \leq 100$ and $^{84}Kr/^{132}Xe < 1$ at ≤ 1300°C as compared to those at ≥1400°C fractions support such a loss.

The uniform composition of trapped Ar, Kr and Xe and the presence of two distinct N-components suggest that the carriers of noble gases and nitrogen are different. Also the light isotopic signature for a major part of nitrogen suggests that carbonaceous chondrites whose $\delta^{15}N \geq 50$‰, could not be the principal precursor material for ureilites. The survival of distinct N-isotopic components is consistent with heterogenous accretion of the ureilite parent body as suggested by the oxygen isotopes (Clayton and Mayeda, 1988). Nitrogen and noble gas studies in acid residues and separated phases of Lahrauli are in progress to identify the carriers of the heavy and light N-carriers and their relation to the associated noble gas components.

References : Bhandari, N., Shah, V.G. and Graham, A. (1981), Meteoritics 16 185; Clayton, R.N. and Mayeda, T.K. (1988) Geochim. Cosmochim. Acta 52 1313; Goodrich, C.A., Jones, J.J. and Berkley, J.L. (1987) Geochim. Cosmochim. Acta 51 2255; Grady, M.M., Wright, I.P., Swart, P.K. and Pillinger, C.T. (1985) Geochim. Cosmochim. Acta 49 903; Grady, M.M. and Pillinger, C.T. (1986) Meteoritics 25 375; Grady, M.M. and Pillinger, C.T. (1988) Nature 331 321; Hohenberg, C.M., Marti, K., Podosek, F.A., Reedy, R. and Shirck, J.R. (1978) Proc. Lunar Planet. Sci. Conf. 9 2311; Murty, S.V.S and Goswami, J.N. (1992) Proc. Lunar Planet. Sci. 23; Sturgeon, G. and Marti, K. (1991) Proc. Lunar Planet. Sci. 21 523; Wacker, J.F. (1986) Geochim. Cosmochim. Acta 50 633; Wilkening, L.L. and Marti, K. (1976) Geochim. Cosmochim. Acta 40 1465.

Preliminary TL subclassification of Yamato unequilibrated ordinary chondrires and comparison with petrographic subgroups

K. NINAGAWA[1], I. YAMAMOTO[1], S. MATSUNAMI[2], H. KOJIMA[3] and K. YANAI[3]

[1]*Okayama University of Science, 1-1, Ridai-cho, Okayama 700*
[2]*Naruto University of Education, Takashima, Naruto, Tokushima 772*
[3]*National Institute of Polar Research, 9-10, Kaga 1-chome, Itabashi-ku, Tokyo 173*

Introduction Unequilibrated ordinary chondrites [UOCs] have been subclassified by olivine heterogeneity, the induced thermoluminescence [TL] sensitivity, carbon content and inert gas content. Metamorphism caused the heterogeneity of Fe contents in olivine to homogeneity. Concurrently metamorphism caused the production of feldspar, which was responsible for the TL, by the devitrification of feldspathic mesostasis and the induced TL sensitivity increased by a factor of 10^3 from type 3.0 to 3.9.

Kojima and Yanai classified Yamato UOCs to 4 subgroups by the Fe-heterogeneity of olivine and low-Ca pyroxene, and Cr_2O_3 contents in olivine.[1)] Low grades of subgroups are less metamorphosed. Yamato UOCs are listed in table 1. This time we investigated TL subtypes of these Yamato UOCs and compared with petrographic subgroups.

Experiments Sears et al. have measured the induced TL sensitivity by usual TL systems with Corning 7-59 and 4-69 filters, which transmitted ultraviolet-blue region.[2)] Their irradiation dose was ~0.2 kGy and the heating rate was 7.5 °C/s. In this TL investigation we used the same filters and the similar irradiation dose, 0.2 kGy. But the heating rate was set to be 1.0 °C/s, because the TL photon-counting system need not so much rapid heating. Dhajala was usually used to normalize the TL sensitivity. But ALH-77214(L3.4) , which relative TL sensitivity was 0.07±0.03 [2)], was used for standard in this classification.

Results The results are summarized in table 1. Subtypes by TL sensitivity is consistent with the petrographic subgroups, except Y-791835 in group 1. On a whole group 1, 2, 3 and 4 correspond to the TL subtypes 3.0~3.3, 3.1~3.4, 3.5~3.8 and 3.6~4, respectively. The TL subtype of Y-791835 was 3.6~3.8 and larger than the others in group 1 by ~0.6. Brecciation involving material of very different petrographic type (>0.4) is rare. But 4 cases, ALH85062 [TL subtype 4, C.V.*1 3.5], LEW 86549 [TL 3.0, C.V. 3.7], RKPA80207 [TL 3.2, C.V. 3.7] and RKPA86700 [TL 3.0, C.V. 3.9] have been reported.[2)] Y-791835 would be this type of breccias.

Ordinary chondrites of type 3.2-3.4 are tending to have TL glow curves, low peak temperature and narrow width, different from those of type 3.6-3.9, high peak temperature and wide width. Guimon et al. argued that this difference was caused by order and disordering of feldspar.[3)] On the other hand Ninagawa et al. suggested that the former was due to the TL emission from normative anorthite mesostasis and the latter normative albite mesostasis.[4)] All high grade chondrites of subgroup 3 and 4 fall in the latter cluster. But Y-793567 in the low grade chondrites falls in the latter cluster while Y-793408, Y-790448 and Y82038 fall in the former cluster.

One of the main subject in this investigation was to identify the primitive chondrites. The primitive chondrites, Semarkona and Bishunpur, have yellow luminescence and unusual TL glow curves.[5)] We also measured the TL using a Corning 4-96 filter instead of the above filters because the Corning 4-96 filter transmit yellow as well as ultraviolet-blue. But no difference was detected in the glow curve shape

*1:Coefficient of variation of the fayalite in the olivine. (C.V. ~ %M.D./0.80)[2)]

Table 1. Petrographic subgroups and TL subtypes

		Olivine	Low-Ca pyroxene	Cr_2O_3 in olivine	TL sensitivity	TL Peak Temp.	TL Peak width	TL Subtype
		(%M.D.)[#1]	(%M.D.)	(wt%)	(Dhajala=1)	(°C)	(°C)	
group 1		L[#2]	L	>0.2%				
Y-793408		40	67	0.19	0.023±0.014	131	110	3.1~3.3
Y-791835		69	61	0.22	0.99±0.61	176	126	3.6~3.8
Y-790448		65	65	0.24	0.0065±0.0041	*	*	3.0~3.2
group 2		L	L	<0.2%				
Y-82038	LL3	50	27	0.11	0.021±0.013	131	91	3.1~3.3
Y-793567	L3	33	45	0.09	0.056±0.034	176	133	3.3~3.4
group 3		D[#3]	L					
Y-791428	H3	2.0	37		1.2±0.7	166	120	3.6~3.8
Y-791429	L3	6.7	24		0.97±0.60	173	119	3.6~3.8
Y-791961	L3	5.2	33		0.49±0.30	202	125	3.5~3.7
Y-793375	L3	5.7	37		0.49±0.30	186	118	3.5~3.7
Y-793396	L3	1.5	35		0.56±0.34	194	119	3.6~3.7
group 4		D	D					
Y-791340	H3	8.6	9.8		1.5±0.95	168	108	3.7~3.8
Y-791087	H3	1.8	16		1.0±0.63	171	120	3.6~3.8
Y-791828	L3	16	27		4.6±2.8	186	108	3.8~4
Standard for the TL sensitivity								
ALH-77214	L3				0.07±0.03[2)]	110	62	3.4

[#1]: Percent mean deviation.

[#2]: Lack mode in the distribution of Fe content.

[#3]: Distinct mode in the distribution of Fe content.

References:

1) Kojima and Yanai (1991): Papers presented to the 16th Symposium on Antarctic Meteorites, 3-4.

2) Sears et al. (1990): Proc. Lunar Planet. Sci. Conf., **21**, 493-512

3) Guimon et al. (1985): Geochim. Cosmochim. Acta, **49**, 1515-1524

4) Ninagawa et al. (1991): Proc. NIPR Symp. Antarct. Meteorites, **4**, 344-351.

5) Ninagawa et al. (1992): Proc. NIPR Symp. Antarct. Meteorites, **5**, in press.

Devitrification and TL sensitivity in an ordinary chondrite

K. NINAGAWA[1], A. MATOBA[1], T. YAMAGUCHI[1], S. FUKUOKA[1]
I. YAMAMOTO[1], S. MATSUNAMI[2] and M. KIMURA[3]

[1]*Okayama University of Science, 1-1, Ridai-cho, Okayama 700*
[2]*Naruto University of Education, Takashima, Naruto, Tokushima 772*
[3]*Ibaraki University, 1-1, Bunkyo 2-chome, Ibaraki 310*

Introduction The induced thermoluminescence [TL] sensitivity of ordinary chondrites increases by a factor of 10^5 from type 3 to type 6, and unequilibrated ordinary chondrites have been classified to subtypes by the induced TL sensitivity.[1)] It has been appreciated that the feldspar is responsible for the TL and is produced by the crystallization of feldspathic mesostases during thermal metamorphism.[2)] On the other hand Matsunami et al. recently showed that amorphous silica glass was responsible for the TL.[3)] Then we applied a TL spatial distribution readout system to a thin section to investigate whether the feldspathic glassy mesostases was responsible for the TL.

Experiments A thin section of Y-74191(L3.6) was made by the usual polishing method with epoxy bond. The thin section together with a bonded slide glass was exposed to γ-rays from ^{60}Co and received a dose of 6.6 kGy. The TL images were measured immediately after irradiation by the TL spatial distribution readout system with no filter. The heating rate was 0.25°C/s and the maximum temperature was limited to 250°C to avoid the degeneration of epoxy bond. The thin section was so large (7x7mm) that the TL was measured several times and a mosaic of TL images was constituted. The chemical compositions of feldspathic mesostases and feldspar were analyzed by an electron probe X-ray microanalyzer [EPMA], JCXA-733 (JEOL LTD), operated at 4 nA beam absorption on PCD (Probe Current Detector).

Results and Discussion Figure 1 (a) shows a photograph of the thin section, Y-74191(L3.6). Devitrification of feldspathic mesostasis [clean glassy or cryptocrystalline mesostasis] was judged through a microscope. Figure 1 (b) shows the mosaic of the TL images at temperature interval 25-250 °C. The chondrule numbers are represented in Fig.1 (b).

The chondrules with cryptocrystalline mesostases or feldspar [8, 18, 41 and 42] showed the TL. The glow curves of 41 and 42 were plotted in Fig.1 (c). The slide glass under the thin section also showed the TL and its glow curve was plotted in Fig.1 (c). A area on a chondrule [45] with cryptocrystalline mesostasis showed the same glow curve as the slide glass [Fig.1 (c)]. This meant that the slide glass under the chondrule showed the TL and the chondrule [45] showed no TL. The chondrules with clean glassy mesostases [35, 36, 57 and 59] showed the TL. The feldspathic glassy mesostases are also responsible for the TL. The glow curves of 35 and 59 were plotted in Fig.1 (d). In the case of a clean glassy mesostasis we found a chondrule [21] with no TL. The devitrification, TL properties and chemical compositions of feldspathic mesostases are summarized in Table 1. The mesostases in chondrules were divided into four groups, I; Cryptocrystalline mesostasis and bright TL, II; Cryptocrystalline mesostasis and no TL, III; Clean glassy mesostasis and bright TL, IV; Clean glassy mesostasis and no TL. But there is no difference between clean glassy and cryptocrystalline mesostasis. This means that the devitrification does not affect the TL property.

There are two types of glow curves, low peak temperature & narrow width [8, 42 and 59], and high peak temperature & wide width [18, 41, 35, 36 and 57]. Guimon et al. argued that this difference was caused by order and disordering of feldspar.[4)] But we reported that the former was due to the TL emission from normative anorthite mesostasis and the latter normative albite

mesostasis.[5] We recognized the same correlation between the TL properties [Peak temp. and Peak width] and molar ratio of Ca/(Ca+Na+K) as shown in Table 1. We found that some mesostases [45 and 21] which showed no TL emission have normative albite compositions. This result also coincides with those of the paper.[5]

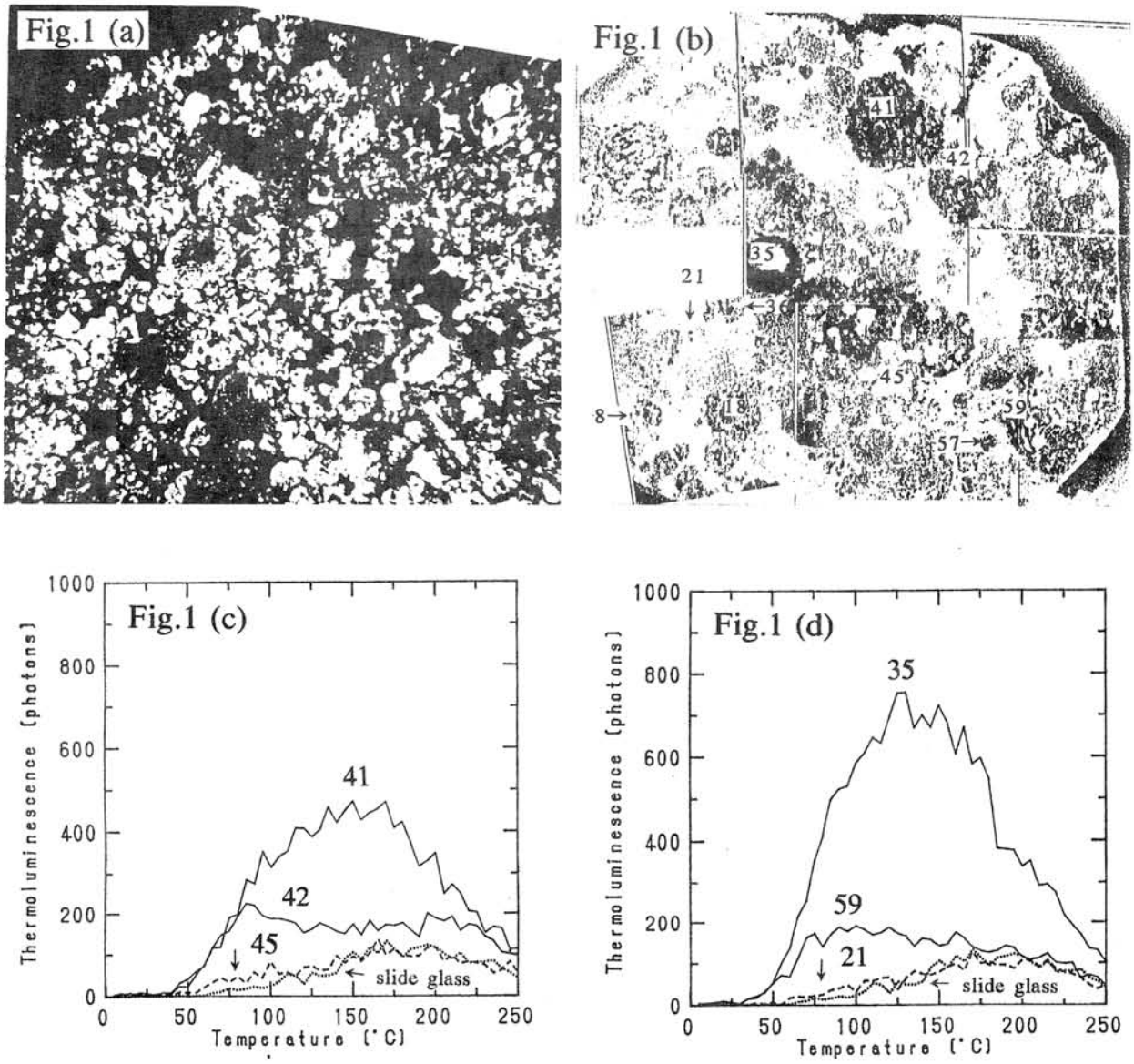

Fig.1 Photograph, mosaic of TL images and glow curves.

(a) Photograph of the thin section, Y-74191(L3.6) in cross-polars. Long dimension is 7.3 mm. (b) Mosaic of TL images at temperature interval 25-250 °C. The position of high TL intensity is put by deep black points. (c) local glow curves of cryptocrystalline mesostases and feldspar. The glow curve of the slide glass is also plotted. (d) local glow curves of clean glassy mesostases. The glow curve of the slide glass is plotted.

Table 1. Devitrification of mesostasis and TL property

Group	I	I	I	I	II
Chondrule number	8	18	41	42	45
ME[#1]: Devitrification	Crypto.[#4]	Crypto.	Crypto.	Feldspar	Crypto.
ME: Norm Fel.[#2]	87-96	59-90	77-89	100	77-89
ME: Ca/(Ca+Na+K)[#3]	79-89	3-17	11-25	70-71	2-25
TL: Bright or No	Bright	Bright	Bright	Bright	No
TL: Peak temp.(°C)	90	130	130	80	----
TL: Peak width (°C)	60	110	110	75	----

Group	III	III	III	III	IV
Chondrule number	35	36	57	59	21
ME: Devitrification	Clean[#5]	Clean	Clean	Clean	Clean
ME: Norm Fel.	53-91	74-90	48-88	70-77	72-86
ME: Ca/(Ca+Na+K)	1-12	4-15	5-18	54-62	10-27
TL: Bright or No	Bright	Bright	Bright	Bright	No
TL: Peak temp.(°C)	125	130	130	95	----
TL: Peak width (°C)	110	105	90	80	----

I. Cryptocrystalline mesostasis and bright TL. II. Cryptocrystalline mesostasis and no TL.
III. Clean glassy mesostasis and bright TL. IV. Clean glassy mesostasis and no TL.
[#1]: Mesostasis, [#2]: Normative feldspar in mesostasis, [#3]: Molar ratio in mesostasis,
[#4]: Cryptocrystalline mesostasis, [#5]: Clean glassy mesostasis.

References:
1) Sears et al. (1990): Proc. Lunar Planet. Sci. Conf., **21**, 493-512.
2) Sears (1988): Nucl. Tracks Radiat. Meas., **14**, 5-17.
3) Matsunami et al. (1992): Proc. NIPR Symp. Antarct. Meteorites, **5**, in press.
4) Guimon et al. (1985): Geochim. Cosmochim. Acta, **49**, 1515-1524.
5) Ninagawa et al. (1991): Proc. NIPR Symp. Antarct. Meteorites, **4**, 344-351.

A transmission electron microscope study of exsolution lamellae of pyroxenes in ordinary chondrites.

Takaaki NOGUCHI[1], Kiyoshi FUJINO[2] and Hiroshi MOMOI[2].
1) Deptartment of Earth Sciences, Ibaraki University, Bunkyo 2-1-1, Mito 310. 2) Department of Earth Sciences, Ehime University, Bunkyo-cho 2-5, Matsuyama 790.

Introduction: Microstucture of pyroxene crystal is a useful indicator of thermal history of pyroxene-bearing rocks. Microstructure of pyroxene in ordinary chondrites has been investigated by some researchers (e. g. Ashworth and Barber, 1977; Ashworth, 1980; Ashworth, 1981; Ashworth et al., 1984; Töpel-Schadt and Müller, 1985; Kitamura et al., 1983; Watanabe et al., 1985). But they did not study systematically microstructure of pyroxene crystals with similar texture in chondrites which belong to various petrologic types. In this study, pyroxenes in porphyritic pyroxene-bearing chondrules were investigated by a transmission electron microscope (TEM). Scanning electron microscope (SEM) with energy dispersive spectrometer (EDS) was also used in order to choose the chondrules investigated. The heterogeneity of chemical composition of pyroxene is different among chondrites which belong to the same petrologic type and different chemical groups (Noguchi, 1990). Therefore, we used the heterogeneity in stead of petrologic types in order to choose meteorites investigated. Meteorites investigated are following: Julesburg (L3), Barratta (L4), McKinney (L4), Homestead (L5), Taiban (L5), Tuan Tuc (L6), ALH-77208 (H4), Ste. Marguerite (H4), Jilin (H5), and Kernouvé (H6).
Results: Julesburg is an unequilibrated L chondrite. Electron microprobe (EPMA) analyses show that it includes heterogeneous olivine and pyroxene. EPMA analyses indicate that Barratta contains fairly homogeneous olivine and heterogeneous pyroxene. Standard deviations of Wo content and Mg # of augite in Barratta are as large as those of augite in Julesburg. In a chondrule in Julesburg, there are exsolution lamellae of pigeonite in augite on the rim of low-Ca clinopyroxene (rim augite). These lamellae have modulated structure and run approximately parallel to (001) and (100). Thickness of them is about several to 10 nm and spacing of them is about 10 to 20nm. Two chondrules in Barratta were investigated. In one chondrule, rim augite includes exsolution lamellae of pigeonite which are similar in shape and size to those shown in Julesburg. The other chondrule contains augite with exsolution lamellae which are finer than those in Julesburg and those in the other chondrule in Barratta. They have bleb-like shape and run neither along (001) nor (100).

Olivine and pyroxene in McKinney, Homestead, ALH-77208, and Ste. Marguerite contain homogeneous olivine and heterogeneous pyroxene. Standard deviations of Wo content of augite in them are as large as those in Julesburg and Barratta. But standard deviations of Mg # of augite are small. In McKinney, pigeonite with exsolution lamellae of augite which are a few tens nm in thick was observed. The spacing of exsolution lamellae is several tens nm. Most of the lamellae run parallel to (001), and the tips of some of the lamellae bend to the direction parallel to (100). Exsolution lamellae of pigeonite in rim augite have similar thickness and spacing among these four chondrites. They are several tens nm in thick. Spacing of them

is from several tens to about 100 nm. Some exsolution lamellae change their direction from parallel to (001) to parallel to (100) of the host augite.

Augite in Jilin is homogeneous as well as low-Ca pyroxene. EPMA analyses also suggest that this meteorite include pyroxene with composition of pigeonite. Backscattered electron images (BEIs) of such pigeonite crystals suggest that they include fine exsolution lamellae (Noguchi, 1988). TEM observation of such pigeonite reveals that the pyroxene has pigeonite structure and that such pigeonite in this meteorite includes fine exsolution lamellae of augite (Fig. 1). It involves exsolution lamellae of augite with about 100 nm in thick, parallel to (001) of host pigeonite. Spacing of augite lamellae is from two to five hundred nm. Some exsolution lamellae of orthopyroxene were also observed. They are several to 20 nm in thick, parallel to (100) of host pigeonite, and associated with stacking faults parallel to (100) of host pigeonite. Contrary to the pigeonite, rim augite has no exsolution lamellae. It contains only stacking faults, parallel to (100), and free dislocations.

Taiban, Tuan Tuc, and Kernouvé include homogeneous augite. In these chondrites, augite has no exsolution lamellae.

L chondrites which were investigated in this study show shock textures such as shock blackening. However, exsolution lamellae of augite in Barratta, McKinney and Homestead seem not to be affected by shock heating, though they show ductile and brittle deformation. Orthopyroxene which is originally protopyroxene and augite in Taiban and Tuan Tuc have many dislocations due to shock deformations.

Discussion

Different cooling history between porphyritic and radial pyroxene chondrules.

Watanabe et al. (1985) indicated that an excentroradial pyroxene chondrule in Fukutomi (L4 to 5) includes pigeonite with spinodal decomposition textures. However, we could not find such pigeonite in porphyritic pyroxene-bearing chondrules investigated here, although Julesburg and Barratta have augite with similar texture to that in the pigeonite in Fukutomi. This textural difference suggests that radial pyroxene chondrules were cooled faster than porphyritic pyroxene-bearing chondrules even under subsolidus temperatures (about 1100 to 800°C, spinodal decomposition develops under such temperatures).

Relationship between EPMA analyses and exsolution lamellae in pigeonite and augite.

EPMA analyses show that ordinary chondrites can be divided into two groups from the viewpoint of standard deviation of Wo content in augite which they include. Wo content of augite is heterogeneous in one group and homogeneous in the other. The latter corresponds to so-called equilibrated ordinary chondrite. Rim augite in the latter contains no exsolution lamellae of pigeonite which are common in the former. If there are homogeneous augite and low-Ca pyroxene in a chondrite, it is reasonable that these pyroxenes were homogenized during metamorphism. However, it is very difficult to explain the coexistence of lamellae-bearing pigeonite and lamellae-free homogeneous augite by such an idea. If rim augite was homogenized by metamorphism, diffusion distance of Ca in augite should be larger than half width of rim augite, about 5μm. On the contrary, diffusion distance of Ca in pigeonite is thought to have

been about a few hundred nm, because the spacing of augite exsolution lamellae in pigeonite is 2 to 5 hundred nm. If metamorphic reequilibration of pyroxene is adopted, it means that Ca diffuses much faster in augite than in pigeonite. It is inconsistent with experimental data (e. g. Fujino et al., in prep.) and observation of exsolution lamellae in augite and pigeonite in terrestrial rocks. Therefore, it may be more reasonable that chemical composition of rim augite was similar to present composition when they crystallized. BEI photographs of (compositional) pigeonite in some H5 chondrites which includes homogeneous augite suggest that such lamellae-bearing pigeonite is common among them (Noguchi, 1988), although the coexistence of such pigeonite and augite was not confirmed by TEM. Rim augite in equilibrated chondrites may not have been formed only by homogenization of primary rim augite and overgrowth of augite on primary augite during metamorphism.

References: Ashworth (1980): Earth Planet. Sci. Lett., 46, 167-177; Ashworth (1981): Proc. R. Soc. Lond. A 374, 179-194; Ashworth and Barber (1977): Phil. Trans. R. Soc. Lond. A. 286, 493-506; Fujino, Naohara, and Momoi (in prep.); Kitamura, Yasuda, Watanabe, and Morimoto (1983) Earth Planet. Sci. Let., 63, 189-201; Noguchi (1988): Papers presented in the 13th NIPR Symp. Anter. Meteor., 38-40; Noguchi (1990): Meteoritics, 25, 393; Töpel-Schadt and Müller (1985): Earth Planet. Sci. Lett., 74, 1-12; Watanabe, Kitamura, and Morimoto (1985) Earth Planet. Sci. Let., 72, 87-98.

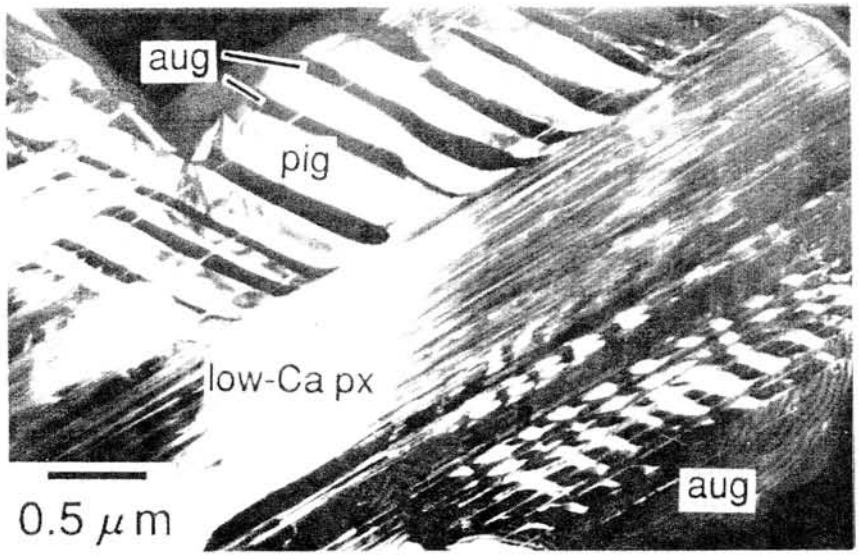

Fig. 1 Dark field electron micrograph of a pyroxene grain in a porphyritic pyroxene-bearing chondrule in Jilin (g=102, pigeonite). This pyroxene grain is composed of low-Ca pyroxene (low-Ca px), lamellae-bearing pigeonite (pig) and rim augite (aug).

ANALYSES FOR DICARBOXYLIC ACIDS IN THE NINGQIANG CARBONACEOUS CHONDRITE

Shimoyama, A., Shigematsu, R., and Wang, D.*

Department of Chemistry, University of Tsukuba, Tsukuba 305
*Institute of Geochemistry, Academic Sinica, Guangzhou Branch, Guangzhou 51064
Guangdong Province, The People's Republic of China

The Ningqiang meteorite has been reported to be an anomalous CV chondrite containing 0.68% carbon [1]. We examined a sample of the chondrite for dicarboxylic acids by the analytical procedures used for Yamato-791198 and Murchison in a companion paper[2].

Our elemental analyses show 0.25% carbon and 0.02% nitrogen in the chondrite sample.

A gas chromatogram for dicarboxylic acids is shown in Fig. 1 with the identities and concentrations of five acids. No other dicarboxylic acids are found on the chromatogram. A chromatogram of procedural blank shows only minor peaks at the retention times 20, 29, and 40 min which are not of dicarboxylic acids. Therefore, the five acids are not due to laboratory contamination introduced in our analyses.

We conclude that the five acids are not indigenous but from terrestrial contamination to the sample by the following reasons:

1. Although succinic, glutaric, and adipic acids are found at the levels of nmol to sub-nmol/g, none of the structural isomers of these acids are found, suggesting not meteoritic origin of these acids.
2. Adipic and phthalic acids are present in concentration more than or similar to succinic and glutaric acids. The former two acids are known to be present as their derivative forms in plasticizer which are found almost everywhere as contaminants.

Various kinds of dicarboxylic acids were found in Yamato-791198 and Muchison by the same analytical method[2] probaby because thery are CM chondrites. On the other hand, the present examination did not find indigenous dicarboxylic acids probably because Ningqiang is a CV chondrite similar to Allende which is known to contain little extractable organic compounds.

References

1. Wang, D. (1988): Abst.13th Symp. Antarct. Meteorites, 25.
2. Shimouama, A. and Shigematsu, R. (1992): A companion paper in this volume.

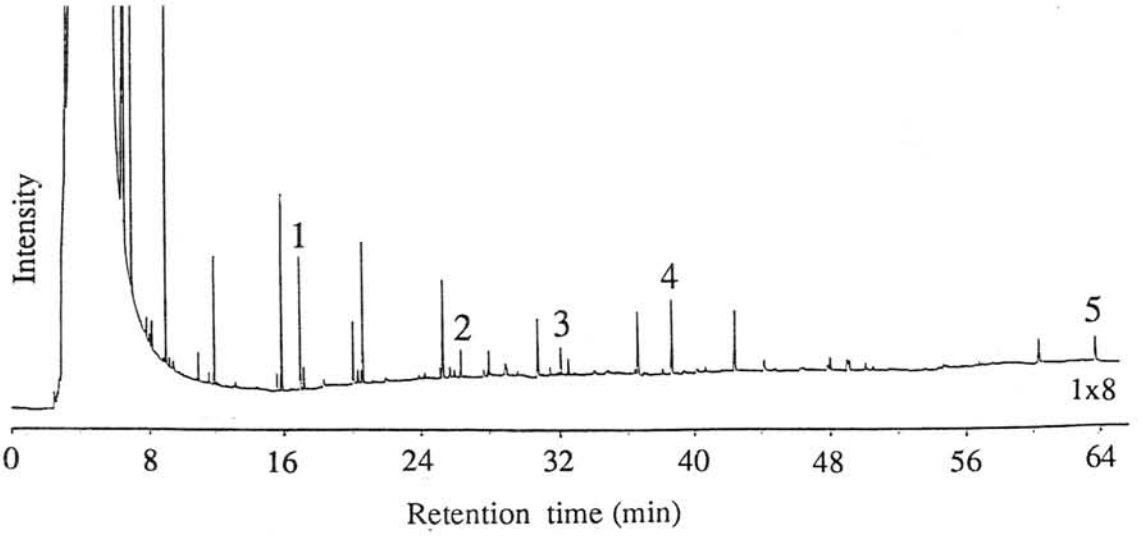

Fig. 1. Gas chromatogram of dicarboxylic acids in the water extract of the Ningqiang chondite. Peak No. 1. oxalic acid (9.1), 2. succinic acid (0.7), 3. glutaric acid (0.1), 4. adipic acid (5.5), 5. phthalic acid (0.6). Numbers in parenthesis are concentration in nmol/g.